ACKNOWLEDGEMENTS

Au terme de ce travail, je tiens à remercier l'ensemble des personnes qui m'ont permis, de près ou de loin, de mener à bien ce projet.

Mes remerciements s'adressent tout d'abord à mon promoteur, le Professeur Véronique Préat, qui a cru en moi, m'a accueillie au sein de son laboratoire pendant ces quatre belles années, m'a toujours aidée et soutenue dans les moments difficiles tant au niveau professionnels qu'à titre privé.

Je tiens également à remercier chaleureusement le Docteur Fabienne Danhier, sans qui je ne serais probablement pas arrivée jusque là. Je la remercie pour son aide précieuse dans l'accompagnement de mon travail ainsi que pour tous les mots justes trouvés pour me faire avancer malgré les embûches. Merci également pour ces nombreuses soirées après le boulot où l'on avait l'impression de trouver l'idée révolutionnaire pour la suite de nos expériences... (Certaines ont quand même porté leurs fruits !!!).

J'aimerais également remercier mon co-promoteur, le Professeur Bernard Gallez, pour ses conseils avisés dans le domaine mystérieux de l'IRM ainsi que pour ses remises en questions nécessaires au bon déroulement de cette thèse.

Ma gratitude s'adresse également au Professeur Olivier Feron, Président du jury, pour le partage de ses connaissances dans le domaine de l'angiogénèse ainsi que pour ces bons conseils. Merci également au Professeur Christine Jérôme et à Vincent Pourcelle, pour les polymères qu'ils m'ont fournis et les techniques de greffage qu'ils m'ont apprises. Je remercie également Sophie Laurent, membre du jury, de m'avoir aidé à la caractérisation de mes particules ainsi que pour les discussions et les judicieux conseils.

Je souhaite exprimer ma reconnaissance aux Professeurs Stephane De Smedt et Frédéric Lagarce d'avoir accepté de faire partie de mon Jury de thèse. Merci pour les discussions passionnantes et les remarques qui ont permis d'enrichir le travail.

Je remercie, bien entendu, tous les membres de l'unité FARG. Merci pour la super ambiance qui règne dans notre laboratoire, pour les chouettes discussions, les conseils avisés en terme de recherche...ou non ! Je tiens à remercier particulièrement Pauline pour sa joie de vivre, nos discussions passionnées, nos fous-rires et notre colocation (certes courte mais intense !!!), Nathalie et Bernard pour votre aide précieuse dans mes manipulations et nos conversations sympathiques et toujours dans la bonne humeur !! Merci aussi à Murielle sans qui la qualité de ce manuscrit laisserait à désirer. Merci pour ta patience devant mon incompétence en terme de traitement de texte !!! Un grand merci à Pierre Danhier de m'avoir appris à dompter cette curieuse machine qu'est la RPE !

Enfin, je voudrais adresser un merci tout particulier à mes parents pour m'avoir soutenue tout au long de ce projet, pour m'avoir rassurée à maintes reprises quand il le fallait. Merci également à Akim pour le calme et la tranquillité qu'il m'a apportés. Ces qualités précieuses qui me font défaut et que j'ai pu puiser en lui. Merci aussi de si bien me comprendre même quand personne n'en est capable. Enfin, un dernier merci à mon petit frère pour les verres de décontraction à l'approche de la défense.

Abbreviations

AMF	Alternative magnetic field
AT	Active targeting
b-FGF	Basic fibroblast growth factor
CH	Chitosan
CMPT	Camptothecin
CNT	Carbon Nanotube
cRGDfk	Cyclo-(Arg-Gly-Asp-D-Phe-Lys)
cRGDfv	Cyclo-(Arg-Gly-Asp-D-Phe-Val)
DAPI	4,6-diamidino-2-phenylindole
DIP	Poly[N-(N',N'-diisopropylaminoethyl)]
DLS	Dynamic Light Scattering
DMEM	Dubelcco's modified Eagle's medium
DOX	Doxorubicin
DTX	Docetaxel
ECM	Extracellular matrix
EGFR	Epidermal growth factor receptor
EMA	European Medicine Agency
EPI	Epirubicin
EPR	Enhanced permeability and retention
ESR	Electron Spin Resonance
FA	Folate
FBP	Folate-binding proteins
FDA	Food and Drug administration
FITC	Fluorescein isothiocyanate
GEM	Gemcitabin
GLUT	Glucose transporter
GRGDS	Glycine-Aginine-Glycine-Aspartare-Serine
HBSS	Hank's buffered salt solution
HeLa	Human cervix epithelial carcinoma
HIF	Hypoxia inducible factor
HPLC	High performance liquid chromatography

HT	Hyperthermia
HUVEC	Human umbilical vein endothelial cells
IAP	Inhibitor of apoptosis proteins
ICAM-1	Intercellular adhesion molecule-1
ICPMS	Inductively coupled plasma mass spectroscopy
IFP	Interstitial fluid pressure
Ig	Immunoglobulin
IL	Interleukin
IP	Intraperitoneal
IV	Intravenous
LCST	Low critical solution temperature
LOD	Limit of detection
LOQ	Limit of quantification
MAb	Monoclonal antibodies
MDR	Multidrug resistance
MMP	Matrix metalloproteinase
MNP	Magnetic nanoparticles
MPS	Mononuclear phagocytic system
MRI	Magnetic resonance imaging
Ms	Saturation magnetization
MT	Magnetic targeting
MTT	3-(4, 5-dimethylthiazol-2-yl)-2,5-diphenyl tetrazolium bromide
MTT	Metotrexate
MTX	Mitoxantrone
NAD	Nicotinamide adenine dinucleotide
NGR	Asparagine-Glycine-Arginine
NHL	Non-Hodgkin’s lymphoma
NIR	Near-infrared
NMRD	Nuclear magnetic resonance dispersion
NP	Nanoparticles
O/W	Oil in water
PBS	Phosphate buffered saline
PCL	Poly(ε-caprolactone)
PDGF	Platelet-derived growth factor

PDI	Polydispersity index
PDT	Photodynamic therapy
PEG	Poly(ethylene glycol)
PET	Positron emission tomography
PGA	Poly(L-glutamic acid)
PHD	Prolyl hydroxylase domain
PLA	Poly(lactic acid)
PLGA	Poly(lactic-coglycolic acid)
PT	Passive targeting
PTT	Photothermic therapy
PTX	Paclitaxel
PVA	Polyvinyl-alcohol
QDs	Quantum dots
RES	Reticulo-endothelial system
RF	Radiofrequency
RFA	Radiofrequency ablation
RGD	Aginine-Glycine-Aspartare
ROS	Reactive oxygen species
scFv	Single-chain antibody fragment
SD	Standard deviation
SEM	Standard error of the mean
SPECT	Single-photon emission computed tomography
SPIO	Superparamagnetic iron oxide
T_1	Longitudinal relaxation time
T_2	Transversal relaxation time
T2WI	T_2 weighted image
TAG	Tumor-associated glycoprotein
TEM	Transmission Electron Microscopy
TKI	Tyrosine kinase inhibitors
TLT	Transplantable liver tumors
TMZ	Temozolomide
TNF	Tumor necrosis factor
US	Ultrasound
UV	Ultraviolet

VCAM	Vascular adhesion molecules
VEGF	Vascular endothelial growth factor
VEGF	Vascular endothelial growth factor
W/O/W	Water in oil in water emulsion
PNP	Polymeric nanoparticles
SCID	Severe combined immunodeficiency
PAA	Poly(acrylamide)
MF	Magnetic field
MST	Mean survival time
PS	Photosensitizer

TABLE OF CONTENTS

CHAPTER I.

INTRODUCTION

TABLE OF CONTENTS

I. TUMOR MICROENVIRONMENT

Tumor microenvironment is one of many areas, which are studied to design new anti-cancer therapies. Indeed, many efforts have been made in research field to develop different therapeutic strategies based on the numerous differences between tumor and normal tissue including vascular abnormalities, oxygenation, perfusion, pH and metabolic states. Therefore, the knowledge and the understanding of tumor microenvironment are crucial. Here, the differences in terms of morphology of tumor vasculature and the pH will be particularly described, as they are the more relevant characteristics for the design of nanocarriers as tumor targeted drug delivery systems.

I.1. ANGIOGENESIS

Angiogenesis refers to the process by which new blood vessels arise from the existing-ones. This process plays a critical role in organ growth in the embryo as well as in wound repair and ovulation in adulthood. Angiogenesis is a highly regulated process by a multitude of stimulators and inhibitors but an imbalance in these regulators contributes to the pathogenesis of various disorders including tumor malignancy. Indeed, even in adulthood, endothelial cells retain their ability of dividing rapidly in response to a physiological stimulus such as hypoxia [Carmeliet, 2005; Distler et al., 2003].

Thus, when tumors reach approximately 2 mm^3, the increased interstitial pressure within the tumor inhibits the diffusion of metabolites and nutrients necessary for tumor growth. A state of cellular hypoxia begins, inducing the sprouting of new blood vessels from the established vasculature. Consequently, oxygen and nutrients are carried to tumor cells, which need them to survive and proliferate [Folkman, 1971; Jain, 1987]. This ability of tumors to progress from a non-angiogenic to angiogenic phenotype (called the “angiogenic switch”) is central to progression of cancer [Carmeliet, 2000; Naumov et al., 2006].

Angiogenesis is a five-step process (Figure 1) in which:

(i) endothelial cells are activated by pro-angiogenic signals
(ii) vessels are destabilized and basement membrane is degraded
(iii) the proliferating endothelial cells migrate through the disintegrated basement membrane

(iv) endothelial cells arrange to form a tube-like structure (lumen formation)

(v) angiogenic remodeling occurs: the vascular tube is stabilized by mural cells (pericytes)

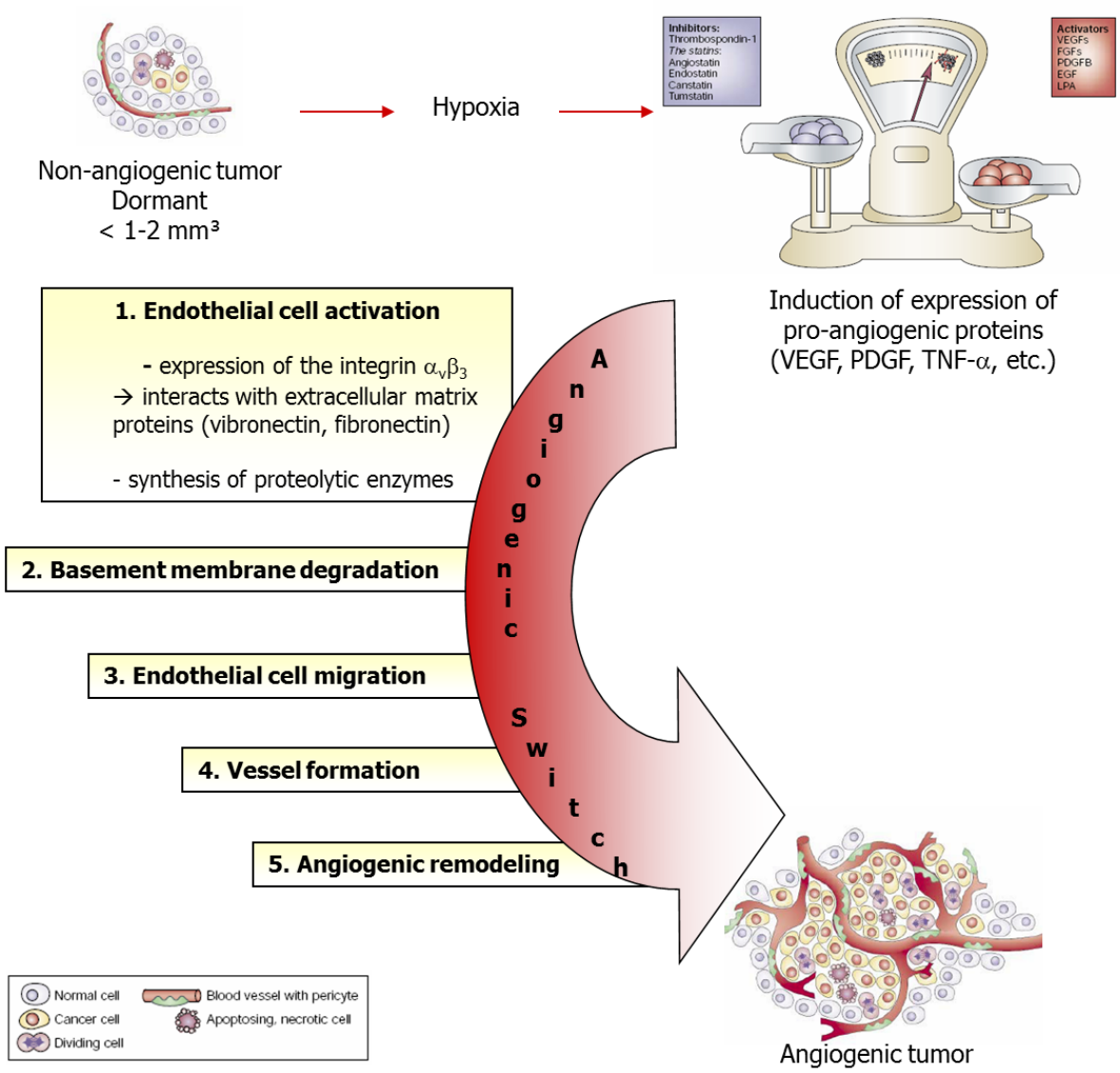

Figure 1. Schematic representation of the 5-step angiogenesis process (adapted from [Danhier et al., 2012b]).

When hypoxia is sensed by the endothelial cells oxygen sensors (e.g. prolyl hydroxylase domain 2 – PHD2), cellular hypoxia inducible factor (HIF) transcription increases, leading to upregulation of pro-angiogenic proteins such as vascular endothelial growth factor (VEGF), platelet derived growth factor (PDGF) or tumor necrosis factor-α (TNF-α) [Carmeliet, 2000; Carmeliet et al., 2011]. Activated endothelial cells express the dimeric transmembrane

integrin $\alpha_v\beta_3$, which interacts with extracellular matrix proteins (e.g., vibronectin, fibronectin) and regulates the migration of the endothelial cell through the extracellular matrix during vessel formation [Avraamides et al., 2008]. The activated endothelial cells synthesize proteolytic enzymes, such as matrix metalloproteinases, used to degrade the basement membrane and the extracellular matrix. The inner layer of endothelial cells undergoes apoptosis leading to formation of the vessel lumen. Immature vasculature undergoes extensive remodeling during which pericytes and smooth-muscle cells stabilize the vessels. This step is often incomplete resulting in irregular shaped, dilated and tortuous tumor blood vessels [Stollman et al., 2009].

I.2. pH

Consistent with the characteristic hypoxia found in tumor tissue, most tumor cells energy production relies on glycolysis. Interestingly, tumor cells have been shown to use this metabolic pathway even when there is enough O_2 to support mitochondrial oxidative phosphorylation. This phenomenon was first reported by Warburg in the 1920s, giving this phenomenon the name of "Warburg effect". This observation led to the hypothesis that cancer cells suffer from impaired mitochondrial metabolism. Such aerobic glycolysis leads to the accumulation of lactate and H^+ into tumor cells [Barar et al., 2013; Feron, 2009; Justus et al., 2013]. Consequently, the export of protons and lactic acid from tumor cells into the extracellular space by transporters including Na^+/H^+ exchangers and monocarboxylate transporters (a lactate/H^+ co-transporter), may lead to acidosis in the tumor microenvironment [Justus et al., 2013]. Indeed, tumor extracellular pH is generally more acidic (pH 6.5) compared to physiological pH (7.3) [Gullotti et al., 2009]. To support high rate proliferation as needed for tumor tissue growing, high glycolytic flux maintenance is needed. Nicotinamide adenine dinucleotide (NAD+) is involved in redox reactions that are essential for conversion of pyruvate to lactic acid produced by cancer cells. Interestingly, the conversion of pyruvate into lactate generates NAD+. This metabolic conversion makes glycolysis self-sufficient as long as elevated glucose uptake is possible [Barar et al., 2013; Feron, 2009]. Therefore, tumor cells implement an abnormally high rate of glucose uptake through an enhanced expression of HIF-1α-dependent glucose transporters (GLUT) [Peppicelli et al., 2014].

I.3. EPR EFFECT

Since solid tumors are rapidly growing tissue, it is of crucial importance for them to facilitate adequate supply of nutrients and oxygen to meet the great demands for growth [Fang et al., 2003]. Therefore, blood vessels in most solid tumors possess unique characteristics that are not usually observed in normal blood vessels (Figure 2):

(i) Extensive angiogenesis and hence, high vascular density [Folkman, 1971]

(ii) Defective vascular architecture. Indeed, tumor vasculature exhibits large gaps in endothelial cell-cell junctions (fenestrations) that lead to an enhanced diffusion of macromolecules to the interstitium space. These fenestrations present a diameter ranging from 10 to 1000 nm. However, it is notworthy that pore cutoff size of porous blood vessels in majority tumors is known to be 380–780 nm [Bae et al., 2011]. Moreover, neoangiogenic vessels are characterized by a lack of smooth muscle layer cells, pericytes and by a tortuous architecture [Greish, 2007; Torchilin, 2000]

(iii) Extensive production of vascular mediators that facilitates extravasation (e.g. matrix metalloproteinases or MMP, Bradykinin, etc…) [Fang et al., 2011; Maeda et al., 2013]

(iv) Irregular blood flow

(v) Impaired lymphatic system leading to an inefficient drainage, thus, affecting the clearance of macromolecules from interstitial tissue [Fang et al., 2003]

(vi) Slow venous return that leads to accumulation in the interstitium of tumor [Jain, 1988; Maeda et al., 2009]

Due to the defective vascular architecture macromolecules can diffuse easily to the interstitium. This phenomenon is referred as the enhanced permeability effect. Moreover, due to the lack of an efficient lymphatic system, the so-entered macromolecules are then retained in the tumor tissue (retention effect). This passive phenomenon has been called the “enhanced permeability and retention (EPR) effect” and was first described by Matsumara and Maeda in 1986 [Matsumura et al., 1986]. According to this concept, it is possible to take advantage of this particular microenvironment to passively target tumor tissue with macromolecular drug or nanocarriers. To benefit from the EPR effect, nanomedicines should be larger than 40 kDa or for macromolecules and 10 nm for nanocarriers, respectively and have long-circulating time to provide a sufficient level of target accumulation [Fang et al., 2011; Torchilin, 2000].

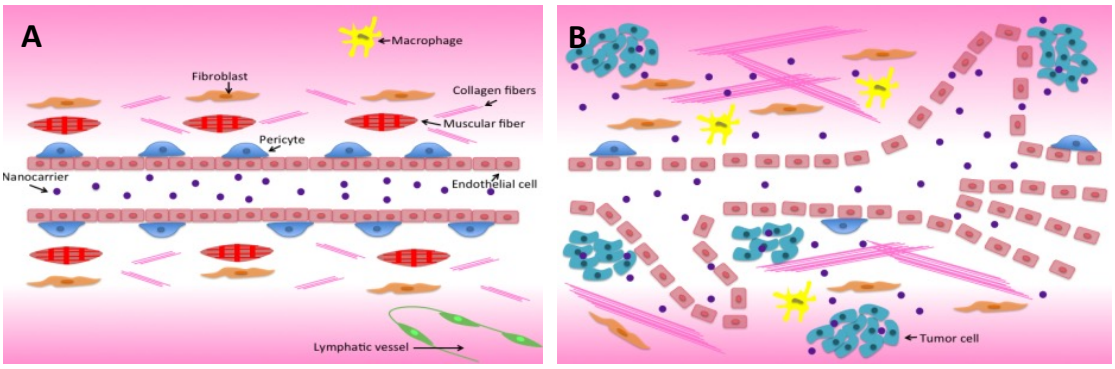

Figure 2. Differences between normal and tumor tissues that explain the passive targeting of nanocarriers via the enhanced permeability and retention effect. (A) Normal tissues is highly structured with pericytes covering the endothelium cells. Fibroblasts, collagen fibers, macrophages and muscular fibers surround them constituting the extracellular matrix. Lymphatic vessels ensure lymphatic drainage. (B) Tumor tissue contains defective blood vessels with many sac-like formations and fenestrations. There is a lack of lymphatic system. (Adapted from [Heldin et al., 2004])

Interestingly, vascular permeability due to fenestration was first observed in inflammation process and in hypoxic areas of infracted myocardium. Although it is still controverted, the essential difference between inflamed and tumor tissue lies in the presence of an efficient lymphatic system in inflamed tissue leading to an enhanced permeability without any retention effect [Maeda et al., 2009; Maeda et al., 2013].

I.4. DRUG TARGETING

A major issue in current cancer therapies is the lack of selectivity, which leads to insufficient drug concentration at the target site and damages in healthy tissues. Consequently, patients frequently suffer from harmful side effects. Hence, researchers have studied over the years innovative targeting strategies to address this problem. The goal of such targeted drug delivery is to be as selective as possible to avoid or minimize accumulation in the healthy tissues [Cukierman et al., 2010; Dandamudi et al., 2007]. Nanoparticles are highly attractive materials to address such a challenge since they allow multiple targeting strategies [Danhier et al., 2010]. Various different concepts have been studied for nanomedicine drug targeting to tumors over the years including passive targeting, active targeting and triggered drug delivery.

I.4.1. Passive targeting

Passive targeting relies on the presence of fenestration in the tumor vascular endothelium that allows the extravasation of nanocarriers to the interstitium by EPR effect [Arias et al., 2011]. Movement of molecules through the vasculature is governed by both vascular morphology (vascular gap size, number…) and blood flow rate. Transport of molecules from the vascular

compartment to the interstitium is mediated by convection, passive diffusion depending on the particle size and, to some extent, by transcytosis [Jain, 1987; Jain, 1990]. While diffusion, defined as a process by which small molecules are transported across the cell membrane according to their gradient of concentration, is the main route for low-molecular weight molecules, convection must be the predominant route for large particles. Convection is based on the movement of molecules within fluids. Since nanoparticles are relatively large, the most predominant transport mode for them should be convection [Florence, 2012; Frenkel, 2008]. However, since convection is governed by the rate of fluid leakage, it will depend on the difference between the vascular and interstitial osmotic pressure. Due to the high interstitial pressure in tumor, convection is maintained at a minimal rate and the major mode of drug transport is even though diffusion [Jain, 1990]. Once nanoparticles enter the interstitium in the absence of anatomically well-defined functioning lymphatic vessels, their accumulation occurs by the EPR effect [Haley et al., 2008] (Figure 3).

To benefit from this EPR effect, nanocarriers have to present several characteristics:

(i) Particles size should be compromised between 50 and 200 nm. Indeed, to ensure an efficient extravasation from the fenestrations in the leaky vasculature nanaoparticles should present a size of less than 700 nm. However, particles of more than 200 nm are often taken up by macrophages resulting in liver and spleen accumulation. On the other hand, nanoparticles of 50-100 nm have a high probability of getting trapped into the hepatic parenchyma [Reddy et al., 2012]. Moreover, particles presenting a size <10 nm will undergo rapid renal clearance [Kwon et al., 2012].

(ii) Nanocarriers should present a long circulation time to optimize accumulation at the target site. Indeed, it takes about 6 hours or longer for drugs in circulation to benefit from the EPR effect [Fang et al., 2003]. Therefore, nanoparticles need to be hidden from the reticulo-endothelial system, which is responsible for the destruction of foreign material through opsonization followed by phagocytosis [Reddy et al., 2012].

(iii) Particles should be neutral to avoid renal elimination and minimize the interaction with plasma protein and thus, prolongs the circulation time by avoiding phagocytosis process [Reddy et al., 2012].

Nevertheless, despite all efforts made to obtain the « perfect candidate », EPR effect have been shown to exhibit some limitations contributing to poor localization of nanomedicines in tumors:

(i) Heterogenous blood supply depending on the tumor type, grade etc. Indeed, the average vascular surface area decreases with tumor growth. Hence, large tumors are less expected to show a good accumulation of drug by EPR than smaller tumors

(ii) Elevated interstitial fluid pressure. As aforementioned, tumors contain region of high interstitial pressure which lowers fluid extravasation

(iii) Large transport distances in the tumor interstitium, which are rendered difficult by the presence of a dense extracellular matrix [Jain, 1990; Nichols et al., 2014]

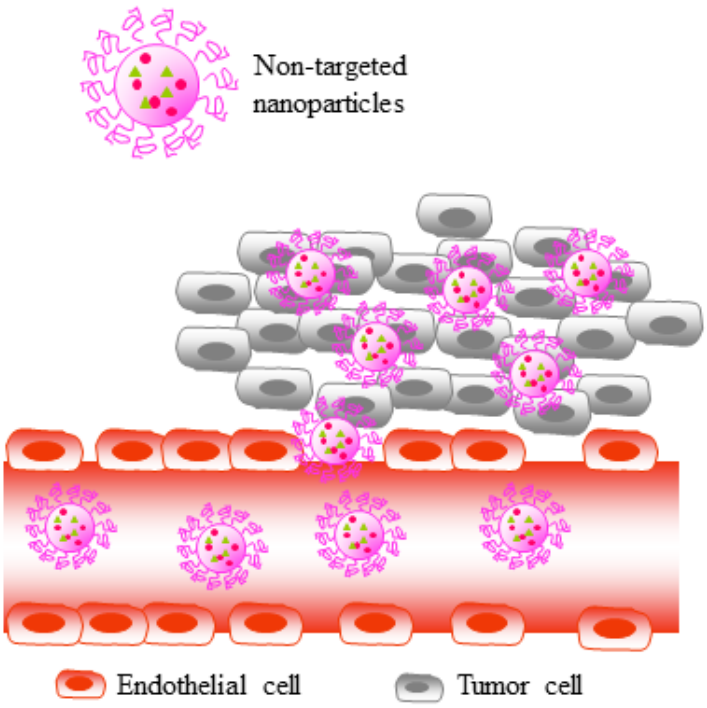

Figure 3. Passive targeting. Nanocarriers reach tumor passively through the leaky vasculature of neoangiogenic vessels (adapted from [Danhier et al., 2012b]).

I.4.2. Active targeting

The principle of this strategy is to target a specific site based on molecular recognition process. Hence, a ligand is coupled to the surface of nanoparticles, which can interact with its

receptor at the target cell site (Figure 4) [Danhier et al., 2009b]. Indeed, since nanoparticles have high surface area-to-volume ratios, they may be surface functionalized with targeting ligands [Kelkar et al., 2011]. Potential methods for active targeting have been extensively investigated. These methods include particles coupled to specific monoclonal antibodies (or antibody fragments) as well as ligand-coated particles targeting proteins overexpressed on endothelial cells of tumor neoangiogenic vessels (e.g., integrin surface receptor) or on cancer cell membranes themselves (e.g., folate receptor) [Arias, 2011]. Ideally, the targeted receptor should be overexpressed by tumor cells or tumor vessels and not expressed by normal cells to ensure a good selectivity of the treatment. This may help to increase both the target-to-background contrast in imaging for diagnostic purpose and the therapeutic concentration at the target of interest, limiting systemic toxicity [Kelkar et al., 2011].

In cancer chemotherapy, two strategies can be used: targeting tumor endothelium or targeting tumor cells. The former aims to kill tumor cells by the lack of oxygen and nutrients. This concept has been first suggested in 1971 by Folkman [Folkman, 1971]. Such tumor endothelium targeting presents some undeniable advantages: (i) nanocarriers can directly reach the target without any need for extravasation; (ii) they can bind to their receptor directly after i.v. injection; (iii) most of endothelial cells markers are expressed by numerous tumor type [Gosk et al., 2008].

While targeting tumor cells, a particular attention is paid to the internalization of nanoparticles for drug delivery inside cancer cells. For this purpose, ligand coupled nanoparticles are useful to facilitate internalization since this approach typically leads to receptor-mediated cell endocytosis [Arias et al., 2011; Cole et al., 2011]. However, since nanoparticles have no means of self-propulsion, reaching the target only depends on the movement of blood passing through the target, wherever it may be. The presence of ligand on the surface does not change anything [Kwon et al., 2012]. Hence, in tumor cells targeting, the chance of targeted-nanoparticles to reach the target only relies on the EPR effect. Ligand-targeted therapeutics are divided into different classes depending on the approach of drug delivery [Allen, 2002]. Main classes to mediate targeting are peptide, monoclonal antibodies or small molecules. These classes can target different receptors among which the most studied are: (i) Integrin, (ii) Folate receptor, (iii) Transferrin receptor and (iv) Human/Epidermal epidermal growth factor receptor 2 [Arias et al., 2011; Kelkar et al., 2011].

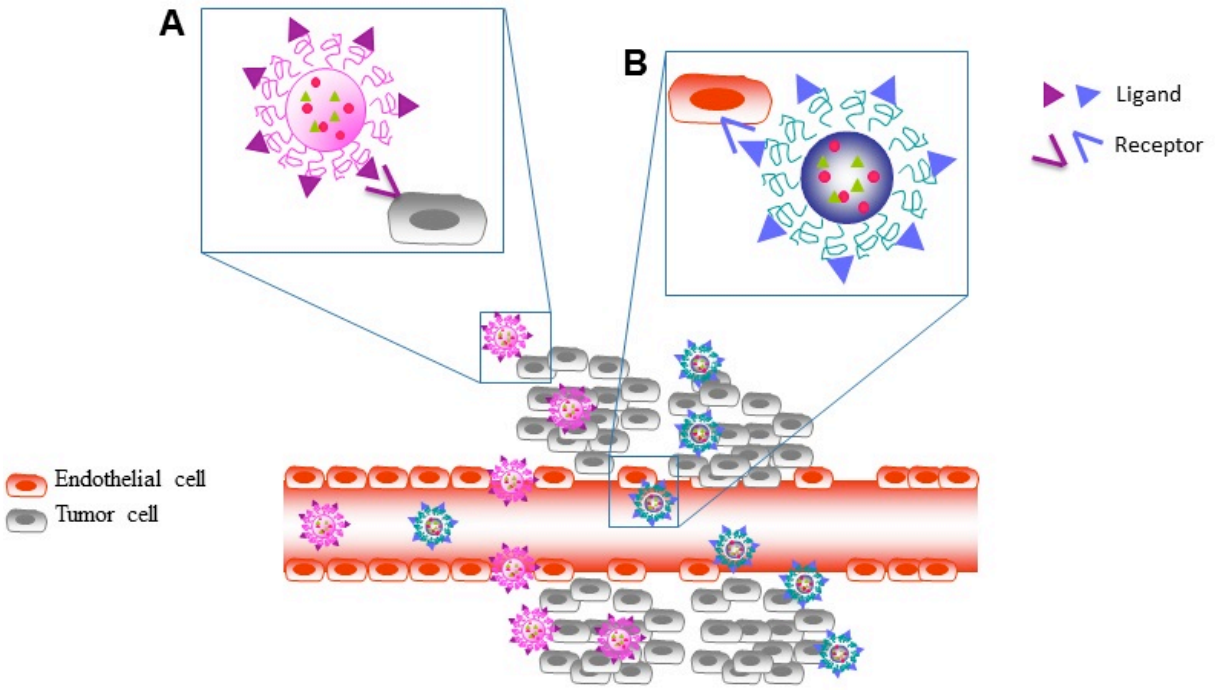

Figure 4. Schematic representation of active targeting modalities of nanocarriers. Targeted nanocarriers presenting targeted ligands on his surface. The ligand can be either a monoclonal antibody or a non-antibody ligand that specifically recognizes an over-expressed receptor at the surface of (A) tumor cells and (B) neoangiogenic endothelial cells (adapted from [Danhier et al., 2012b]).

I.4.2.1. Monoclonal antibodies-mediated targeting

The aim of this strategy is to direct monoclonal antibodies against specific antigen or receptors presented by tumor cells. This could be achieved by using (i) monoclonal antibodies, (ii) antibody fragments, (iii) antibody-drug conjugates and (iv) antibody-conjugated nanocarriers. In this last case, antibodies are coupled to the particle surface of nanocarriers loaded with a cytotoxic drug. Those monoclonal antibody-conjugated nanocarriers are called immunonanocarriers and aim to target specific receptors presented by tumor cells and recognized by the targeting ligand (monoclonal antibody or fragments) [Arias, 2011; Lammers et al., 2012a]. For instance, doxorubicin (DOX)-loaded prostate cell-specific Mab (Mab5D4) conjugated with liposomes enhanced cytotoxicity towards prostate cancer cell lines compared with the non-targeted DOX liposome in vitro [Sawant et al., 2008]. Recently, Talelli *et al.* obtained promising results using nanobody-modified polymeric micelles for tumor targeted combination therapy [Talelli et al., 2013]. However, to date and in spite of significant advances made at the pre-clinical level with regard to active targeting, no

actively targeted-nanocarriers have been approved for clinical use. Nevertheless, several antibody-based therapeutic agents are clinically approved (see Table 1). In this case, antibodies (monoclonal antibodies or fragments) target a specific receptor, interfering with signal transduction pathways regulating proto-oncogenes involved in tumor cells proliferation. For instance, bevacizumab (Avastin®), a tumor angiogenesis inhibitor that binds to VEGF and was approved for treating colorectal cancer in 2004 [Lu et al., 2008] and trastuzumab (anti-ERBB2, Herceptin®) for specific binding to breast cancer cells. Another strategy involves the association of an antibody with a therapeutic agent (e.g., toxin and radioisotope) [Lammers et al., 2012a]. For instance, ^{90}yttrium-ibritumomab tiuxtan (Zevalin®) is the first radioimmunotherapeutic directed against CD-20 an activated-glycosylated phosphoprotein expressed on the surface of B-lymphocytes and is currently approved for the treatment of Rituximab-failed non-Hodgkin's lymphoma [Das et al., 2009; Wiseman et al., 1999]. Denileukin diftitox (Ontak®), a chimeric immunotoxin composed of the modified cytotoxic domain of diphtheria toxin and human interleukin-2 (IL-2) protein, targets cells expressing CD25 [Ansell et al., 2012; Dang et al., 2004]. Gemtuzumab ozogamicin (Mylotarg®), a immunoconjugate between an anti-CD33 antibody (hP67.6) and a toxic calicheamicin-γ1 derivative also received clinical approval [Jurcic, 2001; Sharkey et al., 2006]. Finally, a radiolabeled monoclonal antibody directed against CD-20 (iodine-131 tositumomab, Bexxar®) has been recently approved [Lammers et al., 2012a].

Table 1. Examples of clinically used tumor-targeted antibodies.

Type	Name	Formulation	Indication	Status
Monoclonal Antibody	Herceptin	Anti-ERBB2	Breast cancer	Approved
	Avastin	Anti-VEGF	Colorectal cancer	Approved
	Rituxan	Anti-CD20	NHL	Approved
Antibodies coupled with therapeutics	Ontak	CD25-targeted diphtheria toxin-IL2 fusion protein	T-cell lymphoma	Approved
	Mylotarg	CD33-targeted gemtuzumab ozogamicin	Leukemia	Approved
	Zevalin	CD20-targeted ^{90}yttrium-ibritumomab tiuxtan	NHL	Approved
	Bexxar	CD20-targeted iodine-131-tositumomab	NHL	Approved

I.4.2.2. Integrin targeting

A large number of receptors are overexpressed at the surface of certain tumor cell or tumor neoangiogenic endothelial cells such as receptors for somatostatin analog, VEGF analog, vasoactive intestinal peptide, gastrin-related peptide and RGD peptide. Peptide analog can

easily be conjugated to a drug carrier system to allow tumor-specific targeting of cytotoxic agents by interaction with its receptors [Das et al., 2009]. Peptides are becoming the alternative to other targeting moieties because of their small size, lower immuno-genicity and ease to manufacture.

Integrins are cell surface receptors involved in cell adhesion via interactions with the extracellular matrix (ECM) or counter-receptors on other cells. These cell adhesion molecules are heterodymeric transmembrane glycoproteins consisting of a α and a β subunit. To date, 24 different subtypes of integrins have been discovered arising from different arrangements of the 18 α and 8 β existing subunits [Huveneers et al., 2007; Marelli et al., 2013]. Each subunit is composed of three regions: (i) an intracellular domain, which is connected to the cytoskeleton via associated multi-protein complex, (ii) a single transmembrane region and (iii) an extracellular domain responsible for binding to components of the ECM [Danhier et al., 2012b; Huveneers et al., 2007]. Multiple ligands are known to bind these integrins including ECM molecules (fibronectin, vitronectin, collagen), cell surface proteins such as intracellular adhesion molecule-1 (ICAM-1), vascular adhesion molecules-1 (VCAM-1), growth factors, cytokines and matrix-degrading proteinases. Despite the abundance of integrin ligands, minimal integrin recognition sequences were shown to be shared by most of the ligands. Among those, the tripeptide Arg-Gly-Asp (RGD, see Figure 4A) has been extensively studied since it is recognized by almost half of the integrins [Barczyk et al., 2010; Marelli et al., 2013]. Ligand binding to integrin promotes the so-called "outside-in" signaling, an intracellular signal transduction cascade including the activation of Ras, MAP kinase, focal adhesion kinase (FAK), Src, Rac/Rho/cdc42 GTPases, PKC and PI3K (phosphatidylinositol 3-kinase) resulting in promoting cell survival, proliferation and differentiation [Eliceiri et al., 2001; Huveneers et al., 2007]. Moreover, in cancer, integrins play an important role in angiogenesis by promoting vascular endothelial cell proliferation, migration, invasion and metastasis [Liu, 2006; Marelli et al., 2013]. Noteworthy, given that integrin are devoid of enzymatic activity, this signaling cascade seems to be mediated, at least partly, through growth factor receptor transactivation (VEGFR, EGFR, etc.). This phenomenon is known as "Integrin and growth factor receptor cross-talk" [Huveneers et al., 2007].

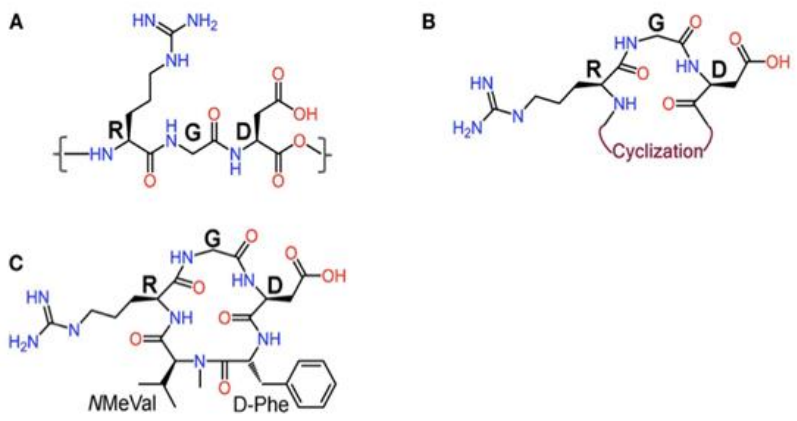

Figure 4. (A) Integrin recognition motif RGD; **(B)** schematic representation of cyclic RGD (*c*RGD); **(C)** Cilengitide – *c*(RGDf-*N*MeVal) (adapted from [Marelli et al., 2013]).

Since we worked with RGD peptide, this thesis will focus on this strategy.

$\alpha_v\beta_3$ Integrin

Numerous integrin sub-types including $\alpha_v\beta_3$, $\alpha_v\beta_5$, $\alpha_v\beta_6$, $\alpha_2\beta_1$, $\alpha_5\beta_1$, $\alpha_6\beta_1$ and $\alpha_6\beta_4$ were shown to be overexpressed at the surface of many cancer cells, showing the important role of integrins in cancer progression [Weis et al., 2011]. Among these integrins, $\alpha_v\beta_3$ is the most extensively studied given its strong implication in the regulation of angiogenesis. Interestingly, whereas many integrins are constitutively expressed in adult tissues, integrin $\alpha_v\beta_3$ was shown to be overexpressed on neoangiogenic endothelial cells [Brooks et al., 1994]. Beside its expression on endothelial cells, $\alpha_v\beta_3$ integrin was shown to be expressed by a multitude of tumor cells including breast cancer cells [Zitzmann et al., 2002]. Therefore, many efforts have been made by researchers to specifically target this integrin in order to make the most of this possible "double sword" [Danhier et al., 2009b; Liu et al., 2013].

Moreover, the presence of $\alpha_v\beta_3$ was correlated with tumor progression and invasiveness in numerous cancer types including ovarian cancer, melanomas, glioblastomas as well as breast, stomach, pancreas and cervix cancers [Baum et al., 2007]. Numerous angiogenic growth factors upregulated in tumor tissue including VEGF, basic fibroblast growth factor (bFGF) interleukin-8, and TNF-α have been shown to promote its expression [Danhier et al., 2009b; Eliceiri et al., 2001]. The angiogenic promoting activity of $\alpha_v\beta_3$ can be partially explained by its functionally active complex with binding to matrix metalloproteinase (MMP-2). Indeed,

after ligand binding, $\alpha_v\beta_3$ induce an intracellular transduction leading to a higher transcription rate of MMP-2 and, hence, to an enhanced matrix degradation activity [Baum et al., 2007]. Finally, $\alpha_v\beta_3$ was shown to play a role in survival by inducing NFκB activation and, hence, inhibition of apoptosis (mediated by the expression of inhibitor of apoptosis proteins, IAP) [von Wnuck et al., 2006].

Numerous studies have shown that the tripeptide arginine–glycine–aspartic acid (RGD) was able to bind preferentially to $\alpha_v\beta_3$ integrin [Danhier et al., 2009b; Garanger et al., 2006; Murphy et al., 2008; Son et al., 2013]. Cilengitide® is a cyclic (RGD) peptide that binds to the integrins and is currently in Phase II clinical trials for the treatment of non-small cell lung cancer and pancreatic cancer.

RGD-based strategies for cancer therapy and diagnosis

Since the discovery of the tripeptide RGD as the cell recognition sequence in fibronectin back in 1984 by Ruoslahti *et al.* and subsequent discovery of the integrins, many efforts have been made to develop RGD-based strategies as both novel cancer therapeutic agents and targeted diagnostic agents [Pierschbacher et al., 1984; Temming et al., 2005].

The arginine-glycine-aspartic (RGD) tripetide sequence originally found in fibronectin turned out to be the cell attachment site of many other adhesive proteins including vitronectin, fibronectin, fibrinogen, lamin, collagen and osteoponin [Liu, 2006; Ruoslahti, 1996]. The expression of $\alpha_v\beta_3$ on both endothelial cells and tumors cells have led researchers to develop RGD-based double targeting, namely anti-angiogenic and anti-tumor strategies [Liu, 2006]. This tripeptide sequence is currently the basic module in almost all the strategies aiming to preferentially bind to $\alpha_v\beta_3$ integrin and other α_v–related integrin [Temming et al., 2005]. The different integrin targeting strategies include: (i) monoclonal antibodies, (ii) RGD-based strategies, (iii) non-RGD antagonists. In this thesis, we will focus on the RGD-based strategies.

Because of its small structure, the RGD sequence can be easily reproduced with synthetic peptides. Indeed, short peptides containing the RGD sequence can mimic cell adhesion proteins [Ruoslahti, 1996]. Furthermore, RGD-affinity and specificity for its integrin as well as metabolic stability and biodistibution can be modulated resulting in optimized smart-engineered RGD peptides analogs. For instance, introduction of some amino-acids flanking the RGD sequence has been shown to improve integrin affinity and selectivity. Similarly,

cyclization (Figure 4 B) is a currently used method to provide conformational restraint and, hence, improve selectivity and specificity [Marelli et al., 2013; Ruoslahti, 1996].

Based on this strategy, Cilengitide®, a very potent RGD-based $\alpha_v\beta_3$ antagonist, was developed by using cyclization and has been clinically tested by Merck for treatment of glioblastoma multiforme (Figure 4 C). However, despite promising preliminary data, failure in phase-III clinical trials has led to its discontinued use as anticancer therapeutic [Marelli et al., 2013]. More recently, N-methylation has been reported as an important element in modulating peptides [Chatterjee et al., 2008].

Beside Cilengitide®, other RGD peptides have been developed among which cRGDfV, cRGDfK and RGD4C, cRGDfX, etc. [Marelli et al., 2013]. These RGD based peptide have been shown to inhibit angiogenesis through $\alpha_v\beta_3$ antagonism via regulation of the VEGF receptor, production of VEGF and stimulation of p53 tumor suppressor gene [Hsu et al., 2007]. In this case, RGD-based strategies were used as anti-cancer treatment using its anti-angiogenic effect.

Beside this anti-angiogenic purpose, RGD can be used as targeting ligand when grafted to the surface of a nanocarrier. The use of nanocarriers such as liposomes, nanoparticles, micelles etc. for RGD-based strategies for cancer therapy offers numerous advantages: (i) carriers have the capacity to be grafted with multiple ligands on their surface exploiting the concept of multivalency [Marelli et al., 2013]; (ii) nanocarriers can incorporate various pharmacological agents e.g. anti-cancer drug [Folkman, 1971]; (iii) due to their large size, these carriers system are not subjected to renal filtration [Kwon et al., 2012]; (iv) the size of these nanocarriers allow passive accumulation trough the leaky vasculature of tumor angiogenic vessels, the so-called EPR effect [Reddy et al., 2012]; (v) grafting of a ligand on their surface promotes receptor-mediated endocytosis of the particles [Prokop et al., 2008].

One of the rationales for using nanocarriers is the delivery of cytostatic agent in the targeted endothelial cells expressing $\alpha_v\beta_3$. Indeed, once internalized through endocytosis, the nanocarrier can release its cytotoxic drug leading to angiogenic endothelial cell death. Thus, subsequent tumor cells death occurs by lack of oxygen and nutrients [Folkman, 1971]. Moreover, since integrin is also expressed on many tumor cells, RGD-grafted nanocarriers

can also kill tumor cells directly, making this RGD-based anti-cancer strategy a double sword [Danhier et al., 2010].

Some examples of developed RGD-targeted nanocarriers are given in Table 2.
The first results to show the inhibition of metastases with this kind of strategy were obtained with targeted nanoparticles loaded with doxorubicin (DOX) [Murphy et al., 2008]. Danhier et al. developed PLGA-based nanoparticles grafted with GRGDS. They showed a high cellular uptake in vitro leading to an improved anticancer efficacy and survival rate in TLT-bearing mice and A-431-bearing mice [Danhier et al., 2012c]. The demonstration of the targeting of the tumor endothelium was performed both *in vitro* and *in vivo* using fluorescence microscopy (Figure 5). Recently, Li *et al*., developed RGD-fatty alcohol-modified docetaxel liposomes and showed a better anti-tumor activity in S-180 sarcoma-bearing mice than the non-modified liposomal form [Li et al., 2014]. Meng *et al.* developed cRGD-based liposomes loaded with paclitaxel and showed a lower tumor microvessel density than for taxol-treated group [Meng et al., 2011]. In si-RNA-based therapy, Yonenaga *et al.* developed RGD-based polycation liposomes bearing siRNA for cancer treatment in B16F10-luc2-bearing mice [Yonenaga et al., 2012]. An elegant study conducted by Han *et al.* showed very interesting *in vivo* results in 3 different ovarian carcinoma models. Their developed RGD grafted chitosan nanoparticles displayed an increased selective intratumoral delivery, effective targeted silencing of multiple growth-promoting genes (POSTN, FAK, and PLXDC1) and significant inhibition of tumor growth [Han et al., 2010].

Table 2. Non-exhaustive examples of developed RGD-targeted nanocarriers loaded with an anticancer-drug for pre-clinical studies.

Formulation	Targeting motif	Drug	Tumor model	Results	References
PEGylated Nanoparticles	cRGD	DOX	R40P murine pancreatic/renal carcinoma cells	15-fold increase in drug efficacy compared to free-DOX treated mice	[Murphy et al., 2008]
PLGA-PEG nanoparticles	GRGDS and peptido-mimetics	PTX DOX	HUVEC, TLT cells, A431, CT-26	High cellular uptake in vitro, improved anticancer efficacy and higher survival rate	[Danhier et al., 2012c]
Liposomes	cRGD	PTX	A549 lung adenocarcinoma	Lower tumor microvessel density than for taxol-treated group	[Meng et al., 2011]
Liposomes	Fatty alcohol modified-RGD	DTX	S-180 sarcoma	Better anti-tumor activity than the non-modified liposomal form	[Li et al., 2014]
polycation liposomes	cRGD	siRNA	B16F10-luc2	High knockdown efficiency	[Yonenaga et al., 2012]
CH nanoparticles	cRGDfk	siRNA	SKOV3ip1, HeyA8, A2780 (ovarian carcinomas)	Increased selective intratumoral delivery, targeted silencing of multiple growth-promoting genes, significant inhibition of tumor growth	[Han et al., 2010]

Abbreviations: CH = chitosan, DOX = doxorubicin, DTX = docetaxel, PTX = paclitaxel

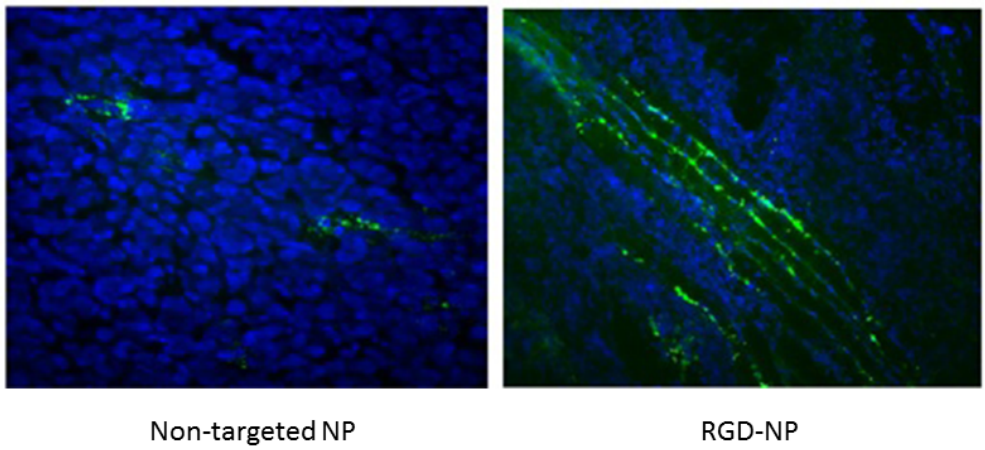

Figure 5. Fluorescent microscopy of TLTs growing in NMRI mice 4 h after injection of non-targeted or RGD-grafted nanoparticles (RGD-NP) containing fluorescent-PLGA (green). Sections were stained with DAPI for nucleus detection (blue) (adapted from [Danhier et al., 2012c]).

RGD-based strategies have also been used for imaging of tumors and angiogenesis. Indeed, since antiangiogenic drugs have been successfully used in cancer patients, molecular imaging for non-invasive assessment of angiogenesis represents potential interest for clinicians [Danhier et al., 2012b]. Such a tool can be used for either detection of angiogenesis and tumor metastasis or monitoring of anti-angiogenic treatment response [Temming et al., 2005]. As for therapeutic purpose, both small RGD-based peptide and RGD-grafted nanocarriers have been developed. For imaging purpose, RGD-targeted nanocarriers also present some advantages. Beyond their advantages concerning passive accumulation via EPR effect and non-renal filtration, two main benefits can be added: (i) numerous imaging labels can be attached to a single nanoparticle leading to an increased signal intensity and (ii) different imaging labels can be used to create functionalized nanoparticles as multimodality imaging systems [Danhier et al., 2012b]. Table 3 gives some examples of the pre-clinical studies in the field of RGD-based strategies for cancer imaging available in the literature. In this case, RGD-peptides or RGD-grafted nanocarriers are coupled with imaging agents. Among those imaging agents, radiotracers and SPIO are the most studied allowing positron emission tomography (PET), single photon emission computed tomography (SPECT) and magnetic resonance imaging (MRI).

Table 3. Examples of the pre-clinical studies of RGD-based strategies for cancer imaging

Formulation	Targeting motif	Imaging agent	Tumor model	Results	References
Galacto-RGD peptides conjugates	cRGDfK	^{18}F	Human M21 melanoma cells	Suitable metabolic stability and low estimated radiation dose	[Haubner et al., 2004]
SPIO-RGD peptides conjugates	cRGDyE	SPIO	HaCaT-ras-A-5RT3 and A341 squamous carcinoma cells	Non-invasively differentiation of tumor with high and lower area fraction of $\alpha_v\beta_3$–positive tumor vessels	[Zhang et al., 2007]
SPIO-RGD peptides conjugates	RGD-Cys	SPIO	A549 non small cell lung cancer cells	Efficient active targeting and labelling of $\alpha_v\beta_3$–expressing tumors	[Xu et al., 2011]
Nanocarriers					
PEGylated Nanoparticles	c(RGDyK)	SPIO	U87MG (brain tumor)	Non-invasive monitoring of the tumor response to VEGF(121)/ rGel therapy at early stages of treatment	[Zhang et al., 2012]
PLG-PEG micelles	cRGDfC	^{64}Cu	U87MG	In vivo monitoring of tumor accumulation by PET	[Xiao et al., 2012]
PEG-PLA micelles	cRGDfK	SPIO	A549 non small cell lung cancer cells	High efficiency in tumor neovasculature detection	[Khemtong et al., 2009]

More recently, optical imaging has emerged as a powerful modality for studying molecular recognitions and molecular imaging in a noninvasive, sensitive, and real-time way. This method presents undeniable advantages including cost-effectiveness, convenience, and non-ionization safety. Moreover, optical imaging and the abovementioned other imaging modalities (MRI, PET, SPECT) have been shown to complete each other [Ye et al., 2011]. Hence, many efforts have been made to develop new RGD-targeted carriers with optical imaging abilities. These novel kinds of nanoparticles include quantum dots (QDs), carbon nanotubes, or gold nanoparticles [Danhier et al., 2012b].

I.4.2.3. Folate receptor targeting

Folate receptors, also known as folate-binding proteins (FBP), are N-glycosylated proteins with high binding affinity to vitamin folic acid. Interestingly, folate receptor is not required for cellular survival and its expression is highly restricted or absent in normal tissues while frequently overexpressed by cancer cells as a consequence of enhanced folate requirements for DNA synthesis [Arias, 2011; Zhao et al., 2008]. Moreover, a correlation between its level of expression and tumor grade and response to chemotherapy has been highlighted [Toffoli et al., 1997]. Therefore, this receptor constitutes an interesting target for cancer therapy. Folate receptors include at least four isoforms, α, β, γ/γ′ and δ. Among these isoforms, the alpha and beta isoform are the most studied [Yu et al., 2010; Zhao et al., 2008]. The alpha isoform folate receptor-α is consistently expressed in several carcinomas, especially in non-mucinous ovarian carcinomas, uterine carcinomas, testicular choriocarcinomas, ependymomas, and pleural mesotheliomas, and less frequently in breast, colon, and renal cell carcinomas [Clifton et al., 2011] whereas the beta isoform was shown to be amplified in activated monocytes, macrophages and overexpressed in chronic myelogenous leukemia (CML) and in 70% of acute myelogenous leukemias (AML). Linking folic acid to nanocarriers has been shown to facilitate tumour-specific delivery of anticancer drugs via receptor-mediated endocytosis [Yu et al., 2010; Zhao et al., 2008].

To date, despite a large number of publications on in vitro and in vivo studies [Lv et al., 2014; Ye et al., 2011], relatively few agents have been translated into the clinic. The recent entry of fartetuzumab, a fully humanized antibody derived from the murine antibody LK26, and vitafolitide, the first folate-drug conjugate to enter into clinical trials as a therapeutic agent, into Phase III trial suggests that Folate receptor targeting is finally reaching a critical point [Teng et al., 2012].

I.4.2.4. Transferrin receptor targeting

Transferrin, a 78 kDa-monomeric glycoprotein, is the main protein involved in the regulation and distribution of circulating iron through the blood and into cells. Cell internalization is governed by receptor-mediated endocytosis after binding to transferrin receptor. Since iron is required for various biological processes including DNA synthesis, cellular metabolism and proliferation, the expression of transferrin receptors have been shown to be upregulated in most active prolifering cell type including cancer cells [Tortorella et al., 2014]. Moreover,

correlation between increased transferrin receptor expression and the level of malignancy has also been determined in a range of cancer type, including bladder transitional cell carcinoma, breast cancer, glioma, lung adenocarcinoma, chronic lymphocytic leukaemia and non-Hodgkin's lymphoma [Singh et al., 2011]. For all these reasons, transferrin receptors have become a high attractive target for cancer therapy. Nanocarriers surface functionalization with the transferrin peptide itself or anti-transferrin receptor antibody has proved to be promising .

To date, four transferrin-conjugated nanocarrier-based drug delivery systems for the encapsulation of anticancer therapeutic compounds have progressed into human clinical trials (see Table 4). All are currently in early stage (Phase I and/or II) trials for the treatment of solid malignancies [van der Meel et al., 2013].

Table 4. Overview of transferrin-targeted nanomedicines undergoing clinical evaluation. Clinical data are extracted from http://www.clinicaltrials.gov (June 2014)

Name	Drug	Formulation	Indication	Clinical phase
MBP-426	oxaliplatin	Tf coupled-liposome	gastro-esophageal (GE) adenocarcinoma	Phase I/II
SGT-53	p53-plasmid DNA	scFv anti-Tf receptor coupled-liposome	Solid tumors	Phase Ib
SGT-94	RB94 plasmid DNA	scFv anti-Tf receptor coupled-liposome	Solid tumors	Phase I
CALAA-01	RRM2 siRNA	Tf coupled nanoparticles	Solid tumors	Phase I

Abbreviations: Tf: transferrin, scFv: single-chain antibody fragment

I.4.2.5. Human/Epidermal epidermal growth factor receptor 2 targeting

The epidermal growth factor receptor (EGFR) is a tyrosine kinase receptor, member of the ErbB family. Ligand binding triggers a signaling cascade promoting cell survival, proliferation, adhesion, migration, differentiation and tissue invasion, while inhibiting apoptosis [Harari, 2004; Trivedi et al., 2014]. Those receptors are important in tumor development via their effect on cell proliferation, migration, angiogenesis and anti-apoptosis. Hence, EGFR is frequently overexpressed in numerous cancer types including breast, uterus, head and neck as well as ovarian, bladder, colon, prostate, kidney, pancreatic and non-small-cell lung cancer associated with poor prognostics [Harari, 2004; Li et al., 2013a]. EGFR are composed of four receptor known as HER-1, HER-2, HER-3 and HER-4, where HER-2 is the most extensively studied. It has become evident that 20-25% of breast cancers are (HER2)-

positive [Li et al., 2013a]. During the past decades, HER-2 has been demonstrated as a validated therapeutic target with dramatically improved survival for patients treated with specific HER-2 targeted therapeutics. Those treatments include monoclonal antibodies and tyrosine kinase inhibitors (TKIs). Table 5 summarizes the different currently available EGFR-targeted therapeutics for clinical use.

Table 5. Exemples of currently available EGFR-targeted therapeutics. Clinical data are extracted from http://www.clinicaltrials.gov (June 2014).

Product name	Other name	Formulation	Target	Indications	Clinical phase
Monoclonal antibody					
trastuzumab	Herceptin®	Humanized murine IgG	HER-2	Breast cancer	Approved
pertuzumab	Omnitarg®	Fully humanized IgG	HER-1, HER-2, HER-3, HER-4	Metastatic breast cancer	Approved
Trastuzumab-DM1	T-DM1	Antibody-drug conjugate trastuzumab-DM1 (anti-microtubule agent)	HER-2	Breast cancer	Phase III
zalutumumab	HuMax-EGFr	Fully humanized IgG	EGFR	Second-line treatment of recurrent SCCHN	Phase III
nimotuzumab	Theraloc	Fully humanized IgG	EGFR	SCCHN	Phase I*
Tyrosine-kinase inhibitors					
lapatinib	Tykerb®	Small molecule	HER-1, HER-2	Breast cancer resistant to trastuzumab	Phase III
neratinib	HKI-272	Small molecule	HER-1, HER-2, HER-4	Metastatic breast cancer	Phase II
afatinib	BIBW-2992	Small molecule	HER-1, HER-2, HER-3, HER-4	Breast cancer resistant to trastuzumab	Phase II
Nanomedicine					
MM-302		Dox-loaded PEG-ylated liposome with scFv** antibody fragments	HER-2	Breast cancer	Phase I
Anti-EGFR Ils-DOX		Dox-loaded immunoliposome coupled with Fab fragments of cetuximab	EGFR	Advanced solid tumor	Phase I

* Approved in countries outside USA and Europe. ** Single-chain antibody fragment

I.4.3. Triggered targeting

Triggered drug delivery is a common term to refer to systems designed to release their contents or react upon exposure to internal or external stimuli. Such environmental-sensitive carriers are essentially polymeric wisely engineered materials able to react rapidly to small modifications in the environment by experiencing rapid changes either in their structure or in their physical properties. Stimuli can be either internal (change in pH or temperature in some tissues or disease stage) or external (magnetic, electric fields, light, ultrasound, etc.) [Arias, 2011; Egusquiaguirre et al., 2012].

Acid-triggered release

As aforementioned, tumor cells initiate several changes in the stroma to supports their growth and progression including slightly acidic pH. Indeed, tumor extracellular pH is generally more acidic (pH 6.5 compared to 7.3 in physiological conditions), due to the increased glycolysis and plasma membrane proton-pump activity of tumor cells. Such differences can be exploited to induce a tumor specific activation of nanocarriers [Abouelmagd et al., 2014; Gullotti et al., 2009].

Particularly, many efforts have been made to develop acidic-sensitive nanocarriers. In designing these nanocarriers, acidic pH changes the ionization status of the polymer used or induces a cleavage of acid-labile linkers resulting in degradation of the carrier, hence releasing the entrapped drug [Arias, 2011].

For instance, Lee *et al*. developed a pH-responsive micelle system using a poly(lactic acid)-b-PEG-b-poly(L-histidine) (PLA-b-PEG-b-polyHis) triblock copolymer with a pKa of 7.0 [Lee et al., 2007]. Below pH 7, the polyHis part is protonated on the nitrogen of the imidazole ring of histidine, allowing the core to release the drug. Hence, this system allows the nanocarrier to remain stable until its entrance in tumor interstitium where drug can be released after micelle destabilization. Similarly, Kim *et al.*, developed pH-sensitive immunoliposomes using small unilamellar vesicles of dioleylphosphatidylethanolamine and cholesteryl hemisuccinate. Those immunoliposomes showed good anti-tumor efficacy *in vivo* [Kim et al., 2009]. Griset *et al.* synthesized cross-linked NPs using acrylate-based hydrophobic polymers with hydroxyl groups that were masked by pH-labile protecting groups (e.g., 2,4,6-trimethoxybenzaldehyde). The NPs were stable at neutral pH, but the protecting group was cleaved and the hydroxyl groups were exposed at mildly acidic pH (pH ≈ 5). This

hydrophobic-to-hydrophilic transformation caused the swelling of NPs and subsequent drug release [Griset et al., 2009].

This pH-triggered release has also been exploited to deliver the encapsulated drug when internalized into late endosomal vesicles to ensure controlled drug release [Griset et al., 2009; Yang et al., 2014b]. An interesting study was conducted by Cajot *et al.* [Cajot et al., 2012]. They developed smart nanocarriers combining acid-triggered drug delivery and active targeting approach. This systems consists of self-assembled hybrid micelles based on 90% wt.% pH-sensitive non-targeted poly(ethylene oxide) – poly(2-vinyl-pyridine) – poly(ε-caprolactone) ($(PEO)_{129}(P2VP)_{43}(PCL)_{17}$) ABC star copolymer, which was co-micellized with 10 wt.% of a biotinylated $(P2VP)_{10}(PEO)_{155}(PCL)_{17}$ ABC linear copolymer. In these micelles, biotin functions, attached to the P2VP polymer part, are protected from blood components during circulation (neutral environment) by a PEO corona. Under acidic conditions (such as tumor environment), the P2VP block is protonated and stretches out of the PEO shell and then exposes biotin at the periphery of micelles (Figure 6).

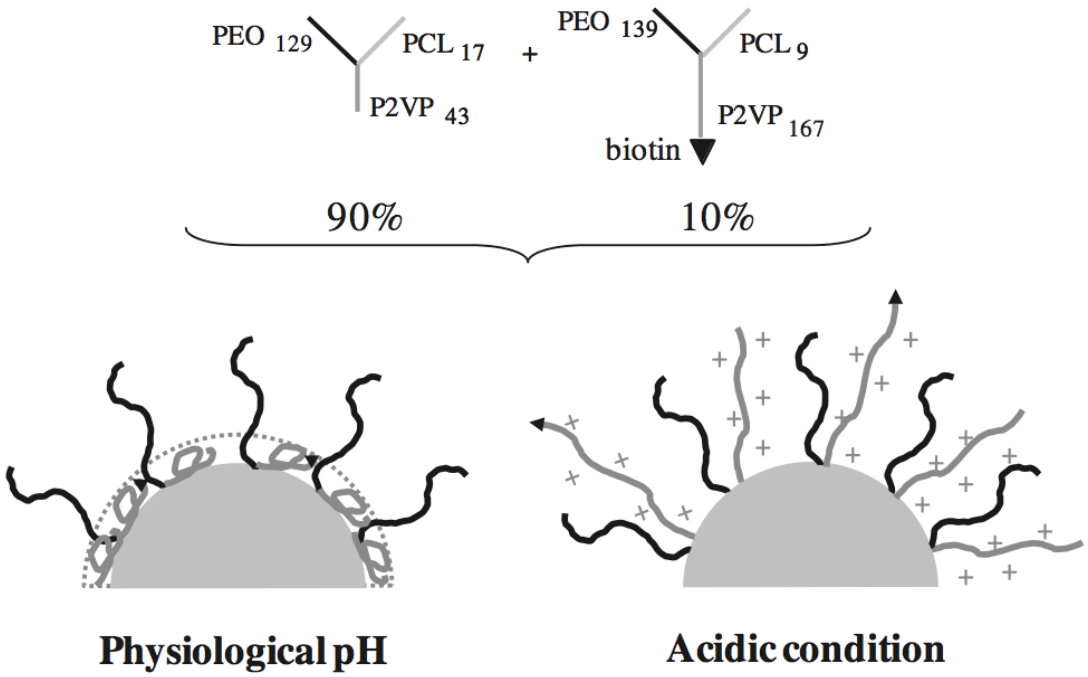

Figure 6. Composition and architecture of the copolymers used for the preparation of the biotinylated hybrid micelles, micelles composition and sketch of the shell evolution depending on the pH, illustrating the principle of ligand camouflage and exposure thanks to pH (adapted from [Cajot et al., 2012]).

Magnetic field

External magnetic field is used in combination with magnetically responsive nanoparticles, so-called "magnetic nanoparticles" (MNP), (i) to accumulate these nanocarriers at the target site, keeping them in place for a given period of time to allow drug release and/or (ii) triggering drug release (See Figure 7). For the first purpose, referred as "magnetic targeting", a static magnetic field is used to guide MNP at the target site (Figure 7A). Indeed, when a permanent magnet is applied externally near the tumor region, the magnetic gradient produced exerts attractive forces on MNP delivered via the circulation. However, this magnetic gradient decreases as the distance with the source (permanent magnet) increases. This constitutes the major limiting factor of this approach to clinical translation [Abouelmagd et al., 2014; Arias, 2011; Cole et al., 2011; Laurent et al., 2011; Reddy et al., 2012]. Nevertheless, constant efforts are made to overcome magnetic barriers. Researchers are currently studying potential solution including improvements in the quality of the source (e.g. using a MRI system magnet as a source [Riegler et al., 2010]), deeply focused targeting [Huang et al., 2010] and magnetic implants [Polyak et al., 2008].

Triggering drug release using magnetic field is referred as "magnetic hyperthermia". This strategy consists in the application of an alternating magnetic field on the target as release trigger after MNP have reached tumor (Figure 7B). This energy is then absorbed by the MNP and converted into heat by the relaxation of rotating magnetic moments induced by the alternating magnetic field. This generated heat can, thereafter, be used to either trigger drug release from a thermo-responsive nano-carrier or act directly by itself on more sensitive tumor cells (discussed in the hyperthermia section) [Cole et al., 2011; Laurent et al., 2011]. The amount of heat generated depends on the nature of magnetic material and of magnetic field parameters [Gupta et al., 2005]. Chen *et al.* and Jordan *et al.*, were the first to study this hyperthermia effect of MNP in 1993 [Chen et al., 2010; Jordan et al., 1993].

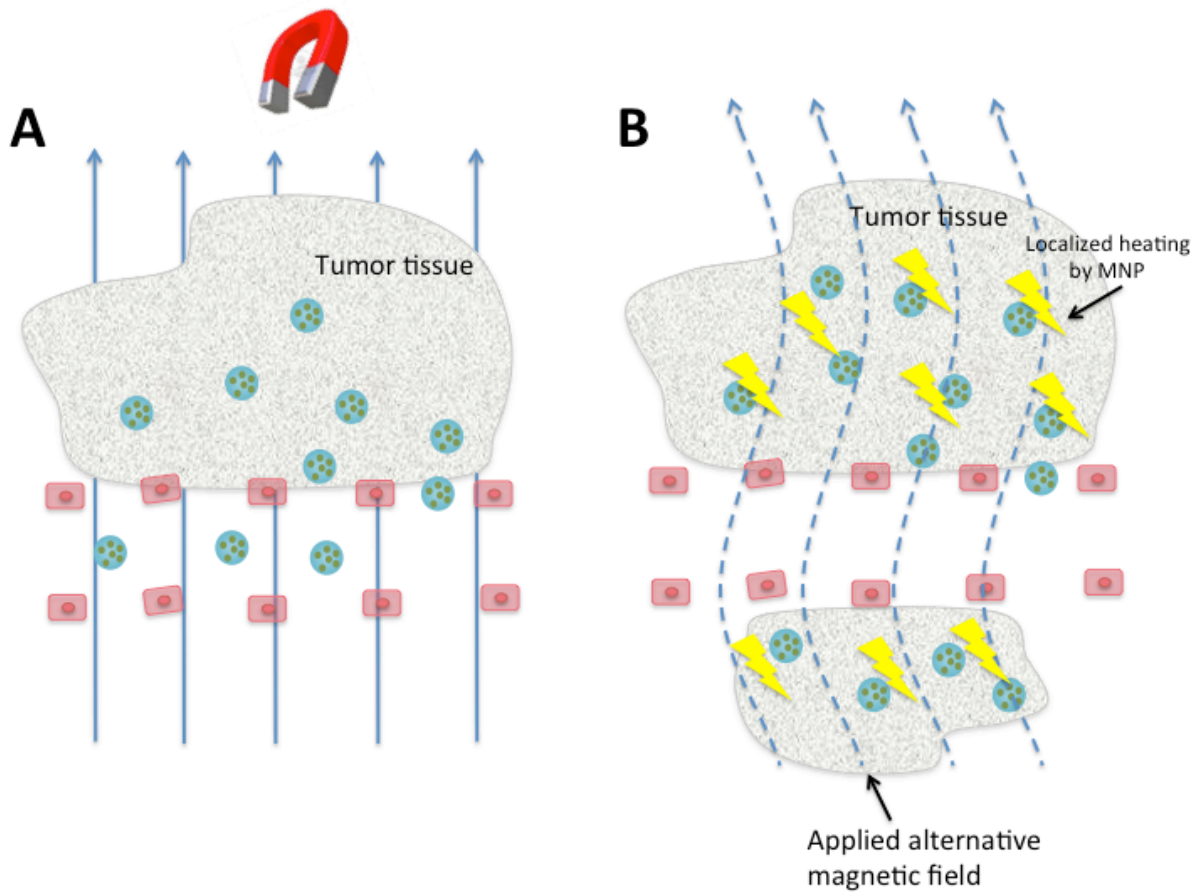

Figure 7. Schematic representation of magnetic triggered drug release. (A) Under application of a static magnetic field placed on the surface of the tumor, the so-formed magnetic gradient attracts magnetic nanoparticles (MNP) through the leaky vasculature into the tumor tissue. (B) After MNP reach tumor tissue, an applied alternative magnetic field induces localized heating by relaxation of rotating MNP (adapted from [Cole et al., 2011]).

Light

Ultraviolet (UV), visible and near-infrared (NIR) lights are widely studied as external stimuli to trigger drug release by inducing structural changes of nanocarriers. This approach is particularly interesting as it provides a non-invasive technique easy to control in terms of intensity and duration of the stimulus. On one hand, UV and short visible lights (< 410 nm) are mostly used as energy source to activate nanocarriers compounds and destabilize their structure to trigger drug release. However, this technique is limited to the close skin surface target as these wave penetration deeps are limited to a few micrometers. This issue limits their application into clinic [Abouelmagd et al., 2014]. On the other hand, long visible and NIR lights can be used to generate reactive oxygen species (ROS) after activation of a compound presented by the drug carrier or the drug itself. Once this photosensitizer-containing drug is delivered to the tumor cell, light radiation activates it and, hence, generates "killer" ROS inducing apoptosis and enhancing drug release. This technique is called photodynamic

therapy (PDT, see Figure 8) [Kelkar et al., 2011; Moses et al., 2013]. PDT is currently an FDA-approved first-line treatment for superficial skin cancers (actinic keratosis and basal cell carcinomas), age-related macular degeneration and is routinely used for obstructive esophageal cancer and some forms of lung cancer [Issa et al., 2010; Kelkar et al., 2011].

Porphyrin derivatives are the most commonly used photosensitizers in PDT. When irradiated with the proper wavelength, the porphyrin produces cytotoxic ROS by reaction between its excited-state and nearby moleculer oxygen [Kelkar et al., 2011]. For instance, Savellano *et al.* conjugated a clinically approved benzoporphyrin derivative (verteporfin) to the anti-EGFR MAb cetuximab, and showed that the conjugate effectively targeted and photodynamically killed EGFR-overexpressing A431 (epidermal carcinoma) and Ovcar5 (ovarian cancer) human cancer cells [Savellano et al., 2005]. Konan *et al.* studied meso-tetra (p-hydroxyphenyl) porphyrin (p-THPP)-loaded nanoparticles and tested their phototoxicities against EMT-6 murine mammary tumor cells [Konan et al., 2003]. The incorporation of the photosensitizer into nanoparticles has been shown to reduce cutaneous photosensitivity post-treatment [Kelkar et al., 2011].

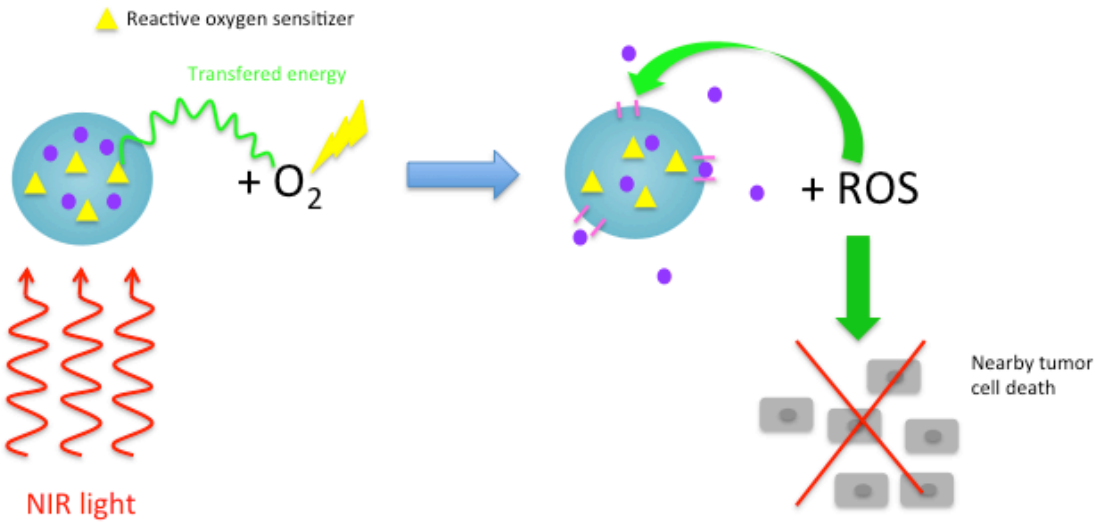

Figure 8. Schematic representation of NIR light triggered delivery. Once the photosensitizer-containing nanocarrier is delivered to the tumor cell, NIR light radiation activates it and, hence, generates "killer" ROS inducing apoptosis and enhancing drug release. This technique is called photodynamic therapy (PDT) (adapted from [Moses et al., 2013]).

Ultrasound

Ultrasound (US) refers to acoustic sound with high frequencies (> 20kHz) above those of audible sound. Those waves have the potency to penetrate deeper in inner organ compared to light waves. Ultrasound generates two kind of effects: (i) thermal (heat generation) and (ii)

non-thermal effects (acoustic cavitation and radiation forces). Both stimuli can be exploited for diagnosis, physical therapy and controlled drug delivery. Non-thermal effects of US induce a variety of biological responses resulting in increased drug or carrier extravasation, BBB disruption and membrane permeabilisation to otherwise cell-impermeable compounds, while thermal effects are mostly used to trigger thermoresponsive drug delivery and tumor tissue thermal ablation [Abouelmagd et al., 2014; Yudina et al., 2012]. Focused US (FUS) is currently used in the clinic for non-invasive treatment of uterine fibroids and prostate tumors. This strategy relies on the application of continuous ultrasound pulses of the order of seconds to reach temperatures around 60–70°C in the ultrasound focal volume inducing coagulative necrosis resulting, hence, in thermal ablation of the diseased tissue [Yudina et al., 2012]. Moreover, efforts have been made in combining high-intensity focused ultrasound (HIFU) exposures, as a source of hyperthermia, with thermosensitive nanocarriers. Li *et al.* demonstrated the feasibility of this approach using Gold nanocages covered with thermally-responsive polymers. They demonstrated experimentally that controlled release could be achieved by the application of HIFU at depths up to 30 mm [Li et al., 2011].

Cavitation, defined as formation and/or activity of gas-filled bubbles in a medium exposed to US, is thought to be responsible for enhancing (i) the permeability of blood vessels, by the generation of local streaming and consequent shear that can open up gaps between endothelial cells [Cool et al., 2013; Hancock et al., 2009] and (ii) the permeability of individual cells through the formation of the transient pores in the plasma membrane, a phenomenon called sonoporation (see Figure 9) [Frenkel, 2008; Geers et al., 2012]. Researchers can make the most of these properties in enhancing drug delivery [Yudina et al., 2012]. Indeed, microbubbles, defined as micron sized (1–10 μm) gas bubbles with a shell composed out of phospholipids, polymers or proteins, can be loaded with a drug and used in association with applied US for drug delivery. Originally, microbubbles were developed as contrast agent in ultrasound imaging [Cool et al., 2013]. At higher acoustical pressures, cavitation will induce violent microbubble oscillations, eventually resulting in microbubble destruction (the so called 'inertial cavitation'). Inertial cavitation is particularly useful in drug delivery as it can trigger both release of drugs from the microbubbles and uptake of the released drugs into the temporary permeabilized cells due to sonoporation [Geers et al., 2012]. For instance, Lentacker *et al.* developed DOX-containing microbubbles and demonstrated a two-fold increase efficacy of DOX-loaded microbubbles in killing melanoma cells after exposure to ultrasound compared to DOX-liposomes [Lentacker et al., 2010]. Finally, another example by

Cool *et al.* gave the *in vivo* proof that ultrasound triggered drug delivery can be enhanced by coupling drug loaded liposomes to microbubbles using indocyanine green-containing liposomes (ICG-liposomes) coupled to perfluorobutane (C4F10) gas containing microbubbles [Cool et al., 2013]. They also showed that the perforations in the blood vessels allow the passage of ICG-liposomes up to 5 h after microbubble and ultrasound treatment.

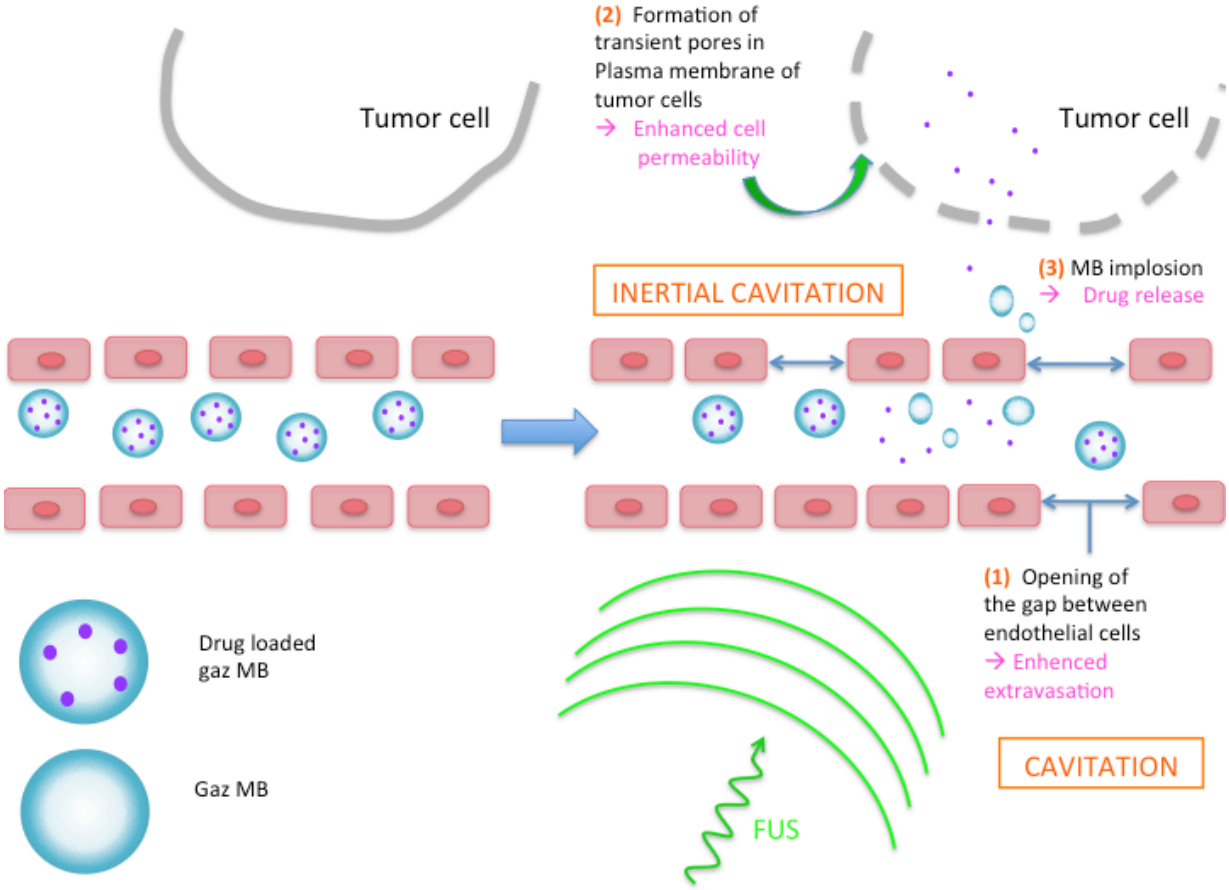

Figure 9. Schematic representation of cavitation-mediated US triggered drug delivery. Applied FUS induce cavitation resulting in (1) opening of the gap between endothelial cells resulting in an enhanced extravasation, (2) formation of transient pores in the plasmic membrane of nearby tumor cells resulting in enhanced cell permeability and (3) microbubbles implosion resulting in drug realease (due to inertial cavitation) (adapted from [Yudina et al., 2012]).

Hyperthermia

The heating of tissue to temperatures above those found in normal physiological conditions, or hyperthermia, has been used in a number of different strategies to treat cancer including thermal ablation, which is the destruction of tumor cells under high hyperthermia. At much lower temperatures hyperthermia (referred as "mild hyperthermia") can be used to induce a number of effects on tissue e.g., increased blood flow, improved perfusion, enhanced oxygenation and increased permeability. Moreover, mild hyperthermia can be used to trigger site-specific drug release from thermo-responsive nanocarriers [May et al., 2013]. Thermo-

sensitive liposomes, micelles and polymeric nanoparticles are the most widely studied stimuli-responsive carrier. Those thermo-sensitive nanocarriers are based on the use of wisely engineered polymer presenting a phase transition temperature. For polymeric micelles, transition phase can lead to an intra-molecular collapse of the polymer leading to the shrinkage of the micelles and subsequent drug release (Figure 10) [Abulateefeh et al., 2011]. This transition phase temperature is known as the low critical solution temperature (LCST) [Arias, 2011]. For instance, Guo *et al.* recently developed thermoresponsive Pluronic F127-poly(d,l-lactic acid) (F127-PLA) copolymer micelles decorated with folate (FA) [Guo et al., 2014]. F-127-PLA micelles had a low critical solution temperature of 39.2 °C close to body temperature. At 37 °C, little amount of encapsulated anticancer drug DOX is released from micelles, while at a slightly elevated temperature (40 °C), the shrinkage of thermoresponsive segments causes a rapid release of DOX and instantly increases the drug concentration locally.

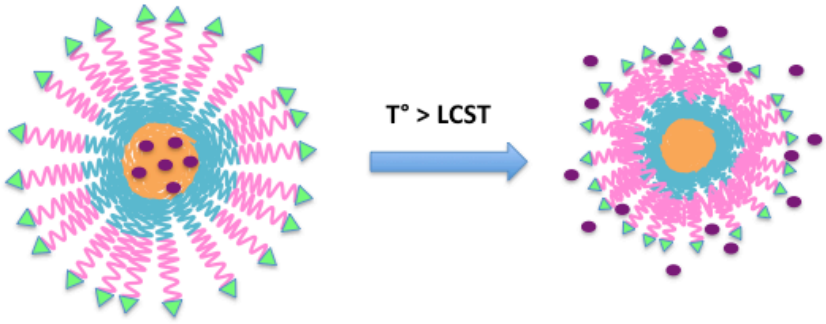

Figure 10. Schematic representation of drug delivery from thermosensitive micelles. When temperature exceeds the LCST, micelles shrinks resulting in drug delivery (adapted from [Guo et al., 2014]).

Local hyperthermia is a phenomenon that can be (i) naturally present under certain pathological conditions (e.g. some carcinomas, inflammation) or (ii) achieved by several external stimuli including the abovementioned light, ultrasound and magnetic field [Abouelmagd et al., 2014; Ta et al., 2013]. For instance, an interesting application was given by Hayashi *et al.* who used alternative magnetic field (AMF) to generate hyperthermia using SPIO-loaded nanoparticles [Hayashi et al., 2014]. They designed the AMF-responsive smart nanoparticles by combining DOX and clustered SPIO core within a containing polymer with a glass-transition temperature (Tg) of 44°C. During exposure to the AMF, the inner Fe_3O_4 nanoparticles cluster produces heat until at least the Tg, leading to the softening of the polymer phase, which allows the release of DOX (Figure 11).

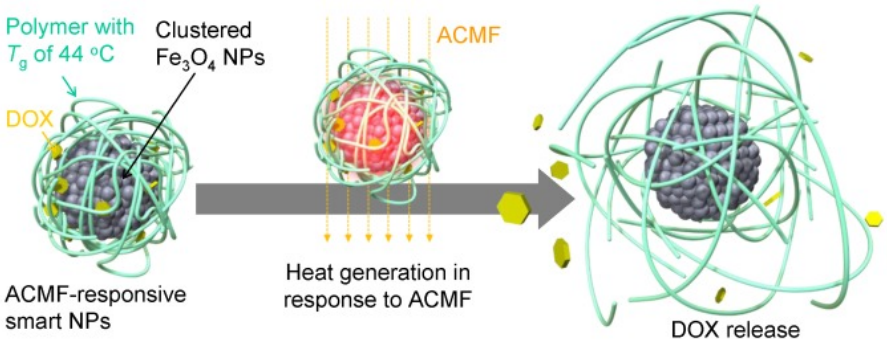

Figure 11. Schematic representation of smart NPs that produce heat in response to alternative magnetic field and sequentially release doxorubicin [Hayashi et al., 2014].
Abbreviations: ACMF = alternating current magnetic field, DOX = Doxorubicine, NPs = nanoparticles, T_g = glass transition temperature

Concerning thermosensitive liposomes, payload release is achieved by taking advantage of the inherent physical properties of liposomal membranes, or more precisely, by tuning the transition temperature between the gel and liquid phases (Tm). At the Tm, the membrane becomes disordered, increasing the permeability of the lipid bilayer to its aqueous contents via passive transfer through the disordered membrane phase boundaries [May et al., 2013]. Thermodox® is a novel formulation of thermosensitive PEGylated liposomal doxorubicin. This system is activated by the application of localised hyperthermia and releases its payload when reaching temperatures between 39 and 42°C [Egusquiaguirre et al., 2012]. Thermodox® is currently being tested in a phase III study to evaluate its efficacy in combination with radiofrequency ablation (RFA) in patients with hepatocellular carcinoma, compared to those receiving RFA alone [www.clinicaltrials.fgov].

Finally, it is noteworthy that most cancer tissues have been shown to possess higher heat-sensitivity over normal tissue. Hence, this property can be used in cancer therapy to destroy the pathological cells by hyperthermia [Cole et al., 2011; Laurent et al., 2011]. The destructive ability of hyperthermia arises from damage to several cellular components such as membranes, the cytoskeleton and cellular process mechanisms such as DNA repair. This strategy has been used by Maier-Hauff *et al*. in a clinical patient trial to treat recurrent glioblastoma by magnetic iron-oxide nanoparticles-mediated hyperthermia [Maier-Hauff et al., 2011].

II. NANOPARTICLES

Over the last decades, numerous nanocarrier platforms have been studied for cancer drug delivery [Acharya et al., 2011; Sultana et al., 2013]. These nanocarriers platforms include liposomes, polymer conjugates, polymeric micelles, nanoparticles and dendrimers (summarized in Figure 12) [Danhier et al., 2010]. We will focus on nanoparticles in this thesis.

II.1. DEFINITIONS

Nanoparticle refers to solid spherical drug carrier system of less than 1µm diameter prepared from natural or synthetic polymers. These nanoparticles have become one of the greats in the field of drug delivery considering the wide range of drugs that can be delivered using this carriers ensuring a sustained drug delivery [Hans et al., 2002; Sultana et al., 2013].

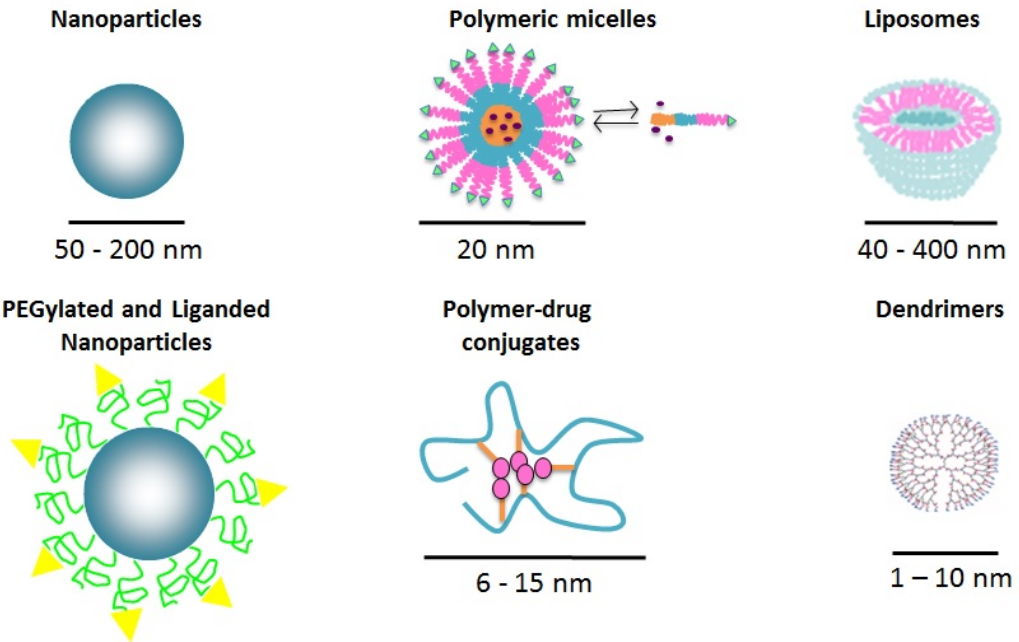

Figure 12. Various types of nanocarriers currently used in drug delivery (adapted from [Danhier et al., 2010]).

II.2. POLYMERS

Among the polymer used to formulate nanoparticles, two categories can be distinguished: (i) natural polymers (i.e. proteins and polysaccharides) and more importantly, (ii) synthetic polymers. Natural polymers for drug delivery and tissue engineering possess good compatibility, but lack of suitable physical properties such as solubility, mechanical strength or stability limits their application [Dash et al., 2012a]. Synthetic polymers have been more

extensively used. Synthetic polymers include Poly(lactic acid) (PLA), poly(glycolic acid) (PGA), the co-polymer of both, Poly(d,l-lactide- co-glycolide) (PLGA) and poly(ε-caprolactone) (PCL). In this thesis, we will focus on PLGA- and PCL-based polymers. Indeed, in the studies presented we used a combination of PLGA, PLGA-PEG and PCL-PEG (see chemical structure in Figure 13).

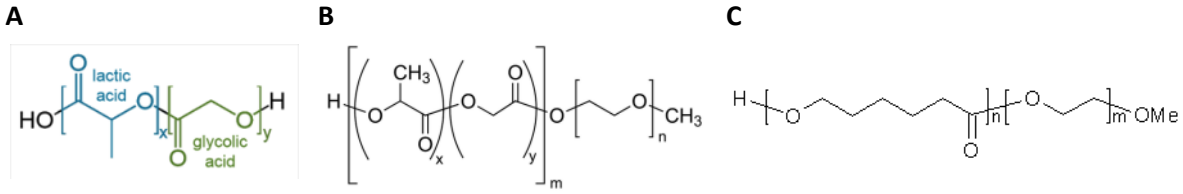

Figure 13. Chemical structures of the three polymers used in this thesis. (A) PLGA, (B) PLGA-PEG, (C) PCL-PEG.

Poly-d,l-lactide- co-glycolide (PLGA)

Because of its biodegradability, Poly(lactic-co-glycolic acid) (PLGA) is one of the most successfully used polymers to formulate nanoparticles. Indeed, its hydrolysis leads to metabolite monomers, lactic acid and glycolic acid, which are endogenous and easily metabolized by the body via the Krebs cycle (Figure 14). Hence, a minimal systemic toxicity is associated with the use of PLGA for drug delivery or biomaterial applications [Danhier et al., 2012a; Kumari et al., 2010]. Interestingly, the US FDA and European Medicine Agency (EMA) approved PLGA in various drug delivery systems in humans, which make it very attractive in a view of a translational approach. Different molecular weights and copolymer compositions are commercially available. Depending on the molecular weight and copolymer ratio, PLGA degradation time can vary from several months to several years. The forms of PLGA are usually identified with regard to the monomers ratio used (e.g., PLGA 75:25 identifies a copolymer whose composition is 75% lactic acid and 25% glycolic acid) [Acharya et al., 2011; Kumari et al., 2010].

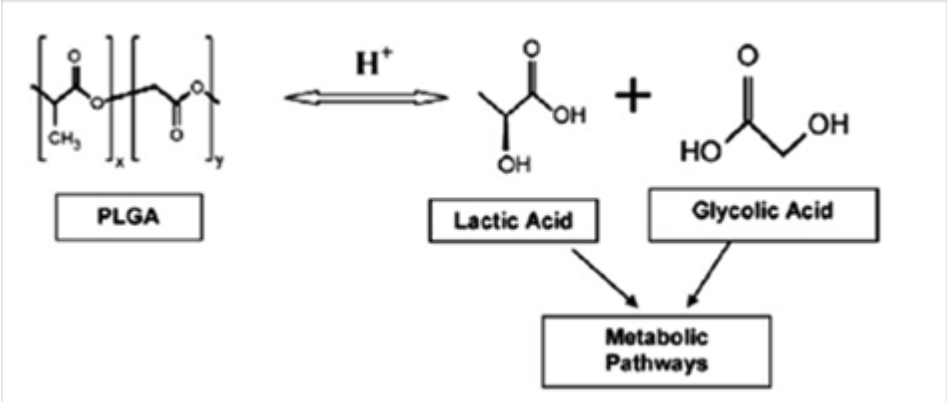

Figure 14. Hydrolysis of PLGA [Kumari et al., 2010]

Many factors are known to influence drug release and efficiency of formulated PLGA-based nanomedicines including surface modification of PLGA, drug encapsulation methods, particle size, additives added during formulation, molecular weight of drug and ratio of lactide to glycolide moieties [Danhier et al., 2012a; Kumari et al., 2010]. PLGA nanoparticles have been extensively used for the encapsulation of various anti-cancer drugs and their successful delivery *in vivo*. These drugs include paclitaxel, doxorubicin, 5-fluorouracil, 9-nitrocamptothecin, cisplatin, triptorelin, dexam- ethasone, xanthone, etc [Danhier et al., 2012a]. On the other hand, recent studies have shown successful formulation of PLGA-based magnetic nanoparticles encapsulating SPIO for imaging applications [Aryal et al., 2013; Lee et al., 2010; Ling et al., 2012].

Poly(ε-caprolactone) (PCL)

Poly(ε-caprolactone) (PCL) is a semicrystalline hydrophobic polyester. At room temperature, PCL is soluble in aromatic solvents and in chlorine solvents (dichloromethane and chloroform), partially soluble in polar solvents, such as acetone and acetonitrile, but insoluble in alcohols and water [Pohlmann et al., 2013] However, PCL hydrophobic nature does not allow easy release of hydrophobic drugs given its long-term degradation (ranging from weeks to months). To overcome this limitation, various types of modification have been developed for successful application in pharmaceutical formulations. Among these, Poly(ethylene glycol) (PEG), a hydrophilic polymer, is frequently used to modify PCL degradation pattern and improve its biodegradability via PCL-PEG co-polymers formation [Dash et al., 2012a; Dash et al., 2012b; Pohlmann et al., 2013]. PCL nanoparticles have been prepared mostly by nanoprecipitation, solvent displacement and solvent evaporation [Danhier et al., 2012a]. PCL nanoparticles have shown their efficacy in encapsulating a wide range of drugs such as paclitaxel, doxorubicin, tamoxifene, insulin and so on [Dash et al., 2012b; Kumari et al., 2010].

II.3. FORMULATION

The drug or molecules of interest may either be entrapped into the particle cavity (so-called "nano-capsules") or homogeneously dispersed into a polymer matrix (so-called "nanospheres") [Sultana et al., 2013]. Polyester nanoparticles are usually prepared using an emulsion-evaporation technique. This technique is commonly used to encapsulate hydrophobic drugs or SPIO and consists in dissolving both polymers and hydrophobic drugs

in an organic solvent (mostly dichloromethane) and incorporating this organic phase into a hydrophilic phase containing a surfactant (polysorbate 80 or polyvinyl-alcohol, PVA) [Danhier et al., 2009a; Garinot et al., 2007; Lee et al., 2010]. Since these two phases are non-miscible, an external source of energy (sonication) is used to induce the nanosized droplets and create this oil-in-water emulsion (O/W). During the last phase of this process, solvent is evaporated and the nanoparticles are collected after centrifugation. This method can be adapted to incorporate hydrophilic drugs into nanoparticles and is called double emulsion W/O/W.

Beside this emulsion-evaporation method, another frequently and easier method used to prepare nanoparticles is the nanoprecipitation method [Danhier et al., 2009b; Hans et al., 2002; Soppimath et al., 2001]. In this technique, acetone is used as organic solvent to dissolve the polymer matrix and the hydrophobic drug. This organic phase is then added dropwise to water. Finally, the same final phase of evaporation and centrifugation is used to remove solvent and collect the so-formed nanoparticles.

II.4. SURFACE MODIFICATION

Surface modification can be done for two purposes: (i) prolong circulation time of the particles and (ii) target tumor specifically.

After intra-venous injection, hydrophobic nanoparticles are recognized by the body as foreign and are, thus rapidly cleared from the systemic circulation by the mononuclear phagocytic system (MPS) and end in the liver or the spleen. While this property of nanoparticles can be an advantage if treating a liver condition, it mostly limits the application of these carriers in many drug delivery systems. A particular attention has been paid to overcome this major concern in the past decades. Since size and surface hydrophobicity determines the amount of adsorbed blood components and proteins (opsonin) and, hence, the opsonization of the particles, surface modification provides a key method to overcome rapid clearance. Of these methods, the most frequently used is the adsorption or grafting of poly-ethylene glycol (PEG) to the surface of nanoparticles. “PEGylation” of nanoparticles surface results in an increase in the blood circulation half-life of the particles by several orders of magnitude (which is of huge interest for target site accumulation). Indeed, PEG grafting creates a hydrophilic protective layer around the nanoparticles, which pushes away opsonin proteins and prevent their adsorption via steric repulsion forces [Hans et al., 2002; Kumari et al., 2010; Soppimath et al., 2001].

The second reason to use a surface modification strategy is to address the particles to a specific receptor present on the target tissue leading in an increased selectivity of the treatment. After specific binding of the particle to its target site, receptor-mediated endocytosis leads to the internalization of the particle [Arias, 2011; Hans et al., 2002]. Most targeting ligands are loaded onto nanoparticle surfaces via a PEG spacer. The rationale for this approach lies in the extension of the ligand from the nanoparticle platform, enhancing its flexibility and, hence, its easier interaction with receptors. An important parameter that affects the targeting moiety is the concentration of surface ligands. Indeed, there could be a rationale for higher ligand densities as a method of increasing the probability of nanoparticle interactions with cell receptors (multivalency). However, this point is subjected to controversy since the presence of increased non-PEG-like material on nanoparticles surface can be related to more MPS uptake as such ligands can be recognized as foreign [Wang et al., 2010].

Among the different methods reported for nanoparticles functionalization, Pourcelle and colleagues developed a “clip photochemistry” method. "Clip photochemistry" is a polymer derivatization methodology based on the photografting of bifunctional photosensitive linkers. This linker, once attached to polymer backbones and activated by UV radiation (creating an activated ester) can be used to introduce a compound of interest bearing primary amine functions on polymer [Danhier et al., 2009a; Pourcelle et al., 2007]. This technique allowed the grafting of the pentapeptide GRGDS (Figure 15) [Pourcelle et al., 2007].

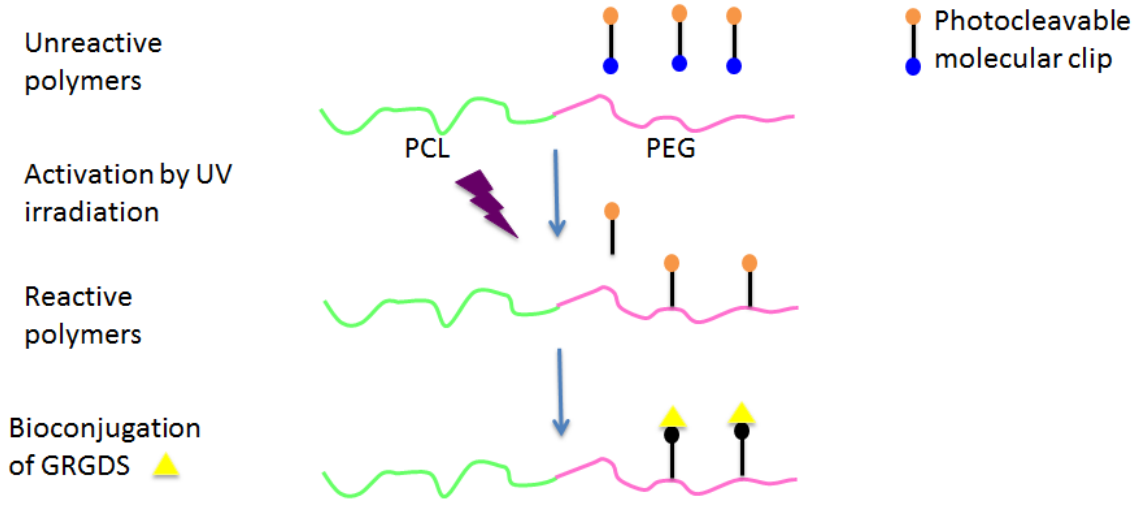

Figure 15. Schematic representation of clip photochemistry. This method covalently links GRGDS peptides mainly on the PEG residue of the PCL-PEG (adaplted from [Pourcelle et al., 2007]).

II.5. PHYSICO-CHEMICAL CHARACTERIZATION

Surface charge is an important parameter in nanoparticles characterization since it has potential effect on receptor binding, physiological barrier penetration and dispersion stability [Lin et al., 2014]. This parameter is commonly assessed by ***zeta potential*** measurement. This technique relies on the measurement of the velocity of the charged species towards the electrode in the presence of an external electric field across the sample solution. The zeta potential can be positive, neutral or negative depending on the nature of the polymer used or the material used for its surface modification. This technique can also be used to estimate the efficiency of surface modification [Soppimath et al., 2001].

The average ***particle size*** and the polydispersity index can be measured by dynamic light scattering (DLS). The principle of DLS is to monitor the temporal fluctuation of light dispersion caused by the Brownian motion of the particles at a fixed scattering angle [Lin et al., 2014].

Another crucial characteristic that need to be assessed is the ***drug loading***. Drugs are either incorporated into the nanoparticles core or adsorbed on the surface of nanoparticles after their production [Kumari et al., 2010]. Ultracentrifugation is a common method to separate nanoparticles from non-encapsulated or non-adsorbed drug. After nanoparticles dissolution and drug content measurement by an appropriate technique, it possible to calculate two parameters: (i) the encapsulation efficiency and (ii) the drug loading. The encapsulation efficiency is defined by the ratio of the encapsulated drug compared to the initial amount of drug, whereas the drug loading is defined as the amount of drug (mg) loaded for 100 mg of polymer [Danhier et al., 2010].

II.6. PHARMACO-KINETICS AND BIODISTRIBUTION

Particles have a long journey from the injection to the tumor site entrance. This journey begins right after the injection while circulating through the blood. At this stage, binding to blood proteins may occur and lead to rapid clearance of the body via the so-called “opsonization” process. This binding phenomenon is dependent on multiple factors including particle charge. Indeed, positive and negatively charged particles are known to amplify complement activation and opsonin fixation. This fixation leads to an enhanced recognition by the MPS (whose 80 to 90% are represented by the non-parenchymal Kupffer cells of the

liver) and, hence, to a rapid clearance. Unmodified particles are known to encounter extremely rapid clearance from the blood stream within minutes to an hour depending on the particle size. Although, even long circulating carriers exhibit relatively rapid clearance depending on the surface charge (as abovementioned) and the size. Actually, particles larger than 200 nm have been shown to accumulate in the spleen and enhance the uptake by the MPS. Besides MPS clearance, particles have been shown accumulate in the liver tissue due to its particular vascular structure (sinusoid capillaries presenting fenestrations) [Nichols and Bae, 2012; Bertrand and Leroux, 2012]. Finally, there is a threshold below which renal filtration occurs passively (70 kDa). Although particles are often large enough to avoid renal filtration, a renal accumulation can be observed. This is probably due to the high part of the cardiac output delivered to the kidney (22%) [Kwon et al., 2012].

III. SPIO NANOPARTICLES

III.1. DEFINITION

Superparamagnetic iron oxides (SPIO) are small synthetic crystalline structure exhibiting a core composed of Fe_2O_3 (also called maghemite) and Fe_3O_4 (magnetite) [Boutry et al., 2009]. Their given name originates from their property to exhibit "superparamagnetism". This property give to SPIO the ability to be magnetized upon the application of an external magnetic field while no longer exhibiting any residual magnetic interaction at magnetic field removal [Laurent et al., 2008; Laurent et al., 2011; Reddy et al., 2012]. SPIO can also be used for drug delivery. To this end, drug can be either directly conjugated to SPIO surface via a covalent link or entrapped in the coating shell of SPIO via physical interactions leading to the so-called "SPIO conjugates" [Zou et al., 2010]. Another common strategy consists in the encapsulation of SPIO along with a drug in nanocarriers. These SPIO-based drug delivery systems are summarized in Figure 16.

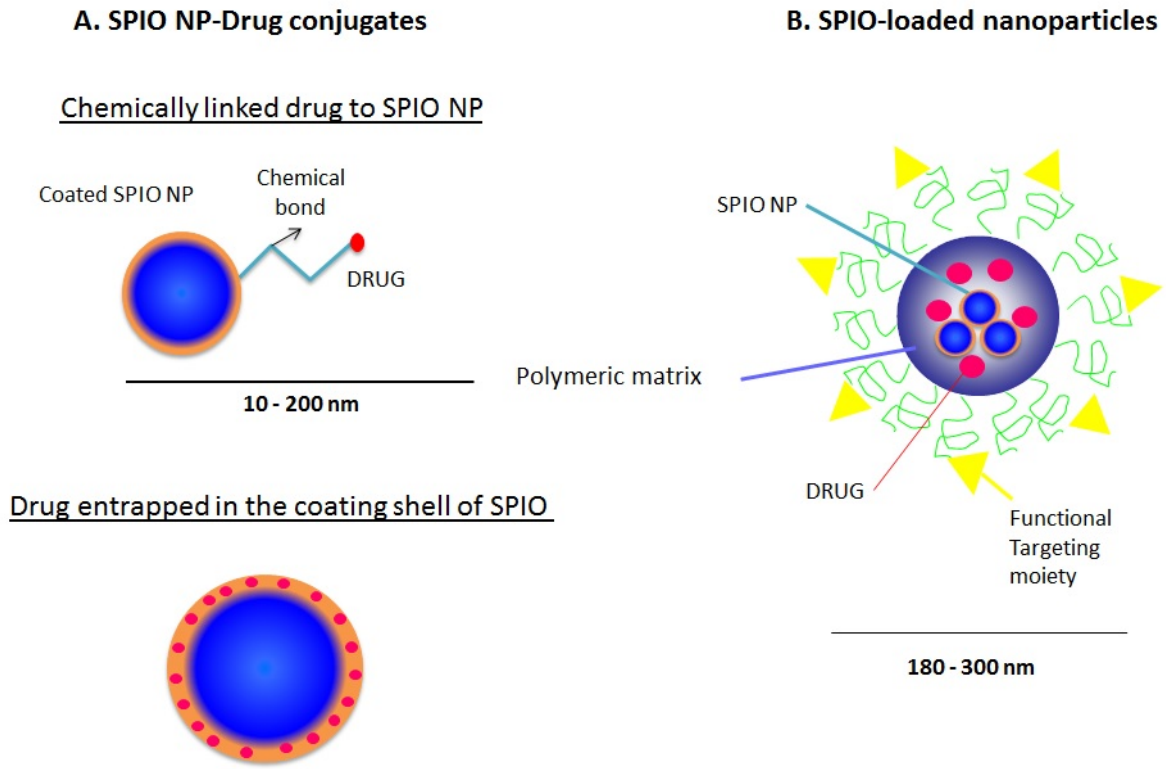

Figure 16. Schematic representation of SPIO-based drug delivery system. (A) SPIO-drug conjugates are represented either by directly conjugated drug to SPIO surface via a covalent link or entrapped in the coating shell of SPIO via physical interactions. (B) SPIO can also be loaded along with a drug into nanoparticles.

During the past decades, SPIO have gained much interest given their high potential in biomedical application. Indeed, such compounds provide simultaneously many advantages [Laurent et al., 2011]:

(i) SPIO can be used as drug carrier platform by direct conjugation to a therapeutic agent

(ii) showing high transverse relaxivity (T_2, T_2^*), SPIO allow strong negative contrast at low concentration, making them attractive candidate for magentic resonance imaging (MRI) contrast enhancement [Danhier et al., 2012d]

(iii) SPIO surface is easily fonctionnalized with ligand, making them suitable candidate for molecular imaging using active targeting approach [Wahajuddin et al., 2012]

(iv) SPIO exhibit low toxicity compared to other MR agent since the iron salvage in the natural body iron store [Wang et al., 2001]

(v) Their capacity to induce local heat when subjected to an externally applied alternative mgnetic field (such called "hyperthermia") [Reddy et al., 2012]

(vi) Finally, SPIO are able to drag a conjugated drug to its target site through the application of an external magnetic field (so-called "magnetic targeting") [Cole et al., 2011]

III.2. METHODS OF FORMULATION

SPIO are prepared by many different routes including micro-emulsion, thermal decomposition and co-precipitation methods [Laurent et al., 2008]. Among these methods, classical co-precipitation technique of iron salts is the most commonly used. This method is based on the precipitation of ferrous (Fe^{2+}) and ferric (Fe^{3+}) salts mixtures in a basic medium to form Fe_3O_4.

$$Fe^{2+} + 2\ Fe^{3+} + 8\ OH^- \longrightarrow Fe_3O_4 + 4\ H_2O$$

This method is the most convenient and the cheapest one. SPIO produced by chemical co-precipitation result in nanoparticles presenting a mean diameter as low as 10 nm and high-purity [Laurent et al., 2008; Laurent et al., 2011; Reddy et al., 2012]. However, the so-prepared naked SPIO present a large surface-to-volume ratio with highly chemical reactivity. Hence, if not covered with a proper surfactant, SPIO tend to aggregate and are easily oxidized

in air, resulting in loss of magnetism and dispersibility [Mahdavi et al., 2013]. Moreover, these SPIO are generally polydispersed and poorly crystallized. Thermal decomposition of iron precursors (generally iron acetylacetonate) under high temperature and in the presence of organic surfactants allows overcoming these problems resulting in monodispersed and uniform crystalline SPIO. Other formulation methods exist including hydrothermal reactions and microemulsion. These methods are currently less explored given their disadvantages (long reaction times, large amount of solvent and surfactant, poor yield) [Laurent et al., 2011; Santhosh et al., 2013].

Size, shape, composition, and surface nature can be controlled by varying the type of the iron salt, the Fe^{2+}/ Fe^{3+} ratio, the reaction temperature, the pH value, and the surfactants [Wang et al., 2013].

III.3. SURFACE MODIFICATION

To avoid aggregation and protect their surface from oxidation, which are crucial characteristics to improve their clinical efficacy, the synthetized SPIO need to be coated. SPIO have been coated with a wide variety of materials. These coating agents can be either physically (electro-static interaction, hydrogen-binding) adsorbed or chemically bound on SPIO surface. Among the coating agents usually used, the most common are biocompatible polymers (dextran and derivatives, siloxane, poly(ethylene glycol), poly(lactic acid), poly(ε-caprolactone), chitosan), inorganic materials (gold and silica) and monomeric stabilizers (carboxylates, phospates) [Laurent et al., 2008; Laurent et al., 2011; Santhosh et al., 2013]. Among the latest, oleic acid is commonly used to stabilize SPIO with strong chemical interraction between the carboxylate group of oleic acid and the iron atom, and to increase lipophilicity in order to facilitate encapsulation in nanoparticles [Mahdavi et al., 2013; Zhang et al., 2006]. In this case stabilization involves steric repulsion forces.

III.4. PHYSICO-CHEMICAL CHARACTERIZATION

Physico-chemical characteristics are of great importance since they influence blood distribution profile, toxicity, circulation time and magnetic properties. Among the physico-chemical characteristics, size and shape are determinants [Wahajuddin et al., 2012]. A common technique to measure the particle core is *transmission electron microscopy* (TEM). This technique allows the determination of the total particle size of the core (crystalline and

amorphous part) and provides an interesting tool to assess size distribution and shape. X-ray diffraction (XRD) can be used to give complementary information to TEM. Indeed, XRD gives informations about the crystalline structure of the particles [Laurent et al., 2008]. Dynamic light scattering (DLS) is also commonly used to assess hydro-dynamic size of the particles. The principle of DLS is to monitor the temporal fluctuation of light dispersion caused by the Brownian motion of the particles at a fixed scattering angle [Lin et al., 2014]. However, it is noteworthy that the hydrodynamic size values obtained by DLS are often much larger than diameters obtained from transmission electron microscopic (TEM) measurements. This effect is particularly relevant for SPIO since there is a great difference between their crystal and their hydrodynamic size [Di Marco et al., 2007].

The coating percentage of SPIO is also crucial to evaluate. Therefore, *thermogravimetric analysis* (TGA) can be used to investigate the formation of strong chemical bonds between the substrates and various molecules such as oleic acid. This technique gives an idea of the percentage of inorganic matters and, consequently, the percentage of coating [van Ewijk et al., 1999].

Finally, magnetic relaxation properties can be obtained by the study of its *nuclear magnetic resonance dispersion* (NMRD) profile. This technique provides the evolution of particles relaxivity as a function of the external magnetic field, where relaxivity can be defined as the relaxation rate enhancement of an aqueous solution induced by 1mmol of iron/L. The fitting of the NMRD profiles by a theoretical relaxation model allows the determination of the ***saturation magnetization*** (M_S), which refers to the maximum magnetization possible. This saturation magnetization arises when all the magnetic dipoles are aligned in an external magnetic field. This parameter allows a good prediction of SPIO susceptibility to an externally applied magnetic field. Indeed, nanoparticles with higher saturation magnetization provide higher sensitivity and efficiency [Kolhatkar et al., 2013].

III.5. PHARMACOKINETICS AND BIODISTRIBUTION

After injection, numerous opsonin proteins, cells, and salts bind to the surface of nanoparticles, known as the opsonization process responsible for easier recognition by the mononuclear phagocytic system (MPS (whose 80 to 90% are represented by the non-parenchymal Kupffer cells of the liver) leading to rapid clearance from the circulation.

Nanoparticles are usually taken up by macrophages in the liver (Kupffer cells – 80 – 90 %), spleen (5 – 8 %) and bone marrow (1 – 2 %) [Yu et al., 2012].

After uptake in specialized macrophages, SPIO are degraded into the lysosomes. The core material is supplied to the iron storage pool of the body (total body iron approximately 4–5 g) and deposited in the liver in the form of ferritin and/or hemosiderin. The natural decomposition of these iron reserves is only possible via hematopoiesis (Fe^{2+} as central atom in the hemoglobin) and the exfoliation of epithelial cells of the skin and bowel. [Ittrich et al., 2013]. Limiting phagocytosis in the liver and spleen decreases the uptake rates for some nanoparticles, resulting in longer blood half-lives and facilitating their clinical application as T_2 agents for the detection of liver lesions. This can be achieved by surface modification yielding stealth nanoparticles. The most common strategy consists in using PEG- or dextran-coated nanoparticles. Moreover, some physicochemical characteristics are important in improving pharmacokinetic profiles of nanoparticles including size, surface charge and shape [Yu et al., 2012]. Thus, SPIO with a small hydrodynamic diameter and neutral and hydrophilic surface are opsonized and phagocytized more slowly than large SPIO with an ionic and hydrophobic coating [Ittrich et al., 2013]. Indeed, particles bearing cationic or anionic surface charges have been shown to be more attractive to phagocytes than neutral particles of the same size [Zahr et al., 2006; Gessner et al., 2002; Dobrovolskaia et al., 2008]. Dextran-coated SPIO have been shown to display a blood clearance half-life of about 10 min with uptake by hepatic RES Kupffer cells accounting for 80% of the injected dose whereas encapsulation in liposomes allowed prolonging the blood clearance half-life to 4 [Ferrucci and Stark, 1990]. The coating material of SPIO is eliminated via other decomposition and elimination paths, e.g. the coating of ferumoxtran-10 (Sinerem®) is degraded via intracellular dextranases and is eliminated primarily by the kidneys (89% in 8 weeks). Although, even long circulating carriers exhibit relatively rapid clearance depending on the surface charge (as abovementioned) and the size. Actually, particles larger than 200 nm have been shown to endure an enhanced uptake by the MPS resulting in accumulation in the liver and spleen. Besides MPS clearance, particles have been shown accumulate in the liver tissue due to its particular vascular structure (sinusoid capillaries presenting fenestrations) [Bertrand et al., 2012; Nichols et al., 2012]. Finally, there is a threshold below which renal filtration occurs passively (70 kDa). Although particles are often large enough to avoid renal filtration, a renal accumulation can be observed. This is probably due to the high part of the cardiac output delivered to the kidney (22%) [Kwon et al., 2012]. It is noteworthy that in most studies, *in vivo* pharmaco-kinetics and biodistribution of SPIO-based nanosystems are not provided.

III.6. VISUALIZING AND QUANTIFYING IRON OXIDES

To date, MRI is the reference method allowing SPIO visualization *in vivo*. However, SPIO quantification, which is crucial to assess the initial iron uptake and adapt formulation as well as for optimizing the administration dose for the subsequent MRI studies, can be assessed by four main traditionnaly used techniques including (i) spectrophotometric techniques (based on Perls' Prussian blue reaction), (ii) inductively coupled plasma mass spectroscopy (ICP-MS), (iii) fluorometry (requiring the presence of a grafted fluorophore), and (iv) relaxometry based on the mesurement of the longitudinal relaxation rate (R_1) of iron resulting from the dissolution of the iron oxyde core [Boutry et al., 2009; Danhier et al., 2012d]. However, despite their sensitivity, all these techniques lack of specificity and do not make the difference between iron species contained in biological fluids and SPIO. Recently, a new technique has been shown to be highly effective in SPIO quantification showing high sensitivity and high specificity, namely, Electron Paramagnetic Resonance spectroscopy also called Electron Spin Resonance (ESR) [Danhier et al., 2012d].

III.6.1. Magnetic Resonance Imaging

Basic principle

Magnetic resonance imaging (MRI) is a non-invasive imaging technique providing high-resolution morphological and functional images. Such a technique is commonly used in diagnostic radiology to detect tissue abnormalities corresponding to a pathological state [Reddy et al., 2012]. Nuclear magnetic resonance on which MRI is based was discovered in the mid-1940s [Bloch, 1946]. More recently, researches in the MRI field have led to its use in functional imaging, which aims to detect or measure changes in metabolism and blood flow revealing physiological activities within a certain tissue [Krishna et al., 2001].

MRI is based on the detection of resonance absorption of nuclei with non-zero nuclear spin. The most commonly used is the ^1H nucleus. Briefly, proton, as charged (positive) spinning particles, generates a characteristic magnetic field called "magnetic moment". Therefore, each proton could be considered as a small rotating magnet. In normal condition, magnetic moments are randomly oriented resulting in a zero "net magnetization". However, when an external magnetic field is applied, all those vectors will align to this external magnetic field in a parallel (low level of energy) or in an anti-parallel way. Since a small excess population is present at the lower energy level, a net magnetization of the entire population is observed, which can be materialized as a vector having the same orientation as the external magnetic

field (Figure 17 A). When a radiofrequency (RF), corresponding to the proton precession frequency (also called "Larmor Frequency"), is applied perpendicularly to the magnetic field (RF pulse), atomic nuclei absorb this energy and entered in the excitation state or resonance which induces the apparition of a transverse magnetization in the x-y plane as seen in Figure 17 B. After RF is stopped, the system returns from this state of imbalance to equilibrium (relaxation) with characteristic time constants, namely T_1 and T_2 and emitting an electromagnetic energy, which is the registered parameter in MRI (Figure 17 C-D). T_1, also called longitudinal relaxation, corresponds to the process whereby proton returns to their equilibrium energy state causing the restoration of initial longitudinal magnetization, while transverse relaxation (T_2) refers to the process involving the loss of transverse magnetization to recover the equilibrium state [Currie et al., 2013; Krishna et al., 2001]

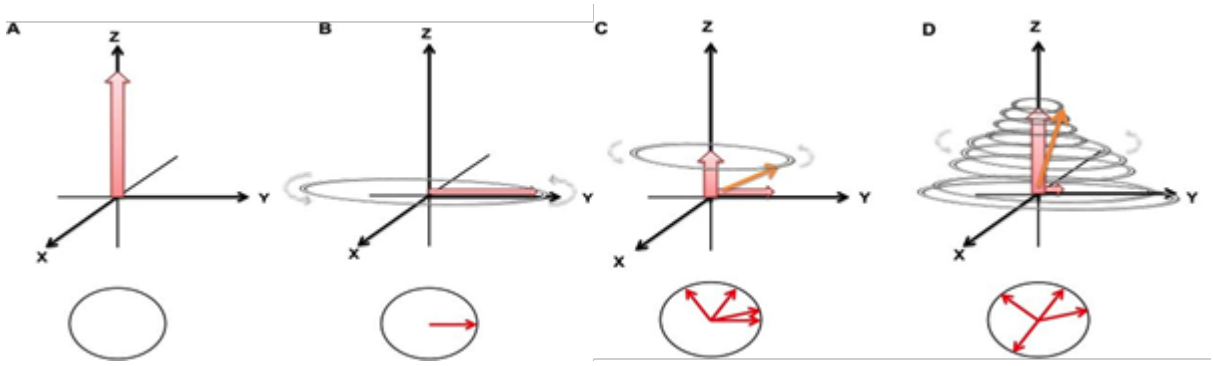

Figure 17. Recovery of longitudinal magnetization following a 90° radiofrequency (RF) pulse. (A) Protons aligned with B_0 produce a sum vector with longitudinal magnetization. (B) When an RF pulse is applied, longitudinal magnetization decreases and transverse magnetization propagates. (C) After the 90° RF pulse, transverse magnetization decreases and longitudinal magnetization begins to recover. During this process, the whole system continues precessing and so the sum vector takes a spiralling motion (D). Recovery of longitudinal magnetisation is termed T1 relaxation and loss of transverse magnetisation is called T2 relaxation [Currie et al., 2013].

Imaging technique based on magnetic resonance spectroscopy such as MRI provides ideal non-invasive imaging modalities. Indeed, this technique responds to a series of criteria needed for such aim including (i) providing high-resolution morphological images, (ii) offering functional information in regard with anatomy, (iii) avoiding the use of ionizing radiation and (iv) being relatively easy to perform [Krishna et al., 2001].

SPIO in MRI

The major limitation of MRI consists of a relatively low sensitivity. Superparamagnetic iron oxides (SPIO) as MRI contrast agent address this limitation. Indeed, SPIO are excellent MRI contrast agent that can produce predominant T_2 relaxation effect with excellent sensitivity

when compared to other MRI agents such as chelates of paramagnetic ion (Gd^{3+}-DTPA), resulting in a strong signal reduction on T_2-weighted images [Ittrich et al., 2013; Reddy et al., 2012]. The magnetic field heterogeneity around the particles, through which water molecules diffuse, induces the dephasing of the proton magnetic moments. Consequently, a T_2 effective transverse relaxation is shortened [Ling et al., 2011].

Currently, SPIO are widely used as MRI contrast agent either free, as a drug carrier platform or encapsulated into nanocarriers for biomedical applications. As such, a variety of free SPIO-based products (generally coated with dextran to stabilize) are already approved or in clinical trial (see table 6).

Table 6. examples of SPIO-based products in clinics (adapted from [Ling et al., 2011]).

Compound	Trade name	Coating agent	Size (nm)	Application	Status
Ferumoxil (AMI-121)	Lumirem, Gastromark	dextran	300	Gastro-intestinal tract	approved
Ferumoxide (AMI-25, SHU555A)	Endorem, Feridex*	dextran	120-180 80-150	Liver tumor imaging	approved
Ferixan (Ferucarbotran, SHU555A)	Resovist*, Cliavist	dextran	60	Focal liver lesions imaging	approved
Ferumoxtran-10 (AMI-227, BMS-180549)	Sinerem* (Europe), Combidex (USA)	Dextran	20-40	Lymph node imaging, atherosclerosis	Late phase clinical
Ferristene (OMP)	Abdoscan	Sulfonated styrene-divinylbenzene copolymer	3500	Gastro-intestinal tract	approved

* withdrawn from the european market

III.6.2. Quantifying SPIO using ESR spectroscopy

Basic principle

In contrast with other existing techniques available for SPIO quantification (spectrophotometric techniques, ICP-MS and relaxometry), Electron Paramagnetic Resonance spectroscopy also called Electron Spin Resonance (ESR) offers a rapid highly sensitive (LOD ≈ nM) non-destructive technique allowing specific dosage of SPIO without taking iron species contained in biological fluids into account [Danhier et al., 2012d; Spasojevic, 2011].

ESR spectroscopy is based on the same principle as MRI. Instead of detecting nuclei, ESR probes species with a single unpaired electron spin residing in a molecular orbital [Sahu et al., 2013]. These species include free radicals, transition metal complex and (super)paramagnetic molecules (e.g. SPIO). Since the total number of unpaired electrons in the sample is proportional to the signal intensity of the ESR spectrum, ESR allows quantification by a double integration technique [Spasojevic, 2011].

Noteworthy, because the magnetic moment of the electron is 658 times greater than that of the proton, ESR exhibits a much higher sensitivity compared to MRI. Moreover, whereas MRI requires high magnetic field (4.7 – 11.4 T) and ends up in a low frequency spectral line width (Hz to kHz), ESR requires only magnetic field of mT order and shows a high frequency spectral line width (≈MHz) [Krishna et al., 2001]. Figure 18 gives a schematic comparison of both techniques.

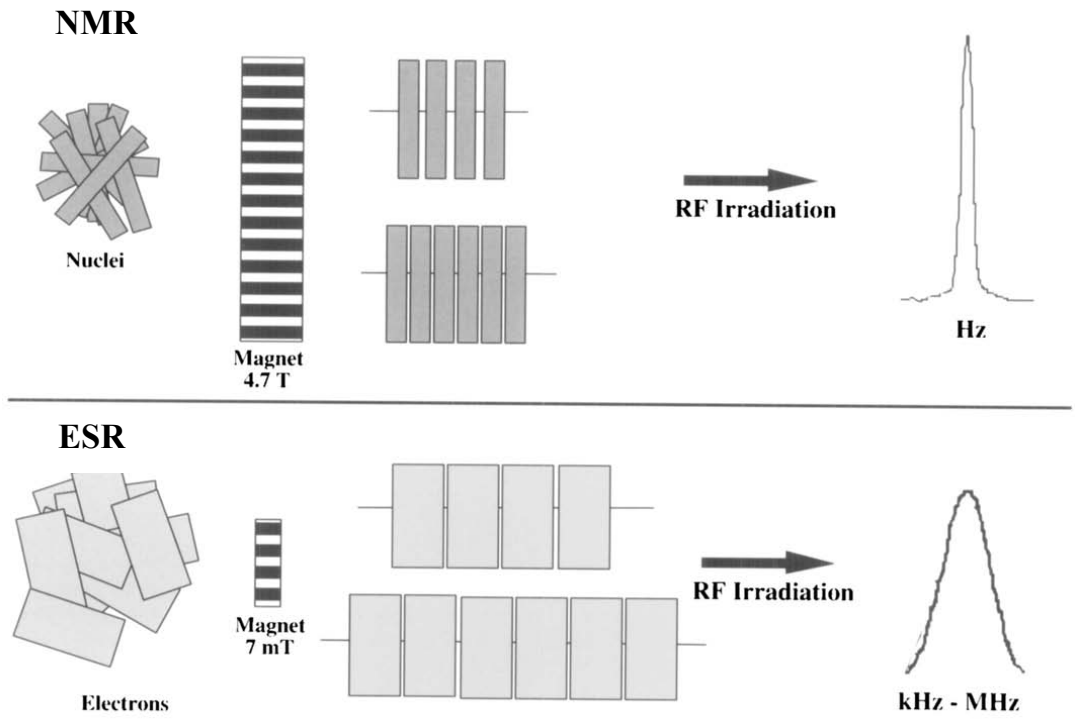

Figure 18. Schematic comparison of `nuclear magnetic resonance (NRM) and ESR spectroscopy principles. The magnetic moments of the protons and electrons are represented as rectangular bars. In the absence of an external magnetic field, individual magnetic moments are aligned randomly. In the presence of an external magnetic field (hatched rectangle), they occupy two energy levels. Irradiation with radiofrequency radiation of appropriate frequency causes resonance absorption, which is shown as an absorption spectrum [Krishna et al., 2001].

Currently, two ESR spectrometers are available depending on the application. For *in vitro* or *ex vivo* quantification, a X-band spectrometer is used. This spectrometer offers high frequency for good sensitivity. However, given its high frequency waves (9 GHz), this spectrometer

does not allow tissue penetration and, hence, *in vivo* measurements. Therefore, L-band spectrometer, working at low frequency (1.2 GHz), provides a wave penetration of 1 cm inside tissue allowing real-time assessment of concentration changes in tissue [Radermacher et al., 2010]. ESR has been extensively used during the past decades in biomedical applications including oxidative stress measurement, oxymetry measurements in the cancer field and membrane fluidity assessment [Spasojevic, 2011].

SPIO in ESR

As superparamagnetic agents, SPIO are suitable for ESR spectroscopy measurement. ESR has already been used to characterize SPIO physicochemical properties, for *ex vivo* biodistribution studies (using X-band) and for real-time assessment of changes in SPIO concentration in a tissue (using L-band) [Danhier et al., 2014; Radermacher et al., 2010]. Moreover, band-X ESR was proven to be more sensitive tool to measure iron oxide in cells compared to the classically used methods [Danhier et al., 2012d]. More recently, ESR spectroscopy was shown to be a promising method for *ex vivo* measurements after cell tracking experiments [Danhier et al., 2014]. However, this technique is not extensively used for these applications yet and is more commonly used for oxidative stress and oxymetry measurements to date.

IV. IRON OXIDES LOADED NANOTHERANOSTICS: MAJOR OBSTACLES TO IN VIVO STUDIES

N. Schleich, F. Danhier* and V. Préat*

Adapted from Journal of Controlled Release, 2014, 198C, 35-54

IV.1. INTRODUCTION

According to the American Cancer Society, approximately 1,6 millions new cancer cases are expected to be diagnosed in 2014 [2014]. Early detection and effective cancer treatments are the most important factors for saving lives [Fan et al., 2014]. Anti-cancer drugs suffer from poor pharmacokinetics and inappropriate biodistribution properties. Consequently, many agents that are shown to be highly effective *in vitro* become relatively ineffective when administered *in vivo* and produce significant toxicity [Lammers et al., 2010]. Numerous drug delivery systems have been designed to address these problems, specifically, nanomedicines, which refer to nano-scaled therapeutics that have been extensively studied. In particular, liposomes, nanoparticles, micelles and antibodies have been demonstrated to be clinically relevant for cancer therapy [Barenholz, 2012; Cecco et al., 2014; Oerlemans et al., 2010]. The first rationale for the use of nanomedicines for cancer therapy is the preferential delivery of nano-vectorized drugs to solid tumors due to enhanced permeability and retention (EPR) effect [Matsumura et al., 1986]. Tumor vessels surrounding the tumors are leaky due to abnormal basement membranes and incomplete endothelial linings, allowing nanomedicines to reach the tumor passively through the leaky vasculature. Therefore, the EPR effect enables higher local drug concentrations at the tumor site when the drug is delivered in a nanovector. The efficacy of *passive targeting* depends primarily on (i) the degree of tumor vascularization and angiogenesis, which is reliant on the tumor type and anatomical site and (ii) the high interstitial fluid pressure and heterogeneous blood flow, which limit drug uptake and homogenous distribution in the tumor [Danhier et al., 2010; Maeda et al., 2000]. Targeting can be improved by grafting ligands to the surface of the nanomedicines, allowing *active targeting* by binding to receptors that are overexpressed by cancer cells or angiogenic endothelial cells [Danhier et al., 2010; Petros et al., 2010]. One potential advantage of targeted delivery may be altered intracellular distribution. Both targeted and non-targeted systems arrive at the tumor via the EPR effect. Subsequently, the tumor cell internalization mechanism is enhanced by the presence of surface ligands [Prokop et al., 2008; Wang et al.,

2010]. It has been demonstrated that ligand-grafted nanoparticles enter cells via receptor-mediated endocytosis [13,14]. Nanomedicines can also enhance drug-circulation times, control drug-release kinetics and enable superior dose scheduling [Petros et al., 2010]. Nanomedicines avoid formulations that contain toxic excipients, which contribute to side effects for many conventional chemotherapeutics. Nanomedicines also may potentially overcome the development of tumor resistance to conventional chemotherapeutics [Jain et al., 2010]. Finally, nanomedicines allow the delivery of more than one therapeutic agent, facilitating combination therapies.

This review aims to provide an overview of the targeted SPIO-based nanotheranostics recently used in pre-clinical studies and the major obstacles to *in vivo* studies and clinical translation. In the first section of this review, we discuss personalized therapy as a biomedical application of theranostics. Then, we summarize the different imaging agents used for theranostic purposes, with a focus on SPIO. In the third section, we detail the recent advances in targeted SPIO-based nanotheranostics that have been used in pre-clinical studies. In the final sections, we discuss their limitations for *in vivo* studies, clinical translation and analyze the clinical perspectives of SPIO-based nanotheranostics.

IV.2. THERANOSTIC NANOMEDICINE

In addition to therapeutic applications, passively and actively targeted nanomedicines are also increasingly being used for diagnostic purposes. Antibodies, liposomes, nanoparticles and micelles may deliver a contrast agent, such as radionuclides and MR imaging probes, to detect cancer as well as visualize the drug delivery process [Lammers et al., 2010]. In addition to nanomedicines that are designed for therapeutic or diagnostic purposes, diagnostic (contrast agent) and therapeutic (anti-cancer drug) agents can be combined within a single multifunctional nanomedicine, known as “theranostic nanomedicine or nanotheranostics” (Figure 19 A). Based on the advances in and close collaboration between several different scientific disciplines, such as chemistry, biology, pharmacy, nanotechnology, medicine and imaging (Figure 19 B), numerous reports have shown that nanomedicine is one the most promising methods for theranostics, although theranostic development is still at an early stage [Ahmed et al., 2012; Lammers et al., 2010; Xie et al., 2010]. Theranostic design requires broad knowledge and a solid understanding of the detection and therapeutic mechanisms. This knowledge includes understanding the molecular mechanisms, diagnostic strategies,

therapeutic efficiency, toxicity, side-effects of materials and nanomedicine preparation techniques for the dual purposes of diagnosis and therapy [Ahmed et al., 2012].

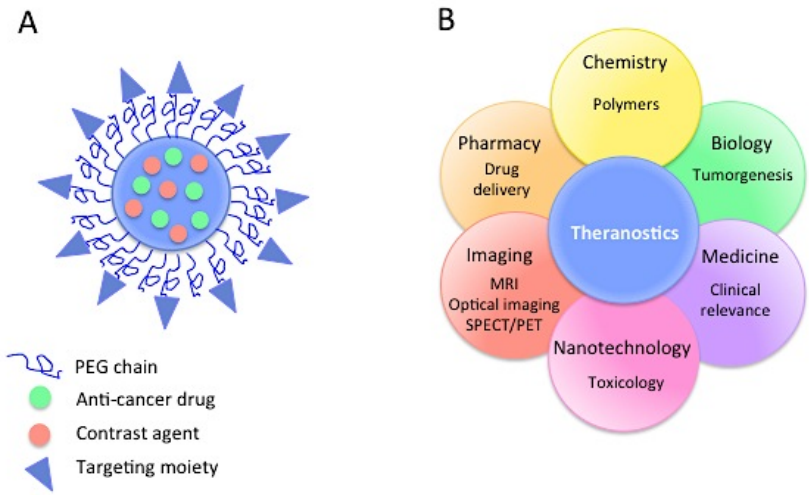

Figure 19. Theranostics. (A) Schematic representation of a theranostic multifunctional nanomedicine. (B) Schematic representation of the interdisciplinary field of theranostics, adapted from [Lammers et al., 2011].

The ideal theranostic nanoparticle should possess several advantageous properties: (i) the ability for selective tumor accumulation, (ii) the capacity to deliver therapeutic doses of anti-cancer drugs and to detect tumors at their earliest stage and (iii) the nanovector must be biocompatible and biodegradable [Fan et al., 2014].

Nanotheranostics can be used for various applications: (i) non-invasive assessment of biodistribution and target site accumulation, (ii) drug release monitoring, (iii) the enhancement of therapeutic efficacy via triggered drug release and (iv) prediction of therapeutic response [Lammers et al., 2010]. Additionally, nanotheranostics can be used to preselect patients, leading to their significant potential for personalized nanomedicine (chemo-) therapeutic interventions. Theranostic strategies include situations where patients are pre-selected based on data from initial target site accumulation studies.

It is important to note that theranostics take their place in its broadest sense. Many publications claim that theranostics can be used for simultaneous diagnosis and treatment. Actually, their suitability for real diagnoses is questionable. The diagnostic purpose of theranostics should not refer to the identification, localization and/or staging of tumors, but to the pre-selection of patients, prediction of potential therapeutic responses, and/or longitudinal monitoring of treatment efficacy [Rizzo et al., 2013]. As exemplified in Figure 20, the first step toward personalized nanomedicine treatment is to pre-select patients on the basis of non-

invasive imaging data examining target site accumulation. If the tumor accumulation is sufficient, patients can be treated with the nanotheranostics, whereas other patients will receive conventional chemotherapy or another intervention. A second personalization step consists of non-invasive monitoring of the response to the first 1 to 3 treatment cycles. During this monitoring, the treatment should be adapted or switched to other therapeutic interventions, if necessary [Lammers et al., 2012b; Rizzo et al., 2013].

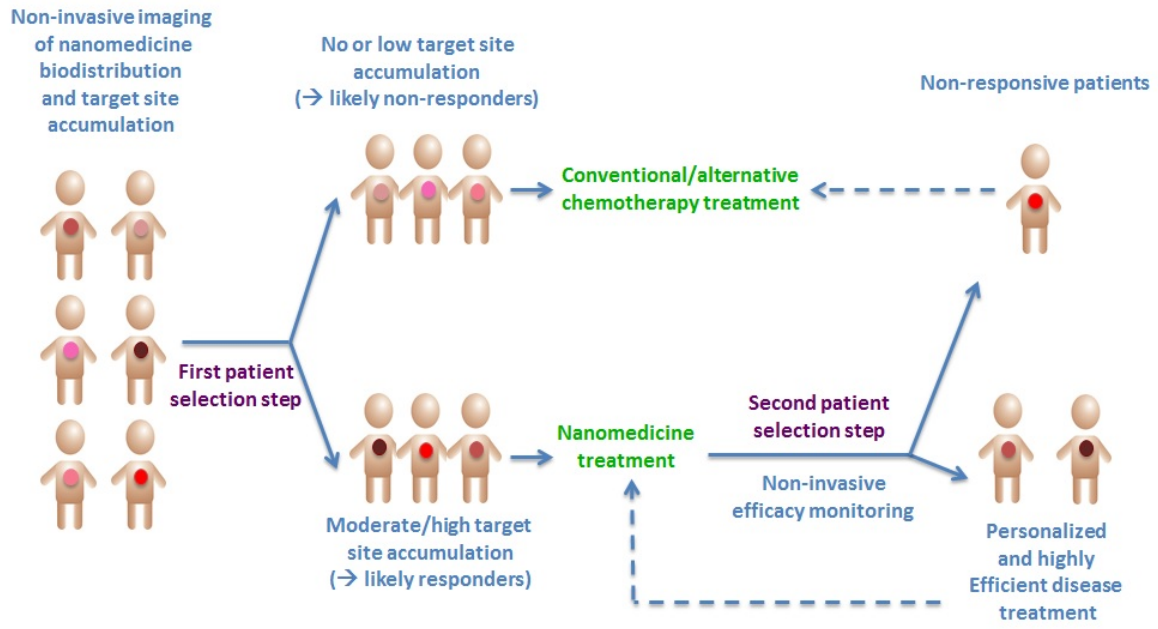

Figure 20. Schematic representation of the rationale for image-guided and personalized nanomedicine (adapted from [Lammers et al., 2012b]).

IV.3. CONTRAST AGENTS AND SPIO

IV.3.1. Imaging techniques and contrast agents for theranostics

The diagnostic aspect of theranostics primarily revolves around imaging mechanisms using different contrast agents. The most commonly used imaging techniques are positron emission tomography (PET), single photon emission computed tomography (SPECT), magnetic resonance imaging (MRI) and different optical imaging techniques (bioluminescence and fluorescence) that have high sensitivity [Danhier et al., 2012b]. Among these techniques, MRI is the most commonly studied technique and a considerable amount of research has been devoted to the use of magnetic particles as contrast agents. Particles of gadolinium, iron oxides, gold, silver and other metals are currently being investigated. The imaging aspect of theranostics can also be exemplified by manganese oxide, quantum dots, microbubbles, radionuclides and silica nanoparticles [Ahmed et al., 2012]. Examples of theranostics using

different contrast agents are presented in Table 7. In this review, we only focus on iron oxides as contrast agents.

Table 7. Examples of currently developed theranostics using different contrast agents for anti-cancer applications.

Contrast agent	Anti-cancer drug	Formulation	Applications	Studies	Ref
Iron oxide	DOX	Polymeric nanoparticles	MRI, CT, PET, therapy	*in vitro, in vivo*	[Maeng et al., 2010; Yang et al., 2011]
Gadolinium	DOX	Liposomes/Silica nanotubes	MRI	*in vitro*	[de Smet et al., 2010; Hu et al., 2010]
Manganese	DNA, DOX	Lipid Micelles	MRI, therapy	*in vitro, preliminary in vivo*	[Howell et al., 2013]
Gold	PTX	Gold nanoparticles	Optical imaging	*in vitro*	[Heo et al., 2012]
Silica	siRNA	Silica nanoparticles	Optical imaging, therapy	*in vitro, in vivo*	[Shen et al., 2014]
QDs	DOX	Lipid Micelles	MRI, optical imaging, therapy	*in vitro, in vivo*	[Park et al., 2008b]
Silver	Silver	Silver nanoparticles	Optical imaging, therapy	*in vitro*	[Mukherjee et al., 2014]
Perfluoro-pentane	DOX	Microbubbles	Ultrasound, therapy	*in vitro, in vivo*	[Gao et al., 2008]
CNT	Intrinsic property	Carbon nanotubes	Optical imaging	*in vitro, in vivo*	[Robinson et al., 2010]
^{99m}Tc	^{90}Y	Polymer conjugates	Scintigraphic imaging, therapy	*in vitro, in vivo*	[Mitra et al., 2004]

Abbreviations: CNT: carbon nanotube; CT: computer tomography; DNA: Deoxyribonucleic acid; DOX: doxorubicin; MRI: magnetic resonance imaging; PET: positron emission tomography, PTX: paclitaxel; siRNA: short interfering ribonucleic acid; QDs: quantum dots;

IV.3.2. Iron oxides

Superparamagnetic iron oxide (SPIO) nanoparticles are contrast agents that have a variety of applications in molecular and cellular MRI. Superparamagnetic nanoparticles are composed of iron oxides, i.e., magnetite (Fe_3O_4), maghemite (Fe_2O_3) or other ferrites. Their given name originates from their ability to exhibit "superparamagnetism". This property allows SPIO to

be magnetized upon external magnetic field application without exhibiting any residual magnetic interactions after magnetic field removal [Corot et al., 2013]. SPIO are prepared using several different methods, including micro-emulsion, thermal decomposition and co-precipitation. Among these methods, the classical iron salt co-precipitation technique is the most commonly used procedure. This method is based on the precipitation of ferrous (Fe^{2+}) and ferric (Fe^{3+}) salt mixtures in a basic medium to form Fe_3O_4 [Laurent et al., 2011; Laurent et al., 2014; Reddy et al., 2012]. To avoid aggregation and prevent surface oxidation, which are crucial for their clinical use, it is necessary to coat the synthetized SPIOs. SPIO have been coated with a wide variety of materials. Among the coating agents usually used, the most common are biocompatible polymers (dextran and its derivatives, siloxane, poly(ethylene glycol), poly(lactic acid), poly(ε-caprolactone), chitosan), inorganic materials (gold and silica) and monomeric stabilizers (carboxylates, phosphates) [Laurent et al., 2011; Laurent et al., 2014; Santhosh et al., 2013].

SPIO are primarily used because of their negative enhancement effect on T_2 and T_2*-weighted sequences [Corot et al., 2013]. However, their effects on T_1 relaxation time are also employed. Different classes of superparamagnetic nanoparticles have been investigated and are classified by their particle size: SPIO (>50 nm), ultra-small superparamagnetic iron oxide (USPIO) (<50 nm) and micron size iron oxide particles (MPIO) (≈ 1000 nm) [Laurent et al., 2011]. SPIO provide significant advantages over traditional contrast agents: (i) high magnetic signal strength, (ii) relatively low cytotoxicity, (iii) longer lasting contrast enhancement, (iv) improved tumor margin delineation and (v) low sensitivity to the number of surrounding water molecules. Additionally, studies have shown that the released iron from SPIO is metabolized by the body, reducing the potential for long-term cytotoxicity [Laurent et al., 2011; Laurent et al., 2014; Rosen et al., 2012].

After intravenous injection, nanoparticles are usually taken up by macrophages in the liver (Kupffer cells), spleen and bone marrow. Limiting phagocytosis in the liver and spleen decreases the uptake rates for some nanoparticles, resulting in longer blood half-lives and facilitating their clinical application as T_2 agents for the detection of liver lesions. Ferumoxides (Endorem®, in Europe or Ferridex® in the United States) and ferucarbotran (Resovist®) have been marketed for this application. However, with the exception of Resovist® in Japan, these two products have been withdrawn from the market after several years of commercialization due to their limited use by radiologists [Corot et al., 2013]. Radiologists consider SPIOs to be negative contrast agents and, consequently, they produce

image contrasts that are more difficult to interpret compared with a positive contrast agent, resulting in hyperintense signals in MRI.

SPIOs can also be used for drug delivery. A drug can be either directly conjugated to the SPIO surface via a covalent link or entrapped in the SPIO coating shell via physical interactions, leading to "SPIO conjugates" [Zou et al., 2010]. However, these strategies suffer from several disadvantages. The drug coating entrapment strategy results in low entrapment efficiency and covalent binding often results in stable linkages that lead to release failures [Wahajuddin et al., 2012]. Another common strategy uses SPIO and drug encapsulation in nanocarriers [Brooks et al., 1994]. This strategy overcomes low efficiency entrapment and offers controlled release of the encapsulated drug. Moreover, SPIO encapsulation in a nanocarrier generally provides optimum magnetic responsiveness [Wahajuddin et al., 2012].

IV.4. PRE-CLINICAL STUDIES OF SPIO-LOADED THERANOSTICS

To improve the pharmacokinetic profile and limiting toxicities associated with conventional treatments, there have been considerable efforts focused on developing targeted drug delivery systems. Consequently, various strategies have been extensively studied during the past decades. These strategies involve (i) passive targeting via the EPR effect, (ii) active targeting involving ligand-mediated targeting and (iii) triggered targeting based on the release of the drug carrier contents in response to a stimulus [Arias, 2011; Lammers et al., 2008; Torchilin, 2004]. These strategies are schematically represented in Figure 21. This review will provide an overview of the different targeting strategies that have been used to improve SPIO-based theranostic delivery because SPIO-based diagnostic agents have been extensively reviewed in the literature [Corot et al., 2013; Peng et al., 2008].

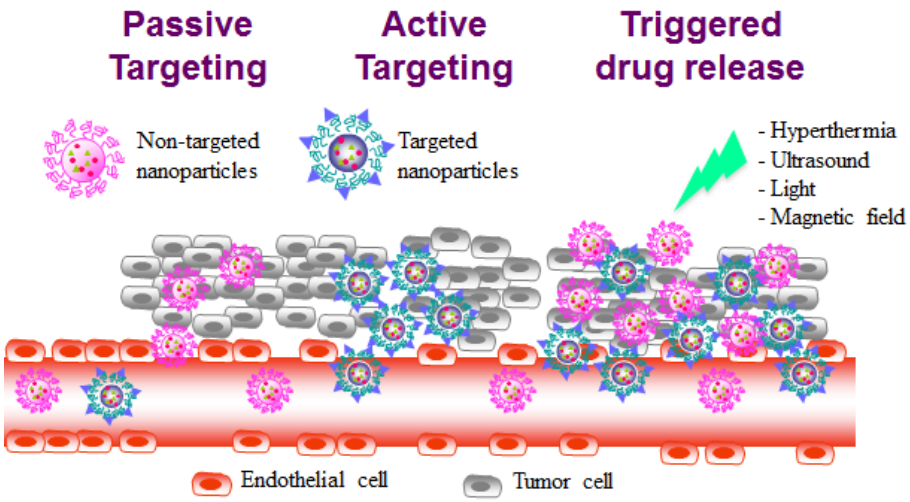

Figure 21. Schematic representation of the different targeting strategies. (i) Passive targeting is based on the so-called enhanced permeability and retention effect (EPR effect) in which nanoparticles can passively enter the interstitium through the leaky vasculature. (ii) Active targeting relies on molecular recognition of a ligand coupled to nanoparticles surface and its receptor at the target cell site. (iii) Triggered drug release refers to the use of stimuli-sensitive carrier materials to trigger drug delivery at the target site. Those externally or internally applied stimuli cover, e.g. hyperthermia, ultrasound, lights and magnetic field.

IV.4.1. Passive targeting

Passive targeting relies on the passive accumulation of the nanovector in the tumor tissue through the leaky vasculature of neo-angiogenic vessels, which is referred to as the EPR effect [Matsumura et al., 1986]. To date, this is the most extensively used targeting strategy for nanotheranostics. Table 8 provides a non-exhaustive list of recent examples of passively targeted SPIO-based theranostics in pre-clinical studies.

Table 8: Examples of passively targeted SPIO-based theranostics in pre-clinical studies.

Formulation	Drug	Cell line	*In vitro/ In vivo MRI*	Results	Ref
PLGA NP	PTX	CT-26	*In vitro*	High tumor regrowth delay, high relaxivity	[Schleich et al., 2013]
PLGA NP	DTXL	PC3	*In vitro*	Effective cellular uptake, good relaxivity	[Ling et al., 2011]
PLGA NP	TMZ	C6 glioma	*In vitro*	Good antiproliferative activity and relaxivity	[Ling et al., 2012]
Silica sphere	curcumin	HL-60	*In vitro*	Time-dependent induction of apoptosis	[Chen et al., 2010]
Silica sphere	DOX	MCF-7	*In vitro* *In vivo*	*In vitro* cytotoxicity and *in vivo* MRI	[Kim et al., 2008]
SPIO-conjugate	MTT	9 L glioma	*In vitro*	*In vitro* cytotoxicity, *in vitro* T2 contrast enhancement MRI	[Kohler et al., 2006]
Polyplex	DNA	HeLa	*In vitro*	Monitoring of DNA release with MRI	[Park et al., 2008a]

Abbreviations: DOX= doxorubicin, DTXL = docetaxel, MTT = methotrexate, NP = nanoparticles, PLGA = poly(lactic-co-glycolide), PT = passive targeting, PTX= paclitaxel, TMZ = temozolomide.

For example, Schleich *et al.* developed dual paclitaxel (PTX)/SPIO loaded PLGA-based nanoparticles for cancer therapy and imaging [Schleich et al., 2013]. They demonstrated the efficiency of the nanoparticles for cellular uptake and MRI contrast enhancement *in vitro* and *in vivo* as an anti-cancer treatment in CT-26 bearing mice. Similarly, Ling *et al.* developed dual docetaxel/SPIO-loaded PLGA-based nanoparticles and demonstrated their efficient *in vitro* cellular uptake, drug release and MRI contrast enhancement in a prostate cancer cell line [Ling et al., 2011]. The same group developed temozolomide/SPIO-loaded PLGA nanoparticles for the imaging and treatment of malignant gliomas and demonstrated their *in vitro* efficacy for cellular uptake, cytotoxicity and MRI contrast enhancement [Ling et al., 2012]. Another example of passively targeted SPIO-based nanotheranostic is provided by Chen *et al.* [Chen et al., 2010]. They developed inorganic silica spheres loaded with SPIO and curcumin as the anti-cancer agent that were further functionalized using gold nanoparticles. These curcumin/SPIO-loaded silica spheres produced a significant time-dependent induction of apoptosis in HL-60 cells (human leukemia cells) and *in vitro* MRI contrast enhancement. Similarly, Kim *et al.* developed PEGylated mesoporous silica materials loaded with both doxorubicin (DOX) and a single SPIO nanocrystal core. These nanoparticles demonstrated DOX-induced toxicity *in vitro* and *in vivo* efficacy as an MRI contrast agent [Kim et al., 2008]. In addition to SPIO-loaded nanotheranostics, Kohler et al. developed a methotrexate-SPIO conjugate (MTT-SPIO), which demonstrated higher *in vitro* anti-tumor efficacy compared with free MTT and significant *in vitro* MRI contrast enhancement in 9 L cultured glioma cells [Kohler et al., 2006]. Finally, Park *et al.* developed a gene delivery-based therapy using a SPIO polyplex in HeLa human cervical tumor cells [Park et al., 2008a]. This *in vitro* study demonstrated that MRI could be a sensitive tool for assessing gene delivery via DNA release from the SPIO-Polyethylene imine (PEI) polyplex, based on the "T_2-magnetic relaxation switch effect" (Figure 22). When packaged with DNA, the particles had an increased T_2 relaxation time, whereas a decrease in T_2 relaxation time was observed when the DNA was released. This phenomenon may be exploited to monitor DNA release using MR imaging.

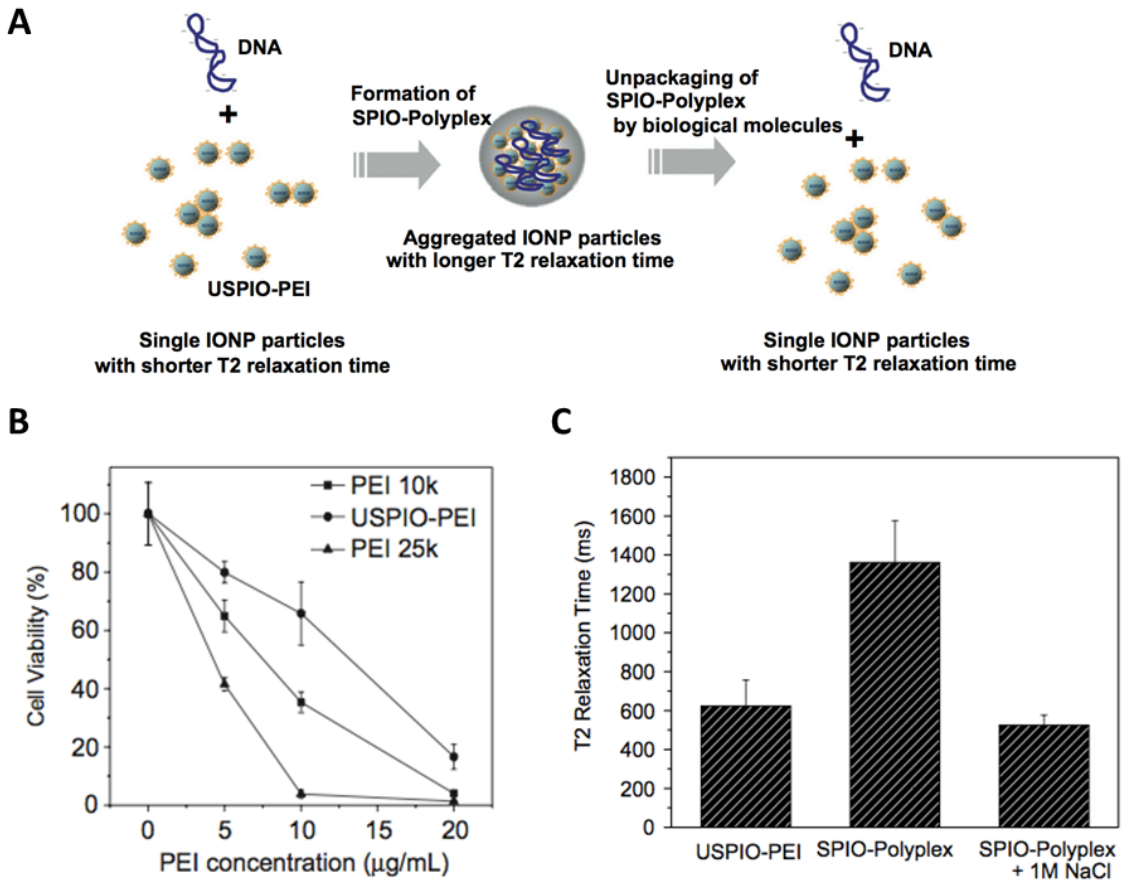

Figure 22. (A) Schematic representation of T_2 magnetic relaxation switch caused by USPIO-PEI condensation with nucleic acids to form a SPIO-polyplex and subsequent unpackaging of the SPIO-polyplex and DNA release. **(B)** *in vitro* toxicity of USPIO-PEI compared with PEI 10k and PEI 25k. Cell viability was determined using the Cell Titer 96 proliferation assay (Promega) 24 h after incubation with polymers. **(C)** T_2 relaxation times of uncomplexed USPIO-PEI, SPIO-polyplex and unpackaged SPIO-polyplex. SPIO-polyplex was unpackaged by the addition of 1 M NaCl. The USPIO concentration in all samples remained constant (adapted from [Park et al., 2008a]).

IV.4.2. Active targeting

Passive targeting has several disadvantages. Specifically, the accumulation resulting from the EPR effect may not be sufficient to induce high intracellular uptake. Therefore, ligand-mediated drug delivery appears to be a powerful tool for overcoming this problem. Passively targeted nanomedicines primarily rely on macropinocytosis for cellular uptake. Conversely, the molecular recognition of a ligand coupled to the nanomedicine surface promotes cellular entry via receptor mediated endocytosis, resulting in enhanced nanovector cellular uptake [Arias, 2011; Cole et al., 2011]. Therefore, the introduction of targeting ligands should increase both drug and contrast agent concentrations in the target-site, resulting in improved anti-tumor activity, reduced toxicity and increased target-to-background contrast during imaging [Kelkar et al., 2011]. In addition to targeting tumor cells directly, nanomedicine can

be directed against neoangiogenic endothelial cells, resulting in subsequent tumor cell death due to oxygen and nutrient deprivation [Danhier et al., 2012b; Folkman, 1971]. Table 9 provides an overview of selected recent examples of actively targeted SPIO-based theranostics in pre-clinical studies.

Table 9. Non-exhaustive examples of actively targeted SPIO-based theranostics in pre-clinical studies.

Formulation	Drug	Functional molecules	Cell line	*In vitro/ In vivo MRI*	Results	Ref
PEG-PCL micelles	DOX	FA	Bel7402	*In vitro*	2.5x higher intracellular accumulation	[Hong et al., 2008]
Wormlike polymer vesicles	DOX	FA	HeLa	*In vitro*	Higher relaxivities compared to Feridex	[Yang et al., 2010]
Silica sphere	PTX/CMPT	FA	PANC-1 and BxPC3 (pancreatic)	*In vitro*	Increased cellular uptake, high relaxivities *in vitro*	[Liong et al., 2008]
SPIO-conjugate	MTT	FA	MCF-7 HeLa	_	In vitro anti-cancer efficacy, Higher internalization compared to the non-targeted SPIO	[Kohler et al., 2005]
Polymeric micelles	DOX	cRGD	SLK (Kaposi's sarcoma)	*In vitro*	Increased cytotoxicity, cellular uptake, relaxivity	[Nasongkla et al., 2006]
Polymeric NP	fumagillin	cRGD, peptido-mimetics	MDA-435	*In vitro In vivo*	Effective angiogenesis MRI, good anti-angiogenic efficacy	[Schmieder et al., 2008]
Polymeric micelles	DOX	LCP	H-2009	*In vitro*	3x increased cellular uptake, high relaxivity	[Guthi et al., 2010]
SPIO conjugates	DOX, ADOX	HuCC49ΔCH2 (anti-TAG-72 antibody)	LS174T A375	*In vitro*	Increased cancer cell targeting, decreased T2 values in *in vitro* MRI, lower IC50 compared to non-specific targeted SPIO	[Zou et al., 2010]

Abbreviations: ADOX = azido-doxorubicin, AT = active targeting, CMPT = camptothecin, DOX= doxorubicin, FA= folate, LCP = lung cancer targeting peptide, MTT = methotrexate, PCL = poly(ε-caprolactone), PEG = poly(ethyleneglycol), TAG-72 = tumor-associated glycoprotein-72

A popular targeting ligand for cancer cells is folate (FA). The folate receptor is a high-affinity, glycosylphosphatidylinositol-anchored protein. Because FA is vital for rapid proliferation, the folate receptor is overexpressed in many tumor types and is highly restricted in healthy tissues. Therefore, FA-conjugates and FA-grafted nanocarriers have been

intensively investigated for both drug delivery and imaging [Shan, 2004]. For example, Hong *et al.* reported the development of SPIO/DOX-loaded PEG-PCL micelles functionalized with folate on their surface (attached to the PEG chain) [Hong et al., 2008]. *In vitro* intracellular accumulation studies demonstrated a 2.5 higher concentration of folate-functionalized micelles compared with non-functionalized micelles in Bel 7402 cells (human hepatic carcinoma cells). Similarly, Yang *et al.* developed SPIO/DOX-loaded wormlike polymer vesicles grafted with FA and tested their magnetic properties in HeLa cells (Figure 23) [Yang et al., 2010]. These theranostic particles displayed higher relaxivities compared with the commercial form Feridex® and improved antitumor efficacy compared with non-functionalized vesicles *in vitro*. However, their theranostic system was not as effective as free doxorubicin. Additionally, Liong *et al.* developed multifunctional inorganic nanoparticles for combined imaging and drug delivery comprised of mesoporous silica nanoparticles containing SPIO and PTX or camptothecin (CMPT) that were functionalized with FA on their surface [Liong et al., 2008]. Finally, Kohler et al. developed MTT-SPIO conjugates as a simultaneous MRI contrast agent and anti-cancer therapy [Kohler et al., 2005]. The conjugate was comprised of iron oxide nanoparticles covalently bound to MTT, a chemotherapeutic drug that can target multiple cancer cells that overexpress folate receptors. The nanoparticles were first surface-modified with (3-aminopropyl)trimethoxysilane to form a self-assembled monolayer and were subsequently conjugated with MTT via amidation between the carboxylic acid end groups on MTT and the amine groups on the particle surface. The authors demonstrated the nanocomposite *in vitro* anti-cancer efficacy using cellular viability studies in human breast cancer cells (MCF-7) and human cervical cancer cells (HeLa). However, they did not assess the imaging ability of the developed theranostic.

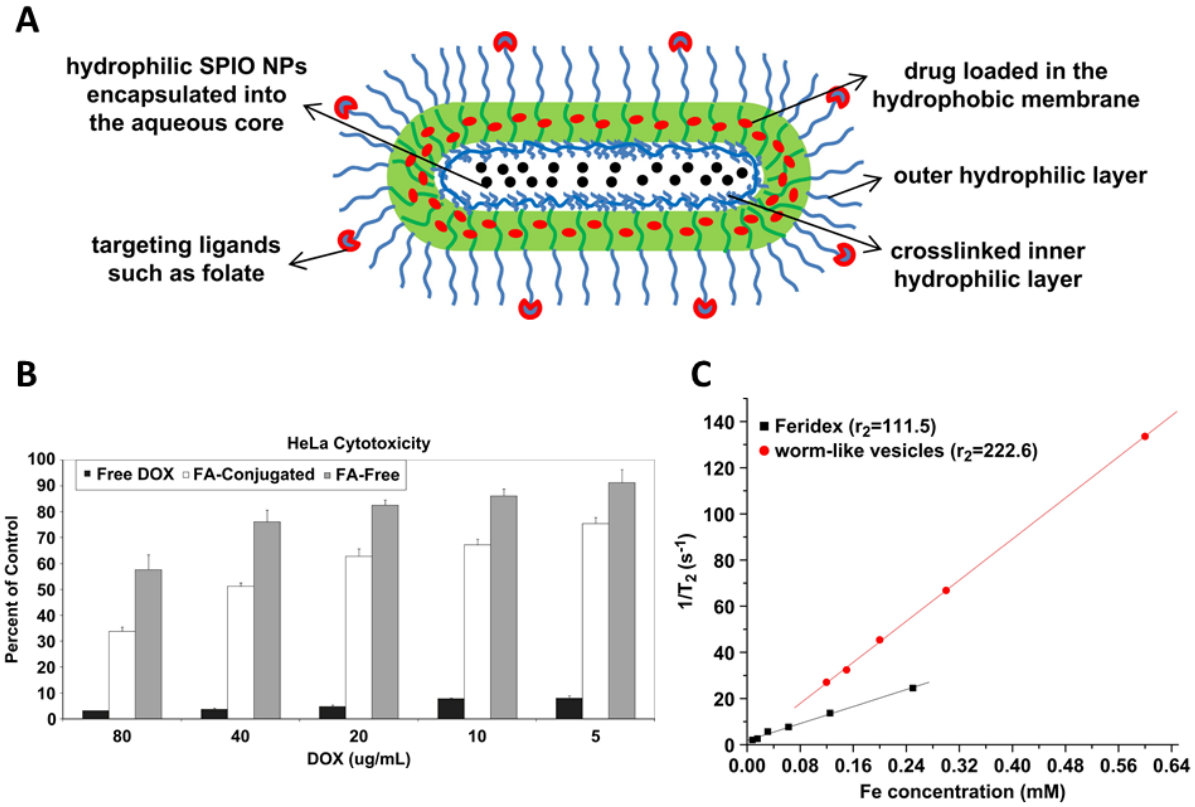

Figure 23. (A) Illustration of the tumor-targeting multifunctional wormlike polymer vesicles formed by triblock copolymers for targeted cancer chemotherapy and imaging; **(B)** Cytotoxicity of free DOX, FA-free and FA-conjugated SPIO/DOX-loaded wormlike polymer vesicles with crosslinked inner hydrophilic PEG layers against HeLa cells at different DOX concentrations (incubation time 48 h); **(C)** T_2 relaxation rates ($1/T_2$, s^{-1}) as a function of iron concentration (mM) for Feridex® and FA-conjugated SPIO/DOX-loaded wormlike polymer vesicles with cross- linked inner hydrophilic PEG layers (adapted from [Yang et al., 2010]).

Another interesting target in cancer therapy is the well-known α_v integrin family. In the integrin family, $\alpha_v\beta_3$ is the most extensively studied because of its strong implication in angiogenesis regulation. Interestingly, integrin $\alpha_v\beta_3$ has been shown to be overexpressed on both neoangiogenic endothelial cells and on the surface of many tumor cell types [Brooks et al., 1994; Danhier et al., 2012b]. Therefore, targeting $\alpha_v\beta_3$ with SPIO-based theranostics may provide interesting insights into angiogenesis using MRI as well as effective tumor cell killing by both indirect (inducing tumor cell death as a consequence of nutrient and oxygen deprivation by killing neoangiogenic endothelial cells) and direct killing of tumor cells expressing $\alpha_v\beta_3$. For this purpose, Nasongkla *et al.* developed multifunctional polymeric micelles loaded with DOX and SPIO functionalized with cRGD [Nasongkla et al., 2006]. The RGD tripeptide sequence has been shown to efficiently bind to $\alpha_v\beta_3$ integrin [Danhier et al., 2012b; Temming et al., 2005]. Similarly, Schmieder *et al.* demonstrated the ability of RGD functionalized fumagillin- (an anti-angiogenic agent) loaded SPIO nanoparticles to improve

drug delivery and angiogenesis imaging in MDA-435 cells [Schmieder et al., 2008]. Guthi *et al.* reported LCP (lung cancer targeting peptide) functionalized multifunctional micelles for targeting $\alpha_v\beta_6$ [Guthi et al., 2010]. These DOX/SPIO-loaded micelles displayed high T_2 relaxivity, increased cytotoxicity and MRI capacity *in vitro*. Finally, Zou *et al.* developed antibody- and fluorescence-SPIO conjugates for MRI and fluorescence cancer cell imaging. DOX and azido-DOX were entrapped into an oleic acid shell coating [Zou et al., 2010]. These conjugates had increased cancer cell targeting, lower IC50 compared with non-specific targeted SPIOs and decreased T_2 values in *in vitro* MRI.

IV.4.3. Triggered drug release

Triggered drug release is a commonly used term to refer to systems designed to release their contents or react upon exposure to internal or external stimuli. The stimuli can either be internal (change in pH or temperature in certain tissues or disease stages) or external (magnetic, electric fields, light, ultrasound, etc.) [Arias, 2011; Egusquiaguirre et al., 2012]. Table 10 presents a non-exhaustive list of triggered-targeted SPIO-based nanotheranostics in pre-clinical studies.

Table 10. Examples of triggered-targeted SPIO-based nanothernanostics in pre-clinical studies.

Formulation	Targeting Type	Drug	Targeting molecules	Cell line	*In vitro/ In vivo MRI*	Results	Ref
PEALCa micelles	pH-triggered	PTX	_	CRC LoVo	*In vitro*	Suppression of cell growth *in vivo* and *in vitro* MRI of delivery	[Feng et al., 2014]
Polymeric micelles	pH-triggered	DOX	FA	Bel-7402	*In vitro*	Enhanced specific drug delivery and MRI diagnosis	[Li et al., 2013a]
β-cyclodextrin-pluronic coated SPIO NP	HT	curcumin	_	A12780CP PC-3 MDA-MB-231	*In vitro*	Higher hyperthermia effects over time, improved therapeutic effects	[Yallapu et al., 2011]
PLGA-PEG NP	HT + AT	SPIO	Anti-EGRF Mab	A-431	*NA*	Decreased tumor size after HT with high tumor accumulation (scintigraphy)	[Baldi et al., 2014]
CHC microbubbles	US	CPT	_	MDA-MB-231	*In vitro In vivo*	More significant transcellular delivery and cytotoxicity	[Yang et al., 2014d]
Squalene based nanoplatform	MT	GEM	_	L1210	*In vitro In vivo*	T2-weighted images of anti-tumor efficacy	[Arias et al., 2011]
SPIO conjugates	MT	EPI	_	MGH-U1 and MGH-U1R	*In vitro In vivo*	10x increase in tumor accumulation, good MRI contrast agents	[Yang et al., 2012]
SPIO conjugates	MT	MTX	_	VX-2	*In vitro In vivo*	Effective anti-cancer activity, MRI to assess tumor accumulation	[Alexiou et al., 2000]

Abbreviations: CHC = carboxymethyl hexanoyl chitosan, CPT = camptothecin, DOX= doxorubicin, EPI = epirubicin, GEM = gemcitabin, FA= folate, (F)US = (focused) ultrasound, HT = Hyperthermia, MT = magnetic targeting, MTX = mitoxantrone, Ref = references

Acid triggered drug release

Acid triggered drug release is based upon the particular microenvironment in tumor tissues characterized by a slightly more acidic pH compared with physiological pH (pH 5 - 6.5 compared to 7.3 in physiological conditions) [Gullotti et al., 2009]. Several research groups have used this characteristic to develop a labile link between the drug and carrier or labile self-assembling micelles to provide tumor specific drug release. For example, Feng *et al.* recently developed polyethylene glycol (PEG), poly (N-(N', N'-diisopropylaminoethyl) aspartamide) (P(Asp-DIP)) and poly (lysine-cholic acid) (P(Lys-Ca)) (PEALCa) micelles loaded with SPIO and PTX for cancer therapy [Feng et al., 2014]. In physiological conditions, the polymers organize themselves to form micelles with the hydrophobic drug and hydrophilic SPIO loaded in the core, whereas at a lower pH, the pH-sensitive P(Asp-DIP) interlayer undergoes a hydrophobic-hydrophilic transition leading to micelle destabilization and content release. The authors reported that these micelles effectively suppressed human

colorectal carcinoma LoVo cell growth *in vivo* and effective delivered the micelles for MRI *in vivo*. Similarly, Li *et al.* studied acid-triggered core cross-linked nanomicelles loaded with DOX and SPIO for drug delivery and magnetic resonance imaging in liver cancer cells [Li et al., 2013a]. These micelles were comprised of folate-poly(ethylene glycol)-b-poly[N-(N',N'-diisopropylaminoethyl) (DIP) glutamic acid (GA)] (folated-PEG-P[GA-DIP]) amphiphilic block copolymers. DIP was grafted to ~50% of the poly(L-glutamic acid) (PGA)'s carboxyl groups for nanomicelle stability. Micelle stability is ensured by the ionic interaction between the electronegative carboxylic function of non-grafted PGA (COO-) and the positively charged, namely N,N-diisopropyl, tertiary amine group. In acidic conditions (e.g., endosome, lysosome), the carboxylic groups are protonated, resulting in a weaker interaction between the two polymers and drug release (Figure 24 A). The authors demonstrated the micelle efficacy as a contrast agent for MRI *in vitro* and assessed in vitro cellular uptake (Figure 24 B-C).

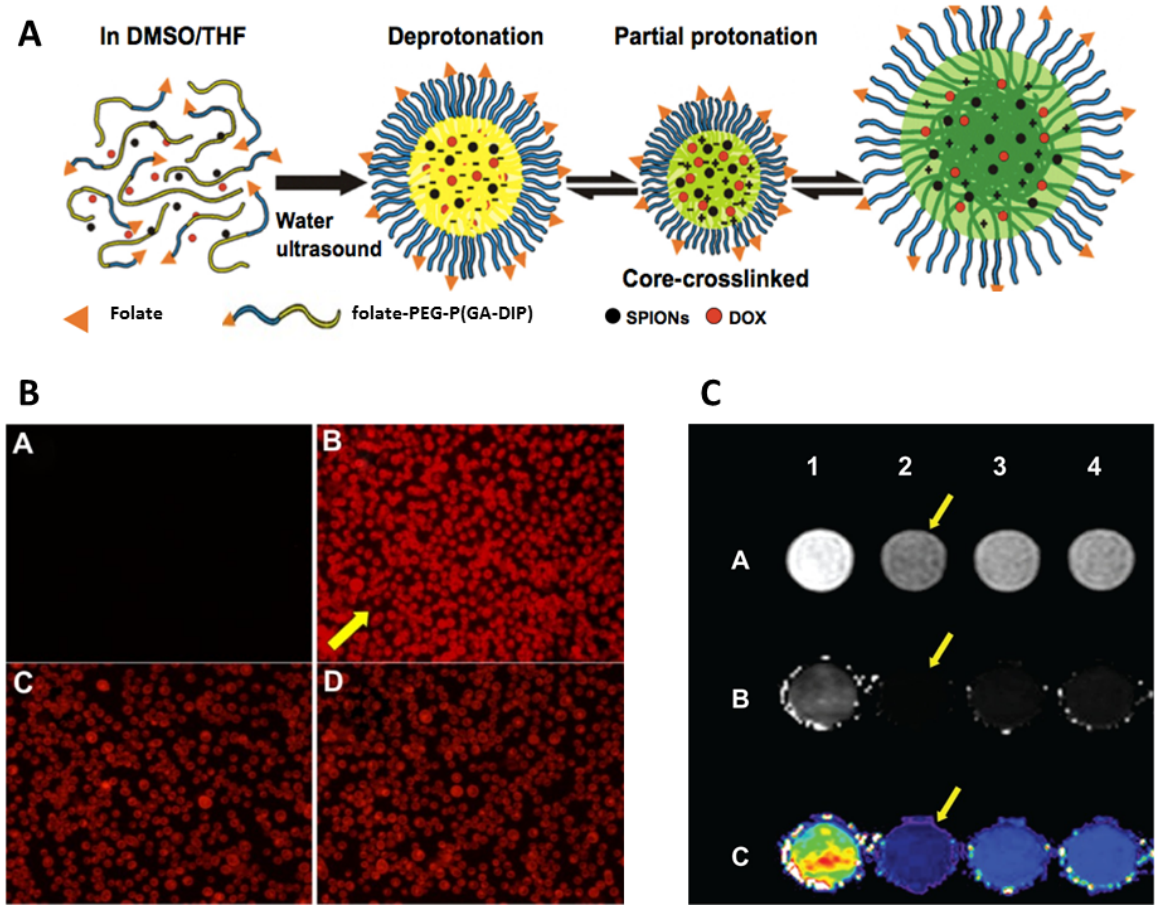

Figure 24. Acid-triggered self-assembly of folate-PEG-P(GA-DIP) nanomicelles loaded with DOX and SPIO. **(A)** Schematic representation of nanomicelle assembly following medium acidification. **(B)** *In vitro* cellular uptake. Bel-7402 cells were incubated with different samples. Arrow: clear DOX fluorescence in targeted group. (A) PBS control; (B) Targeted group: folate-PEG-P(GA-DIP); (C) Non-targeted group: PEG-P(GA-DIP); (D) The competitive inhibition group: folate-PEG-P(GA- DIP) and 1 mM free folic acid. **(C)** *In vitro* MRI. T_2-weighted (A), T_2-mapping (B), and colored (C) T_2-mapping images. (1) Gelatin contrast of cells not incubated with micelles; (2) Targeted group: folate-PEG-P(GA-DIP); (3) Non-targeted group: PEG-P(GA-DIP); (4) Competitive inhibition group: folate- PEG-P(GA-DIP) micelles with 1 mM free folic acid. Arrow: clear decreased signal in targeted group (adapted from[Li et al., 2013a].

Abbreviations: DOX, doxorubicin; DMSO, dimethyl sulfoxide; folate-PEG-P(GA-DIP), folate-poly(ethylene glycol)-b-poly[N-(N',N'-diisopropylaminoethyl) glutamine]; SPIONs, superparamagnetic iron oxide nanoparticles; THF, tetrahydrofuran.

Hyperthermia

The majority or cancer tissues have been shown to have higher heat-sensitivity compared with normal tissue. Therefore, hyperthermia can be used in cancer therapies to destroy pathological cells. Moreover, SPIOs have been shown to react after the application of an alternating magnetic field (AMF) by absorbing this energy and converting it into heat. This generated heat can subsequently be used to destroy cancer cells [Cole et al., 2011; Laurent et al., 2011]. Multiple encouraging preclinical data led to the first clinical trials in 2007, which were conducted by two groups, Johansen and colleagues and Maier-Hauff and colleges, using aminosilane-coated SPIO in patients with locally recurrent prostate cancer and glioblastoma multiform, respectively [Johannsen et al., 2005; Maier-Hauff et al., 2011]. After those clinical trials, numerous SPIO-loaded theranostics have been used in hyperthermia-based pre-clinical studies.

This strategy has been successfully applied by Yallapu *et al.* using β-cyclodextrin-pluronic coated SPIO nanoparticles [Yallapu et al., 2011]. Magnetic nanoparticles loaded with curcumin had promising results for hyperthermia and MRI in ovarian, breast and prostate cancer cells. More recently, an elegant study performed by Baldi *et al.* demonstrated the efficacy of anti-human epidermal growth factor receptor (EGFR)-targeted and ^{99m}Tc functionalized PLGA-PEG nanoparticles loaded with SPIO (Figure 25 A) for both hyperthermia tumor regression (Figure 25 B) and *in vivo* imaging capacity using PET (Figure 25 C) [Baldi et al., 2014]. The tumor site was clearly visible in the PET images, indicating nanosystem accumulation. However, substantial liver accumulation was observed (Figure 25 C). A substantial decrease in tumor size was correlated with an increase in nanoparticle accumulation resulting from the EGFR-targeting moieties and local temperature.

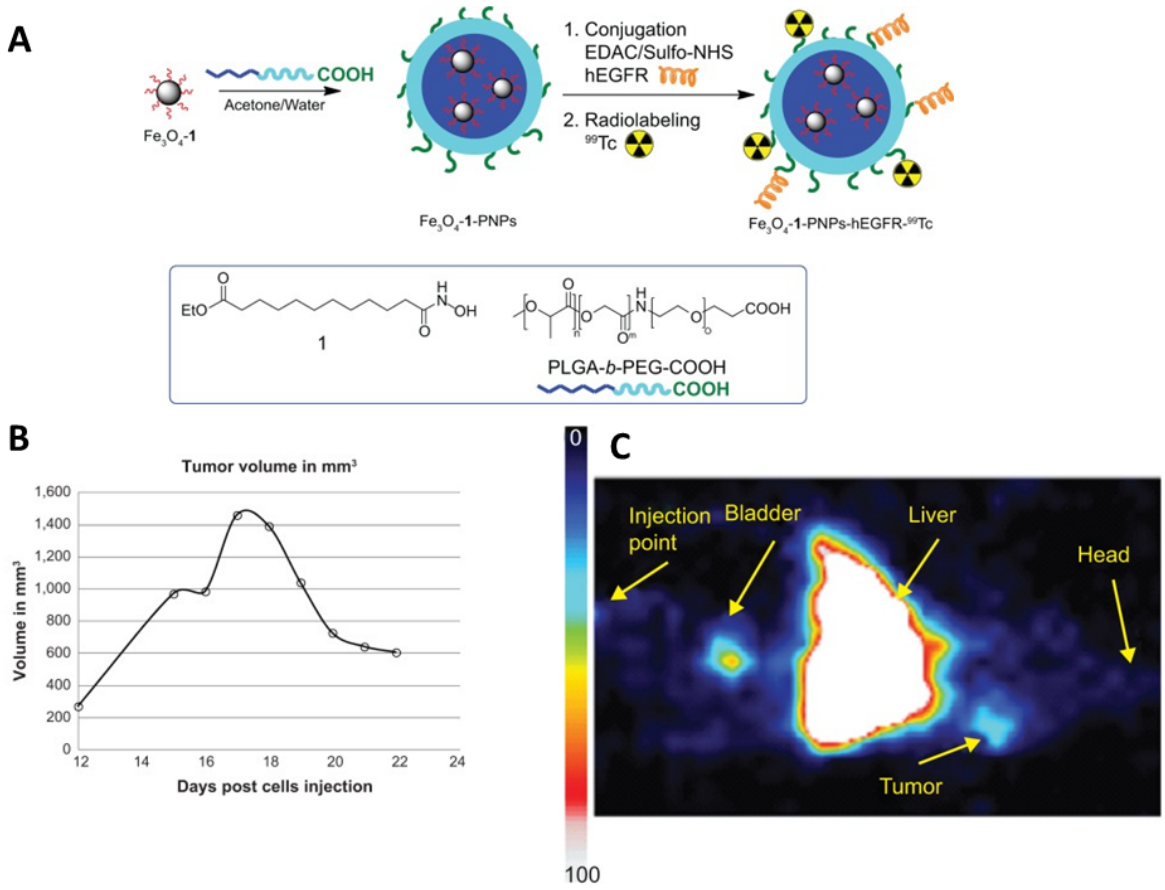

Figure 25. (A) Schematic representation of the synthesis of anti-human epidermal growth factor receptor (EGFR)-targeted and 99mTc functionalized PLGA-PEG nanoparticles loaded with SPIO **(B)** Mouse tumor volume on day 12 through day 24, showing a decrease in tumor volume. **(C)** *In vivo* scintigraphic image of hybrid radiolabeled Fe_3O_4-1-PNP-hEGFR-^{99m}Tc in an A431 tumor-bearing SCID mouse model (adapted from [Baldi et al., 2014]).
Abbreviations: *hEGFR = human epidermal growth factor receptor; PNP = polymeric nanoparticles; SCID = severe combined immunodeficiency.*

Ultrasound

Ultrasound (US, acoustic sound with frequencies > 20 kHz) can produce different effects, which are classified into thermal and non-thermal effects. Thermal effects are commonly used for thermal ablation of diseased tissue as a non-invasive alternative to surgery. Experimental clinical trials have shown promising results for various tumor types, including prostate and pancreatic cancer [Malietzis et al., 2013]. US non-thermal effects, mainly cavitation, induce a variety of biological responses, resulting in increased drug or carrier extravasation, blood–brain barrier (BBB) disruption and membrane permeabilization to otherwise cell-impermeable compounds. Meanwhile, thermal effects are primarily used to trigger thermoresponsive drug delivery and tumor tissue thermal ablation [Abouelmagd et al., 2014; Yudina et al., 2012]. For example, Yang *et al.* developed carboxymethyl hexanoyl chitosan (CHC)-based microbubbles, encapsulating both SPIO and CPT along with sulfur hexafluoride (SF6) gas,

for cancer therapy and imaging (Figure 26) [Yang et al., 2014c]. They used US to combine US-triggered release with US-enhanced cellular uptake. The authors demonstrated the efficacy of their system for *in vivo* MRI, US imaging and *in vitro* cytotoxicity in MDA-MB-231 human breast cancer cells. However, few studies have researched simple US-triggered targeting. The majority of researchers use combined targeting delivery systems for SPIO-based theranostics, which will be discussed below.

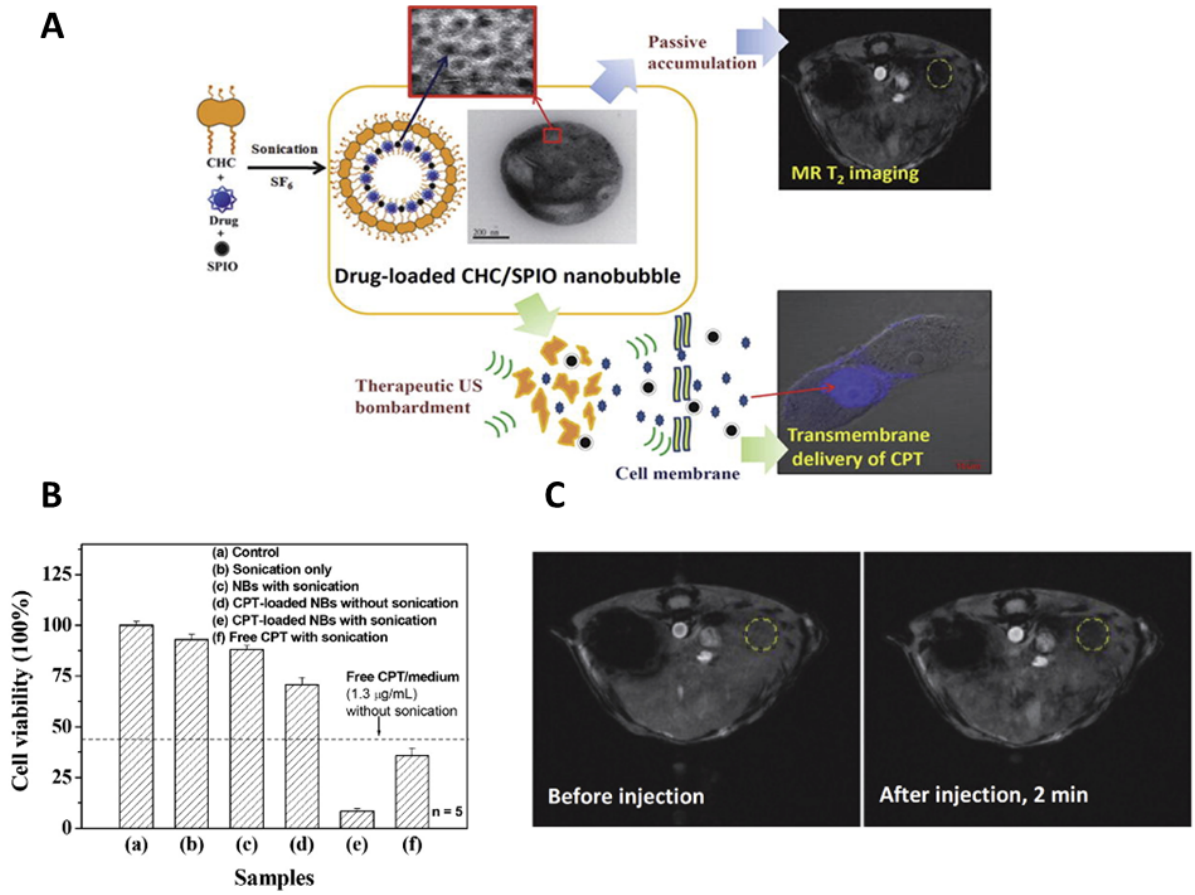

Figure 26. (A) Schematic representation of bubble-forming material (CHC) together with SPIO nanoparticles to prepare MR image-guided nanobubbles to efficiently encapsulate a hydrophobic drug (CPT) and exert US-triggered toxicity to enhance membrane drug permeation; **(B)** Cell viability of breast tumor cells (MDA-MB-231) cultured under different conditions. (a) Control group (cells without CPT and without sonication) (b) Cells sonicated for 20 min. (c) Cells cultured with CHC/SPIO NB suspension (without CPT) with sonication for 20 min. (d) Cells cultured with CPT-loaded CHC/SPIO NB suspension without sonication for 20 min. (e) Cells cultured with CPT-loaded CHC/SPIO NB suspension with sonication for 20 min. (f) Cells cultured with CPT-containing medium under sonication for 20 min; **(C)** In vivo MR images of mouse liver acquired before and after injection of CHC/SPIO NB suspension (adapted from [Yang et al., 2014c]).

Magnetic targeting

Due to their superparamagnetic properties, an external magnetic field can be used to guide SPIO-based theranostics directly to the tumor. When a permanent magnet is applied

externally near the tumor region, the magnetic gradient produced exerts attractive forces on magnetic nanoparticles delivered via the circulation [Reddy et al., 2012]. Lübbe *et al*. were the pioneers in this field, using an external magnetic field to guide a treatment [Lubbe et al., 1996]. Subsequently, numerous studies have used this method, employing magnetic field strengths ranging from 0.4 to 4 T. For example, Arias *et al.*, reported a magnetically responsive squalene-based nanoplatform for theranostic purposes [Arias et al., 2011]. This concept was based on the inclusion of SPIO nanocrystals into nanoparticles constructed by self-assembling molecules of a squalenoyl gemcitabine (SQgem) bioconjugate. This nanoplatform simultaneously allows (i) the targeting of a gemcitabine prodrug to an experimental solid tumor under the influence of a magnetic field produced by an external permanent magnet placed on the tumor surface and (ii) the imaging of the targeted tumor nodule. Yang *et al.* developed epirubicin (EPI) conjugated SPIO for magnetically targeted cancer therapy [Yang et al., 2012]. This EPI-SPIO conjugate increased accumulation 10-fold in tumors following intra-arterial injection and magnetic targeting using a 0.4T neodyme permanent magnet and displayed *in vivo* MRI contrast enhancement. Finally, Alexiou *et al.,* examined a mitoxantrone (MTX)-SPIO conjugate that accumulated in the tumor tissue of VX-2 squamous carcinoma-bearing rabbits using a 1.7 T electromagnet [Alexiou et al., 2000]. Complete remission of the rabbits was induced after treatment with the magnetically targeted MTX-SPIO conjugate and MRI was used for the *in vivo* visualization of particle accumulation (Figure 27).

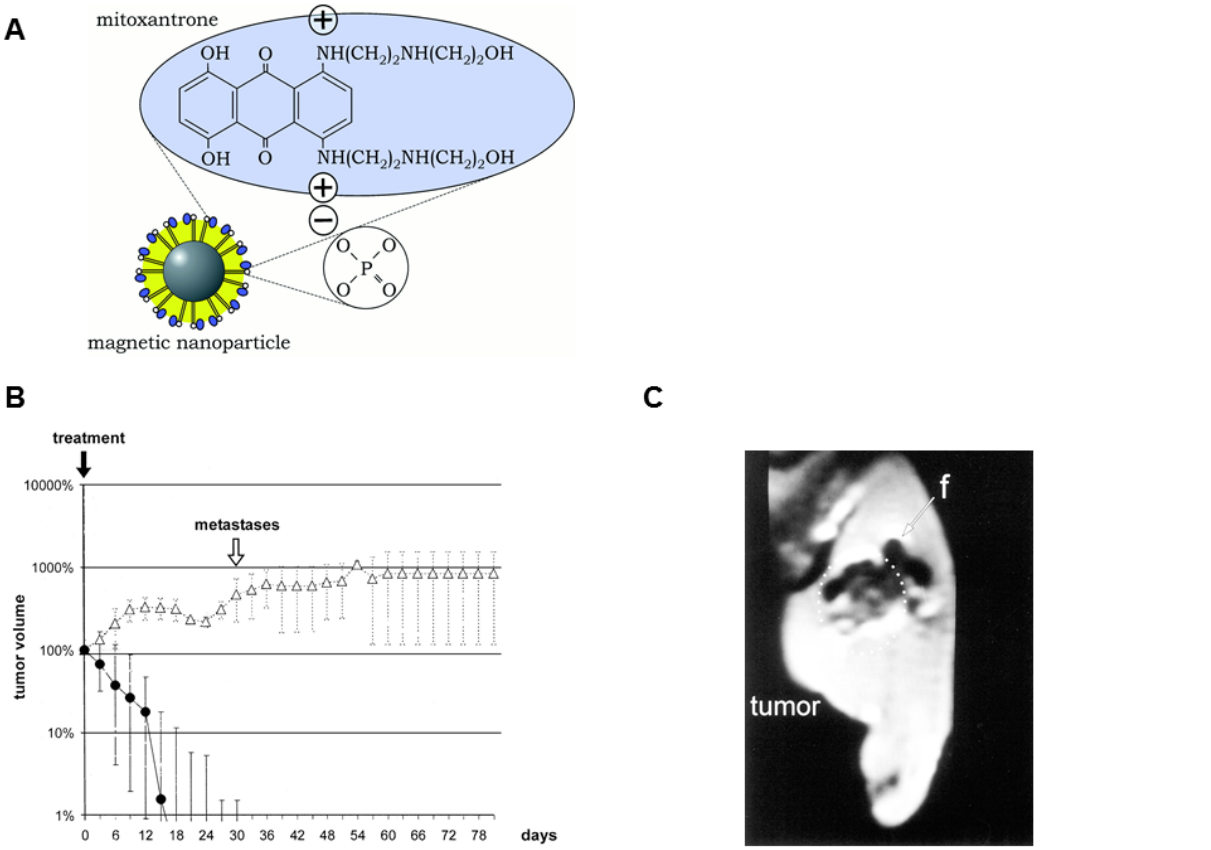

Figure 27. (A) Schematic representation of the mitoxantrone-conjugated SPIO nanoparticles. **(B)** Effect of i.a. injection of MTX-SPIO conjugate after magnetic drug targeting (●) compared with control group (no treatment △). **(C)** MRI of tumor hind limbs of rabbits after i.a. injection and magnetic drug targeting (1h exposure). The "f-narrow" points out the accumulation of SPIO (adapted from [Alexiou et al., 2000]).

Combined targeting strategies

Considering the different disadvantages of each simple targeting strategy, many efforts have been made to develop multifunctional platforms with combined targeting strategies. Table 11 gives non-exhaustive examples of combined-targeted multifunctional SPIO-based nanothernanostics in pre-clinical studies.

Table 11. Non-exhaustive examples of combined-targeted multifunctional SPIO-based nanothernanostics in pre-clinical studies.

Formulation	Targeting Type	Drug	Functional molecules	Cell line	*In vitro/ In vivo MRI*	Results	Ref
SPIO conjugates	AT + pH triggered	DOX	cRGDfC ^{64}Cu	U87MG cells	*In vitro*	*In vitro* MRI contrast enhancement, Enhanced tumor accumulation (PET)	[Yang et al., 2011]
Liposomes	MT + HT + AT	DOX	FA	KB and HeLa cells	*In vitro*	Improved cellular uptake and cytotoxicity	[Pradhan et al., 2010]
Phospholipid-based microbubbles	MT + FUS	DOX	_	C6 glioma cells	*In vitro* *In vivo*	BBB opening and highly effective drug delivery	[Fan et al., 2013]
PEG-PLGA-PCL NP	MT+AT	PTX	GRGDS	CT-26 cells	*In vitro* *In vivo*	High tumor accumulation, drastic tumor growth delay, strong contrast enhancement	[Schleich et al., 2014]
PEG-PAA NP	PDT + AT	_	F3	9L glioma cells	*In vitro* *In vivo*	Significant improvement in survival rate, *in vivo* MRI	[Reddy et al., 2006]
PEGylated SPIO nanoclusters	PDT + MT	_	_	4T1 (mammary carcinoma)	*In vitro* *In vivo*	Dramatically delayed tumor growth and MF-enhanced PDT	[Li et al., 2013b]
SPIO conjugates Gold nanoshell	PTT + AT	_	C225 (anti-EGFR Mab)	A431 cells FaDu, OSC19, and HN5	*In vitro* *In vivo*	Thermal ablation, *in vitro* MRI contrast enhancement	[Melancon et al., 2011].

Abbreviations: AT = active targeting, BBB = blood brain barrier, DOX = doxorubicin, FA = folate, FUS = focused ultrasound, HT = hyperthermia, MF = magnetic field, MT = magnetic targeting, PAA= poly(acrylamide), PDT = Photodynamic therapy, PTT = photothermic therapy

The classical approach for combining targeting strategies consists of combining the active and acid-triggered drug release strategies. Yang *et al.* used this strategy and developed ^{64}Cu labeled SPIO-DOX conjugates linked by an acid labile bond that was further functionalized with cRGD [Yang et al., 2011]. This system exhibited high *in vitro* MRI contrast enhancement and tumor accumulation using PET.

Another strategy combines magnetic targeting (MT) with SPIO induced hyperthermia. For example, Pradhan *et al.* combined these two strategies along with active targeting for

theranostic purposes [Pradhan et al., 2010]. They developed folate functionalized SPIO/DOX-loaded liposomes and tested their efficacy for improving cellular uptake and cytotoxicity *in vitro*.

More recently, Fan et al. developed a US/MRI dual contrast agent using SPIO-labeled phospholipid based microbubbles that incorporated DOX (Figure 28 A) [Fan et al., 2013]. They combined magnetic targeting (for tumor accumulation) along with focused US to induce BBB opening and therapeutic agent delivery in a glioma-bearing rat. This study demonstrated enhanced anti-tumor efficacy mediated by the DOX-loaded microbubbles combined with focused US in an *in vitro* cytotoxicity experiment (Figure 28 B) and contrast enhancement after focused US and 40 min of magnetic targeting (Figure 28 C).

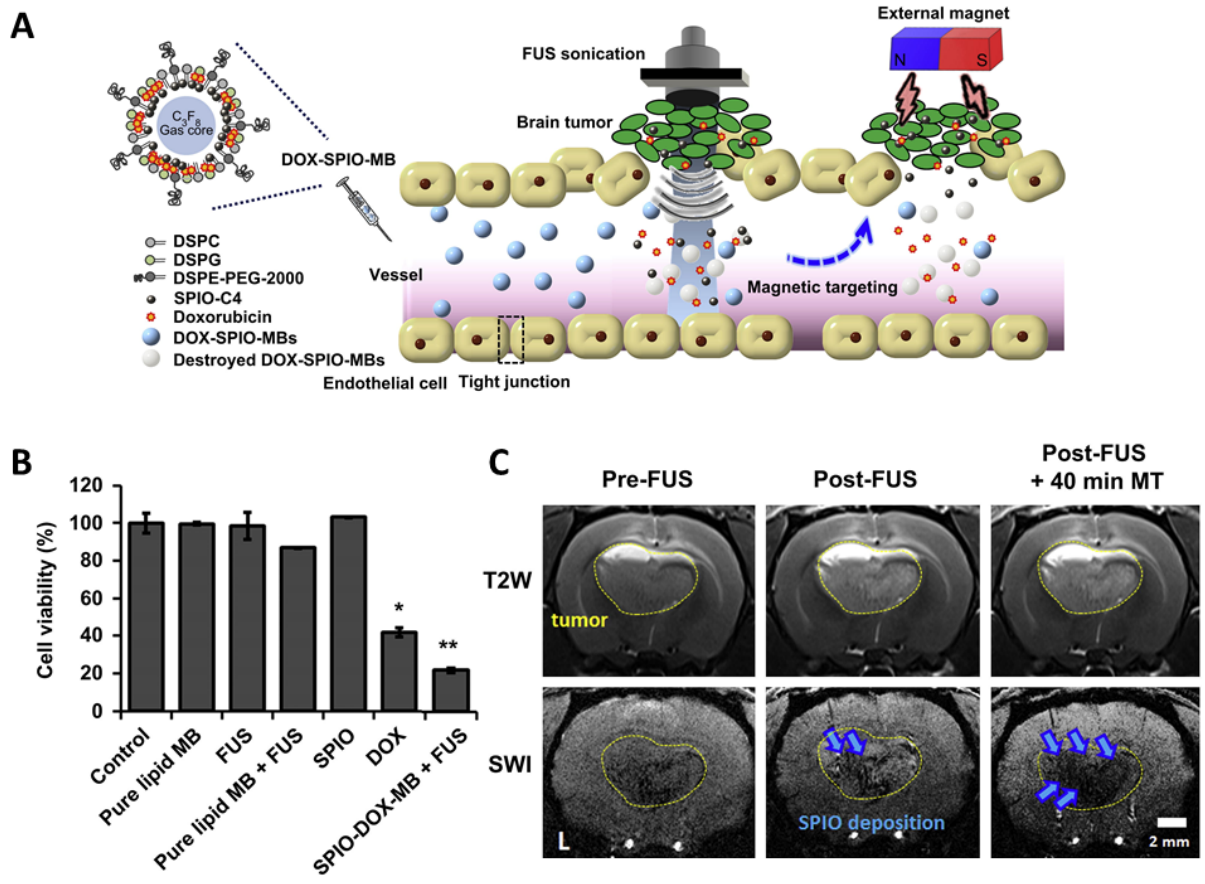

Figure 28. (A) Schematic illustration of DOX-SPIO-MBs and their controlled release into brain tissue, triggered by focused US, and enhanced SPIO deposition using external MT. **(B)** In vitro cytotoxicity experiment. **(C)** In vivo MRI T_2-weighted (T_2W) images (to confirm tumor location) and susceptibility weighted images (SWI) (to confirm SPIO deposition) obtained before and after focused US sonication with MT for 40 min. Arrow: Location of SPIO deposition [Fan et al., 2013]).

Abbreviations: DSPC = 1,2-distearoyl-sn-glycero-3-phospho-choline, DSPE-PEG2000 = 1,2-distearoyl-sn-glycero-3-phosphoethanolamine-N-[methoxy(poly(ethyleneglycol))-2000], DSPG = 1,2-dioctadecanoyl-sn-glycero-3-phospho-(1'-rac-glycerol), DOX-SPIO-MBs = SPIO labeled microbubbles incorporating DOX, FUS = Focused ultrasound, MT = Magnetic targeting

Our group recently developed another strategy that combined magnetic and active targeting. We developed RGD-functionalized PTX/SPIO-loaded PLGA-based nanoparticles and separately compared the double active and magnetic targeting strategy to passive, active and magnetic targeting. These SPIO-based multifunctional theranostics displayed a high tumor accumulation using the combined strategy (RGD+MT, figure 29 B), as demonstrated by the ex vivo biodistribution that corresponds to a strong contrast enhancement of the tumor region by *in vivo* MRI. This high tumor accumulation was correlated to drastically enhanced survival time and long-term survival in mice (figure 29 C) [Schleich et al., 2014].

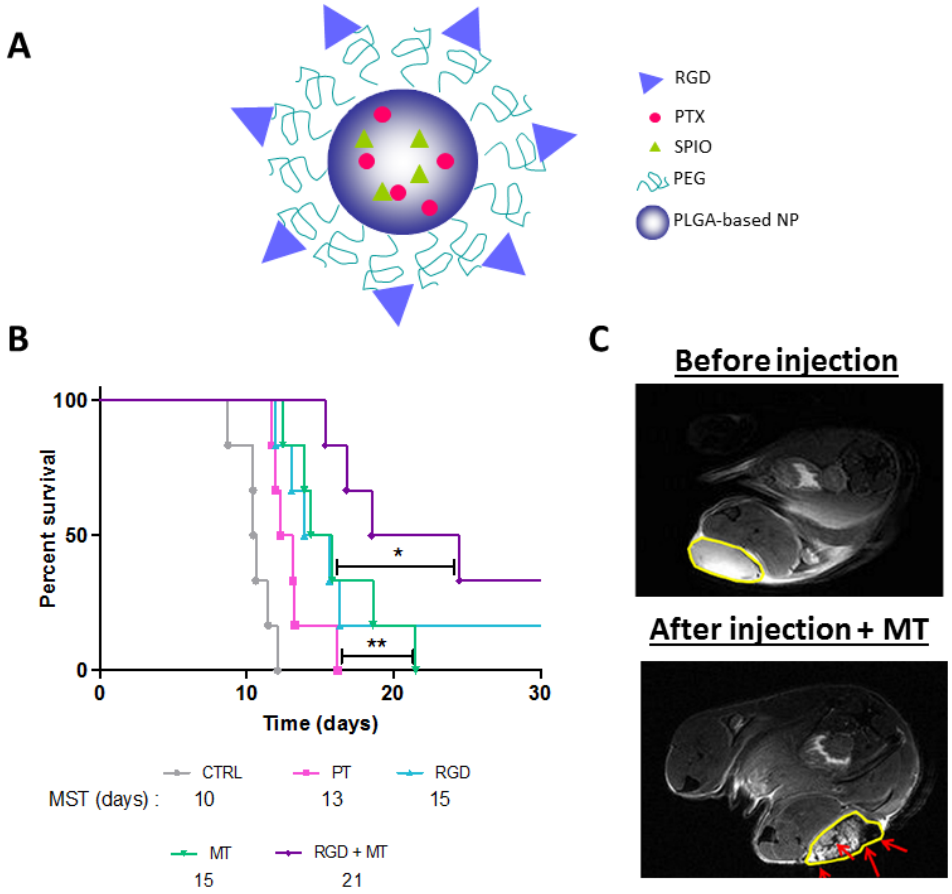

Figure 29. (A) Schematic representation of the SPIO/PTX-loaded PLGA-based multifunctional nanoparticles. **(B)** Kaplan-Meyer survival plot. Mice treated with the combination RGD+MT had significantly longer survival times compared with the other targeting strategies. **(C)** T_2-weighted MR images before injection and 4 h after injection and subsequent magnetic targeting (adapted from [Schleich et al., 2014]).
Abbreviations: CTRL = control, MST = mean survival time, MT = magnetic targeting, PT = passive targeting.

Long visible and NIR lights can be used to generate reactive oxygen species (ROS) after the activation of a compound presented by the drug carrier or the drug itself. After delivery of a photosensitizer-containing drug to the tumor cell, light radiation activates the drug, generating "killer" ROS, which induce apoptosis and enhance drug release. This technique is called

photodynamic therapy (PDT) [Alexiou et al., 2000; Kelkar et al., 2011; Moses et al., 2013]. PDT has been investigated for several decades, but light-associated toxicity limits its clinical application. Therefore, the classical strategy combines PDT and active targeting to increase specificity and limit potential damage to healthy tissue [Wang et al., 2014]. For example, in a study conducted by Reddy *et al.*, vascular targeted PEGylated Photofrin/SPIO-loaded poly(acrylamide) nanoparticles were developed for the treatment of glioma [Reddy et al., 2006]. The vascular targeting capacity was accomplished by the functionalization of the particles using the F3-peptide. *In vivo* MRI was used to assess biodistribution and the efficacy of the active targeting prior to PDT. There was a significant improvement in the survival rate of 9L glioma-bearing rats treated with this combined targeting therapy compared with the group treated with PDT alone (Figure 30).

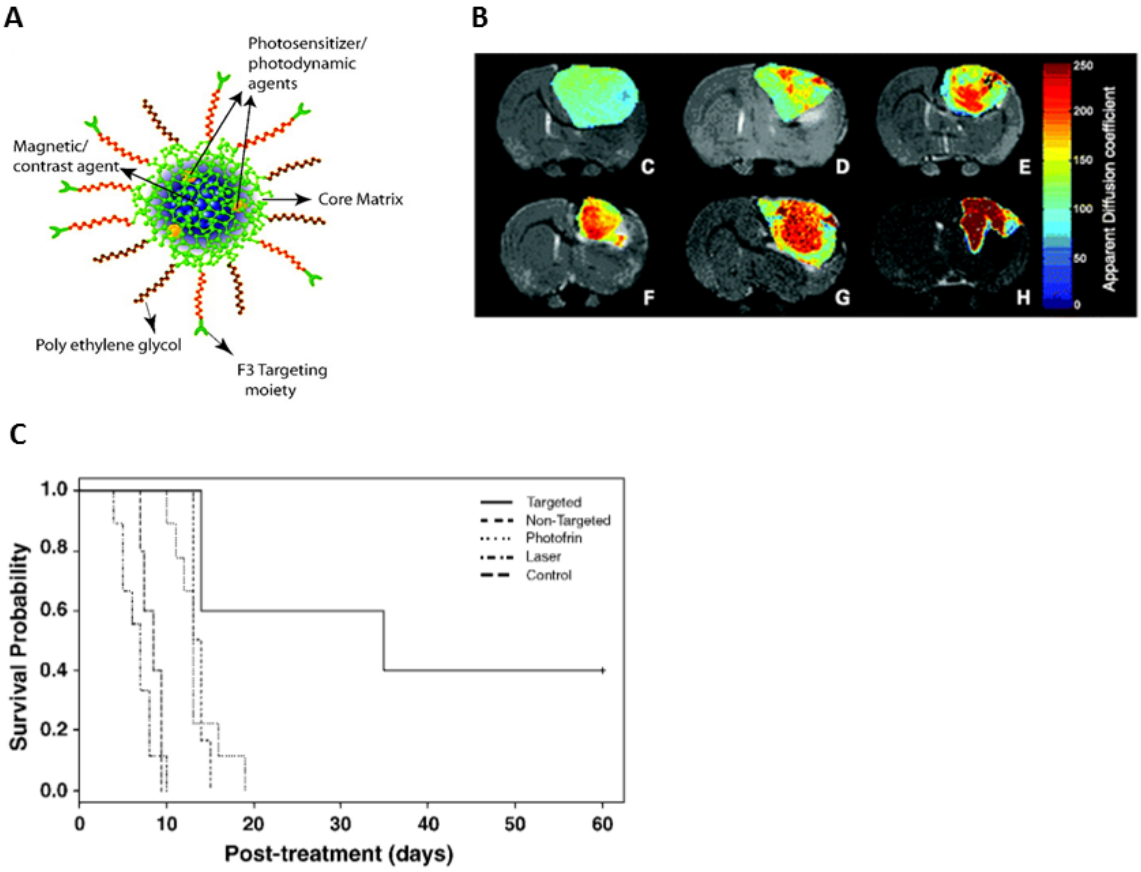

Figure 30. (A) Schematic representation of the vascular targeted PEGylated Photofrin/SPIO-loaded poly(acrylamide) nanoparticles. **(B)** T_2-weighted magnetic resonance images at day 8 after treatment from (C) a representative control tumor and tumors treated with (D) laser light only, (E) i.v. administration of Photofrin plus laser light, and (F) non-targeted nanoparticles containing Photofrin plus laser light and (G) targeted nanoparticles containing Photofrin plus laser light. The image shown in (H) is from the same tumor shown in (G), which was treated with the F3-targeted nanoparticle preparation but at day 40 after treatment**. (C)** Kaplan-Meier survival plot for 9L tumor. Survival curves for brain tumor animals: untreated, laser only, i.v. Photofrin + laser treated, non-targeted nanoparticles containing Photofrin + laser, and F3-targeted Photofrin-containing nanoparticles + laser treated (Adapted from [Reddy et al., 2006]).

A recent example of combined PDT-magnetic targeting is provided by Li *et al.,* who developed PEGylated iron oxide nanoclusters loaded with chlorin e6, a photosensitizer, for targeted, NIR light induced, photodynamic therapy [Li et al., 2013b]. SPIO were used for both their MRI contrast agent properties and the magnetic targeting potential. To further improve tumor accumulation, an external magnet was placed, allowing magnetic targeting.

Another light-mediated strategy uses NIR light to induce local heating and, consequently, hyperthermia-induced cell death, known as photothermic therapy (PTT) [Alexiou et al., 2000; Kelkar et al., 2011; Moses et al., 2013]. Melancon *et al*. developed a SPIO-coated gold nanoshell functionalized with C225, an anti-EGFR monoclonal antibody, for head and neck cancer treatment [Melancon et al., 2011]. They used these C225-SPIO@Au nanoshells to image guide thermal ablation (using *in vivo* MRI). They used the PTT thermic effect by applying an NIR laser to induce local hyperthermia and destroy the tumor tissue.

IV.5. DISCUSSION: MAJOR OBSTACLES FOR IN VIVO AND CLINICAL STUDIES

SPIO have been extensively used during the last decade because of their (i) high surface functionalization for forming SPIO-conjugates, (ii) high efficiency as MRI contrast agents, (iii) high potential for multi-modal imaging and (iv) high potential for theranostic purposes. To further improve functionality, release kinetics (controlled release) and drug protection against degradation, nanoparticles encapsulating SPIO have recently received particular attention. These nanoparticular systems are interesting candidates that provide multifunctional platforms for theranostic applications [Cohen et al., 2013; Laurent et al., 2011].

The concept of theranostics has received increasing interest in recent years. Nanotheranostics can be used for various biomedical applications including (i) non-invasive assessment of biodistribution and target site accumulation, (ii) monitoring of drug release, (iii) enhancement of therapeutic efficacy via triggered drug release and (iv) prediction of therapeutic response [Lammers et al., 2010]. Furthermore, the potential of theranostic platforms to promote personalized therapy has become clear. Because of the potential major adverse effects of current available anti-cancer therapies and patient inter- and intra-variability, it is important to pre-select patients, based on drug biodistribution, that will likely respond to therapies [Kumagai et al., 2009]. Patients that have good tumor accumulation and less undesirable accumulation in healthy tissues are more likely to be treatment-responsive and have minimal adverse effects.

Despite these exciting potential biomedical applications and as seen in the tables presented above, only a few *in vivo* MRI studies of nanotheranostics have been successfully conducted in pre-clinical models. Furthermore, the majority of nanotheranostics designed for personalized therapy have only demonstrated *in vitro* efficacy. Moreover, if researchers describe *in vivo* data, that data generally only assesses one of the two purposes of theranostics, either therapeutic efficacy or imaging efficacy [Mura et al., 2012]. Studies that have shown *in vitro* and *in vivo* efficacy for therapeutic and imaging purposes are mostly represented by studies combining multiple strategies. This observation raises the question: what are the obstacles responsible for so few successful *in vivo* MRI studies? The answer to this question is that SPIO-loaded theranostics have some limitations that lead to challenging *in vivo* and clinical translations.

Impaired biodistribution

As previously discussed, following i.v. injection, a significant proportion of SPIO-based nanoparticles are sequestered by the liver and spleen [Kwon et al., 2012; Nichols et al., 2012]. This phenomenon can be explained by their capture by the MPS (i.e., Kupffer cells) due to the size of the particles (often larger than 100 nm) and their interaction with plasma proteins (opsonins). It is noteworthy that only a small proportion of the injected dose actually reaches the tumor [Laurent et al., 2014; Reddy et al., 2012]. This phenomenon has led the researchers to usually use SPIO-loaded nanoparticles as a contrast agent for liver imaging [Lu et al., 2009]. Various physico-chemical parameters have been shown to modulate this biodistribution, including particle size, surface charge and surface modifications (PEGylation) (see Figure 31). Another strategy for improving tumor accumulation is to use an external magnetic field to guide the therapy to the tumor site and maintain its position using magnetic force, known as magnetic targeting [Laurent et al., 2014; Reddy et al., 2012]. However, even if this strategy has shown drastic improvement of nanoparticles accumulation in tumor site, a major fraction of the injected dose is still found in the liver [Nichols et al., 2012; Schleich et al., 2014].

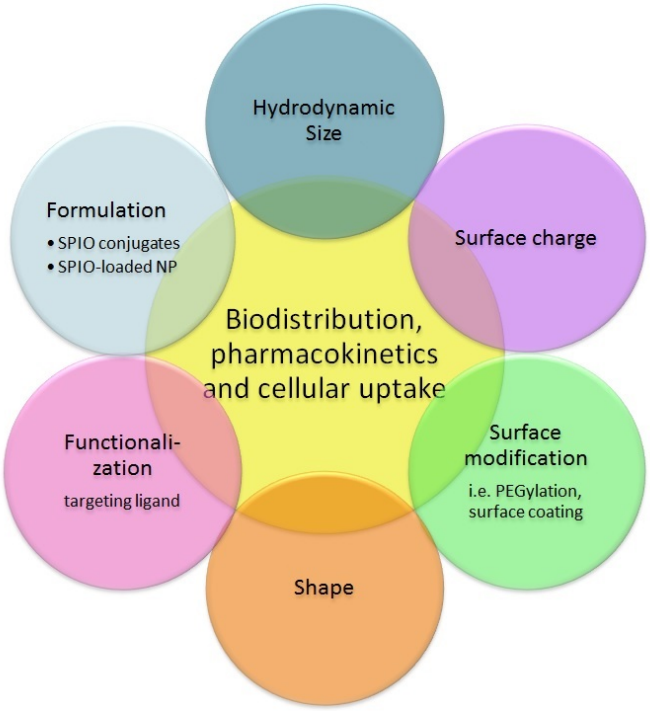

Figure 31. Illustration of the association of SPIO-based nanoparticles physicochemical properties with their biodistribution, pharmacokinetics and cellular uptake.

Formulation challenges

SPIO-based nanotheranostics have formulation challenges that limit their market entry. The vast majority of multifunctional nanomedicine systems described in the literature suffer from high manufacturing and material costs, as well as complexity or limitations in their production processes [Peer et al., 2007]. This particular point will be discussed in more details in the discussion section of this thesis.

Limitations for passive targeting

Since passive targeting is highly dependent on tumor vascularization and given this vascularization is highly heterogeneous depending on the tumor type, the patient (inter-variability) and the disease stage or even on the tumor areas (intra-variability), EPR effect is a highly heterogeneous phenomenon [Bae et al., 2011; Maeda, 2012]. This point will be discussed in more details in the discussion section of this thesis.

Limitations for active targeting

In its first conception, as imagined by Paul Ehrlich in 1908 as a "magic bullet", ligand-mediated targeting was thought to improve both biodistribution of the targeted nanomedicine and tumor accumulation, resulting in enhanced efficacy. However, because targeted nanomedicines have no means of self-propulsion, reaching the target site and subsequently accumulating in the tumor tissue, relies on EPR-mediated extravasation, which has several disadvantages as outlined above [Kwon et al., 2012; Lammers et al., 2008]. Therefore, the advantage of functionalizing nanoparticles is the higher chance of internalization. The mechanisms of tumor internalization for non-targeted nanoparticles mostly involve macropinocytosis [Kocbek et al., 2013; Kumari et al., 2011]. Conversely, functionalized nanoparticles are internalized via receptor-mediated endocytosis. Consequently, functionalized nanoparticle intratumor distribution shifts from the extracellular compartment to the tumor cell intracellular compartment, which improves anti-cancer efficacy [Prokop et al., 2008]. Targeting neoangiogenic endothelial cells may provide an interesting alternative because nanomedicines do not need to enter the interstitium to reach their target; therefore, they do not rely on EPR-mediated extravasation to exert their activity. This targeting can be easily achieved using RGD ligand-grafted nanomedicines.

Furthermore, since PEGylation is a common technique improving nanocarriers stealthness to avoid capture by the MPS, ligand grafting, by covering PEG corona, can lower the amount of available PEG and, thereby, can alter pharmacokinetic and biodistribution profile [van der Meel et al., 2013]. Hence, it is of great importance for novel nanomedicines to verify the efficacy of targeting strategy in vivo and to document the dose- and time- dependency of targeting to guide protocol design in a view of a translational approach [Duncan and Gaspar, 2011]. To date, many receptors have been explored in tumor targeting. Knowledge of basic cell biology, tumor biology, immunology, and cancer biology would be required to develop smart nanocarriers and to guide researchers in the choice of the proper ligand to attach. This choice should take several knowledge into account including tumor-specific receptors allowing endocytosis, tumor-specific biomarkers, tissue-specific and tumor-specific homing proteins, and tumor-specific enzymes allowing selective uptake into cells or accumulation in tumor microenvironments [Kim, 2007].

Limitations for magnetic targeting

Magnetic targeting has gained more and more interest in the last decade. Many research groups have now demonstrated its potential in increasing tumor accumulation through magnetic attraction [Alexiou et al., 2000; Arias et al., 2011; Yang et al., 2012]. However, the success of this targeting strategy is limited by the distance between the magnets and the target site. Hence, magnetic targeting should be more effective in regions closer to the magnets limiting its application to superficial tumors [Alexiou et al., 2000; Laurent et al., 2011]. This point will be discussed in more details in the discussion section of this thesis.

Limitations for other strategies

Ultrasound therapy also has several limitations. The challenges for ultrasound-enhanced drug delivery are the same as for the other targeting strategies, namely formulation challenges. There is a crucial need to develop a new generation of delivery vehicles that have sizes smaller than 200 nm, which are tailor-made for cavitation-enhanced drug delivery and may profit from high extravasation into tumor tissues [Ibsen et al., 2013; Mo et al., 2012].

PDT also has limitations in terms of light penetration. The singlet oxygen produced by the photochemical reaction between the sensitizer and light can only diffuse 0.02 μm, limiting tissue damage to the penetration depth of the light used to activate the photosensitizer [Nyst et al., 2009]. Although this strategy allows more selective and irreversible destruction of tumor cells than conventional therapies, there are several challenges that need to be addressed for better clinical acceptance. First, the efficiency of this strategy is limited by light penetration depth, restricting the use of PDT relatively superficial lesions [Chatterjee et al., 2008]. Second, using PDT requires specialized equipment and training [Jerjes et al., 2012]. Finally, the most important challenge that needs to be addressed is the high concentration of photosensitizer (PS) needed at the target site for clinical efficiency. Poor cancer cell uptake and inefficient tumor delivery of PS agents are the two main limiting factors for the current application of PDT in cancer therapy [Li et al., 2013b].

Combined strategies

Given the limitations of each targeting strategy taken individually, there is a crucial need for merging advanced targeted delivery systems to further improve selectivity of the currently available treatment. In this context, there is a rationale to combine different strategies in a same nanomedicine to overcome the limitations of each one taken separately, making those multi-modal nanotheranostics.

IV.6. CLINICAL PERSPECTIVES AND OPINION

Few clinical trials using nanotheranostics have provided proof-of-principle for personalized nanomedicine. PK2, galactosamine-modified pHPMA-GFLA-GFLG-doxorubicin convincingly showed efficient target site localization [Seymour et al., 2002]. ^{111}labeled PEGylated liposomes accumulated highly efficiently in the primary tumor mass of a Kaposi's sarcoma patient, as well as in a number of secondary metastatic lesions. This observation explains why patients suffering from Kaposi's sarcoma that are characterized by a dense, highly leaky, EPR-vascular network generally respond well to Doxil® treatment [Harrington et al., 2001; Lammers et al., 2012b]. VEGF-R2-targeted microbubbles are also a clinically relevant example of theranostics and are currently used in early-stage trials for prostate cancer staging and monitoring by ultrasound imaging [Kiessling et al., 2012].

To our knowledge, no clinical trial has been performed with SPIO-based theranostics. Nevertheless, advances in the development of SPIO-based magnetic nanoparticles (without anti-cancer drug) have demonstrated that it is a promising method for cancer treatment by hyperthermia. The advantage of these nanoparticles is their ease of tumor targeting and fewer side effects than chemotherapy and radiotherapy, as proven by the results of current/ongoing clinical trials. These trials have evaluated both tumor accumulation with magnetic targeting and anti-cancer efficacy combined with radiotherapy or via hyperthermia [Laurent et al., 2011; Maier-Hauff et al., 2011]. These trials are encouraging for the development of SPIO-based nanotheranostics in the future.

In our opinion, scientists, clinicians and pharmaceutical companies researching nanomedicines should investigate the image guidance of their nanomedicines during the initial phase of clinical testing. Because of the co-encapsulation possibility of contrast agents and anti-cancer drugs, theranostics should be considered a tool for earliest phases of clinical trials. This would allow the collection of important information about their nanomedicine: (i) the initial biodistribution and target site accumulation of the nanomedicine and (ii) during follow-up, the response monitoring of the nanomedicine. These two results could then be correlated [Lammers et al., 2012b]. However, an essential question remains unanswered: why do so many papers describe nanomedicines while only a few nanomedicines are commercialized? This question has been discussed in this review. To summarize, one major reason is the EPR effect is undoubtedly larger in animal model tumors than in patients [Jain et al., 2010]. Although there appears to be a clear EPR effect in clinical tumors, practical information on the extent of the EPR effect in most solid tumors is needed for the

development of nanomedicine. In this context, SPIO-based theranostics, via their non-invasive biodistribution visualization and the importance of the EPR, should address this shortcoming. Assuming that there will be a clear correlation between tumor concentration and therapeutic efficacy, it will be highly important to properly differentiate between low and high levels of target site accumulation. These studies should also guide the specific use of nanomedicines in clinical applications.

V. ANTI-CANCER DRUGS

Among all the anti-cancer drugs currently used, paclitaxel and doxorubicin are the most widely used for the treatment of various cancers and have been used in this thesis.

V.1. PACLITAXEL

Paclitaxel (PTX) is the first of a new class of microtubule stabilizing agents. PTX is a diterpenoid pseudoalkaloid ($C_{47}H_{51}NO_{14}$, MW 853 Da) isolated in 1960s from the bark of Pacific Yew (*Taxus brevifolia*; Taxaceae) (Figure 32). Its anti-tumor activity is due to the entire taxane molecule [Wani et al., 1971].

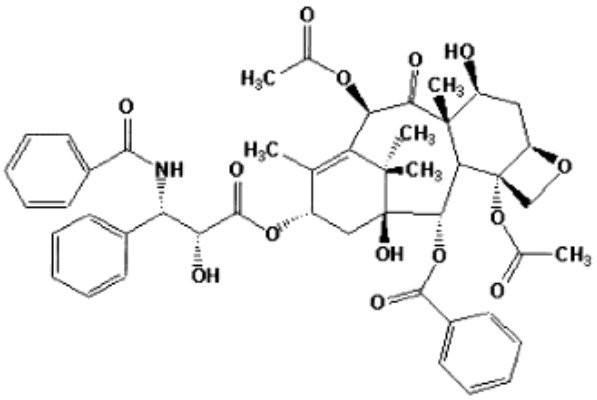

Figure 32: Structure of paclitaxel.

Unlike other microtubule agents, such as *Vinca* alkaloids, which induce the disassembly of microtubules, PTX stabilizes microtubules and inhibits depolarization back to tubulin [Schiff et al., 1979; Wall et al., 1995]. Microtubules are cylindrical structure (made up of proteins, mainly tubulin) involved in various essential cellular functions including mitosis. They represent a fundamental constitutive part of eukaryotic cell's cytoskeleton [Marchetti et al., 2002]. PTX acts by disruption of the dynamic equilibrium within the microtubule system causing an increase in mass and number of microtubules which are extremely stable. Therefore, the elongation and shortening required for cell division or the vital functions in the interphase cannot occur [Fan, 1999]. Thus, PTX blocks cells in the late G_2 phase and M phase of the cell cycle [Singla et al., 2002]. Consequently, the more the cells are undergoing mitosis the more they are sensitive to PTX [Marchetti et al., 2002].

Currently, the use of PTX is approved for the treatment of breast cancer, non-small cell lung cancer, ovarian cancer and Kaposi's Sarcoma [paclitaxel RCP]. However, PTX was shown to

have neoplasic activity against a variety of other cancers such as ovarian carcinoma, colon, head, non-small cell lung cancer and AIDS related Kaposi's sarcoma [Horwitz, 1992].

PTX presents a low therapeutic index and treatments are always associated with serious side-effects due to non-specific activity. Indeed, all cells presenting a high turn-over will be more sensitive to PTX with consequences for the patient like neutropenia, thrombocytopenia, asymptomatic bradycardia, arrhythmias, ischemia, nausea, vomiting, diarrhea, elevation of liver function, alopecia, myopathy, fatigue, pulmonary embolism, etc [Panchagnula, 1998; Rowinsky et al., 1995].

The usually dose is 135-175 mg/m² and is given as 3 and 24 h perfusion in a weekly or a 3-weekly schedule. Pharmacokinetics of PTX shows wide variability. Terminal half-life was found to be in the range of 1.3-8.6 h. PTX undergoes cytochrome P450 (mainly CYP2C8 and CYP3A4) mediated hepatic metabolism and is mainly eliminated in feces. The majority of the drug (89-98%) binds to plasma proteins [Singla et al., 2002] (paclitaxel RCP).

Some resistance has been associated with taxanes such as an increased multidrug resistance (MDR). Indeed, natural alkaloids enter the cell by passive diffusion, which is related to the presence of cellular membrane proteins such as P-glycoprotein, inducing resistance [Marchetti et al., 2002].

Paclitaxel is poorly soluble in water and thus, until recently, its commercially available preparations are using a vehicle composed of non-ionic solvent Cremophor® EL (polyethoxylated castor oil) and ethanol (1:1) (Taxol®, 6 mg/ml, Bristol-Meyers Squibb) which is diluted with 5-20-fold in 0.9% sodium chloride injection or 5% dextrose injection. However, some side-effects associated with paclitaxel, such as hypersensitivity reactions requiring premedication with antihistamines or corticosteroids, myelosuppression, and peripheral neuropathy, are known to be worsened by Cremophor® EL [Gupta et al., 2014]. Cremophor® EL was also shown to cause vasodilatation, labored breathing, lethargy and hypotension [Friedland et al., 1993]. Moreover, Cremophor® EL has been shown to influence the pharmacokinetic profile of paclitaxel resulting in a non-linear kinetics of total concentration, when administrated as Taxol® [Friedland et al., 1993] whereas unbound concentrations were been proven to follow linear kinetics [Friedland et al., 1993]. A more recent study demonstrated the influence of Cremophor® EL on the pharmacokinetics of paclitaxel metabolites showing that total concentrations of 6α-hydroxypaclitaxel and p-3'-hydroxypaclitaxel, two primary metabolites, were strongly dependent on predicted Cremophor EL concentrations [Friedland et al., 1993].

In recent years, a growing interest has emerged in the design of biocompatible Cremophor-free formulation of PTX. Polymer-based drug carriers represent an attractive issue because of the diversity of existing polymers presenting various physico-chemical properties. Polymeric micelles, nanoparticles, liposomes, polymer-drug conjugates have been extensively studied with varying degree of success [Gaucher et al., 2010; Lammers et al., 2008].

In 2005, a cremophor-free formulation has been introduced into the market. Indeed, 130 nm albumin-bound paclitaxel nanoparticle (ABRAXANE® ABI-007) is a new generation formulation of paclitaxel that allow avoiding the use of Cremophor®, resulting in a safer administration without requiring the use of premedications to avoid hypersensitivity. Abraxane® gained its initial FDA approval for metastatic breast cancer patients who failed combination chemotherapy [Gradishar et al., 2005].

V.2. DOXORUBICIN

Doxorubicin (DOX) is an anthracycline drug isolated from *Streptomyces peucetius*, a soil bacterium [Arcamone et al., 1969]. DOX has shown great efficacy in cancer cell killing. It has been used for more than 40 years for the treatment of solid tumors arising in the breast, endometrial tissue, ovarian tissue, osteosarcomas, multiple myeloma, soft tissue sarcomas and non-Hogkin's lymphoma [Gewirtz, 1999; Yang et al., 2014a] (doxorubicin RCP]). Despite the extensive clinical utilization of this drug, the mechanism by which DOX induces cell death remains the subject of controversy. Indeed, multiple mechanisms have shown to be involved:

(i) DOX was been shown to induce topoisomerase II poisoning by trapping this enzyme at cleavage site resulting in double-strand DNA breaks and, thus, cell death [Forrest et al., 2012; Gewirtz, 1999]. Indeed, when the attempt to repair the breaks in DNA fails, the apoptosis pathway is triggered and cellular growth is inhibited at phases G1 and G2 [Tacar et al., 2013]

(ii) Due to its planar conformational structure (Figure 33), DOX acts as a DNA intercalator. Intercalation takes place at site containing adjacent GC base via specific hydrogen-bond formation. The formation of these DNA-adducts has been shown to activate DNA damage responses and induce cell death [Forrest et al., 2012]

(iii) Recently, DOX has been demonstrated to have a role in blocking cancer cells proliferation through stimulation of ceramide synthesis [Denard et al., 2012]

(iv) The quinone structure of DOX can be oxidized to a semiquinone radical by numerous NAD(P)H-oxidoreductases, leading to oxidative stress via superoxide generation and DNA damage [Saltiel et al., 1983; Yang et al., 2014a]

The degree and type of cell death caused by DOX varies according to the administered dose and cell line treated [Tacar et al., 2013].

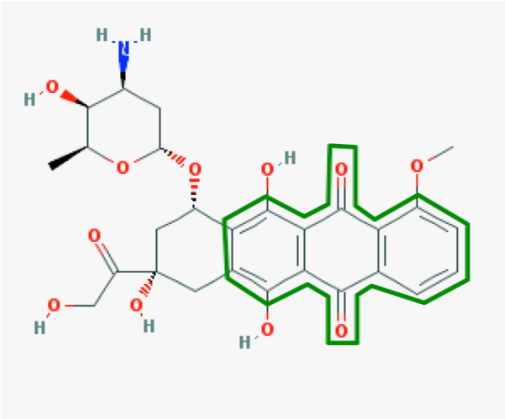

Figure 33. Doxorubicin molecular structure with the anthraquinone core (in green) (adapted from [Forrest et al., 2012]).

A major adverse effect limits, however, its clinical application as a free-drug. Indeed, DOX induces cardiotoxicity. This well-known phenomenon shows an overall prevalence of 1.7 % to 6.8% and is highly dependent on the total dose [Saltiel et al., 1983]. The mechanisms of DOX toxicity to cardiomyocytes involve ROS generation leading to both apoptosis and cell autophagy [Tacar et al., 2013].

DOX is administered through a drip-drip at doses varying between 15 and 90 mg/m^2 during 30 minutes corresponding to approximately 5 µM of initial plasma concentration. This plasma concentration declines rapidly to 25-250 nM within 1 hour [Gewirtz, 1999]. To limit DOX-induced cardiotoxicity and improve pharmacokinetics parameters, PEGylated liposomal DOX is commonly used. Indeed, liposomes have a circulation half-life of approximately 73.9 h, whereas free doxorubicin has a half-life of <10 min. Pegylated liposomal encapsulation also reduces plasma levels of free DOX and, consequently, reduces drug delivery to normal tissue, leading to a decrease in cardiotoxicity risk [O'Brien et al., 2004]. Currently, two commercial forms of these liposomes are available: CAELYX™ and Doxil® (U.S.A.). Pegylated liposomal doxorubicin has been investigated in a variety of cancer types, including breast cancer, gynecologic malignancies, multiple myeloma, non-Hodgkin's lymphoma, gastrointestinal malignancies, and non-small cell lung cancer. Pegylated liposomal doxorubicin is approved by the FDA and EMA for the treatment of metastatic ovarian cancer

in patients with disease refractory to both paclitaxel- and platinum-based chemotherapy regimens, for the treatment of metastatic breast cancer in patients who are at increased cardiac risk, in the second-line treatment of multiple myeloma in combination with bortezomib and in the treatment of Kaposi's sarcoma in patient with a CD4 lymphocytes rate lower than 200 /mm^3 (Caelyx and Doxil RCP).

VI. REFERENCES

2014. http://www cancer org/.

Abouelmagd,S.A., Hyun,H., Yeo,Y., 2014. Extracellularly activatable nanocarriers for drug delivery to tumors. Expert Opin Drug Deliv, 1-18.

Abulateefeh,S.R., Spain,S.G., Aylott,J.W., Chan,W.C., Garnett,M.C., Alexander,C., 2011. Thermoresponsive polymer colloids for drug delivery and cancer therapy. Macromol Biosci, 11, 1722-1734.

Acharya,S., Sahoo,S.K., 2011. PLGA nanoparticles containing various anticancer agents and tumour delivery by EPR effect. Adv Drug Deliv Rev, 63, 170-183.

Ahmed,N., Fessi,H., Elaissari,A., 2012. Theranostic applications of nanoparticles in cancer. Drug Discov Today, 17, 928-934.

Alexiou,C., Arnold,W., Klein,R.J., Parak,F.G., Hulin,P., Bergemann,C., Erhardt,W., Wagenpfeil,S., Lubbe,A.S., 2000. Locoregional cancer treatment with magnetic drug targeting. Cancer Res, 60, 6641-6648.

Allen,T.M., 2002. Ligand-targeted therapeutics in anticancer therapy. Nat Rev Cancer, 2, 750-763.

Ansell,S.M., Tang,H., Kurtin,P.J., Koenig,P.A., Nowakowski,G.S., Nikcevich,D.A., Nelson,G.D., Yang,Z., Grote,D.M., Ziesmer,S.C., Silberstein,P.T., Erlichman,C., Witzig,T.E., 2012. Denileukin diftitox in combination with rituximab for previously untreated follicular B-cell non-Hodgkin's lymphoma. Leukemia, 26, 1046-1052.

Arcamone,F., Cassinelli,G., Fantini,G., Grein,A., Orezzi,P., Pol,C., Spalla,C., 1969. Adriamycin, 14-hydroxydaunomycin, a new antitumor antibiotic from S. peucetius var. caesius. Biotechnol Bioeng, 11, 1101-1110.

Arias,J.L., 2011. Drug targeting strategies in cancer treatment: an overview. Mini Rev Med Chem, 11, 1-17.

Arias,J.L., Reddy,L.H., Othman,M., Gillet,B., Desmaele,D., Zouhiri,F., Dosio,F., Gref,R., Couvreur,P., 2011. Squalene based nanocomposites: a new platform for the design of multifunctional pharmaceutical theragnostics. ACS Nano, 5, 1513-1521.

Aryal,S., Key,J., Stigliano,C., Ananta,J.S., Zhong,M., Decuzzi,P., 2013. Engineered magnetic hybrid nanoparticles with enhanced relaxivity for tumor imaging. Biomaterials, 34, 7725-7732.

Avraamides,C.J., Garmy-Susini,B., Varner,J.A., 2008. Integrins in angiogenesis and lymphangiogenesis. Nat Rev Cancer, 8, 604-617.

Bae,Y.H., Park,K., 2011. Targeted drug delivery to tumors: myths, reality and possibility. J Control Release, 153, 198-205.

Baldi,G., Ravagli,C., Mazzantini,F., Loudos,G., Adan,J., Masa,M., Psimadas,D., Fragogeorgi,E.A., Locatelli,E., Innocenti,C., Sangregorio,C., Comes,F.M., 2014. In vivo anticancer evaluation of the hyperthermic efficacy of anti-human epidermal growth factor receptor-targeted PEG-based nanocarrier containing magnetic nanoparticles. Int J Nanomedicine, 9, 3037-3056.

Barar,J., Omidi,Y., 2013. Dysregulated pH in Tumor Microenvironment Checkmates Cancer Therapy. Bioimpacts, 3, 149-162.

Barczyk,M., Carracedo,S., Gullberg,D., 2010. Integrins. Cell Tissue Res, 339, 269-280.

Barenholz,Y., 2012. Doxil(R)--the first FDA-approved nano-drug: lessons learned. J Control Release, 160, 117-134.

Baum,O., Hlushchuk,R., Forster,A., Greiner,R., Clezardin,P., Zhao,Y., Djonov,V., Gruber,G., 2007. Increased invasive potential and up-regulation of MMP-2 in MDA-MB-231 breast cancer cells expressing the beta3 integrin subunit. Int J Oncol, 30, 325-332.

Bertrand,N., Leroux,J.C., 2012. The journey of a drug-carrier in the body: an anatomo-physiological perspective. J Control Release, 161, 152-163.

Bloch,F., 1946. Nuclear Induction. Phys Rev, 70, 460-474.

Boutry,S., Forge,D., Burtea,C., Mahieu,I., Murariu,O., Laurent,S., Vander,E.L., Muller,R.N., 2009. How to quantify iron in an aqueous or biological matrix: a technical note. Contrast Media Mol Imaging, 4, 299-304.

Brooks,P.C., Clark,R.A., Cheresh,D.A., 1994. Requirement of vascular integrin alpha v beta 3 for angiogenesis. Science, 264, 569-571.

Cajot,S., Van,B.K., Paillard,A., Passirani,C., Garcion,E., Benoit,J.P., Varshney,S.K., Jerome,C., 2012. Smart nanocarriers for pH-triggered targeting and release of hydrophobic drugs. Acta Biomater, 8, 4215-4223.

Carmeliet,P., 2000. Mechanisms of angiogenesis and arteriogenesis. Nat Med, 6, 389-395.

Carmeliet,P., 2005. Angiogenesis in life, disease and medicine. Nature, 438, 932-936.

Carmeliet,P., Jain,R.K., 2011. Molecular mechanisms and clinical applications of angiogenesis. Nature, 473, 298-307.

Cecco,S., Aliberti,M., Baldo,P., Giacomin,E., Leone,R., 2014. Safety and efficacy evaluation of albumin-bound paclitaxel. Expert Opin Drug Saf, 13, 511-520.

Chatterjee,D.K., Fong,L.S., Zhang,Y., 2008. Nanoparticles in photodynamic therapy: an emerging paradigm. Adv Drug Deliv Rev, 60, 1627-1637.

Chen,W., Xu,N., Xu,L., Wang,L., Li,Z., Ma,W., Zhu,Y., Xu,C., Kotov,N.A., 2010. Multifunctional magnetoplasmonic nanoparticle assemblies for cancer therapy and diagnostics (theranostics). Macromol Rapid Commun, 31, 228-236.

Clifton,G.T., Sears,A.K., Clive,K.S., Holmes,J.P., Mittendorf,E.A., Ioannides,C.G., Ponniah,S., Peoples,G.E., 2011. Folate receptor alpha: a storied past and promising future in immunotherapy. Hum Vaccin, 7, 183-190.

Cohen,Y., Shoushan,S.Y., 2013. Magnetic nanoparticles-based diagnostics and theranostics. Curr Opin Biotechnol, 24, 672-681.

Cole,A.J., Yang,V.C., David,A.E., 2011. Cancer theranostics: the rise of targeted magnetic nanoparticles. Trends Biotechnol, 29, 323-332.

Cool,S.K., Geers,B., Roels,S., Stremersch,S., Vanderperren,K., Saunders,J.H., De Smedt,S.C., Demeester,J., Sanders,N.N., 2013. Coupling of drug containing liposomes to microbubbles improves ultrasound triggered drug delivery in mice. J Control Release, 172, 885-893.

Corot,C., Warlin,D., 2013. Superparamagnetic iron oxide nanoparticles for MRI: contrast media pharmaceutical company R&D perspective. Wiley Interdiscip Rev Nanomed Nanobiotechnol, 5, 411-422.

Cukierman,E., Khan,D.R., 2010. The benefits and challenges associated with the use of drug delivery systems in cancer therapy. Biochem Pharmacol, 80, 762-770.

Currie,S., Hoggard,N., Craven,I.J., Hadjivassiliou,M., Wilkinson,I.D., 2013. Understanding MRI: basic MR physics for physicians. Postgrad Med J, 89, 209-223.

Dandamudi,S., Campbell,R.B., 2007. The drug loading, cytotoxicty and tumor vascular targeting characteristics of magnetite in magnetic drug targeting. Biomaterials, 28, 4673-4683.

Dang,N.H., Hagemeister,F.B., Pro,B., McLaughlin,P., Romaguera,J.E., Jones,D., Samuels,B., Samaniego,F., Younes,A., Wang,M., Goy,A., Rodriguez,M.A., Walker,P.L., Arredondo,Y., Tong,A.T., Fayad,L., 2004. Phase II study of denileukin diftitox for relapsed/refractory B-Cell non-Hodgkin's lymphoma. J Clin Oncol, 22, 4095-4102.

Danhier,F., Ansorena,E., Silva,J.M., Coco,R., Le Breton A., Preat,V., 2012a. PLGA-based nanoparticles: an overview of biomedical applications. J Control Release, 161, 505-522.

Danhier,F., Feron,O., Preat,V., 2010. To exploit the tumor microenvironment: Passive and active tumor targeting of nanocarriers for anti-cancer drug delivery. J Control Release, 148, 135-146.

Danhier,F., Le Breton A., Preat,V., 2012b. RGD-based strategies to target alpha(v) beta(3) integrin in cancer therapy and diagnosis. Mol Pharm, 9, 2961-2973.

Danhier,F., Lecouturier,N., Vroman,B., Jerome,C., Marchand-Brynaert,J., Feron,O., Preat,V., 2009a. Paclitaxel-loaded PEGylated PLGA-based nanoparticles: in vitro and in vivo evaluation. J Control Release, 133, 11-17.

Danhier,F., Pourcelle,V., Marchand-Brynaert,J., Jerome,C., Feron,O., Preat,V., 2012c. Targeting of tumor endothelium by RGD-grafted PLGA-nanoparticles. Methods Enzymol, 508, 157-175.

Danhier,F., Vroman,B., Lecouturier,N., Crokart,N., Pourcelle,V., Freichels,H., Jerome,C., Marchand-Brynaert,J., Feron,O., Preat,V., 2009b. Targeting of tumor endothelium by RGD-grafted PLGA-nanoparticles loaded with paclitaxel. J Control Release, 140, 166-173.

Danhier,P., De Preter G., Boutry,S., Mahieu,I., Leveque,P., Magat,J., Haufroid,V., Sonveaux,P., Bouzin,C., Feron,O., Muller,R.N., Jordan,B.F., Gallez,B., 2012d. Electron paramagnetic resonance as a sensitive tool to assess the iron oxide content in cells for MRI cell labeling studies. Contrast Media Mol Imaging, 7, 302-307.

Danhier,P., De Preter G., Magat,J., Godechal,Q., Porporato,P.E., Jordan,B.F., Feron,O., Sonveaux,P., Gallez,B., 2014. Multimodal cell tracking of a spontaneous metastasis model: comparison between MRI, electron paramagnetic resonance and bioluminescence. Contrast Media Mol Imaging, 9, 143-153.

Das,M., Mohanty,C., Sahoo,S.K., 2009. Ligand-based targeted therapy for cancer tissue. Expert Opin Drug Deliv, 6, 285-304.

Dash,T.K., Konkimalla,V.B., 2012a. Polymeric modification and its implication in drug delivery: poly-epsilon-caprolactone (PCL) as a model polymer. Mol Pharm, 9, 2365-2379.

Dash,T.K., Konkimalla,V.B., 2012b. Poly-Đö-caprolactone based formulations for drug delivery and tissue engineering: A review. Journal of Controlled Release, 158, 15-33.

de Smet,M., Langereis,S., van den Bosch,S., Grull,H., 2010. Temperature-sensitive liposomes for doxorubicin delivery under MRI guidance. J Control Release, 143, 120-127.

Denard,B., Lee,C., Ye,J., 2012. Doxorubicin blocks proliferation of cancer cells through proteolytic activation of CREB3L1. Elife, 1, e00090.

Di Marco,M., Sadun,C., Port,M., Guilbert,I., Couvreur,P., Dubernet,C., 2007. Physicochemical characterization of ultrasmall superparamagnetic iron oxide particles (USPIO) for biomedical application as MRI contrast agents. Int J Nanomedicine, 2, 609-622.

Distler,J.H., Hirth,A., Kurowska-Stolarska,M., Gay,R.E., Gay,S., Distler,O., 2003. Angiogenic and angiostatic factors in the molecular control of angiogenesis. Q J Nucl Med, 47, 149-161.

Egusquiaguirre,S.P., Igartua,M., Hernandez,R.M., Pedraz,J.L., 2012. Nanoparticle delivery systems for cancer therapy: advances in clinical and preclinical research. Clin Transl Oncol, 14, 83-93.

Eliceiri,B.P., Cheresh,D.A., 2001. Adhesion events in angiogenesis. Curr Opin Cell Biol, 13, 563-568.

Fan,C.H., Ting,C.Y., Lin,H.J., Wang,C.H., Liu,H.L., Yen,T.C., Yeh,C.K., 2013. SPIO-conjugated, doxorubicin-loaded microbubbles for concurrent MRI and focused-ultrasound enhanced brain-tumor drug delivery. Biomaterials, 34, 3706-3715.

Fan,W., 1999. Possible mechanisms of paclitaxel-induced apoptosis. Biochem Pharmacol, 57, 1215-1221.

Fan,Z., Fu,P.P., Yu,H., Ray,P.C., 2014. Theranostic nanomedicine for cancer detection and treatment. Yao Wu Shi Pin Fen Xi, 22, 3-17.

Fang,J., Nakamura,H., Maeda,H., 2011. The EPR effect: Unique features of tumor blood vessels for drug delivery, factors involved, and limitations and augmentation of the effect. Adv Drug Deliv Rev, 63, 136-151.

Fang,J., Sawa,T., Maeda,H., 2003. Factors and mechanism of "EPR" effect and the enhanced antitumor effects of macromolecular drugs including SMANCS. Adv Exp Med Biol, 519, 29-49.

Feng,S.T., Li,J., Luo,Y., Yin,T., Cai,H., Wang,Y., Dong,Z., Shuai,X., Li,Z.P., 2014. pH-Sensitive Nanomicelles for Controlled and Efficient Drug Delivery to Human Colorectal Carcinoma LoVo Cells. PLoS One, 9, e100732.

Feron,O., 2009. Pyruvate into lactate and back: from the Warburg effect to symbiotic energy fuel exchange in cancer cells. Radiother Oncol, 92, 329-333.

Florence,A.T., 2012. "Targeting" nanoparticles: the constraints of physical laws and physical barriers. J Control Release, 164, 115-124.

Folkman,J., 1971. Tumor angiogenesis: therapeutic implications. N Engl J Med, 285, 1182-1186.

Forrest,R.A., Swift,L.P., Rephaeli,A., Nudelman,A., Kimura,K., Phillips,D.R., Cutts,S.M., 2012. Activation of DNA damage response pathways as a consequence of anthracycline-DNA adduct formation. Biochem Pharmacol, 83, 1602-1612.

Frenkel,V., 2008. Ultrasound mediated delivery of drugs and genes to solid tumors. Adv Drug Deliv Rev, 60, 1193-1208.

Friedland,D., Gorman,G., Treat,J., 1993. Hypersensitivity reactions from taxol and etoposide. J Natl Cancer Inst, 85, 2036.

Gao,Z., Kennedy,A.M., Christensen,D.A., Rapoport,N.Y., 2008. Drug-loaded nano/microbubbles for combining ultrasonography and targeted chemotherapy. Ultrasonics, 48, 260-270.

Garanger,E., Boturyn,D., Coll,J.L., Favrot,M.C., Dumy,P., 2006. Multivalent RGD synthetic peptides as potent alphaVbeta3 integrin ligands. Org Biomol Chem, 4, 1958-1965.

Garinot,M., Fievez,V., Pourcelle,V., Stoffelbach,F., des Rieux A., Plapied,L., Theate,I., Freichels,H., Jerome,C., Marchand-Brynaert,J., Schneider,Y.J., Preat,V., 2007. PEGylated PLGA-based nanoparticles targeting M cells for oral vaccination. J Control Release, 120, 195-204.

Gaucher,G., Marchessault,R.H., Leroux,J.C., 2010. Polyester-based micelles and nanoparticles for the parenteral delivery of taxanes. J Control Release, 143, 2-12.

Geers,B., Dewitte,H., De Smedt,S.C., Lentacker,I., 2012. Crucial factors and emerging concepts in ultrasound-triggered drug delivery. J Control Release, 164, 248-255.

Gewirtz,D.A., 1999. A critical evaluation of the mechanisms of action proposed for the antitumor effects of the anthracycline antibiotics adriamycin and daunorubicin. Biochem Pharmacol, 57, 727-741.

Gosk,S., Moos,T., Gottstein,C., Bendas,G., 2008. VCAM-1 directed immunoliposomes selectively target tumor vasculature in vivo. Biochim Biophys Acta, 1778, 854-863.

Gradishar,W.J., Tjulandin,S., Davidson,N., Shaw,H., Desai,N., Bhar,P., Hawkins,M., O'Shaughnessy,J., 2005. Phase III trial of nanoparticle albumin-bound paclitaxel

compared with polyethylated castor oil-based paclitaxel in women with breast cancer. J Clin Oncol, 23, 7794-7803.

Greish,K., 2007. Enhanced permeability and retention of macromolecular drugs in solid tumors: a royal gate for targeted anticancer nanomedicines. J Drug Target, 15, 457-464.

Griset,A.P., Walpole,J., Liu,R., Gaffey,A., Colson,Y.L., Grinstaff,M.W., 2009. Expansile nanoparticles: synthesis, characterization, and in vivo efficacy of an acid-responsive polymeric drug delivery system. J Am Chem Soc, 131, 2469-2471.

Gullotti,E., Yeo,Y., 2009. Extracellularly activated nanocarriers: a new paradigm of tumor targeted drug delivery. Mol Pharm, 6, 1041-1051.

Guo,X., Li,D., Yang,G., Shi,C., Tang,Z., Wang,J., Zhou,S., 2014. Thermo-triggered drug release from actively targeting polymer micelles. ACS Appl Mater Interfaces, 6, 8549-8559.

Gupta,A.K., Gupta,M., 2005. Synthesis and surface engineering of iron oxide nanoparticles for biomedical applications. Biomaterials, 26, 3995-4021.

Gupta,N., Hatoum,H., Dy,G.K., 2014. First line treatment of advanced non-small-cell lung cancer - specific focus on albumin bound paclitaxel. Int J Nanomedicine, 9, 209-221.

Guthi,J.S., Yang,S.G., Huang,G., Li,S., Khemtong,C., Kessinger,C.W., Peyton,M., Minna,J.D., Brown,K.C., Gao,J., 2010. MRI-visible micellar nanomedicine for targeted drug delivery to lung cancer cells. Mol Pharm, 7, 32-40.

Haley,B., Frenkel,E., 2008. Nanoparticles for drug delivery in cancer treatment. Urol Oncol, 26, 57-64.

Han,H.D., Mangala,L.S., Lee,J.W., Shahzad,M.M., Kim,H.S., Shen,D., Nam,E.J., Mora,E.M., Stone,R.L., Lu,C., Lee,S.J., Roh,J.W., Nick,A.M., Lopez-Berestein,G., Sood,A.K., 2010. Targeted gene silencing using RGD-labeled chitosan nanoparticles. Clin Cancer Res, 16, 3910-3922.

Hancock,H.A., Smith,L.H., Cuesta,J., Durrani,A.K., Angstadt,M., Palmeri,M.L., Kimmel,E., Frenkel,V., 2009. Investigations into pulsed high-intensity focused ultrasound-enhanced delivery: preliminary evidence for a novel mechanism. Ultrasound Med Biol, 35, 1722-1736.

Hans,M.L., Lowman,A.M., 2002. Biodegradable nanoparticles for drug delivery and targeting. Current Opinion in Solid State and Materials Science, 6, 319-327.

Harari,P.M., 2004. Epidermal growth factor receptor inhibition strategies in oncology. Endocr Relat Cancer, 11, 689-708.

Harrington,K.J., Mohammadtaghi,S., Uster,P.S., Glass,D., Peters,A.M., Vile,R.G., Stewart,J.S., 2001. Effective targeting of solid tumors in patients with locally advanced cancers by radiolabeled pegylated liposomes. Clin Cancer Res, 7, 243-254.

Haubner,R., Kuhnast,B., Mang,C., Weber,W.A., Kessler,H., Wester,H.J., Schwaiger,M., 2004. [18F]Galacto-RGD: synthesis, radiolabeling, metabolic stability, and radiation dose estimates. Bioconjug Chem, 15, 61-69.

Hayashi,K., Nakamura,M., Miki,H., Ozaki,S., Abe,M., Matsumoto,T., Sakamoto,W., Yogo,T., Ishimura,K., 2014. Magnetically responsive smart nanoparticles for cancer treatment with a combination of magnetic hyperthermia and remote-control drug release. Theranostics, 4, 834-844.

Heldin,C.H., Rubin,K., Pietras,K., Ostman,A., 2004. High interstitial fluid pressure - an obstacle in cancer therapy. Nat Rev Cancer, 4, 806-813.

Heo,D.N., Yang,D.H., Moon,H.J., Lee,J.B., Bae,M.S., Lee,S.C., Lee,W.J., Sun,I.C., Kwon,I.K., 2012. Gold nanoparticles surface-functionalized with paclitaxel drug and biotin receptor as theranostic agents for cancer therapy. Biomaterials, 33, 856-866.

Hong,G., Yuan,R., Liang,B., Shen,J., Yang,X., Shuai,X., 2008. Folate-functionalized polymeric micelle as hepatic carcinoma-targeted, MRI-ultrasensitive delivery system of antitumor drugs. Biomed Microdevices, 10, 693-700.

Horwitz,S.B., 1992. Mechanism of action of taxol. Trends Pharmacol Sci, 13, 134-136.

Howell,M., Mallela,J., Wang,C., Ravi,S., Dixit,S., Garapati,U., Mohapatra,S., 2013. Manganese-loaded lipid-micellar theranostics for simultaneous drug and gene delivery to lungs. J Control Release, 167, 210-218.

Hsu,A.R., Veeravagu,A., Cai,W., Hou,L.C., Tse,V., Chen,X., 2007. Integrin alpha v beta 3 antagonists for anti-angiogenic cancer treatment. Recent Pat Anticancer Drug Discov, 2, 143-158.

Hu,K.W., Hsu,K.C., Yeh,C.S., 2010. pH-Dependent biodegradable silica nanotubes derived from Gd(OH)3 nanorods and their potential for oral drug delivery and MR imaging. Biomaterials, 31, 6843-6848.

Huang,Z., Pei,N., Wang,Y., Xie,X., Sun,A., Shen,L., Zhang,S., Liu,X., Zou,Y., Qian,J., Ge,J., 2010. Deep magnetic capture of magnetically loaded cells for spatially targeted therapeutics. Biomaterials, 31, 2130-2140.

Huveneers,S., Truong,H., Danen,H.J., 2007. Integrins: signaling, disease, and therapy. Int J Radiat Biol, 83, 743-751.

Ibsen,S., Schutt,C.E., Esener,S., 2013. Microbubble-mediated ultrasound therapy: a review of its potential in cancer treatment. Drug Des Devel Ther, 7, 375-388.

Issa,M.C., Manela-Azulay,M., 2010. Photodynamic therapy: a review of the literature and image documentation. An Bras Dermatol, 85, 501-511.

Ittrich,H., Peldschus,K., Raabe,N., Kaul,M., Adam,G., 2013. Superparamagnetic iron oxide nanoparticles in biomedicine: applications and developments in diagnostics and therapy. Rofo, 185, 1149-1166.

Jain,R.K., 1987. Transport of molecules in the tumor interstitium: a review. Cancer Res, 47, 3039-3051.

Jain,R.K., 1988. Determinants of tumor blood flow: a review. Cancer Res, 48, 2641-2658.

Jain,R.K., 1990. Vascular and interstitial barriers to delivery of therapeutic agents in tumors. Cancer Metastasis Rev, 9, 253-266.

Jain,R.K., Stylianopoulos,T., 2010. Delivering nanomedicine to solid tumors. Nat Rev Clin Oncol, 7, 653-664.

Jerjes,W., Hamdoon,Z., Hopper,C., 2012. Photodynamic therapy in the management of potentially malignant and malignant oral disorders. Head Neck Oncol, 4, 16.

Johannsen,M., Gneveckow,U., Eckelt,L., Feussner,A., Waldofner,N., Scholz,R., Deger,S., Wust,P., Loening,S.A., Jordan,A., 2005. Clinical hyperthermia of prostate cancer using magnetic nanoparticles: presentation of a new interstitial technique. Int J Hyperthermia, 21, 637-647.

Jordan,A., Wust,P., Fahling,H., John,W., Hinz,A., Felix,R., 1993. Inductive heating of ferrimagnetic particles and magnetic fluids: physical evaluation of their potential for hyperthermia. Int J Hyperthermia, 9, 51-68.

Jurcic,J.G., 2001. Antibody therapy for residual disease in acute myelogenous leukemia. Crit Rev Oncol Hematol, 38, 37-45.

Justus,C.R., Dong,L., Yang,L.V., 2013. Acidic tumor microenvironment and pH-sensing G protein-coupled receptors. Front Physiol, 4, 354.

Kelkar,S.S., Reineke,T.M., 2011. Theranostics: combining imaging and therapy. Bioconjug Chem, 22, 1879-1903.

Khemtong,C., Kessinger,C.W., Ren,J., Bey,E.A., Yang,S.G., Guthi,J.S., Boothman,D.A., Sherry,A.D., Gao,J., 2009. In vivo off-resonance saturation magnetic resonance

imaging of alphavbeta3-targeted superparamagnetic nanoparticles. Cancer Res, 69, 1651-1658.

Kiessling,F., Fokong,S., Koczera,P., Lederle,W., Lammers,T., 2012. Ultrasound microbubbles for molecular diagnosis, therapy, and theranostics. J Nucl Med, 53, 345-348.

Kim,I.Y., Kang,Y.S., Lee,D.S., Park,H.J., Choi,E.K., Oh,Y.K., Son,H.J., Kim,J.S., 2009. Antitumor activity of EGFR targeted pH-sensitive immunoliposomes encapsulating gemcitabine in A549 xenograft nude mice. J Control Release, 140, 55-60.

Kim,J., Kim,H.S., Lee,N., Kim,T., Kim,H., Yu,T., Song,I.C., Moon,W.K., Hyeon,T., 2008. Multifunctional uniform nanoparticles composed of a magnetite nanocrystal core and a mesoporous silica shell for magnetic resonance and fluorescence imaging and for drug delivery. Angew Chem Int Ed Engl, 47, 8438-8441.

Kocbek,P., Kralj,S., Kreft,M.E., Kristl,J., 2013. Targeting intracellular compartments by magnetic polymeric nanoparticles. Eur J Pharm Sci, 50, 130-138.

Kohler,N., Sun,C., Fichtenholtz,A., Gunn,J., Fang,C., Zhang,M., 2006. Methotrexate-immobilized poly(ethylene glycol) magnetic nanoparticles for MR imaging and drug delivery. Small, 2, 785-792.

Kohler,N., Sun,C., Wang,J., Zhang,M., 2005. Methotrexate-modified superparamagnetic nanoparticles and their intracellular uptake into human cancer cells. Langmuir, 21, 8858-8864.

Kolhatkar,A.G., Jamison,A.C., Litvinov,D., Willson,R.C., Lee,T.R., 2013. Tuning the magnetic properties of nanoparticles. Int J Mol Sci, 14, 15977-16009.

Konan,Y.N., Berton,M., Gurny,R., Allemann,E., 2003. Enhanced photodynamic activity of meso-tetra(4-hydroxyphenyl)porphyrin by incorporation into sub-200 nm nanoparticles. Eur J Pharm Sci, 18, 241-249.

Krishna,M.C., Devasahayam,N., Cook,J.A., Subramanian,S., Kuppusamy,P., Mitchell,J.B., 2001. Electron paramagnetic resonance for small animal imaging applications. ILAR J, 42, 209-218.

Kumagai,M., Kano,M.R., Morishita,Y., Ota,M., Imai,Y., Nishiyama,N., Sekino,M., Ueno,S., Miyazono,K., Kataoka,K., 2009. Enhanced magnetic resonance imaging of experimental pancreatic tumor in vivo by block copolymer-coated magnetite nanoparticles with TGF-beta inhibitor. J Control Release, 140, 306-311.

Kumari,A., Yadav,S.K., 2011. Cellular interactions of therapeutically delivered nanoparticles. Expert Opin Drug Deliv, 8, 141-151.

Kumari,A., Yadav,S.K., Yadav,S.C., 2010. Biodegradable polymeric nanoparticles based drug delivery systems. Colloids Surf B Biointerfaces, 75, 1-18.

Kwon,I.K., Lee,S.C., Han,B., Park,K., 2012. Analysis on the current status of targeted drug delivery to tumors. J Control Release, 164, 108-114.

Lammers,T., Aime,S., Hennink,W.E., Storm,G., Kiessling,F., 2011. Theranostic nanomedicine. Acc Chem Res, 44, 1029-1038.

Lammers,T., Hennink,W.E., Storm,G., 2008. Tumour-targeted nanomedicines: principles and practice. Br J Cancer, 99, 392-397.

Lammers,T., Kiessling,F., Hennink,W.E., Storm,G., 2010. Nanotheranostics and image-guided drug delivery: current concepts and future directions. Mol Pharm, 7, 1899-1912.

Lammers,T., Kiessling,F., Hennink,W.E., Storm,G., 2012a. Drug targeting to tumors: principles, pitfalls and (pre-) clinical progress. J Control Release, 161, 175-187.

Lammers,T., Rizzo,L.Y., Storm,G., Kiessling,F., 2012b. Personalized nanomedicine. Clin Cancer Res, 18, 4889-4894.

Laurent,S., Forge,D., Port,M., Roch,A., Robic,C., Vander,E.L., Muller,R.N., 2008. Magnetic iron oxide nanoparticles: synthesis, stabilization, vectorization, physicochemical characterizations, and biological applications. Chem Rev, 108, 2064-2110.

Laurent,S., Mahmoudi,M., 2011. Superparamagnetic iron oxide nanoparticles: promises for diagnosis and treatment of cancer. Int J Mol Epidemiol Genet, 2, 367-390.

Laurent,S., Saei,A.A., Behzadi,S., Panahifar,A., Mahmoudi,M., 2014. Superparamagnetic iron oxide nanoparticles for delivery of therapeutic agents: opportunities and challenges. Expert Opin Drug Deliv, 1-22.

Lee,E.S., Oh,K.T., Kim,D., Youn,Y.S., Bae,Y.H., 2007. Tumor pH-responsive flower-like micelles of poly(L-lactic acid)-b-poly(ethylene glycol)-b-poly(L-histidine). J Control Release, 123, 19-26.

Lee,P.W., Hsu,S.H., Wang,J.J., Tsai,J.S., Lin,K.J., Wey,S.P., Chen,F.R., Lai,C.H., Yen,T.C., Sung,H.W., 2010. The characteristics, biodistribution, magnetic resonance imaging and biodegradability of superparamagnetic core-shell nanoparticles. Biomaterials, 31, 1316-1324.

Lentacker,I., Geers,B., Demeester,J., De Smedt,S.C., Sanders,N.N., 2010. Design and evaluation of doxorubicin-containing microbubbles for ultrasound-triggered doxorubicin delivery: cytotoxicity and mechanisms involved. Mol Ther, 18, 101-108.

Li,W., Cai,X., Kim,C., Sun,G., Zhang,Y., Deng,R., Yang,M., Chen,J., Achilefu,S., Wang,L.V., Xia,Y., 2011. Gold nanocages covered with thermally-responsive polymers for controlled release by high-intensity focused ultrasound. Nanoscale, 3, 1724-1730.

Li,X., Li,H., Yi,W., Chen,J., Liang,B., 2013a. Acid-triggered core cross-linked nanomicelles for targeted drug delivery and magnetic resonance imaging in liver cancer cells. Int J Nanomedicine, 8, 3019-3031.

Li,Y., Zheng,X., Sun,Y., Ren,Z., Li,X., Cui,G., 2014. RGD-fatty alcohol-modified docetaxel liposomes improve tumor selectivity in vivo. Int J Pharm, 468, 133-141.

Li,Z., Wang,C., Cheng,L., Gong,H., Yin,S., Gong,Q., Li,Y., Liu,Z., 2013b. PEG-functionalized iron oxide nanoclusters loaded with chlorin e6 for targeted, NIR light induced, photodynamic therapy. Biomaterials, 34, 9160-9170.

Lin,P.C., Lin,S., Wang,P.C., Sridhar,R., 2014. Techniques for physicochemical characterization of nanomaterials. Biotechnol Adv, 32, 711-726.

Ling,Y., Wei,K., Luo,Y., Gao,X., Zhong,S., 2011. Dual docetaxel/superparamagnetic iron oxide loaded nanoparticles for both targeting magnetic resonance imaging and cancer therapy. Biomaterials, 32, 7139-7150.

Ling,Y., Wei,K., Zou,F., Zhong,S., 2012. Temozolomide loaded PLGA-based superparamagnetic nanoparticles for magnetic resonance imaging and treatment of malignant glioma. Int J Pharm, 430, 266-275.

Liong,M., Lu,J., Kovochich,M., Xia,T., Ruehm,S.G., Nel,A.E., Tamanoi,F., Zink,J.I., 2008. Multifunctional inorganic nanoparticles for imaging, targeting, and drug delivery. ACS Nano, 2, 889-896.

Liu,S., 2006. Radiolabeled multimeric cyclic RGD peptides as integrin alphavbeta3 targeted radiotracers for tumor imaging. Mol Pharm, 3, 472-487.

Liu,Z., Wang,F., 2013. Development of RGD-based radiotracers for tumor imaging and therapy: translating from bench to bedside. Curr Mol Med, 13, 1487-1505.

Lu,J., Jackson,J.K., Gleave,M.E., Burt,H.M., 2008. The preparation and characterization of anti-VEGFR2 conjugated, paclitaxel-loaded PLLA or PLGA microspheres for the systemic targeting of human prostate tumors. Cancer Chemother Pharmacol, 61, 997-1005.

Lu,J., Ma,S., Sun,J., Xia,C., Liu,C., Wang,Z., Zhao,X., Gao,F., Gong,Q., Song,B., Shuai,X., Ai,H., Gu,Z., 2009. Manganese ferrite nanoparticle micellar nanocomposites as MRI contrast agent for liver imaging. Biomaterials, 30, 2919-2928.

Lubbe,A.S., Bergemann,C., Huhnt,W., Fricke,T., Riess,H., Brock,J.W., Huhn,D., 1996. Preclinical experiences with magnetic drug targeting: tolerance and efficacy. Cancer Res, 56, 4694-4701.

Lv,Y., Yang,B., Jiang,T., Li,Y.M., He,F., Zhuo,R.X., 2014. Folate-conjugated amphiphilic block copolymers for targeted and efficient delivery of doxorubicin. Colloids Surf B Biointerfaces, 115, 253-259.

Maeda,H., 2012. Vascular permeability in cancer and infection as related to macromolecular drug delivery, with emphasis on the EPR effect for tumor-selective drug targeting. Proc Jpn Acad Ser B Phys Biol Sci, 88, 53-71.

Maeda,H., Bharate,G.Y., Daruwalla,J., 2009. Polymeric drugs for efficient tumor-targeted drug delivery based on EPR-effect. Eur J Pharm Biopharm, 71, 409-419.

Maeda,H., Nakamura,H., Fang,J., 2013. The EPR effect for macromolecular drug delivery to solid tumors: Improvement of tumor uptake, lowering of systemic toxicity, and distinct tumor imaging in vivo. Adv Drug Deliv Rev, 65, 71-79.

Maeda,H., Wu,J., Sawa,T., Matsumura,Y., Hori,K., 2000. Tumor vascular permeability and the EPR effect in macromolecular therapeutics: a review. J Control Release, 65, 271-284.

Maeng,J.H., Lee,D.H., Jung,K.H., Bae,Y.H., Park,I.S., Jeong,S., Jeon,Y.S., Shim,C.K., Kim,W., Kim,J., Lee,J., Lee,Y.M., Kim,J.H., Kim,W.H., Hong,S.S., 2010. Multifunctional doxorubicin loaded superparamagnetic iron oxide nanoparticles for chemotherapy and magnetic resonance imaging in liver cancer. Biomaterials, 31, 4995-5006.

Mahdavi,M., Ahmad,M.B., Haron,M.J., Namvar,F., Nadi,B., Rahman,M.Z., Amin,J., 2013. Synthesis, surface modification and characterisation of biocompatible magnetic iron oxide nanoparticles for biomedical applications. Molecules, 18, 7533-7548.

Maier-Hauff,K., Ulrich,F., Nestler,D., Niehoff,H., Wust,P., Thiesen,B., Orawa,H., Budach,V., Jordan,A., 2011. Efficacy and safety of intratumoral thermotherapy using magnetic iron-oxide nanoparticles combined with external beam radiotherapy on patients with recurrent glioblastoma multiforme. J Neurooncol, 103, 317-324.

Malietzis,G., Monzon,L., Hand,J., Wasan,H., Leen,E., Abel,M., Muhammad,A., Price,P., Abel,P., 2013. High-intensity focused ultrasound: advances in technology and experimental trials support enhanced utility of focused ultrasound surgery in oncology. Br J Radiol, 86, 20130044.

Marchetti,P., Urien,S., Cappellini,G.A., Ronzino,G., Ficorella,C., 2002. Weekly administration of paclitaxel: theoretical and clinical basis. Crit Rev Oncol Hematol, 44 Suppl, S3-13.

Marelli,U.K., Rechenmacher,F., Sobahi,T.R., Mas-Moruno,C., Kessler,H., 2013. Tumor Targeting via Integrin Ligands. Front Oncol, 3, 222.

Matsumura,Y., Maeda,H., 1986. A new concept for macromolecular therapeutics in cancer chemotherapy: mechanism of tumoritropic accumulation of proteins and the antitumor agent smancs. Cancer Res, 46, 6387-6392.

May,J.P., Li,S.D., 2013. Hyperthermia-induced drug targeting. Expert Opin Drug Deliv, 10, 511-527.

Melancon,M.P., Lu,W., Zhong,M., Zhou,M., Liang,G., Elliott,A.M., Hazle,J.D., Myers,J.N., Li,C., Stafford,R.J., 2011. Targeted multifunctional gold-based nanoshells for magnetic resonance-guided laser ablation of head and neck cancer. Biomaterials, 32, 7600-7608.

Meng,S., Su,B., Li,W., Ding,Y., Tang,L., Zhou,W., Song,Y., Caicun,Z., 2011. Integrin-targeted paclitaxel nanoliposomes for tumor therapy. Med Oncol, 28, 1180-1187.

Mitra,A., Nan,A., Ghandehari,H., McNeill,E., Mulholland,J., Line,B.R., 2004. Technetium-99m-Labeled N-(2-hydroxypropyl) methacrylamide copolymers: synthesis, characterization, and in vivo biodistribution. Pharm Res, 21, 1153-1159.

Mo,S., Coussios,C.C., Seymour,L., Carlisle,R., 2012. Ultrasound-enhanced drug delivery for cancer. Expert Opin Drug Deliv, 9, 1525-1538.

Moses,B., You,Y., 2013. Emerging strategies for controlling drug release by using visible/near IR light. Medicinal Chemistry, 3, 192-198.

Mukherjee,S., Chowdhury,D., Kotcherlakota,R., Patra,S., Vinothkumar,B., Bhadra,M.P., Sreedhar,B., Patra,C.R., 2014. Potential theranostics application of bio-synthesized silver nanoparticles (4-in-1 system). Theranostics, 4, 316-335.

Mura,S., Couvreur,P., 2012. Nanotheranostics for personalized medicine. Adv Drug Deliv Rev, 64, 1394-1416.

Murphy,E.A., Majeti,B.K., Barnes,L.A., Makale,M., Weis,S.M., Lutu-Fuga,K., Wrasidlo,W., Cheresh,D.A., 2008. Nanoparticle-mediated drug delivery to tumor vasculature suppresses metastasis. Proc Natl Acad Sci U S A, 105, 9343-9348.

Nasongkla,N., Bey,E., Ren,J., Ai,H., Khemtong,C., Guthi,J.S., Chin,S.F., Sherry,A.D., Boothman,D.A., Gao,J., 2006. Multifunctional polymeric micelles as cancer-targeted, MRI-ultrasensitive drug delivery systems. Nano Lett, 6, 2427-2430.

Naumov,G.N., Akslen,L.A., Folkman,J., 2006. Role of angiogenesis in human tumor dormancy: animal models of the angiogenic switch. Cell Cycle, 5, 1779-1787.

Nichols,J.W., Bae,Y.H., 2012. Odyssey of a cancer nanoparticle: from injection site to site of action. Nano Today, 7, 606-618.

Nichols,J.W., Bae,Y.H., 2014. EPR: Evidence and fallacy. J Control Release.

Nyst,H.J., Tan,I.B., Stewart,F.A., Balm,A.J., 2009. Is photodynamic therapy a good alternative to surgery and radiotherapy in the treatment of head and neck cancer? Photodiagnosis Photodyn Ther, 6, 3-11.

O'Brien,M.E., Wigler,N., Inbar,M., Rosso,R., Grischke,E., Santoro,A., Catane,R., Kieback,D.G., Tomczak,P., Ackland,S.P., Orlandi,F., Mellars,L., Alland,L., Tendler,C., 2004. Reduced cardiotoxicity and comparable efficacy in a phase III trial of pegylated liposomal doxorubicin HCl (CAELYX/Doxil) versus conventional doxorubicin for first-line treatment of metastatic breast cancer. Ann Oncol, 15, 440-449.

Oerlemans,C., Bult,W., Bos,M., Storm,G., Nijsen,J.F., Hennink,W.E., 2010. Polymeric micelles in anticancer therapy: targeting, imaging and triggered release. Pharm Res, 27, 2569-2589.

Panchagnula,R., 1998. Pharmaceutical aspects of paclitaxel. International Journal of Pharmaceutics, 172, 1-15.

Park,I.K., Ng,C.P., Wang,J., Chu,B., Yuan,C., Zhang,S., Pun,S.H., 2008a. Determination of nanoparticle vehicle unpackaging by MR imaging of a T(2) magnetic relaxation switch. Biomaterials, 29, 724-732.

Park,J.H., von,M.G., Ruoslahti,E., Bhatia,S.N., Sailor,M.J., 2008b. Micellar hybrid nanoparticles for simultaneous magnetofluorescent imaging and drug delivery. Angew Chem Int Ed Engl, 47, 7284-7288.

Peer,D., Karp,J.M., Hong,S., Farokhzad,O.C., Margalit,R., Langer,R., 2007. Nanocarriers as an emerging platform for cancer therapy. Nat Nanotechnol, 2, 751-760.

Peng,X.H., Qian,X., Mao,H., Wang,A.Y., Chen,Z.G., Nie,S., Shin,D.M., 2008. Targeted magnetic iron oxide nanoparticles for tumor imaging and therapy. Int J Nanomedicine, 3, 311-321.

Peppicelli,S., Bianchini,F., Calorini,L., 2014. Extracellular acidity, a "reappreciated" trait of tumor environment driving malignancy: perspectives in diagnosis and therapy. Cancer Metastasis Rev, 33, 823-832.

Petros,R.A., DeSimone,J.M., 2010. Strategies in the design of nanoparticles for therapeutic applications. Nat Rev Drug Discov, 9, 615-627.

Pierschbacher,M.D., Ruoslahti,E., 1984. Cell attachment activity of fibronectin can be duplicated by small synthetic fragments of the molecule. Nature, 309, 30-33.

Pohlmann,A.R., Fonseca,F.N., Paese,K., Detoni,C.B., Coradini,K., Beck,R.C., Guterres,S.S., 2013. Poly(-caprolactone) microcapsules and nanocapsules in drug delivery. Expert Opin Drug Deliv, 10, 623-638.

Polyak,B., Fishbein,I., Chorny,M., Alferiev,I., Williams,D., Yellen,B., Friedman,G., Levy,R.J., 2008. High field gradient targeting of magnetic nanoparticle-loaded endothelial cells to the surfaces of steel stents. Proc Natl Acad Sci U S A, 105, 698-703.

Pourcelle,V., Devouge,S., Garinot,M., Preat,V., Marchand-Brynaert,J., 2007. PCL-PEG-based nanoparticles grafted with GRGDS peptide: preparation and surface analysis by XPS. Biomacromolecules, 8, 3977-3983.

Pradhan,P., Giri,J., Rieken,F., Koch,C., Mykhaylyk,O., Doblinger,M., Banerjee,R., Bahadur,D., Plank,C., 2010. Targeted temperature sensitive magnetic liposomes for thermo-chemotherapy. J Control Release, 142, 108-121.

Prokop,A., Davidson,J.M., 2008. Nanovehicular intracellular delivery systems. J Pharm Sci, 97, 3518-3590.

Radermacher,K.A., Boutry,S., Laurent,S., Vander Elst,L.V., Mahieu,I., Bouzin,C., Magat,J., Gregoire,V., Feron,O., Muller,R.N., Jordan,B.F., Gallez,B., 2010. Iron oxide particles covered with hexapeptides targeted at phosphatidylserine as MR biomarkers of tumor cell death. Contrast Media Mol Imaging, 5, 258-267.

Reddy,G.R., Bhojani,M.S., McConville,P., Moody,J., Moffat,B.A., Hall,D.E., Kim,G., Koo,Y.E., Woolliscroft,M.J., Sugai,J.V., Johnson,T.D., Philbert,M.A., Kopelman,R., Rehemtulla,A., Ross,B.D., 2006. Vascular targeted nanoparticles for imaging and treatment of brain tumors. Clin Cancer Res, 12, 6677-6686.

Reddy,L.H., Arias,J.L., Nicolas,J., Couvreur,P., 2012. Magnetic nanoparticles: design and characterization, toxicity and biocompatibility, pharmaceutical and biomedical applications. Chem Rev, 112, 5818-5878.

Riegler,J., Wells,J.A., Kyrtatos,P.G., Price,A.N., Pankhurst,Q.A., Lythgoe,M.F., 2010. Targeted magnetic delivery and tracking of cells using a magnetic resonance imaging system. Biomaterials, 31, 5366-5371.

Rizzo,L.Y., Theek,B., Storm,G., Kiessling,F., Lammers,T., 2013. Recent progress in nanomedicine: therapeutic, diagnostic and theranostic applications. Curr Opin Biotechnol, 24, 1159-1166.

Robinson,J.T., Welsher,K., Tabakman,S.M., Sherlock,S.P., Wang,H., Luong,R., Dai,H., 2010. High Performance In Vivo Near-IR (>1 mum) Imaging and Photothermal Cancer Therapy with Carbon Nanotubes. Nano Res, 3, 779-793.

Rosen,J.E., Chan,L., Shieh,D.B., Gu,F.X., 2012. Iron oxide nanoparticles for targeted cancer imaging and diagnostics. Nanomedicine, 8, 275-290.

Rowinsky,E.K., Donehower,R.C., 1995. Paclitaxel (taxol). N Engl J Med, 332, 1004-1014.

Ruoslahti,E., 1996. RGD and other recognition sequences for integrins. Annu Rev Cell Dev Biol, 12, 697-715.

Sahu,I.D., McCarrick,R.M., Lorigan,G.A., 2013. Use of electron paramagnetic resonance to solve biochemical problems. Biochemistry, 52, 5967-5984.

Saltiel,E., McGuire,W., 1983. Doxorubicin (adriamycin) cardiomyopathy. West J Med, 139, 332-341.

Santhosh,P.B., Ulrih,N.P., 2013. Multifunctional superparamagnetic iron oxide nanoparticles: promising tools in cancer theranostics. Cancer Lett, 336, 8-17.

Savellano,M.D., Hasan,T., 2005. Photochemical targeting of epidermal growth factor receptor: a mechanistic study. Clin Cancer Res, 11, 1658-1668.

Sawant,R.M., Cohen,M.B., Torchilin,V.P., Rokhlin,O.W., 2008. Prostate cancer-specific monoclonal antibody 5D4 significantly enhances the cytotoxicity of doxorubicin-loaded liposomes against target cells in vitro. J Drug Target, 16, 601-604.

Schiff,P.B., Fant,J., Horwitz,S.B., 1979. Promotion of microtubule assembly in vitro by taxol. Nature, 277, 665-667.

Schleich,N., Po,C., Jacobs,D., Ucakar,B., Gallez,B., Danhier,F., Préat,V., 2014. Comparison of active, passive and magnetic targeting to tumors of multifunctional paclitaxel/SPIO-loaded nanoparticles for tumor imaging and therapy. J Control Release.

Schleich,N., Sibret,P., Danhier,P., Ucakar,B., Laurent,S., Muller,R.N., Jerome,C., Gallez,B., Preat,V., Danhier,F., 2013. Dual anticancer drug/superparamagnetic iron oxide-loaded PLGA-based nanoparticles for cancer therapy and magnetic resonance imaging. Int J Pharm, 447, 94-101.

Schmieder,A.H., Caruthers,S.D., Zhang,H., Williams,T.A., Robertson,J.D., Wickline,S.A., Lanza,G.M., 2008. Three-dimensional MR mapping of angiogenesis with alpha5beta1(alpha nu beta3)-targeted theranostic nanoparticles in the MDA-MB-435 xenograft mouse model. FASEB J, 22, 4179-4189.

Seymour,L.W., Ferry,D.R., Anderson,D., Hesslewood,S., Julyan,P.J., Poyner,R., Doran,J., Young,A.M., Burtles,S., Kerr,D.J., 2002. Hepatic drug targeting: phase I evaluation of polymer-bound doxorubicin. J Clin Oncol, 20, 1668-1676.

Shan,L., 2004. Polyethylene glycol-coated and folic acid-conjugated superparamagnetic iron oxide nanoparticles.

Sharkey,R.M., Goldenberg,D.M., 2006. Targeted therapy of cancer: new prospects for antibodies and immunoconjugates. CA Cancer J Clin, 56, 226-243.

Shen,J., Kim,H.C., Su,H., Wang,F., Wolfram,J., Kirui,D., Mai,J., Mu,C., Ji,L.N., Mao,Z.W., Shen,H., 2014. Cyclodextrin and Polyethylenimine Functionalized Mesoporous Silica Nanoparticles for Delivery of siRNA Cancer Therapeutics. Theranostics, 4, 487-497.

Singh,M., Mugler,K., Hailoo,D.W., Burke,S., Nemesure,B., Torkko,K., Shroyer,K.R., 2011. Differential expression of transferrin receptor (TfR) in a spectrum of normal to malignant breast tissues: implications for in situ and invasive carcinoma. Appl Immunohistochem Mol Morphol, 19, 417-423.

Singla,A.K., Garg,A., Aggarwal,D., 2002. Paclitaxel and its formulations. Int J Pharm, 235, 179-192.

Son,H.N., Nam,J.O., Kim,S., Kim,I.S., 2013. Multiple FAS1 domains and the RGD motif of TGFBI act cooperatively to bind alphavbeta3 integrin, leading to anti-angiogenic and anti-tumor effects. Biochim Biophys Acta, 1833, 2378-2388.

Soppimath,K.S., Aminabhavi,T.M., Kulkarni,A.R., Rudzinski,W.E., 2001. Biodegradable polymeric nanoparticles as drug delivery devices. J Control Release, 70, 1-20.

Spasojevic,I., 2011. Free radicals and antioxidants at a glance using EPR spectroscopy. Crit Rev Clin Lab Sci, 48, 114-142.

Stollman,T.H., Ruers,T.J.M., Oyen,W.J.G., Boerman,O.C., 2009. New targeted probes for radioimaging of angiogenesis. Methods, 48, 188-192.

Sultana,S., Khan,M.R., Kumar,M., Kumar,S., Ali,M., 2013. Nanoparticles-mediated drug delivery approaches for cancer targeting: a review. J Drug Target, 21, 107-125.

Ta,T., Porter,T.M., 2013. Thermosensitive liposomes for localized delivery and triggered release of chemotherapy. J Control Release, 169, 112-125.

Tacar,O., Dass,C.R., 2013. Doxorubicin-induced death in tumour cells and cardiomyocytes: is autophagy the key to improving future clinical outcomes? J Pharm Pharmacol, 65, 1577-1589.

Talelli,M., Oliveira,S., Rijcken,C.J., Pieters,E.H., Etrych,T., Ulbrich,K., van Nostrum,R.C., Storm,G., Hennink,W.E., Lammers,T., 2013. Intrinsically active nanobody-modified polymeric micelles for tumor-targeted combination therapy. Biomaterials, 34, 1255-1260.

Temming,K., Schiffelers,R.M., Molema,G., Kok,R.J., 2005. RGD-based strategies for selective delivery of therapeutics and imaging agents to the tumour vasculature. Drug Resist Updat, 8, 381-402.

Teng,L., Xie,J., Teng,L., Lee,R.J., 2012. Clinical translation of folate receptor-targeted therapeutics. Expert Opin Drug Deliv, 9, 901-908.

Toffoli,G., Cernigoi,C., Russo,A., Gallo,A., Bagnoli,M., Boiocchi,M., 1997. Overexpression of folate binding protein in ovarian cancers. Int J Cancer, 74, 193-198.

Torchilin,V.P., 2000. Drug targeting. Eur J Pharm Sci, 11 Suppl 2, S81-S91.

Torchilin,V.P., 2004. Targeted polymeric micelles for delivery of poorly soluble drugs. Cell Mol Life Sci, 61, 2549-2559.

Tortorella,S., Karagiannis,T.C., 2014. Transferrin receptor-mediated endocytosis: a useful target for cancer therapy. J Membr Biol, 247, 291-307.

Trivedi,S., Concha-Benavente,F., Srivastava,R.M., Jie,H.B., Gibson,S.P., Schmitt,N.C., Ferris,R.L., 2014. Immune biomarkers of anti-EGFR monoclonal antibody therapy. Ann Oncol.

van der Meel,R., Vehmeijer,L.J., Kok,R.J., Storm,G., van Gaal,E.V., 2013. Ligand-targeted particulate nanomedicines undergoing clinical evaluation: current status. Adv Drug Deliv Rev, 65, 1284-1298.

van Ewijk,G.A., Vroege,G.J., Philipse,A.P., 1999. Convenient preparation methods for magnetic colloids. Journal of Magnetism and Magnetic Materials, 201, 31-33.

von Wnuck,L.K., Keul,P., Ferri,N., Lucke,S., Heusch,G., Fischer,J.W., Levkau,B., 2006. Integrin-mediated transcriptional activation of inhibitor of apoptosis proteins protects smooth muscle cells against apoptosis induced by degraded collagen. Circ Res, 98, 1490-1497.

Wahajuddin, Arora,S., 2012. Superparamagnetic iron oxide nanoparticles: magnetic nanoplatforms as drug carriers. Int J Nanomedicine, 7, 3445-3471.

Wall,M.E., Wani,M.C., 1995. Camptothecin and taxol: discovery to clinic--thirteenth Bruce F. Cain Memorial Award Lecture. Cancer Res, 55, 753-760.

Wang,D., Fei,B., Halig,L.V., Qin,X., Hu,Z., Xu,H., Wang,Y.A., Chen,Z., Kim,S., Shin,D.M., Chen,Z.G., 2014. Targeted Iron-Oxide Nanoparticle for Photodynamic Therapy and Imaging of Head and Neck Cancer. ACS Nano.

Wang,M., Thanou,M., 2010. Targeting nanoparticles to cancer. Pharmacol Res, 62, 90-99.

Wang,Y.X., Hussain,S.M., Krestin,G.P., 2001. Superparamagnetic iron oxide contrast agents: physicochemical characteristics and applications in MR imaging. Eur Radiol, 11, 2319-2331.

Wang,Y.X., Xuan,S., Port,M., Idee,J.M., 2013. Recent advances in superparamagnetic iron oxide nanoparticles for cellular imaging and targeted therapy research. Curr Pharm Des, 19, 6575-6593.

Wani,M.C., Taylor,H.L., Wall,M.E., Coggon,P., McPhail,A.T., 1971. Plant antitumor agents. VI. The isolation and structure of taxol, a novel antileukemic and antitumor agent from Taxus brevifolia. J Am Chem Soc, 93, 2325-2327.

Weis,S.M., Cheresh,D.A., 2011. alphaV integrins in angiogenesis and cancer. Cold Spring Harb Perspect Med, 1, a006478.

Wiseman,G.A., White,C.A., Witzig,T.E., Gordon,L.I., Emmanouilides,C., Raubitschek,A., Janakiraman,N., Gutheil,J., Schilder,R.J., Spies,S., Silverman,D.H., Grillo-Lopez,A.J., 1999. Radioimmunotherapy of relapsed non-Hodgkin's lymphoma with zevalin, a 90Y-labeled anti-CD20 monoclonal antibody. Clin Cancer Res, 5, 3281s-3286s.

Xiao,Y., Hong,H., Javadi,A., Engle,J.W., Xu,W., Yang,Y., Zhang,Y., Barnhart,T.E., Cai,W., Gong,S., 2012. Multifunctional unimolecular micelles for cancer-targeted drug delivery and positron emission tomography imaging. Biomaterials, 33, 3071-3082.

Xie,J., Lee,S., Chen,X., 2010. Nanoparticle-based theranostic agents. Adv Drug Deliv Rev, 62, 1064-1079.

Xu,F., Lei,D., Du,X., Zhang,C., Xie,X., Yin,D., 2011. Modification of MR molecular imaging probes with cysteine-terminated peptides and their potential for in vivo tumour detection. Contrast Media Mol Imaging, 6, 46-54.

Yallapu,M.M., Othman,S.F., Curtis,E.T., Gupta,B.K., Jaggi,M., Chauhan,S.C., 2011. Multi-functional magnetic nanoparticles for magnetic resonance imaging and cancer therapy. Biomaterials, 32, 1890-1905.

Yang,F., Teves,S.S., Kemp,C.J., Henikoff,S., 2014a. Doxorubicin, DNA torsion, and chromatin dynamics. Biochim Biophys Acta, 1845, 84-89.

Yang,H.W., Hua,M.Y., Liu,H.L., Tsai,R.Y., Pang,S.T., Hsu,P.H., Tang,H.J., Yen,T.C., Chuang,C.K., 2012. An epirubicin-conjugated nanocarrier with MRI function to overcome lethal multidrug-resistant bladder cancer. Biomaterials, 33, 3919-3930.

Yang,K.N., Zhang,C.Q., Wang,W., Wang,P.C., Zhou,J.P., Liang,X.J., 2014b. pH-responsive mesoporous silica nanoparticles employed in controlled drug delivery systems for cancer treatment. Cancer Biol Med, 11, 34-43.

Yang,P.S., Tung,F.I., Chen,H.P., Liu,T.Y., Lin,Y.Y., 2014c. A novel bubble-forming material for preparing hydrophobic-agent-loaded bubbles with theranostic functionality. Acta Biomater, 10, 3762-3774.

Yang,X., Grailer,J.J., Rowland,I.J., Javadi,A., Hurley,S.A., Steeber,D.A., Gong,S., 2010. Multifunctional SPIO/DOX-loaded wormlike polymer vesicles for cancer therapy and MR imaging. Biomaterials, 31, 9065-9073.

Yang,X., Hong,H., Grailer,J.J., Rowland,I.J., Javadi,A., Hurley,S.A., Xiao,Y., Yang,Y., Zhang,Y., Nickles,R.J., Cai,W., Steeber,D.A., Gong,S., 2011. cRGD-functionalized, DOX-conjugated, and (6)(4)Cu-labeled superparamagnetic iron oxide nanoparticles for targeted anticancer drug delivery and PET/MR imaging. Biomaterials, 32, 4151-4160.

Yang,Y., Yu,K., Zhang,H., Dai,J., Deng,Z., 2014d. In vitro assessment of the dual-targeting behavior of a peptide-based magnetic resonance imaging contrast agent. Int J Mol Med, 33, 215-220.

Ye,Y., Chen,X., 2011. Integrin targeting for tumor optical imaging. Theranostics, 1, 102-126.

Yonenaga,N., Kenjo,E., Asai,T., Tsuruta,A., Shimizu,K., Dewa,T., Nango,M., Oku,N., 2012. RGD-based active targeting of novel polycation liposomes bearing siRNA for cancer treatment. J Control Release, 160, 177-181.

Yu,B., Tai,H.C., Xue,W., Lee,L.J., Lee,R.J., 2010. Receptor-targeted nanocarriers for therapeutic delivery to cancer. Mol Membr Biol, 27, 286-298.

Yudina,A., Moonen,C., 2012. Ultrasound-induced cell permeabilisation and hyperthermia: strategies for local delivery of compounds with intracellular mode of action. Int J Hyperthermia, 28, 311-319.

Zhang,C., Jugold,M., Woenne,E.C., Lammers,T., Morgenstern,B., Mueller,M.M., Zentgraf,H., Bock,M., Eisenhut,M., Semmler,W., Kiessling,F., 2007. Specific targeting of tumor angiogenesis by RGD-conjugated ultrasmall superparamagnetic iron oxide particles using a clinical 1.5-T magnetic resonance scanner. Cancer Res, 67, 1555-1562.

Zhang,F., Huang,X., Zhu,L., Guo,N., Niu,G., Swierczewska,M., Lee,S., Xu,H., Wang,A.Y., Mohamedali,K.A., Rosenblum,M.G., Lu,G., Chen,X., 2012. Noninvasive monitoring of orthotopic glioblastoma therapy response using RGD-conjugated iron oxide nanoparticles. Biomaterials, 33, 5414-5422.

Zhang,L., He,R., Gu,H.C., 2006. Oleic acid coating on the monodisperse magnetite nanoparticles. Applied Surface Science, 253, 2611-2617.

Zhao,X., Li,H., Lee,R.J., 2008. Targeted drug delivery via folate receptors. Expert Opin Drug Deliv, 5, 309-319.

Zitzmann,S., Ehemann,V., Schwab,M., 2002. Arginine-glycine-aspartic acid (RGD)-peptide binds to both tumor and tumor-endothelial cells in vivo. Cancer Res, 62, 5139-5143.

Zou,P., Yu,Y., Wang,Y.A., Zhong,Y., Welton,A., Galban,C., Wang,S., Sun,D., 2010. Superparamagnetic iron oxide nanotheranostics for targeted cancer cell imaging and pH-dependent intracellular drug release. Mol Pharm, 7, 1974-1984.

CHAPTER II.

AIMS OF THE THESIS

AIMS OF THE THESIS

(i) The first aim of the thesis was to **develop and characterize PLGA-based nanoparticles as multifunctional entities** by co-encapsulation of an anti-cancer drug (PTX/DOX) and contrast agents (SPIO) for both anti-cancer therapy and magnetic resonance imaging;

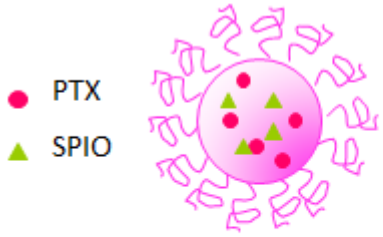

(ii) The second aim of the thesis was **to compare four targeting strategies** of these multifunctional nanoparticles in terms of anti-tumor efficacy, biodistribution and magnetic resonance imaging capabilities. The four targeting strategies compared were passive targeting (PT), active αvβ3 targeting (RGD), magnetic targeting (MT) and the combination of the two latest (RGD+MT).

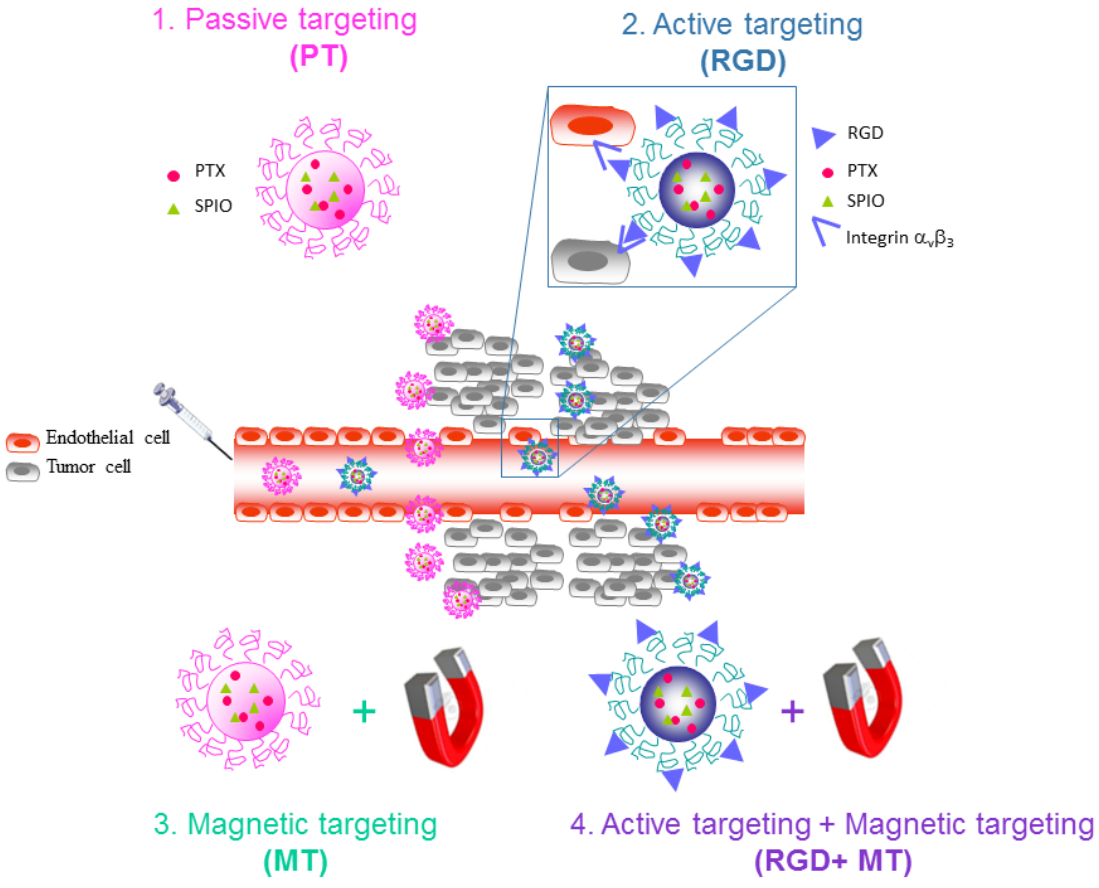

CHAPTER III.

DUAL PACLITAXEL/SUPERPARAMAGNETIC IRON OXIDE-LOADED PLGA-BASED NANOPARTICLES FOR CANCER THERAPY AND MAGNETIC RESONANCE IMAGING

TABLE OF CONTENTS

DUAL PACLITAXEL/SUPERPARAMAGNETIC IRON OXIDE-LOADED PLGA-BASED NANOPARTICLES FOR CANCER THERAPY AND MAGNETIC RESONANCE IMAGING

N. Schleich, P. Sibret, P. Danhier, B. Ucakar, S. Laurent, R. Muller,
C. Jérôme, B. Gallez, V. Préat*, F. Danhier*

Adapted from International Journal of Pharmaceutics, 2013, 447(1-2), 94-101.

ABSRACT

We developed dual paclitaxel (PTX)/superparamagnetic iron oxide (SPIO)-loaded PLGA-based nanoparticles for a theranostic purpose. Nanoparticles presented a spherical morphology and a size of 240 nm. The PTX and iron loading were 1.84 ± 0.4 and 10.4 ± 1.93 mg/100 mg respectively. Relaxometry studies and phantom MRI demonstrated their efficacy as T_2 contrast agent. Significant cellular uptake by CT26 cells of nanoparticles was shown by Prussian blue staining and fluorescent microscopy. While SPIO did not show any toxicity in CT-26 cells, PTX-loaded nanoparticles had a cytotoxic activity. PTX-loaded nanoparticle (5 mg/kg) with or without co-encapulated SPIO induced *in vivo* a regrowth delay of CT26 tumors. Together these multifunctional nanoparticles may be considered as future nanomedicine for simultaneous molecular imaging, drug delivery and real-time monitoring of therapeutic response.

KEYWORDS

PLGA-nanoparticles, SPIO, Paclitaxel, Cancer therapy, Magnetic Resonance Imaging

I. INTRODUCTION

Theranostics is a newly emerging concept which involves simultaneous execution of therapeutic and diagnostic approaches for personalized medicine. Nanoparticles (NP) can be designed to encapsulate a wide variety of chemotherapeutic and diagnostic agents for the delivery of these agents to tumor cells [Lammers et al., 2010]. Nanoparticles can target tumors by a passive process. Passive targeting implies that nanoparticles are smaller than the fenestrations of endothelial cells and can therefore enter the interstitium to be finally entrapped in the tumor. The combination of leaky vasculature and poor lymphatic drainage results in the well-known Enhanced Permeability and Retention (EPR) effect [Maeda et al., 2000].

Paclitaxel (PTX), a major anti-cancer drug has anti-neoplasic activity particularly against various types of solid tumors [Singla et al., 2002]. PTX disrupts the dynamic equilibrium within the microtubule system and blocks cells in the late G_2 phase and M phase of the cell cycle, thereby inhibiting cell replication [Schiff et al., 1979]. PTX is poorly soluble in water. To enhance its solubility and allow its parenteral administration, PTX is currently formulated at 6 mg/ml in a vehicle composed of a mixture of Cremophor® EL and ethanol (1:1) (Taxol®) [Weiss et al., 1990].

Magnetic resonance imaging (MRI) is a non-invasive imaging technique, presenting a high spatial resolution which is suitable for cancer detection and therapeutic response assessment [Brindle, 2008]. However, its low sensitivity represents a major limitation. Superparamagnetic iron oxide (SPIO) as MRI contrast agent addresses this limitation. SPIO can produce predominant T_2 relaxation effect, resulting in a signal reduction on T_2-weighted images. The magnetic field heterogeneity around the particles, through which water molecules diffuse, induces the dephasing of the proton magnetic moments. Consequently, a T_2 effective transverse relaxation is shortened [Bjornerud et al., 2004; Ling et al., 2011].

Recently, numerous publications have reported various polymer-based nanocarriers (Poly(lactide-co-glycolide) (PLGA), Poly (L-lactic acid) PLLA, N-(2-hydroxypropyl)methacrylamide (HPMA), poly(e-caprolactone)) for magnetic-imaging [Hamoudeh et al., 2007; Ling et al., 2011; Lu et al., 2009; Talelli et al., 2009]. These theranostics successfully allowed the non-invasive assessment of the biodistribution, the visualization of drug distribution, the optimization of strategies, the prediction and real-time monitoring of therapeutic responses [Lammers et al., 2010]. However, these SPIO-loaded nanocarriers are generally limited because of (i) their lack of functional groups on their

surface for covalent modification, (ii) their low capacity of drug loading and (iii) the fact that most of polymers used are not approved by the FDA, limiting their potential translation to the clinic.

Previously, we developed PTX-loaded PEGylated PLGA-based nanoparticles showing a lower IC_{50} *in vitro* and improved *in vivo* anti-tumor efficacy when compared to Taxol®, due to the EPR effect [Danhier et al., 2009a]. (PLGA) was chosen for its biodegradability properties, its biocompatibility and its approval by the FDA [Danhier et al., 2012]). Poly(ε-caprolactone-b-ethylene glycol) (PCL-b-PEG), an amphiphilic copolymer, was added to take advantage of the repulsive properties of PEG, to provide a higher stability of nanoparticles in biological fluids and to allow the grafting of a targeting ligand [Fievez et al., 2009; Garinot et al., 2007; Pourcelle et al., 2007]. We also previously developed RGD-grafted PTX-loaded PEGylated PLGA-based nanoparticles showing an effective $\alpha_v\beta_3$ targeting of the tumor endothelium [Danhier et al., 2009c].

In this study, we aimed at developing these previously described PTX-loaded PEGylated PLGA-based nanoparticles as an effective nanocarrier for dual encapsulation of anti-cancer drug (PTX) and SPIO for a theranostic purpose. Hence, SPIO were prepared by the co-precipitation technique and were encapsulated in PLGA-based nanoparticles. The physico-chemical properties of nanoparticles were characterized by different techniques such as transmission electron microscopy (TEM), dynamic light scattering (DLS) method, electron spin resonance (ESR) spectroscopy or inductively coupled plasma mass spectroscopy (ICP-MS). Their magnetic properties were evaluated using relaxometry and MRI. Furthermore, we investigated the *in vitro* cellular uptake and cytotoxicity of nanoparticles. Finally, the *in vivo* anti-tumor efficacy was assessed on CT-26 tumor-bearing mice.

II. MATERIALS AND METHODS

II.1. MATERIALS

Iron(II) chloride, iron(III) chloride, oleic acid, sodium hydroxide, chlorhydric acid, 4,6-diamidino-2-phenylindole (DAPI), 3-(4, 5-dimethylthiazol-2-yl)-2,5-diphenyltetrazolium bromide) (MTT), polyvinylalcohol (PVA, MW=30-70kDa), poly(lactic-co-glycolic acid) (PLGA, lactide/glycolide molar ratio of 50:50 MW: 7000-17000), paclitaxel (PTX) and doxorubicin (DOX) were purchased from Sigma-Aldrich (St. Louis, MO, USA). Perls' Prussian blue kit and commercial SPIO Molday Ion™ were purchased from BioPAL (Worcester, UK). PLGA-*b*-PEG (MW=10 040–4600), PCL-*b*-PEG (MW=13 100-5000) and FITC-PLGA were synthesized as previously described [Danhier et al., 2010; Garinot et al., 2007]. Dulbecco's modified Eagle's medium (DMEM), fetal bovine serum (FBS), trypsin–EDTA and penicillin–streptomycin mixtures were from Gibco® BRL (Carlsbad, CA, USA). Murine colon carcinoma CT26 cells were kindly given by Goldyne Savad Institute of Gene Therapy, Hadassah-Hebrew University Hospital (Jerusalem, Israël). Water used in all experiment was prepared by Aqualab purification system.

II.2. SYNTHESIS OF SUPERPARAMAGNETIC IRON OXIDES (SPIO) COATED WITH OLEIC ACID

Hydrophobic superparamagnetic iron oxides (SPIO) were synthesized using a classical co-precipitation technique of ferrous and ferric salts in alkaline medium [Massart, 1981]. Briefly, 10 mmol iron(III) chloride and 5 mmol iron(II) chloride were mixed together in 12 ml of an hydrochloride aqueous solution (HCl 1M). This solution was then added dropwise to an aqueous solution of NaOH 1M containing 3.1 g of oleic acid with stirring on a magnetic stir plate for 20 minutes under a nitrogen-gas atmosphere at 80°C. The black precipitate was separated using a magnet, washed three times using absolute ethanol and then dissolved in 50 ml of dichloromethane (DCM). The solution was then placed in an ultrasonic bath for 10 minutes and centrifuged (4416 rcf, 10 min) to remove the undispersed residue.

Hydrophilic SPIO used as SPIO aqueous solution (SPIO sol) were also synthesized. Briefly 1 ml of DCM dispersion of SPIO coated with oleic acid (40 mg/ml) was added to a suspension of tetramethylammonium 11-aminoundecanoate in DCM (40 mg in 2 ml). After 24 h

magnetic stirring, the precipitate was washed three times with DCM and dispersed in water [Yang et al., 2010].

II.3. PREPARATION OF PLGA-BASED NANOPARTICLES LOADED WITH SPIO AND PACLITAXEL OR DOXORUBICIN

Both nanoparticles loaded with SPIO and DOX (SPIO/DOX-NP) and nanoparticles loaded with SPIO and paclitaxel (SPIO/PTX-NP) were prepared by an emulsion-diffusion-evaporation method [Danhier et al., 2009a; Garinot et al., 2007]. Briefly, PLGA (14 mg/ml), PLGA-PEG (3 mg/ml) and PCL-PEG (3 mg/ml) were dissolved in 2ml DCM containing SPIO (Fe concentration: 15 mg/ml). Doxorubicin HCl (0,2 mg/ml) was dissolved in 1ml DCM containing 0.001 mg/ml triethanolamine beforehand and stirred overnight [Shieh et al., 2011] whereas paclitaxel (3 mg) was added directly. This organic solution was then added to an aqueous solution (4.5 ml) containing 3 % (p/v) PVA and emulsified using a vortex for 2 min followed by sonication (2 x 30 sec, 50W). The mixture was then added dropwise and under magnetic stirring into an aqueous solution containing 1 % PVA and stirred overnight to evaporate the organic solvent. To remove the non-encapsulated drug, the suspension was filtered (1,2 µm) and washed three times with water using ultracentrifugation (11 000 g, 30 min, 4°C) and suspended in 2 ml water. FITC covalently labeled PLGA was used to prepare fluorescent nanoparticles [Freichels et al., 2011]. PTX-loaded nanoparticles (PTX-NP) and SPIO-loaded nanoparticles (SPIO-NP) were also prepared using the same protocol.

II.4. PHYSICO-CHEMICAL CHARACTERIZATION OF NANOPARTICLES LOADED WITH SPIO AND PACLITAXEL OR DOXORUBICIN

II.4.1. Thermogravimetric analysis of SPIO

The coating percentage of SPIO with oleic acid was assessed by thermogravimetric analysis (TGA) on a TA Instrument Q500 model, under dry nitrogen flow, with a heating rate of 15°C/min from RT to 600°C, in an open platinum pan.

II.4.2. Particles size and morphology determination

The hydrodynamic particle size and size polydispersity of nanoparticles was assessed using a dynamic light scattering method (Nano ZS, Malvern instruments, UK). The Zeta (ζ) potential of the nanoparticles was measured in KCL 1 mM with a Malvern Nano ZS at 25 °C. The

morphology of the particles was achieved using transmission electron microscopy (TEM). TEM was carried out with a Philips CM 100 operating at a voltage of 100 kV, equipped with a Megaview G2 camera. Samples for TEM experiments were prepared by spin coating a drop of nanoparticles in DCM on a carbon-coated TEM grid.

II.4.3. Determination of SPIO loading content

The iron content was measured by Electron Spin Resonance (ESR) spectroscopy using a Bruker EMX ESR spectrometer operating at 9 GHz (Bruker Biospin GmBh, Germany) validated by inductively coupled plasma mass spectroscopy (ICP-MS) measurements (Agilent 7500ce instrument). This method allow a sensitive quatification with a LOD and a LOQ of, respectively, 91 and 304 ng Fe ml^{-1} [Danhier et al., 2012]. The solution to be tested was drawn into a 75 µl glass capillary tubes as such, no transformation needed, and this capillary was placed in the spectrometer for measurement at room temperature. Typical parameters were selected for ESR measurements: 3 mT modulation amplitude, 10.11 mW power, 325.1 mT center field, and field 400 mT sweep width. Double integration of the iron oxides ESR spectra was used to quantify signal intensity.

II.4.4. Determination of drug loading content

The DOX content was assessed by determining the absorbance at 480 nm with a UV–Visible spectrophotometer (HP8453 from Hewlett Packard). The PTX content was determined using high-performance liquid chromatography (HPLC) with UV detection at 227 nm (Agilent 1100 series, Agilent Technologies, Diegem, BE), as previously described after dissolution of particles in acetonitrile (50:50), vortex (5 min) and filtration (0,22 µm) [Danhier et al., 2009c]. The mobile phase consisted of acetonitrile and water (70:30 v/v, respectively) at a rate of 1ml/min. The column used was a CC 125/4 Nucleod UR 100-5 C18. Standard solutions of 5 to 100 µg/ml of PTX dissolved in acetonitrile were used for calibration (correlation coefficient = 0.99, LOD = 1.6 µg/ml, LOQ = 5 µg/ml, coefficients of variation < 4.5 %). The drug loading was defined as the amount of drug (mg) loaded for 100 mg of polymer whereas the encapsulation efficiency was defined by the ratio of the encapsulated drug compared to the initial amount of drug [Danhier et al., 2010].

II.5. MAGNETIC PROPERTIES

II.5.1. Relaxometry by proton NMRD

Nuclear Magnetic Relaxation Dispersion (NMRD) profiles were recorded at 37°C on a Fast Field Cycling Relaxometer (Stelar, Mede, Italy) over a magnetic field range from 0.01-40 MHz. Additional longitudinal (R_1) and transverse (R_2) relaxation rate measurements at 20 and 60 MHz were respectively obtained on Minispec mq 20 and mq 60 spin analyzers (Bruker, Karlsruhe, Germany). The fitting of the NMRD profiles by a theoretical relaxation model allows the determination of the crystal radius (r) and the specific magnetization (M_S). The proton NMRD curves were fitted using data-processing software, including different theorical models describing the nuclear relaxation phenomena [Laurent et al., 2010; Roch et al., 2005; Roch et al., 1999].

II.5.2. Phantom MRI

T_2 relaxivity was obtained using a 11,7 T animal Biospec MR system (Bruker Biospec, Ettlingen, Germany). Phantom MRI of SPIO-NP was carried out at various iron concentration from 0 µg/ml to 30 µg/ml (0, 5, 10, 15, 20, 25 and 30 µg/ml) in 10 % gelatin using a T_2-weighted multi-slice multi-echo (MSME) sequence. The imaging parameters were: repetition time (TR) = 2500 msec, echo time (TE) = 30 msec, field of view (FOV) = 3.00 cm, flip angle (FA) = 180.0°.

II.6. *IN VITRO* CELL LINE EXPERIMENT

II.6.1. In vitro cellular uptake

CT26 colon carcinoma cells were seeded at a density of $1x10^5$ cells per well in Lab-tekII® chamber slide system in DMEM supplemented with 10 % fetal bovine serum (FBS), 1 % of a penicillin/streptomycin mixture and 1 % L-Glutamine. Cells were incubated for 24 h in a 5% CO_2 incubator (37°C). Then, 100 µl of SPIO/DOX-NP suspension labeled with FITC was added to the medium for 1 h, 2 h or 4 h. After incubation, cells were fixed at room temperature for 15 min with 4% paraformaldehyde. Following cell fixation, cells were incubated with 4,6-diamidino-2-phenylindole (DAPI) at a concentration of 0,2 µg/ml in phosphate buffer saline (PBS) for 15 min protected from light, washed twice with PBS and once with water to avoid salt crystals formation.

The intracellular iron oxides were visualized using a Prussian blue staining. After 2 h of incubation with SPIO/DOX-NP suspension at 80 µg/ml of Fe concentration, CT-26 were washed three times with PBS, fixed with 4 % paraformaldehyde for 15 min and incubated for 30 min with 2 ml working solution provided by the Prussian blue kit comprising equal volume of 2 % HCl and 2 % potassium ferrocyanide (II) trihydrate (bioPAL). Wells were finally washed twice with PBS and once with water.

The stained plates were observed using either a fluorescent microscope (Axioskop 40, Zeiss) fitted with three excitation filters: 340/380 nm (blue), 470/490 nm (green), 515/560 nm (red) or without filter for iron oxide visualization. Photographs were taken with an AxioCam MRc5 camera (Zeiss).

II.6.2. In vitro cytotoxicity

The cytotoxicity of SPIO, SPIO-NP and SPIO/PTX-NP was determined by a MTT cell proliferation assay as previously described [Danhier et al., 2009b; Mosmann, 1983]. Briefly, CT26 colon carcinoma cells were seeded at a density of 10^4 cell per well in 96-well plates. Next day, cells were incubated with the different formulations: SPIO solution, SPIO-NP, PTX-NP at 3 different iron concentrations (20 µg/ml, 10 µg/ml and 2 µg/ml) and SPIO/PTX-NP. All the concentrations of SPIO used were based on the corresponding PTX aforementioned concentrations when SPIO and PTX are co-loaded (Fe concentrations: 106.8 µg/ml, 53.4 µg/ml and 10.7 µg/ml). After 24h, supernatants were removed. Wells were then washed twice with PBS and incubated with DMEM containing MTT (5 mg/ml) for an additional 2 h. After MTT solution removal, DMSO was added to dissolve the formazan crystals. Absorbance was measured at 570 nm using a BioRad microplate reader. Untreated cells were taken as control with 100 % viability, and Triton X-100 1% was used as a positive control of cytotoxicity. Cells without addition of MTT were used as blank to calibrate the spectrophotometer to zero absorbance.

II.7. IN VIVO EVALUATION

II.7.1. Animal and tumor models

All experiments were performed in compliance with guidelines set by national regulations and were approved by the ethical committee for animal care of the health science sector of the

Université Catholique de Louvain. CT26 colon carcinoma cells were inoculated subcutaneously in the right flank of BALB/c mice ($5x10^4$ cells per mouse).

II.7.2. In vivo anti-tumor efficacy

The effect of SPIO/PTX-NP on tumor growth was assessed by daily measurements of tumor volume with an electronic caliper. CT26 cells were injected subcutaneously in the right flank of the mice to allow easy and reproducible tumor volume measurements. Mice were randomly assigned to a treatment group when tumor reached a volume of 27 ± 5 mm³. Treatment was injected trough the tail vein. Five groups were defined (6 mice per group): group1: PBS injection, group 2: injection of a SPIO solution (SPIO sol; Fe dose: 13.5 mg/kg), group 3: injection of SPIO loaded nanoparticles (SPIO-NP; Fe dose: 13.5 mg/kg), group 4: injection of PTX loaded nanoparticles (PTX-NP) at a concentration of 5 mg/kg PTX and group 5: injection of SPIO-PTX co-loaded nanoparticles (SPIO/PTX-NP; PTX dose: 5 mg/kg – Fe dose: 13.5 mg/kg). The end point of the experiment was determined as the moment when tumor reached 600 mm³. At this point, mice were sacrificed. Tumor growing ratio was calculated as the volume measured each day (mm³) compared to the volume measured at day 1 (day of treatment injection).

II.8. STATISTICAL ANALYSES

All results are expressed as mean ± standard deviation (SD). Two-way ANOVA, Bonferroni post test, Kaplan-Meier survival rate and T-test were performed, using the software GraphPad Prism 5 for Windows, to demonstrate statistical differences (p<0,05).

III. RESULTS AND DISCUSSION

III.1. PHYSICO-CHEMICAL CHARACTERIZATION

To ensure dispersibility in organic solvent and hydrophobicity of particles, SPIO were coated with oleic acid by a simple adsorption process (Figure 1). Coating efficacy was assessed by the percent by mass of inorganic matters using TGA. SPIO showed a percentage of 39.5 % inorganic matters representing SPIO suggesting a coating of 60.5 %. This coating is needed to prevent the formation of large aggregates when exposed to the biological system or DCM for nanoparticle preparation [van Ewijk et al., 1999].

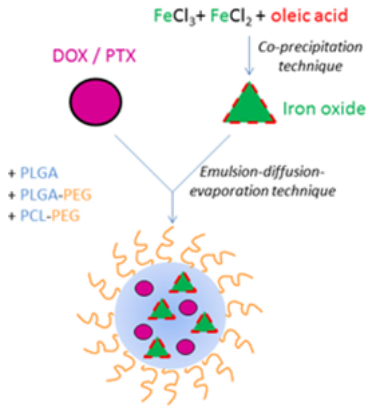

Figure 1. Schematic representation of SPIO/PTX-loaded PLGA-based nanoparticles

SPIO were also characterized in terms of size and morphology using transmission electron microscopy (TEM) (Figure 2A). TEM results showed a spherical morphology with relatively uniform sizes ranging from 6 to 12 nm. Apparent aggregation was not detected.

PLGA-based nanoparticles were prepared using an emulsion-diffusion-evaporation method [Garinot et al., 2007] (Figure 1). This method was selected comparing the results obtained either by the nanoprecipitation or by the emulsion method after several adjusts (data not shown). As shown in Table 1, all the PLGA-based nanoparticles presented neutral ζ potentials and similar sizes between 235 nm and 244 nm (p>0.05) except for the PLGA-based nanoparticles loaded with both SPIO and doxorubicin (SPIO/DOX-NP), which presented a slightly larger size (285 nm). It is well known that the EPR effect is exploited to allow nanocarriers the passive targeting of tumors. Thus, the particle size plays an important role. Endothelial pores have sizes varying from 10 to 1000 nm. It was further established that the optimal particles size is ranging from 20 to 400 nm [Danhier et al., 2010; Maeda et al., 2000]. PTX/SPIO-loaded nanoparticles are thus convenient to benefit from the EPR effect.

Table 1. Particle size, ζ potential, drug loading and SPIO loading of PLGA-based nanoparticles loaded with either SPIO (SPIO-NP), paclitaxel (PTX-NP), SPIO and paclitaxel (SPIO/PTX-NP) or with SPIO and doxorubicin (SPIO/DOX-NP) (n=3).

	SPIO-NP	**PTX-NP**	**SPIO/PTX-NP**	**SPIO/DOX-NP**
Size (nm)	235 ± 8	238 ± 8	243 ± 9	285 ± 1
ζ potential (mV)	0 ± 0.04	0 ± 0.01	0 ± 0.01	-2 ± 0.56
Drug loading (mg/100 mg polymer)	-	1.8 ± 0.3	1.8 ± 0.4	0.5 ± 0.0
SPIO loading (mg/100 mg polymer)	9 ± 1.5	-	10 ± 1.9	9 ± 0.6

The size and morphology of SPIO-PTX-loaded nanoparticles were also investigated by TEM. Particles were spherical and presented a narrow distribution without aggregation. Particles size appeared to be approximately 50 nm. Only iron oxides induced differences in transmission and consequently in contrast. The measured size does not probably constitute the real size of nanoparticles, in comparison with the hydrodynamic diameter measured by DLS. The polymers shape was visible in grey areas surrounding black spots (SPIO). Interestingly, size, morphology or distribution of nanoparticles were not affected by the co-encapsulation of SPIO and PTX (Figures 2B,C).

All formulations presented a similar SPIO loading around 10 mg/100 mg of polymer (p>0.05) which is similar to those found in the literature [Guthi et al., 2010; Hu et al., 2012; Lee et al., 2010] The Fe concentration was the same when quantified by ESR spectroscopy or by ICP-MS.

PTX loading was not affected by the co-encapsulation of SPIO. The PTX loading was 1.8 mg/100 mg polymer. Drug loading is crucial for formulations of drug delivery systems because it directly affects the therapeutic dose available for the targeted tissue. Interestingly, the drug loading of nanoparticles, formulated by an emulsion-diffusion-evaporation method using PVA as emulsifier, was 4.5-fold higher than with the same method, described previously, using sodium cholate and 2.5-fold higher than with the nanoprecipitation technique [Danhier et al., 2009a]. Moreover, the drug loading of nanoparticles was 2.8 to 4.8-fold higher than those described in previous studies [Hu et al., 2012; Singh et al., 2011]. However, other studies using either other contrast agent or other polymers have shown better paclitaxel loading (7,5-17 mg/100 mg polymer) [Bao et al., 2014; Yoon et al., 2012]. Due to the small amount of doxorubicin used to formulate SPIO/DOX-NP (0.5 mg/100 mg of polymer), the encapsulation efficiency reached 100%.

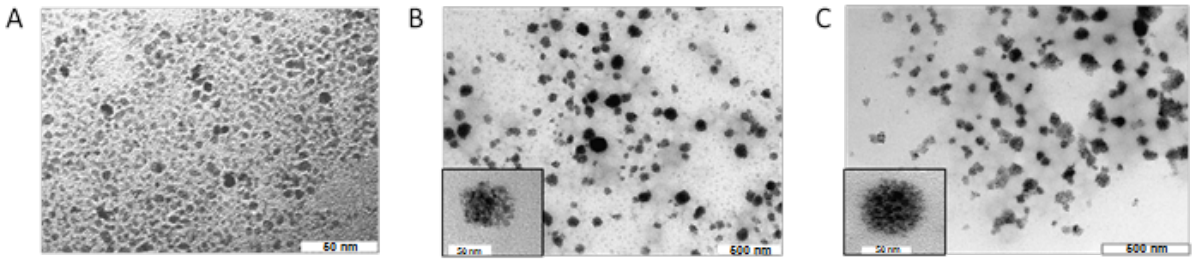

Figure 2. TEM micrographs of (A) SPIO, (B) SPIO-NP and (C) SPIO/PTX-NP.

III.2. MAGNETIC PROPERTIES OF SPIO AND SPIO-NP

III.2.1. Relaxometry studies

The relaxivity of SPIO is defined as the efficiency to enhance the relaxation rate of the neighboring water protons and is expressed in $s^{-1}mM^{-1}$. The relaxivities of SPIO are summarized in Table 2. Noticeably, the r_2/r_1 ratios of SPIO are higher than those of Resovist® [Allkemper et al., 2002], indicating that SPIO could be considered as highly efficient T_2 contrast agents.

The NMRD profiles, which display the evolution of proton longitudinal relaxivity as a function of the applied field, illustrates typically superparamagnetic relaxation profiles both for SPIO-loaded nanoparticles and SPIO/PTX-loaded nanoparticles (Figure 3). The shape of the NMRD profile of superparamagnetic iron oxide nanoparticle suspensions is governed (i) by the size, the crystallinity and the magnetization of the magnetic cores, (ii) by the diffusion of solvent close to the particle cores, and (iii) by the interaction between superparamagnetic cores, as they affect the anisotropy energy [Roch et al., 1999]. Table 3 shows the parameters obtained from the theoretical fitting of the NMRD profiles. The specific magnetization (M_S), the crystal radius (r) and the Néel relaxation time (τ_N) highlight the superparamagnetism properties of SPIO. Interestingly, the presence of PTX into nanoparticles did not change significantly the relaxometric properties.

Table 2. Longitudinal ($r1$) and transverse ($r2$) relaxivities of SPIO-NP, SPIO/PTX-NP and Resovist® at 20 and 60 MHz in water (37°C).
NA Not available

	20 MHz			**60 MHz**		
	$\mathbf{r_1}$ $\mathbf{(mM^{-1}s^{-1})}$	$\mathbf{r_2}$ $\mathbf{(mM^{-1}s^{-1})}$	$\mathbf{r_2/r_1}$	$\mathbf{r_1}$ $\mathbf{(mM^{-1}s^{-1})}$	$\mathbf{r_2}$ $\mathbf{(mM^{-1}s^{-1})}$	$\mathbf{r_2/r_1}$
SPIO-NP	3.4	134.4	39.5	1.1	139	126.4
SPIO/PTX- NP	3.8	127	33.4	1.3	137	105.4
Resovist® [Allkemper et al., 2002]	25	119	4.8	NA	NA	NA

Table 3. Parameters obtained from the theoretical fitting of the NMRD profiles.

	SPIO-NP	**SPIO/PTX-NP**
M_s (Am^2/kg)	14,5 ± 0,1	15,1 ± 0,1
r (nm)	16,1 ± 0,1	15,9 ± 0,1
t_N (ns)	5,88 ± 0,08	5,78 ± 0,08

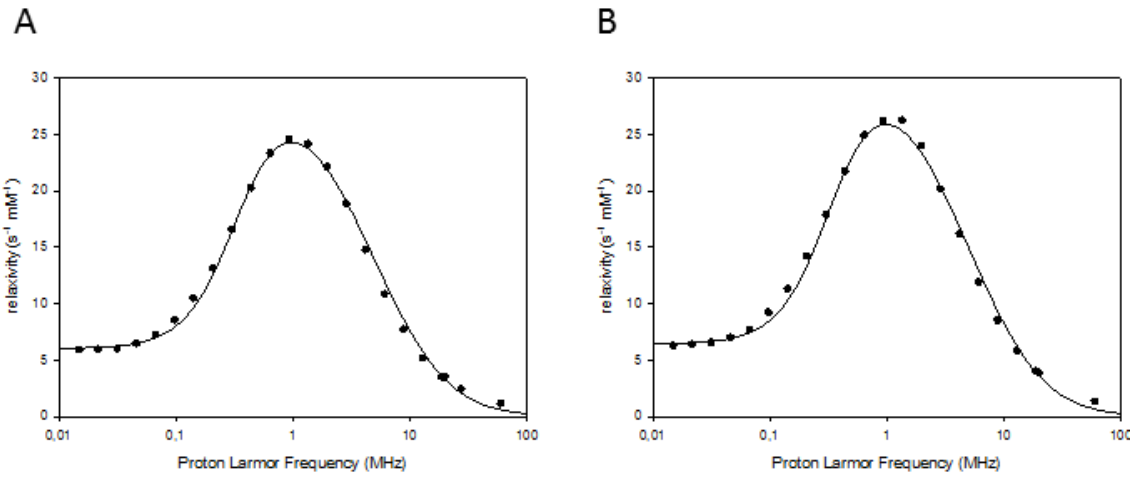

Figure 3. ^{1}H NMRD relaxivity profiles of (A) SPIO-loaded nanoparticles and (B) SPIO/PTX-loaded nanoparticles.

III.2.2. Phantom MRI

Various concentrations of SPIO in aqueous solution (SPIO sol) and PLGA-based nanoparticles loaded with SPIO (SPIO-NP) ranging from 0 to 30µg/ml (Fe concentrations: 0-5-10-15-20-25-30µg/ml) were investigated by T_2-weighted MRI to assess their T_2 enhancing capability. Commercial SPIO (BioPAL, Worcester, UK) were used as a reference at the same concentrations (Figure 4). This pilot experiment confirmed that the magnetism of the

synthesized SPIO was detectable by MRI either when freely suspended in water (SPIO sol) or when encapsulated in PLGA-based nanoparticles (SPIO-NP). For all treatments, the signal intensity of MRI decreased as the SPIO concentration increased. It is important to note that synthesized SPIO presented similar relaxation rates ($R_2 = T_2^{-1}$) profiles than commercialized SPIO (BioPAL). Furthermore, as shown on Figure 4A, the transverse relaxation rates (T_2^{-1}) of all treatments were well fitted by a line within the analyzed range of iron concentration. Nevertheless, compared to SPIO sol, SPIO-NP relaxed more slowly indicating that the presence of PLGA surrounding SPIO could slightly affect T_2 enhancing capability.

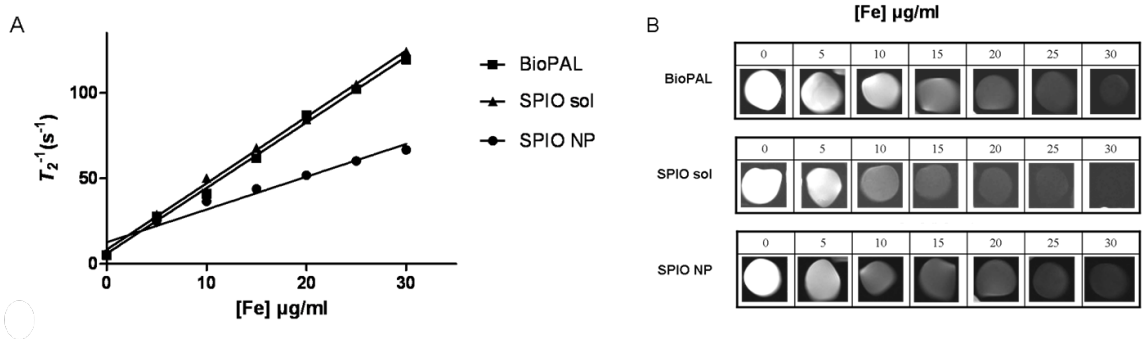

Figure 4: (A) T_2 relaxation rate of commercial SPIO (BioPAL, Worcester, UK), an aqueous suspension hydrophilic SPIO (SPIO sol) and SPIO loaded nanoparticles (SPIO NP) as a function of Fe concentration (µg/ml) (B) T2-weighted MR images as a function of Fe concentration (µg/ml, TE=30msec).

III.3. IN VITRO CELLULAR UPTAKE

To assess the uptake of SPIO/DOX-NP, fluorescent NP were used. Fluorescein isothiocyanate (FITC) was grafted covalently on PLGA to label polymer matrix (green fluorescence). Doxorubicin was chosen because of its natural fluorescence (red fluorescence) to follow the drug into cells. Nuclei of cells were labeled using DAPI staining (blue fluorescence). Figure 5 A shows that DOX fluorescence increased with the incubation time of the formulation. Moreover, the red and blue fluorescence were co-localized indicating that DOX was able to reach the nucleus which is its site of action. FITC-fluorescence indicated that polymeric nanoparticles have also been internalized by cells allowing a broad distribution of free DOX and SPIO in the cytosol. After 4 h, the blue fluorescence (DAPI) was co-localized with DOX, indicating that DOX accumulated in nuclei. The cellular uptake was thus time-dependent, as reported previously [Danhier et al., 2009a].

Figure 5 B shows the entrapment of SPIO stained in intense blue color into the cells. Obviously, there was no blue color appearance in cells of the control group. Conversely, cells incubated with SPIO/PTX-NP (Fe concentration = 80µg/ml) were stained in intensive blue

color. Consistent with previous publications, blue areas or spots could be seen in almost every cell [Ling et al., 2012]. SPIO-loaded PLGA nanoparticles were internalized by cells PLGA nanoparticles are mostly internalized through fluid phase pinocytosis and also through clathrin-mediated endocytosis [Petros et al., 2010].

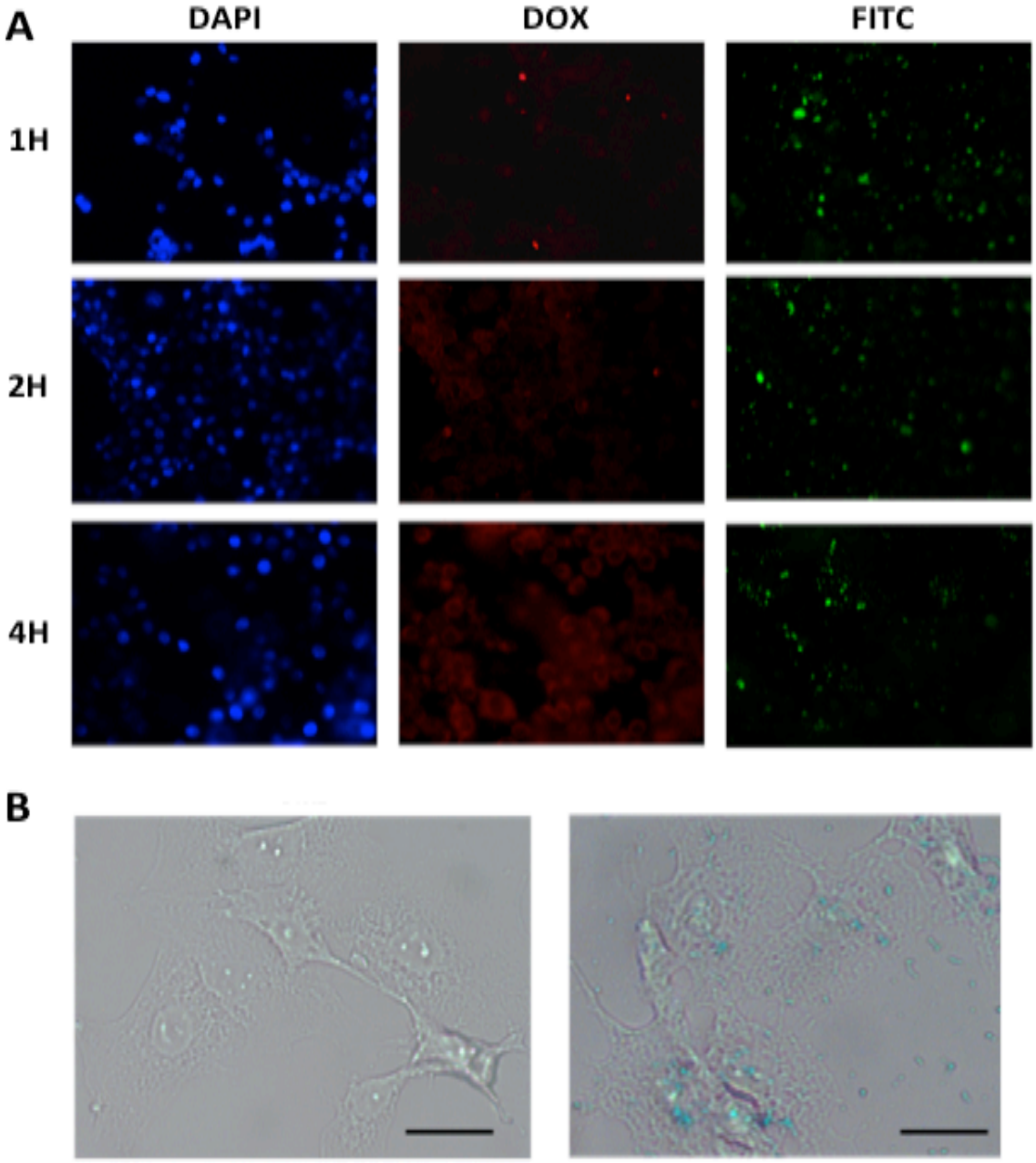

Figure 5. Nanoparticles uptake by CT26 cells. (A) Fluorescence microscopy of CT26 cells (1 x 10^5) after 1, 2 or 4 h of incubation with SPIO/DOX-NP followed by DAPI staining (magnification = 40x). (B) Prussian blue staining images after 4h of incubation with SPIO/PTX-NP at a Fe concentration of 80µg/ml, treated with Prussian blue liquid for 30 min. Black lines correspond to 10µm.

III.4. IN VITRO CYTOTOXICITY

The cytotoxicity of multifunctional nanoparticles was evaluated by the MTT test in CT26 colon carcinoma cells after 24 h incubation (Figure 6). The range of PTX concentrations (2 to 20 µg/ml) corresponds to plasma levels of the drug achievable in human [Raymond et al., 1997]. The range of Fe concentrations (106.8 µg/ml, 53.4 µg/ml and 10.7 µg/ml) corresponds to the concentrations present in solution of the different tested concentrations of PTX. An aqueous solution containing hydrophilic SPIO was used to test the toxicity of free SPIO (without entrapment into nanoparticles; SPIO sol). Consistent with other published data [Ling et al., 2011], SPIO (in solution or entrapped into NP) did not present any cytotoxic activity. The addition of PTX in formulations induced cell death. Compared with SPIO or SPIO-NP, the viability of cells treated with PTX-NP and SPIO/PTX-NP was decreased (p<0.01). This PTX cytotoxicity was increased in dose-dependent manner. Hence, PTX anti-tumor efficacy was maintained while encapsulated in PLGA-based nanoparticles in presence or in absence of SPIO.

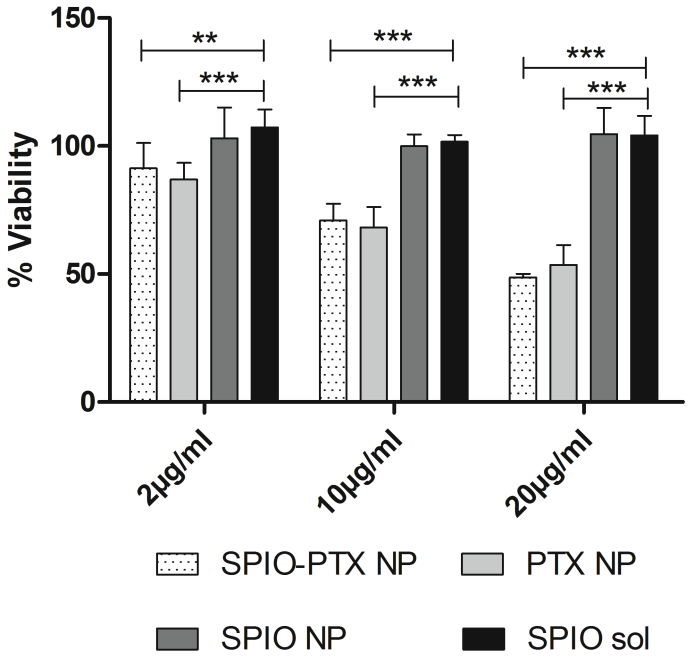

Figure 6. Viability of CT26 cells incubated with a solution of hydrophilic SPIO (SPIO sol, SPIO concentration corresponding to SPIO/PTX-NP formulation: Fe concentration of 106.8 µg/ml, 53.4 µg/ml and 10.7 µg/ml), paclitaxel-free nanoparticles (SPIO-NP, same concentrations as above), nanoparticles loaded with paclitaxel (PTX-NP, PTX concentrations 2, 10 and 20 µg/ml) and nanoparticles loaded with paclitaxel and SPIO (SPIO/PTX-NP). Cell viability was determined by the MTT assay. Untreated cells were taken as a negative control and Triton X-100 1% was used as a positive control. The results were expressed as mean values ± standard deviation (n=5). **p < 0.01, ***p < 0.001.

III.5. IN VIVO ANTI-TUMOR EFFICACY

The *in vivo* anti-tumor efficacy of multifunctional nanoparticles was evaluated in CT26-tumor-bearing mice (Figure 7). In a previous study of our group, paclitaxel-loaded nanoparticles were been shown to display a better efficacy compared with Taxol® [Danhier et al., 2009a]. Therefore we did not use this control. Consistent with *in vitro* cytotoxicity data, all treatments containing PTX (PTX-NP and SPIO/PTX-NP) induced a higher delay in tumor growth than other treatments (Figure 7A). Moreover, SPIO sol and SPIO-NP did not inhibit the tumor growth when compared with the PBS control group (Figure 7A). Kaplan-Meier survival rate was performed (Figure 7B). PTX-NP and SPIO/PTX-NP exhibited higher survival rates than the untreated group (PBS) with median survival rates of 13 and 15 days, respectively, compared to 9 days ($p<0.05$ and $p<0.01$). No significant difference was observed between the two PTX-based treatment ($p>0.05$). Additionally, SPIO sol and SPIO-NP presented median survival times of 10.2 and 10 days ($p>0.05$), which are not statistically different than the control PBS group ($p>0.05$).

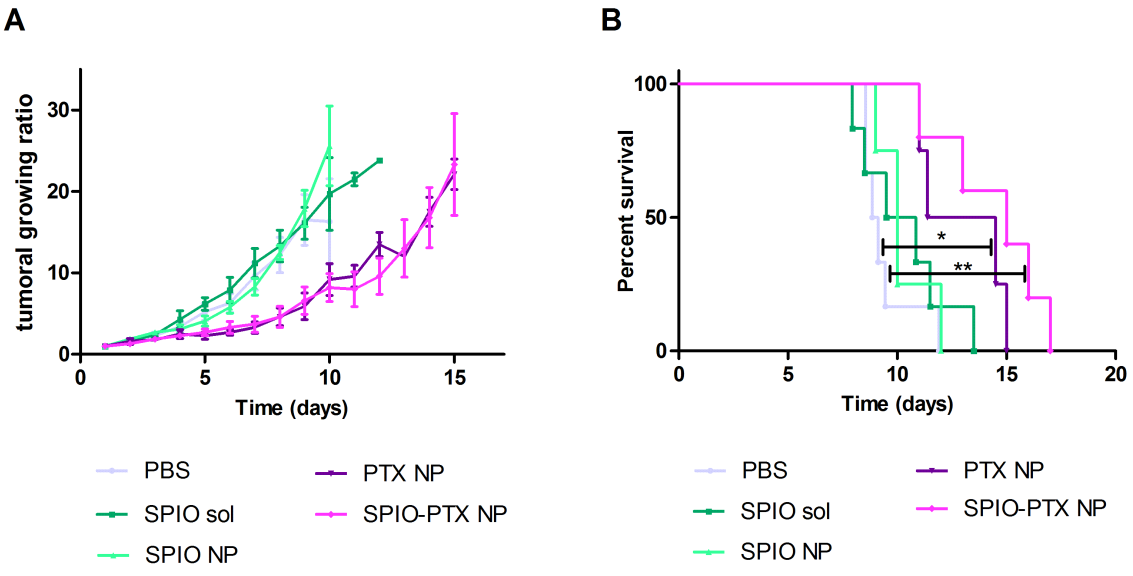

Figure 7. (A) Tumor growth curves of CT26-tumor bearing mice treated with free SPIO in aqueous solution (SPIO sol), SPIO loaded nanoparticles (SPIO-NP), paclitaxel-loaded nanoparticles (PTX-NP) (PTX dose = 5 mg/kg), paclitaxel and SPIO co-loaded nanoparticles (SPIO/PTX-NP) (PTX dose = 5 mg/kg) or untreated (PBS). The treatment was injected in the tail vein of the mice when tumors reached 27±5mm (n=6/group). Results are presented as the average tumor growing ratio ± SEM versus time after treatment injection. (B) Survival rates of tumor-bearing mice.

IV. CONCLUSIONS

Based on previous developed PLGA-based nanoparticles for anti-tumor drugs delivery, we aimed to extent these nanoparticles as multifunctional entities by co-encapsulation of an anti-cancer drug (PTX) and contrast agents (SPIO) for both anti-cancer therapy and magnetic resonance imaging. We successfully co-encapsulated SPIO and PTX in PLGA-based nanoparticles. We demonstrated that these nanoparticles inhibited the growth of CT26 cells. PTX/SPIO-loaded nanoparticles could be used as potential tumor-targeting MRI contrast agents, thanks to the high uptake of nanoparticles by cells as well as their magnetic characteristics. Together these results, these multifunctional nanoparticles may be considered as future nanomedicine for simultaneous targeting imaging, drug delivery and real-time monitoring of therapeutic response.

V. REFERENCES

Allkemper,T., Bremer,C., Matuszewski,L., Ebert,W., Reimer,P., 2002. Contrast-enhanced blood-pool MR angiography with optimized iron oxides: effect of size and dose on vascular contrast enhancement in rabbits. Radiology, 223, 432-438.

Bao,Q.Y., Zhang,N., Geng,D.D., Xue,J.W., Merritt,M., Zhang,C., Ding,Y., 2014. The enhanced longevity and liver targetability of Paclitaxel by hybrid liposomes encapsulating Paclitaxel-conjugated gold nanoparticles. Int J Pharm, 477(1-2), 408-15.

Bjornerud,A., Johansson,L., 2004. The utility of superparamagnetic contrast agents in MRI: theoretical consideration and applications in the cardiovascular system. NMR Biomed, 17, 465-477.

Brindle,K., 2008. New approaches for imaging tumour responses to treatment. Nat Rev Cancer, 8, 94-107.

Danhier,F., Ansorena,E., Silva,J.M., Coco,R., Le Breton A., Preat,V., 2012. PLGA-based nanoparticles: an overview of biomedical applications. J Control Release, 161, 505-522.

Danhier,F., Feron,O., Preat,V., 2010. To exploit the tumor microenvironment: Passive and active tumor targeting of nanocarriers for anti-cancer drug delivery. J Control Release, 148, 135-146.

Danhier,F., Lecouturier,N., Vroman,B., Jerome,C., Marchand-Brynaert,J., Feron,O., Preat,V., 2009a. Paclitaxel-loaded PEGylated PLGA-based nanoparticles: in vitro and in vivo evaluation. J Control Release, 133, 11-17.

Danhier,F., Magotteaux,N., Ucakar,B., Lecouturier,N., Brewster,M., Preat,V., 2009b. Novel self-assembling PEG-p-(CL-co-TMC) polymeric micelles as safe and effective delivery system for paclitaxel. Eur J Pharm Biopharm, 73, 230-238.

Danhier,F., Vroman,B., Lecouturier,N., Crokart,N., Pourcelle,V., Freichels,H., Jerome,C., Marchand-Brynaert,J., Feron,O., Preat,V., 2009c. Targeting of tumor endothelium by RGD-grafted PLGA-nanoparticles loaded with paclitaxel. J Control Release, 140, 166-173.

Fievez,V., Plapied,L., des Rieux A., Pourcelle,V., Freichels,H., Wascotte,V., Vanderhaeghen,M.L., Jerome,C., Vanderplasschen,A., Marchand-Brynaert,J., Schneider,Y.J., Preat,V., 2009. Targeting nanoparticles to M cells with non-peptidic ligands for oral vaccination. Eur J Pharm Biopharm, 73, 16-24.

Freichels,H., Danhier,F., Preat,V., Lecomte,P., Jerome,C., 2011. Fluorescent labeling of degradable poly(lactide-co-glycolide) for cellular nanoparticles tracking in living cells. Int J Artif Organs, 34, 152-160.

Garinot,M., Fievez,V., Pourcelle,V., Stoffelbach,F., des Rieux A., Plapied,L., Theate,I., Freichels,H., Jerome,C., Marchand-Brynaert,J., Schneider,Y.J., Preat,V., 2007. PEGylated PLGA-based nanoparticles targeting M cells for oral vaccination. J Control Release, 120, 195-204.

Guthi,J.S., Yang,S.G., Huang,G., Li,S., Khemtong,C., Kessinger,C.W., Peyton,M., Minna,J.D., Brown,K.C., Gao,J., 2010. MRI-visible micellar nanomedicine for targeted drug delivery to lung cancer cells. Mol Pharm, 7, 32-40.

Hamoudeh,M., Al,F.A., Canet-Soulas,E., Bessueille,F., Leonard,D., Fessi,H., 2007. Elaboration of PLLA-based superparamagnetic nanoparticles: characterization, magnetic behaviour study and in vitro relaxivity evaluation. Int J Pharm, 338, 248-257.

Hu,J., Qian,Y., Wang,X., Liu,T., Liu,S., 2012. Drug-loaded and superparamagnetic iron oxide nanoparticle surface-embedded amphiphilic block copolymer micelles for integrated chemotherapeutic drug delivery and MR imaging. Langmuir, 28, 2073-2082.

Lammers,T., Kiessling,F., Hennink,W.E., Storm,G., 2010. Nanotheranostics and image-guided drug delivery: current concepts and future directions. Mol Pharm, 7, 1899-1912.

Laurent,S., Bridot,J.L., Elst,L.V., Muller,R.N., 2010. Magnetic iron oxide nanoparticles for biomedical applications. Future Med Chem, 2, 427-449.

Lee,P.W., Hsu,S.H., Wang,J.J., Tsai,J.S., Lin,K.J., Wey,S.P., Chen,F.R., Lai,C.H., Yen,T.C., Sung,H.W., 2010. The characteristics, biodistribution, magnetic resonance imaging and biodegradability of superparamagnetic core-shell nanoparticles. Biomaterials, 31, 1316-1324.

Ling,Y., Wei,K., Luo,Y., Gao,X., Zhong,S., 2011. Dual docetaxel/superparamagnetic iron oxide loaded nanoparticles for both targeting magnetic resonance imaging and cancer therapy. Biomaterials, 32, 7139-7150.

Ling,Y., Wei,K., Zou,F., Zhong,S., 2012. Temozolomide loaded PLGA-based superparamagnetic nanoparticles for magnetic resonance imaging and treatment of malignant glioma. Int J Pharm, 430, 266-275.

Lu,J., Ma,S., Sun,J., Xia,C., Liu,C., Wang,Z., Zhao,X., Gao,F., Gong,Q., Song,B., Shuai,X., Ai,H., Gu,Z., 2009. Manganese ferrite nanoparticle micellar nanocomposites as MRI contrast agent for liver imaging. Biomaterials, 30, 2919-2928.

Maeda,H., Wu,J., Sawa,T., Matsumura,Y., Hori,K., 2000. Tumor vascular permeability and the EPR effect in macromolecular therapeutics: a review. J Control Release, 65, 271-284.

Massart,R., 1981. Preparation of aqueous magnetic liquids in alkaline and acidic media. Magnetics, IEEE Transactions on, 17, 1247-1248.

Mosmann,T., 1983. Rapid colorimetric assay for cellular growth and survival: application to proliferation and cytotoxicity assays. J Immunol Methods, 65, 55-63.

Petros,R.A., DeSimone,J.M., 2010. Strategies in the design of nanoparticles for therapeutic applications. Nat Rev Drug Discov, 9, 615-627.

Pourcelle,V., Devouge,S., Garinot,M., Preat,V., Marchand-Brynaert,J., 2007. PCL-PEG-based nanoparticles grafted with GRGDS peptide: preparation and surface analysis by XPS. Biomacromolecules, 8, 3977-3983.

Raymond,E., Hanauske,A., Faivre,S., Izbicka,E., Clark,G., Rowinsky,E.K., Von Hoff,D.D., 1997. Effects of prolonged versus short-term exposure paclitaxel (Taxol) on human tumor colony-forming units. Anticancer Drugs, 8, 379-385.

Roch,A., Gossuin,Y., Muller,R.N., Gillis,P., 2005. Superparamagnetic colloid suspensions: Water magnetic relaxation and clustering. Journal of Magnetism and Magnetic Materials, 293, 532-539.

Roch,A., Muller,R.N., Gillis,P., 1999. Theory of proton relaxation induced by superparamagnetic particles. 110, 5403-5411.

Schiff,P.B., Fant,J., Horwitz,S.B., 1979. Promotion of microtubule assembly in vitro by taxol. Nature, 277, 665-667.

Shieh,M.J., Hsu,C.Y., Huang,L.Y., Chen,H.Y., Huang,F.H., Lai,P.S., 2011. Reversal of doxorubicin-resistance by multifunctional nanoparticles in MCF-7/ADR cells. J Control Release, 152, 418-425.

Singh,A., Dilnawaz,F., Mewar,S., Sharma,U., Jagannathan,N.R., Sahoo,S.K., 2011. Composite polymeric magnetic nanoparticles for co-delivery of hydrophobic and hydrophilic anticancer drugs and MRI imaging for cancer therapy. ACS Appl Mater Interfaces, 3, 842-856.

Singla,A.K., Garg,A., Aggarwal,D., 2002. Paclitaxel and its formulations. Int J Pharm, 235, 179-192.

Talelli,M., Rijcken,C.J., Lammers,T., Seevinck,P.R., Storm,G., van Nostrum,C.F., Hennink,W.E., 2009. Superparamagnetic iron oxide nanoparticles encapsulated in biodegradable thermosensitive polymeric micelles: toward a targeted nanomedicine suitable for image-guided drug delivery. Langmuir, 25, 2060-2067.

van Ewijk,G.A., Vroege,G.J., Philipse,A.P., 1999. Convenient preparation methods for magnetic colloids. Journal of Magnetism and Magnetic Materials, 201, 31-33.

Weiss,R.B., Donehower,R.C., Wiernik,P.H., Ohnuma,T., Gralla,R.J., Trump,D.L., Baker,J.R., Jr., Van Echo,D.A., Von Hoff,D.D., Leyland-Jones,B., 1990. Hypersensitivity reactions from taxol. J Clin Oncol, 8, 1263-1268.

Yang,X., Grailer,J.J., Rowland,I.J., Javadi,A., Hurley,S.A., Steeber,D.A., Gong,S., 2010. Multifunctional SPIO/DOX-loaded wormlike polymer vesicles for cancer therapy and MR imaging. Biomaterials, 31, 9065-9073.

Yoon,H.Y., Saravanakumar,G., Heo,R., Choi,S.H., Song,I.C., Han,M.H., Kim,K., Park,J.H., Choi,K., Kwon,I.C., Park,K., 2012. Hydrotropic magnetic micelles for combined magnetic resonance imaging and cancer therapy. J Control Release, 160(3), 692-698.

CHAPTER IV.

COMPARISON OF ACTIVE, PASSIVE AND MAGNETIC TARGETING TO TUMORS OF MULTIFUNCTIONAL PACLITAXEL/SPIO-LOADED NANOPARTICLES FOR TUMOR IMAGING AND THERAPY

COMPARISON OF ACTIVE, PASSIVE AND MAGNETIC TARGETING TO TUMORS OF MULTIFUNCTIONAL PACLITAXEL/SPIO-LOADED NANOPARTICLES FOR TUMOR IMAGING AND THERAPY

N. Schleich, C. Po, D. Jacobs, B. Ucakar, B. Gallez, F. Danhier*, V. Préat*

Adapted from Journal of Controlled Release, in press, doi: 10.1016/j.jconrel.2014.07.059

ABSTRACT

Multifunctional nanoparticles combining therapy and imaging have the potential to improve cancer treatment by allowing personalized therapy. Herein, we aimed to compare *in vivo* different strategies in terms of targeting capabilities: (1) passive targeting via the EPR effect, (2) active targeting of $\alpha_v\beta_3$ integrin via RGD grafting, (3) magnetic targeting via a magnet placed on the tumor and (4) the combination of the magnetic targeting and the active targeting of $\alpha_v\beta_3$ integrin. For a translational approach, PLGA-based nanoparticles loaded with paclitaxel and superparamagnetic iron oxides were used. Electron Spin Resonance spectroscopy and Magnetic Resonance Imaging (MRI) were used to both quantify and visualize the accumulation of multifunctional nanoparticles into the tumors. We demonstrate that compared to untargeted or single targeted nanoparticles, the combination of both active strategy and magnetic targeting drastically enhanced (i) nanoparticle accumulation into the tumor tissue with a 8–fold increase compared to passive targeting (1.12% and 0.135% of the injected dose, respectively), (ii) contrast in MRI (imaging purpose) and (iii) anti-cancer efficacy with a median survival time of 22 days compared to 13 for the passive targeting (therapeutic purpose). Double targeting of nanoparticles to tumors by different mechanisms could be a promising translational approach for the management of therapeutic treatment and personalized therapy.

KEYWORDS

Theranostic, Nanoparticle, Tumor Targeting, Paclitaxel, SPIO, MRI

TABLE OF CONTENTS

I. INTRODUCTION

Multifunctional nanoparticles combining therapy and imaging have the potential to improve cancer treatment by allowing personalized therapy. Based on the advances made in different scientific disciplines, such as chemistry, biology, pharmacy, nanotechnology, medicine and imaging, many reports have shown that the use of nanotheranostics is one the most promising methods, although this is still at an early stage [Ahmed et al., 2012; Lammers et al., 2010; Xie et al., 2010].

Theranostic refers to the combination of a therapeutic and a diagnostic agent in a same unique vector. This term is commonly used to describe multifunctional system combining therapeutic and imaging abilities [Lammers et al., 2010]. Such a tool could be helpful in non-invasive assessment of the biodistribution, visualization of drug distribution, optimization of strategies, prediction and real-time monitoring of therapeutic responses [Janib et al., 2010; Lammers et al., 2010].

Additionally, nanotheranostics can be used for preselecting patients, seeming to hold significant potential for personalizing nanomedicine (chemo-) therapeutic interventions. Theranostics strategies range from set-ups in which patients are pre-selected on the basis of initial target site accumulation studies. It is important to note that theranostics take their place in its broadest sense. Many publications claim that theranostics can be used for the simultaneous diagnosis and treatment. The diagnosis purpose of theranostics should not refer to the identification, the localization and/or the staging of tumors but to the pre-selection of patients, to the prediction of potential therapeutic responses, and/or to the longitudinal monitoring of treatment efficacy [Rizzo et al., 2013]. The first step toward personalized nanomedicine treatment is to pre-select patients on the basis of non-invasive imaging insights on target site accumulation. A second personalization step consists in the non-invasive monitoring of the response of the first cycles of treatment. During this monitoring, the treatment should be adapted, if necessary [Rizzo et al., 2013].

Different tumoral targeting strategies have been described in the literature. However, *in vivo* quantification of the accumulation of theranostic nanoparticles targeting tumors by different strategies has not been yet studied [Danhier et al., 2010; Danhier et al., 2012b]. Hence, we evaluated *in vivo* in parallel three tumoral targeting strategies.

Passive targeting is based on the so-called enhanced permeability and retention (EPR) effect [Maeda et al., 2000]. This strategy relies on the presence of fenestrations in the endothelium of tumor vessels. These fenestrations allow the entry of macromolecules or nanoparticle into the tumor tissue (enhanced permeability effect). Moreover, the deficiency of the lymphatic system in tumor tissue prevents the recapture of these macromolecules leading to a retention effect [Danhier et al., 2010; Maeda et al., 2000; Taurin et al., 2012].

Active targeting consists in coupling a ligand to the surface of nanoparticles that can interact with its receptor at the target cell site [Danhier et al., 2012b; Danhier et al., 2009b]. Although angiogenesis is a physiological process by which new blood vessels are formed, it is also at the root of tumor growth and metastasis. Since angiogenesis is controlled by the endothelial cells, it is of great interest to target tumor endothelial cells. $\alpha_v\beta_3$ is an adhesion integrin overexpressed at the surface of the endothelial cells of neo-angiogenic vessels involved in the angiogenic process. Its expression is correlated with the malignancy of tumor. Moreover, $\alpha_v\beta_3$ is also overexpressed at the surface of many tumor cells. Therefore, many efforts have been made by researchers to specifically target this integrin in order to make the most of this "double sword" [Danhier et al., 2009b; Liu et al., 2013]. Numerous studies have shown that the tripeptide arginine–glycine–aspartic acid (RGD) was able to bind preferentially to particular $\alpha_v\beta_3$integrin [Danhier et al., 2009b; Garanger et al., 2006; Murphy et al., 2008; Son et al., 2013].

More recently, *magnetic drug targeting* has been studied. In this approach, magnetic nanoparticles are guided to tumor site using magnetic fields [Arias et al., 2011; Cole et al., 2011].

Many groups have demonstrated differential levels of tumor growth between tumors treated by targeted or untargeted drug-loaded nanoparticles. However, only few have shown *in vivo* efficacy in both therapeutic and diagnostic approach. We hypothesized that the combination of both active strategy and magnetic targeting could enhance multifunctional nanoparticles concentration into the tumor tissue leading, therefore, to a better anti-cancer efficacy (therapeutic purpose) and increased contrast enhancement in MRI (diagnosis purpose). Our main objective was to directly evaluate different targeting strategies *in vivo* using two complementary techniques: (1) the Electron Spin Resonance (ESR) spectroscopy, a very sensitive quantification tool [Danhier et al., 2012a; Radermacher et al., 2009] and (2) the 11.7

T Magnetic Resonance Imaging (MRI), a quantification and an imaging tool [Radermacher et al., 2012].

The present study relies on previously developed and described nanoparticles [Schleich et al., 2013]. These dual paclitaxel/superparamagnetic iron oxide-loaded PEGylated PLGA-based nanoparticles showed strong magnetic properties, and *in vivo* anti-tumor efficacy. In a view of a translational approach, poly(lactide-co-glycolide)(PLGA) was chosen for its biodegradability properties, its biocompatibility and its approval in parenteral products by the FDA.

Hence, different strategies have been compared in terms of targeting capabilities: (1) *passive targeting* via the EPR effect, (2) *active targeting* of $\alpha_v\beta_3$ integrin via RGD grafting, (3) *magnetic targeting* via a magnet placed on the tumor and (4) the combination of the magnetic targeting and the active targeting of $\alpha_v\beta_3$ integrin (Figure 1).

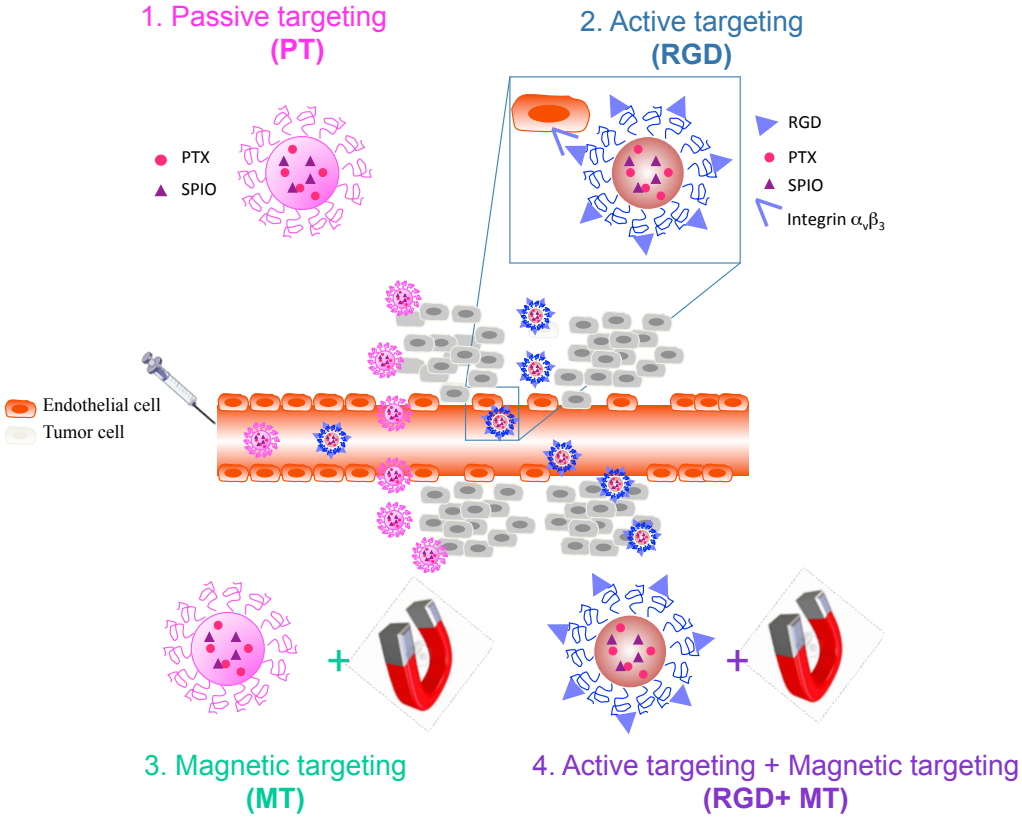

Figure 1. Schematic representation of the different tumor targeting strategies compared in the present study. (1) *passive targeting* via the EPR effect (PT), (2) *active targeting* of $\alpha_v\beta_3$ integrin via RGD grafting (RGD), (3) *magnetic targeting* via a magnet of 1.1 T placed on the tumor (MT) and (4) the combination of the magnetic targeting and the active targeting of $\alpha_v\beta_3$ integrin (RGD+MT).

We aimed at comparing different targeting strategies for multifunctional nanoparticles in terms of anti-cancer efficacy, biodistribution, and MRI contrast agent efficiency. The most

effective targeting strategy was obtained by the use of a combination of active strategy using RGD-grafted nanoparticles and magnetic targeting.

II. MATERIAL AND METHODS

II.1. NANOPARTICLES FORMULATION

Superparamagnetic iron oxides (SPIO) coated with oleic acid were synthetized by a co-precipitation technique of ferrous and ferric salts in alkaline medium as previously described [Schleich et al., 2013]. All nanoparticles formulations were prepared by an emulsion-diffusion-evaporation method [Danhier et al., 2010; Garinot et al., 2007; Schleich et al., 2013]. Briefly, PLGA (Sigma Aldrich, 28 mg/ml), PLGA-PEG (6 mg/ml) and PCL-PEG (6 mg/ml), synthesized as previously described [Danhier et al., 2009b; Garinot et al., 2007], were dissolved in 2 ml dichloromethane containing SPIO (30 mg/ml) and paclitaxel (PTX) (Chemieliva) (1.5 mg/ml) [Schleich et al., 2013]. This organic solution was then added to an aqueous solution (4.5 ml) containing 3 % (p/v) PVA and emulsified using a vortex for 2 min followed by sonication (2 x 30 s, 50 W). The mixture was then added dropwise and under magnetic stirring into an aqueous solution containing 1 % PVA and stirred overnight to evaporate the organic solvent. To remove the non-encapsulated drug and oleic acid-coated SPIO, the suspension was filtered (1,2 µm) and washed three times with water using ultracentrifugation (11 000 g, 30 min, 4°C) and suspended in 2 ml water. Two different types of nanoparticles were prepared:

(1) SPIO/PTX-loaded nanoparticles (SPIO/PTX-NP)
(2) SPIO/PTX-loaded nanoparticles grafted with the RGD peptide on their surface (SPIO/PTX-NP RGD)

For the latest formulation, we used exactly the same method while PCL-PEG was replaced by PCL-PEG-RGD that was synthetized by photografting as previously described [Pourcelle et al., 2009].

II.2. PHYSICO-CHEMICAL CHARACTERIZATION

The *hydrodynamic particle* size and size polydispersity of nanoparticles was assessed using a dynamic light scattering method (Nano ZS, Malvern instruments, UK).

The *Zeta* (ζ) *potential* of the nanoparticles was measured in KCl 1 mM with a Malvern Nano ZS at 25 °C.

Iron content was measured by Electron Spin Resonance (ESR) using a Bruker EMX ESR spectrometer operating at 9 GHz (BrukerBiospinGmBh) validated by inductively coupled plasma mass spectroscopy (ICP-MS) measurements (Agilent 7500ce instrument) [Danhier et

al., 2009a]. Typical parameters were selected for ESR measurements: 3 mT modulation amplitude, 10.11mW power, 325.1 mT center field, and 400 mT sweep width field. Double integration of the iron oxides ESR spectra was used to quantify signal intensity.

PTX content was determined using high-performance liquid chromatography (HPLC) with UV detection at 227 nm (Agilent 1100 series, Agilent Technologies), as previously described after dissolution of the particles by acetonitrile [Danhier et al., 2009a]. The mobile phase consisted of acetonitrile and water (70:30 v/v, respectively) at a rate of 1ml/min. The column used was a CC 125/4 Nucleod UR 100-5 C18.The drug loading was defined as the amount of drug (mg) loaded for 100 mg of polymer whereas the encapsulation efficiency was defined by the ratio of the encapsulated drug compared to the initial amount of drug [Danhier et al., 2010; Schleich et al., 2013].

Saturation magnetisation values were obtained from the fitting by a theoretical relaxation model of Nuclear Magnetic Relaxation Dispersion (NMRD) profiles recorded at 37°C on a Fast Field Cycling Relaxometer (Stelar, Mede, Italy) over a magnetic field range from 0.01-40 MHz. The proton NMRD curves were fitted using data-processing software, including different theorical models describing the nuclear relaxation phenomena [Danhier et al., 2010; Schleich et al., 2013].

II.3. ANIMAL MODELS

All experiments were performed in compliance with guidelines set by national regulations and were approved by the ethical committee for animal care of the medical sector of the Université catholique de Louvain. CT26 colon carcinoma was chosen because of its sensitivity to PTX [Yang et al., 2012] and of its angiogenic properties [Lyons et al., 2007]. CT26 colon carcinoma cells were inoculated subcutaneously in the right flank or in the right leg (to avoid respiratory artifacts in MRI studies) of BALB/c mice ($5x10^4$ cells per mouse) depending on the experiment. For all the experiments, mice were divided into 5 groups:

Group 1: control group (injected with PBS for *in vivo* anti-tumor efficacy study and histological study and SPIO-loaded nanoparticles for *ex vivo* biodistribution and MRI,

Group 2: mice treated by SPIO/PTX-NP (*passive targeting, PT*),

Group 3: mice treated by SPIO/PTX-NP grafted with RGD peptide (*active targeting or RGD*), Group 4: mice treated with SPIO/PTX-NP magnetic guided by placing a 1.1 T neodyme-iron-bore external magnet (Webcraft GmbH) on the surface of the tumor during 1 or 4 h (*magnetic targeting or MT*),

Group 5: mice treated with SPIO/PTX-NP using both magnetic and active targeting (*RGD+MT*).

For magnetic targeting, the magnet was placed directly in contact of the tumor surface and fixed by a bandage. The bandage was fixed as the space between the magnet and the skin would not be exceeding 0.3 cm. The exposure time varies from 1h (ESR spectroscopy) to 4h (*in vivo* anti-tumor efficacy, ESR spectroscopy and MRI experiments as well as histological studies).

PTX and Fe doses were 5 mg/kg and 27.1 mg/kg, respectively, for *in vivo* anti-tumor efficacy experiment and 2.5 mg/kg and 13.5 mg/kg for other experiments. For tumor inoculation, mice were anesthetized by intra-peritoneal injections of a mixed ketamine (100 mg/kg) and xylazine (10 mg/kg). For *in vivo* MRI experiments, mice were maintained under anesthesia during the entire experiment using 1-2 % isoflurane (Abbott) inhalation in air.

II.4. *IN VIVO* ANTI-TUMOR EFFICACY

The effect of SPIO/PTX-NP on tumor growth was assessed by daily measurements of tumor volume with an electronic caliper. CT26 cells were injected subcutaneously in the right flank of the mice to allow easy and reproducible tumor volume measurements. Mice were randomly assigned to a treatment group when tumor reached a volume of 27 ± 5 mm^3. Treatments were injected trough the tail vein. Five groups were defined as aforementioned (n=6): PBS, PT, RGD, MT and RGD+MT. In this experiment, the magnet was placed on the surface of the tumor during 4 h. The end point of the experiment was determined as the moment when tumor reached 600 mm^3. At this point, mice were sacrificed.

II.5. *EX VIVO* BIODISTRIBUTION STUDY BY ESR SPECTROSCOPY

The biodistribution of the different treatments was assessed using ESR spectroscopy (X-band). CT26 cells were subcutaneously inoculated in the right flank of the mice. When tumor reached 50-100 mm^3 in volume, mice were randomly dispersed into 5 groups as aforementioned (n=6): CTRL, PT, RGD, MT and RGD+MT. The control group was a group injected with SPIO-loaded nanoparticles. For mice treated with magnetic targeting, the external magnet was maintained on the tumor until sacrifice. Treatments were injected in the tail vein of the mouse. 1 or 4 h post-treatment, mice were first taken a retro-orbital blood sample and were then sacrificed for dissection in order to remove liver, lungs and tumor. Thereafter, samples were frozen in liquid nitrogen, dehydrated for 24 h in a freeze-dryer

(Labconco), crushed into a fine powder, weighed and analyzed by ESR spectroscopy to determine iron concentration in each tissue.

II.6. *IN VIVO* MR IMAGING

For these experiments, CT26 cells were injected subcutaneously in the right leg of the mice to avoid respiratory artifacts. Mice were enrolled in the study when tumor reached 50-100 mm^3 in diameter. The same amount of SPIO/PTX-NP or SPIO/PTX-NP-RGD were injected, and the same groups were defined (n=5): PT, RGD, MT and RGD + MT. Each mouse was imaged before and 1 h after treatment injection in the tail vein in order to use each mouse as its own control.

MR experiments were performed using a 11.7 T Bruker Biospec horizontal MR System (Bruker Biospin). RF transmission and reception were achieved with a quadrature volume resonator (inner diameter 40 mm). At first, mice were anesthetized by isoflurane inhalation 3 % in $_{air}$ and they were placed in an MRI compatible cradle. The breathing rate was assessed via a breathing pillow, placed under the thorax, and kept at 70 breaths/minute by adjusting the isoflurane concentration. The body temperature was maintained at 37°C by a warm waterbed and monitored using a rectal probe. Vital functions were monitored during the whole anesthesia period using SamPC Monitor (version 6.17, Small Animal Instruments Inc). Anatomical images of the mice were provided by T_2-weighted axial images acquired with a Rapid Acquisition with Relaxation Enhancement sequence (RARE; TR/TE: 2500/30 ms, RARE factor: 6, 10 slices non-contiguous with a gap of 0.08 mm, resolution: 125 x 125 x 800 μm^3). T_2 maps were acquired with the same geometry than the anatomical images using a Multi Slice Multi Echo sequence (MSME; TR/TE: 2500/10 ms; 16 echoes). Quantitative T_2 maps were calculated from the MSME multi-echo trains and assuming mono-exponential decays, using ImageJ (ImageJ version, 1.48 NIH). The volume of interest (VOI) corresponding to the tumor volume were manually delineated on a slice by slice basis on the anatomical images acquired before and after treatment injection, for each animal. These VOIs were applied on corresponding maps to determine the T_2 values. Relative standard deviations (RSD) were calculated as RSD = $SD/mean\ T_2$, where SD is the standard deviation of the mean T_2 value [Oakes et al., 2014].

II.7. HISTOLOGICAL STUDY OF TUMOR TISSUES

The accumulation of multifunctional nanoparticles in tumor tissue was visualized by histological analysis of tumor tissue after Prussian's blue staining. After MR imaging, mice were sacrificed and tumor tissues were surgically removed and fixed in 4% paraformaldehyde and imbedded in paraffin. Representative 5 µm tumor cross-sections were cut and mounted on glass slides. Thereafter sections were placed in a bath containing 5% Potassium hexacyanoferrate (II) trihydrate (Sigma Aldrich) and 5% HCl in distilled water for 30 min at room temperature and protected from light. Tumor sections were counterstained with a 0.1% nuclear fast red aqueous solution (Sigma Aldrich) containing 5% aluminum sulfate for 5 min.

II.8. STATISTICAL ANALYSIS

All results arising from *in vivo* antitumor efficacy and *ex vivo* biodistribution are expressed as mean ± SEM. Two-way ANOVA, Bonferroni post-test, Kaplan-Meier survival rate and t-test were performed using the software GraphPad Prism 5 for Windows, to demonstrate statistical differences ($p<0,05$). MRI results were expressed as mean RSD ± SD. One-way ANOVA and Bonferroni post-test were performed using the software GraphPad Prism 5 for Windows, to demonstrate statistical differences ($p<0,05$).

III. RESULTS

III.1. PHYSICO-CHEMICAL CHARACTERIZATION

Physico-chemical features of the nanoparticles are summarized in Table 1. Nanoparticles co-loaded with SPIO and PTX presented a similar size of about 240 nm when grafted with RGD or not. They all presented a neutral ζ potential and drug encapsulation efficiency approximately 25%. This corresponds to a paclitaxel-loading of around 1.8 mg/100 mg of polymer. SPIO-loading was about 10 mg/100 mg of polymer. Moreover, they all presented a saturation magnetization around 15 Am^2/kg. In a previous study, we evaluated the drug release from nanoparticles [Danhier et al., 2009b]. Briefly, after the initial burst release for about 4 h (50%), the release rate of PTX slowed down and became an almost zero-order rate of release (75% released in 11 days)

Table 1: Physico-chemical properties of nanoparticles. Size, ζ potential, drug encapsulation efficiency, drug loading, SPIO loading and saturation magnetization (M_{sat}) of SPIO-loaded nanoparticles (SPIO-NP), paclitaxel-loaded nanoparticles (PTX-NP), co-loaded SPIO/paclitaxel nanoparticles (SPIO/PTX-NP) and co-loaded SPIO/paclitaxel nanoparticles grafted with RGD (*n*=5).

	SPIO-NP	SPIO/PTX-NP	SPIO/PTX-NP RGD
Size (nm)	235.8 ± 8.9	243 ± 9.9	245 ± 1.2
Zeta ζ potential (mV)	-0.16 ± 0.04	-0.02 ± 0.01	-0.42 ± 0.6
Drug encapsulation efficiency (%)	/	24.8 ± 4.9	25.2 ± 2.8
PTX loading (mg/100 mg of polymer)	/	1.84 ± 0.4	1.85 ± 0.2
SPIO-loading (mg/100mg of polymer)	9.0 ± 1.5	10.4 ± 1.9	10.1 ± 0.6
M_{sat} (Am^2/kg or emu/g)	14,5 ± 0,1	15,1 ± 0,1	14,1 ± 0,1

III.2. *IN VIVO* ANTI-TUMOR EFFICACY

The *in vivo* anti-tumor efficacy of the different targeting strategies was evaluated in CT26-tumor-bearing mice (Figure 2). All PTX-loaded nanoparticles induced a higher delay in tumor growth than the control group (PBS) (Figure 2A). Moreover, all the groups treated with an active targeting (RGD, MT and RGD + MT) induced a higher delay compared with PT (Figure 2A). Kaplan-Meier survival rate was performed (Figure 2B). PT exhibited higher survival rate than the untreated group (PBS) with median survival rate of 13 compared to 10

days (p<0.01). No significant difference was observed between RGD and MT with median survival times of 14.7 and 15 days (p>0.05), which are statistically different from the PBS group (p<0.01) and from the PT group (p<0.01). Moreover, one long-term survival mouse was found in the RGD group. Finally, mice treated with the combination of active and magnetic targeting (RGD + MT) exhibited the highest survival rate with a median survival time of 21.5 days (p<0.05). In this group, there were two long-term survival mice. The benefits of the combination of RGD+MT are illustrated in Figure 2C. The time to reach a tumor-growing ratio of 13 (endpoint of the PBS group) was prolonged by both RGD and MT treatments compared to the control group (11.7, 12.1, respectively compared to 8.6; p<0.001 and p<0.0001, respectively). Mice treated with RGD-grafted nanoparticles and magnetically targeted nanoparticles (MT) showed an equivalent time to reach a tumor-growing ratio of 13 (p>0.05). The time to reach a tumor-growing ratio of 13 was enhanced when mice were treated with RGD-grafted nanoparticles combined with the magnetic targeting (RGD+MT) when compared to MT or RGD alone (14.8 days versus 12.1 and 11.7 days, respectively; p<0.01and p<0.05).

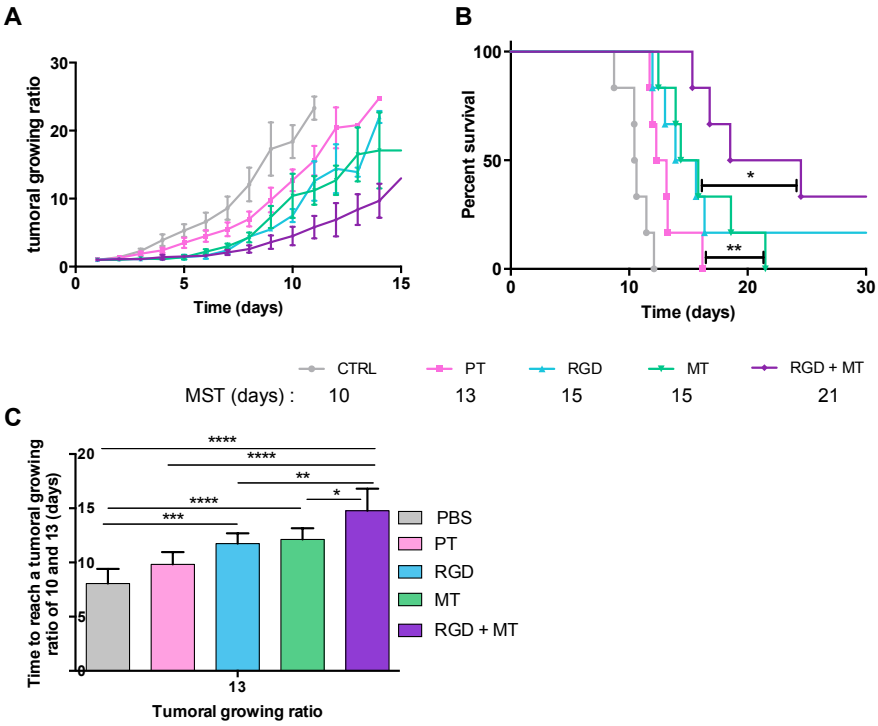

Figure 2. Tumoral growing ratio and survival rates of CT26-tumor bearing mice. (A) Tumor growth curves of CT26-tumor bearing mice treated with co-loaded SPIO/PTX nanoparticles (PT) (PTX dose = 5 mg/kg), SPIO/PTX-NP grafted with RGD-peptide (RGD), SPIO/PTX-NP followed by 4 hours of magnetic targeting (MT) and SPIO/PTX-NP RGD followed by 4 hours of magnetic targeting (RGD + MT) or untreated (PBS). The treatment was injected in the tail vein of the mice when tumors reached 27±5 mm (n=6). Results are presented as the average tumor growing ratio ± SEM versus time after treatment injection.
(B) Survival rates of tumor-bearing. Mean survival times (MST) in days were calculated for each group. (C) Comparison of time for tumor to reach a growing ratio of 13 (in days).
* p<0.05, ** p<0.01, *** p<0.001, **** p<0.0001

III.3. BIODISTRIBUTION USING ESR SPECTROSCOPY

Biodistribution studies of SPIO/PTX-loaded NP are illustrated in Figure 3. Iron accumulation in blood, tumor tissue, liver and lungs was measured using ESR spectroscopy. Blood samples did not show any statistical differences in terms of iron concentration with a mean concentration around 2 ng/mg of blood for all groups (data not shown). Concerning the iron accumulation in tumor tissues (Figure 3A), no significant difference was observed between 1 h and 4 h after injection even when using magnetic targeting. Mice treated with RGD showed a 2.5-fold accumulation increase in tumor tissue compared to the group treated with PT with 0.35 % of the injected dose and 0.135 %, respectively ($p<0.05$). This accumulation rose to 5-fold in MT (0.737%, $p<0.001$). The highest iron concentration was obtained in mice treated with the combination of RGD+MT with a 8–fold increase in iron accumulation (1.12 % of the injected dose). The iron uptake by the liver (Figure 3B) was dominant for all treatment groups with iron concentration rising up to 35 % of the injected dose. However, after 4 h of MT, this iron uptake was drastically reduced to 11.29 % of the injected dose ($p<0.001$). Interestingly, RGD-, MT- and RGD+MT-treated group showed a highly significant decrease of the iron accumulation in lungs compared to control and PT-treated groups with 0.52 %, 0.43 % and 0.47 % of the injected dose for RGD-, MT- and RGD+MT-treated group, respectively compared to 1.31 % and 1.21 % of the injected dose for control and PT-treated group after 1h ($p<0.001$, Figure 3C).

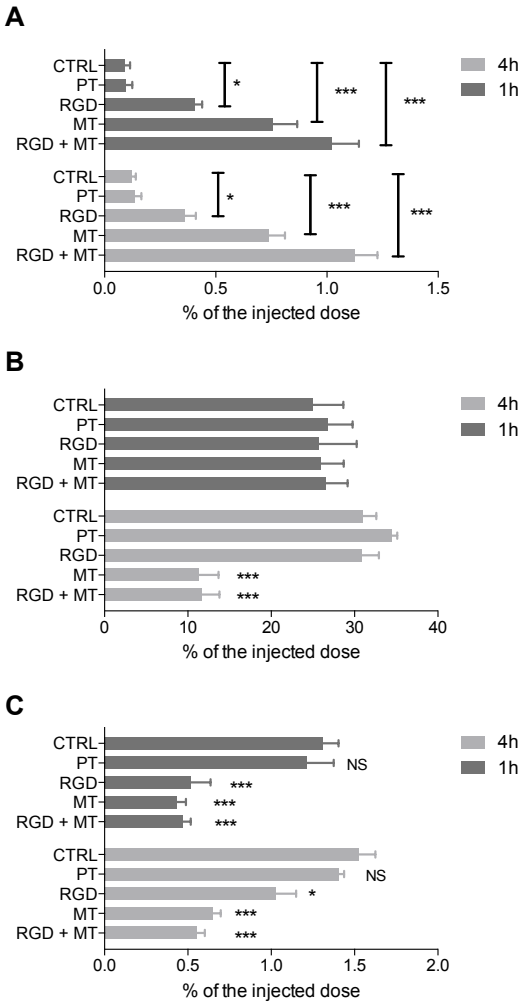

Figure 3. Biodistribution of multifunctional nanoparticles. Biodistribution of multifunctional nanoparticles using ESR spectroscopy, 1 or 4 hours after injection of the treatment. 5 groups were defined: SPIO-loaded nanoparticles (CTRL), PT, RGD, MT and RGD + MT. (A) Iron accumulation in tumor tissue in ng/mg of tissue (n=5). (B) Iron accumulation in liver (n=5). (C) Iron accumulation in lungs (n=5).
*p<0.05, ***p<0.001, NS: Not Significant

III.4. HISTOLOGICAL ANALYSIS

Figure 4 shows representative histological sections of tumor tissues stained with Prussian's blue to label the SPIO nanoparticles. Blue spots indicating the presence of SPIO are pointed out by white arrows. As seen in Figure 4A, no blue coloration was observed in untreated tumor tissue. Only a few blue spots were observed in tumor treated with PT (Figure 4B). There were more blue spots in tissues of mice treated by RGD (Figure 4C). These blue spots were even more numerous in tumor tissue when using MT (Figure 4D). Nevertheless, the most colored sections were obtained for mice of the RGD+MT group (Figure 4E).

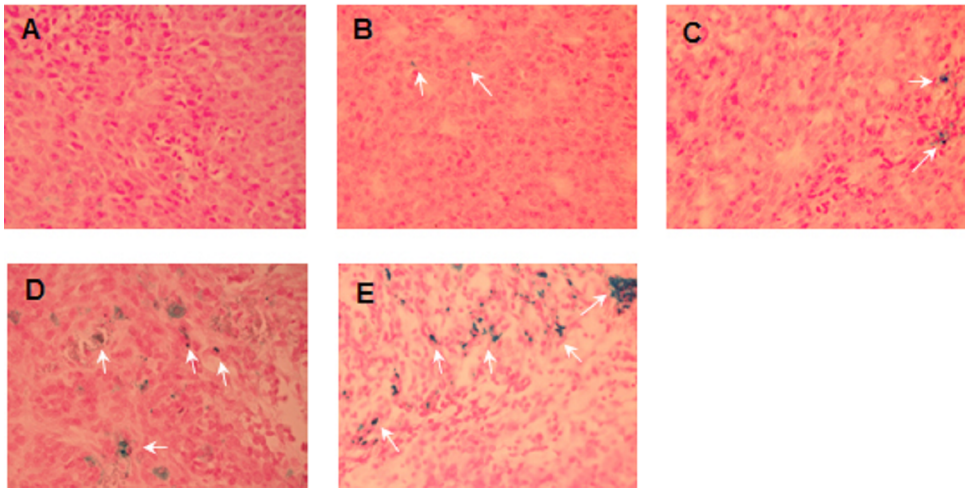

Figure 4. **Histological study of tumor tissue using Prussian's blue staining**. A: CTRL, B: SPIO/PTX-NP treated mouse, C: SPIO/PTX-NP RGD treated mouse, D: SPIO/PTX-NP treated group with magnetic targeting. E: SPIO/PTX-NP RGD treated group with magnetic targeting.

III.5. IN VIVO MRI

To detect the contrast enhancement provided by the injection of the different treatments, MR imaging of mice were performed before and 4 h after injection. T_2-weighted images, obtained with different TE from MSME sequence, showed very low signal intensity in the areas characterized by the presence of SPIO (Figure 5, red arrows). For this reason, the T_2 value corresponding to these areas could not be determined. To estimate the local disturbance induced by SPIO in MRI, RSD of T_2 is commonly used [Oakes et al., 2014]. Injection of the passive targeted nanoparticles (PT) induced no visible darkening of the tumor region (Figure 5A). No significant change in RSD was observed (p>0.05) (Figure 6). Mice treated with actively targeted nanoparticles (RGD) showed a slight darkening of the tumor region with a few darker spots located into the tumor tissue pointed out by narrow-head (Figure 5B). This effect was reflected by a 3-times increase tendency in RSD after injection (p>0.05) (Figure 6). As for mice treated with magnetic targeted treatment (MT), many dark spots were clearly found in the tumor region (Figure 5C) inducing a 30–fold increase in RSD after injection (p<0.001) (Figure 6). The combination of magnetic targeting and active targeting induced

also a high darkening contrast (Figure 5D) translated into a 40–fold increase in RSD after injection (p<0.001) (Figure 6). The difference between MT and RGD+MT was not significant (p>0.05) but a tendency of a larger increase in RSD was observed for RGD+MT (3.4 ± 0.42 vs 4.4 ± 0.67, for MT and RGD+MT, respectively).

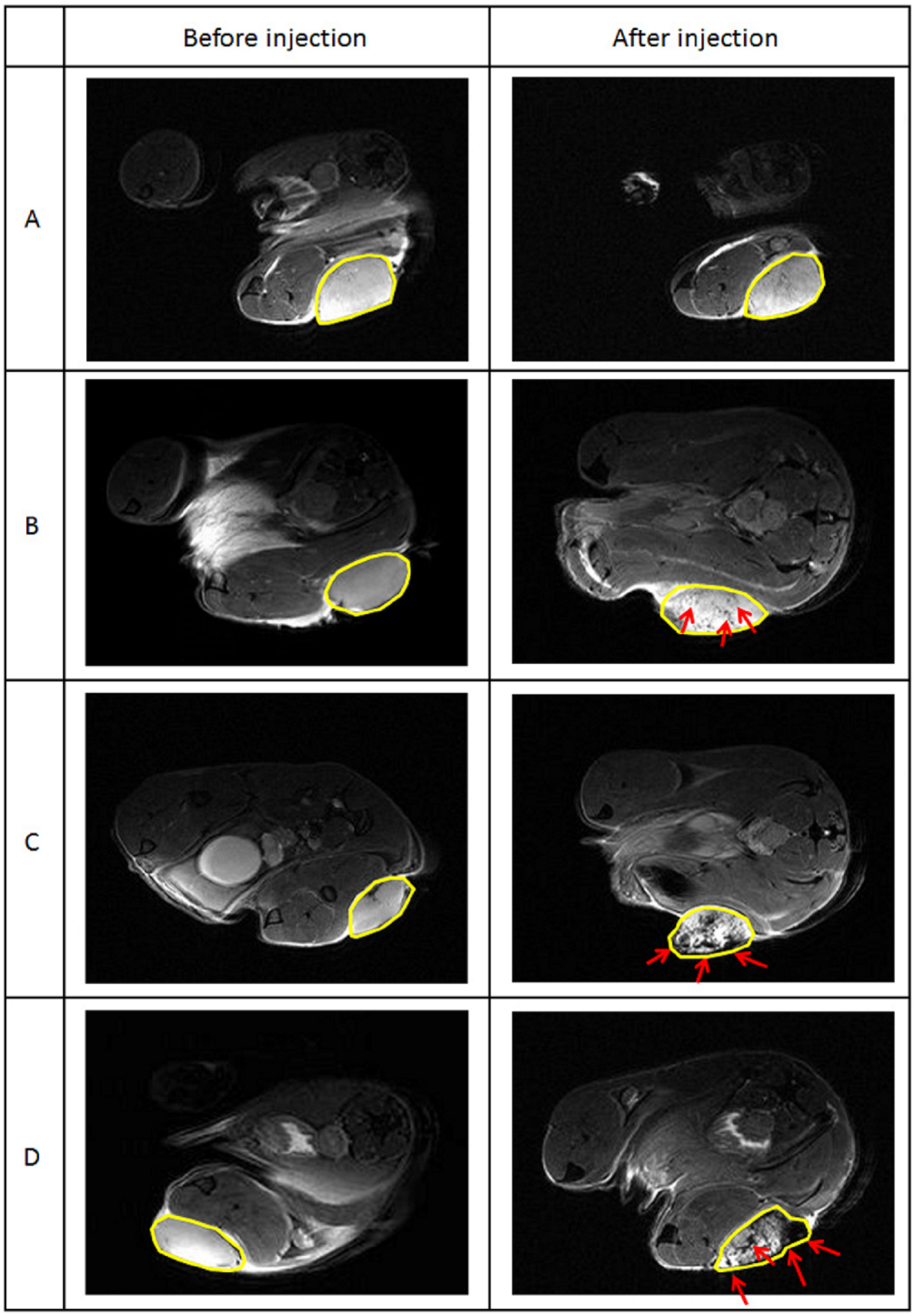

Figure 5. MRI imaging. T_2-weighted images, obtained from MSME sequence (TE = 10 ms) of CT26-tumor bearing mice pre-injection and 4 h after injection. The position of dark region in tumor was pointed by red head-narrows (n=5). A: PT, B: RGD, C: MT, D: RGD+MT.

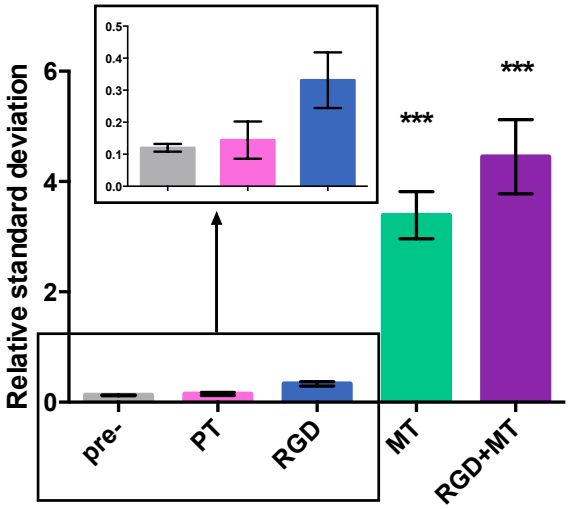

Figure 6. MRI quantification. Mean RSD (Relative Standard Deviation) calculation of the tumor region pre- and 4 h after injection of PT, RGD, MT and RGD+MT (results expressed as mean ± SD, n=5).
***p<0.001

IV. DISCUSSION

A major challenge to address in cancer therapy lies in improving the amount of drug reaching the tumor to have an efficient treatment while limiting the damages to healthy tissues. Therefore, different targeting strategies have been developed [Danhier et al., 2010; Kwon et al., 2012]. In this study, we compared four targeting strategies of multifunctional nanoparticles loaded with an anti-cancer drug and a imaging agent in terms of anti-tumor efficacy, biodistribution and magnetic resonance imaging capabilities: passive targeting (PT), active $\alpha_v\beta_3$ targeting (RGD), magnetic targeting (MT) and the combination of the two latest (RGD+MT). The current multifunctional nanoparticles incorporated SPIO for their diagnostic and superparamagnetic properties and PTX for its therapeutic properties.
All experiments (PTX anti-cancer efficacy, biodistribution, MRI and histological studies) were consistent with each other indicating that active targeting (RGD) was more effective than passive targeting (PT). Magnetic targeting (MT) showed a better efficacy compared to active targeting (RGD) in biodistribution, MRI and histological studies. PTX anti-cancer efficacy, biodistribution and histological studies confirmed that the most effective targeting was obtained using a double targeting (RGD+MT).

Magnetic resonance imaging (MRI) is a clinical widely used non-invasive imaging technique, presenting a high spatial resolution, which is suitable for cancer detection and therapeutic response assessment [Brindle, 2008; Liu et al., 2013]. However, its major limitation consists of a relatively low sensitivity. Superparamagnetic iron oxides (SPIO) as MRI contrast agent address this limitation. SPIO can produce predominant T_2 relaxation effect, resulting in a signal reduction on T_2-weighted images. The magnetic field heterogeneity around the particles, through which water molecules diffuse, induces the dephasing of the proton magnetic moments. Consequently, a T_2 effective transverse relaxation is shortened. Moreover, with their high magnetic properties, SPIO are among the most suitable candidate to achieve magnetic targeting abilities by using an external magnet [Laurent et al., 2011]. However, when SPIO concentration is very high, a fitting deficiency can occur and lead to difficulties in measuring T_2 values. Indeed, high concentration of SPIO in the tumor produced a too fast decrease of the T_2 value resulting in a non-exponential relationship. Thus, it was impossible to measure a proper T_2 value at these sites. Therefore, we measured a relative standard deviation of these T_2 values in the ROI. RSD is a measure of tumor heterogeneity after the

SPIO injection. This method is commonly used in MRI when T_2 signal is too heterogeneous [Mitra et al., 2004].

Recently, numerous publications have reported various polymer-based nanocarriers (PLGA, PLLA, HPMA, PCL, etc.) for magnetic-imaging [Hamoudeh et al., 2007; Lin et al., 2012; Ling et al., 2011; Talelli et al., 2009]. These SPIO-loaded nanocarriers are generally limited because of (i) their lack of functional groups on their surface for covalent modification, (ii) their low capacity of drug loading and (iii) the fact that the use of most of polymers used are not approved by the FDA/EMA, limiting their potential translation to the clinic [Schleich et al., 2013]. So far, many researchers have shown the interest of an active targeting [Danhier et al., 2009b; Lin et al., 2012; Zhang et al., 2012] or of the magnetic targeting [Arias et al., 2011; Yang et al., 2012]. However, only few have shown *in vivo* efficacy in both therapeutic and imaging approach.

In vivo anti-tumor efficacy study showed a significant longer regrowth delay with a longer survival time for mice treated with actively-targeted nanoparticles (RGD) compared to the passively-targeted nanoparticles. This result is consistent with our previous study [Danhier et al., 2009b]. The potential advantage of targeted delivery may result from an altered intracellular distribution. Both targeted and non-targeted systems arrive at the tumor site via the EPR effect, after which the mechanism of tumor cell internalization is enhanced by the presence of surface ligands via a receptor-mediated endocytosis [Prokop et al., 2008; Wang et al., 2010]. On the contrary, non-targeted nanoparticles mainly enter into the cells via pinocytosis [Melancon et al., 2012; Petros et al., 2010; Stromhaug et al., 1997]. Furthermore, this better anti-tumor efficacy can be easily explained by the increased accumulation in tumor tissue. Indeed, *ex-vivo* biodistribution, histological studies and MRI confirmed the iron concentration increase in tumor tissue suggesting a better accumulation of nanoparticles. However, despite this better accumulation in tumor tissue, a major issue that remains to be solved is the massive uptake by the liver. This phenomenon is well known and described in the literature [Bertrand et al., 2012]. Zhang *et al*. reported an accumulation of RGD-grafted magnetite PLGA-based nanoclusters of 35% of the injected dose in the liver [Zhang et al., 2012]. For this reason, SPIO-loaded nanoparticles are usually used as contrast agent for liver imaging [Lu et al., 2009].

Magnetic targeting showed a better nanoparticles accumulation in tumor compared to active targeting in *ex-vivo* biodistribution, histological study and MRI. As expected, this better accumulation was correlated with a longer survival time and a longer regrowth delay compared to the passively-targeted group. Lübbe *et al*. were the pioneers in using an external magnetic field to guide a treatment [Lubbe et al., 1996]. Later, numerous studies used this method with magnetic field strength ranging from 0.4 to 4 T [Alexiou et al., 2000; Arias et al., 2011; Chertok et al., 2008; Kim et al., 2009]. The success of magnetic targeting is limited by inadequate magnetic gradients, thus, by the distance between the magnets and the target site. The magnetic targeting would be more effective in regions closer to the magnets. In this experiment, a 1.1 T neodyme permanent magnet was used to create an external magnetic field to accumulate the treatment in the tumor. For superficial tumors, this strategy can be easily done by placing the permanent magnet outside of the body at the surface of the tumor [Alexiou et al., 2000; Arias et al., 2011; Lubbe et al., 1996].

The most impressive results were undoubtedly obtained with the combination of both active and magnetic strategies. Indeed, the double targeting-treated group of mice showed the most important regrowth delay compared to all the other groups. Moreover, two mice were long-time survivor in the RGD+MT-treated group. Unsurprisingly, this better anti-cancer efficacy was correlated with a higher nanoparticles accumulation in tumor (shown by both ESR spectroscopy and histological studies). The lack of difference in the T_2 RSD of MT and RGD + MT could be due to the very fast decrease in the T_2 value obtained in both groups leading to the fitting deficiency as aforementioned. Moreover, MRI is less sensitive compared to ESR spectroscopy [Danhier et al., 2014] Furthermore, using such a combination could be useful to potentialize the effect of the active targeting. Indeed, since active targeting is a saturable process [Kranenborg et al., 1998] and sometimes lacks of selectivity, it becomes more and more interesting to combine several targeting strategies [Al-Jamal, 2013].

These results confirmed our hypothesis. Indeed, there was a rationale to think that two targeting strategies would show better results compared to a simple strategy. Many groups have studied a double targeting strategy for a delivery purpose. Recently, Fang et al., used a combination of MT and lactoferrin [Fang et al., 2014]. Yang et al., have studied a double RGD and NGR targeting [Yang et al., 2014]. However, to our knowledge, this is the first study having investigated the combination of both $\alpha_v\beta_3$ integrin-targeting and magnetic targeting for a theranostic purpose. RGD targeting is a very promising strategy since it can target both neoangiogenic endothelial cells and tumors cells. Moreover, $\alpha_v\beta_3$ plays an

important role in angiogenesis [Desgrosellier et al., 2010]. Finally, in our previous study, we demonstrated the efficacy of targeting to tumor endothelium of RGD-grafted nanoparticles and their better anti-tumor efficacy [Danhier et al., 2012b].

Solid tumors are known to be highly heterogeneous either depending on the cancer type, patient or even on the disease stage (inter-tumor heterogeneity). Moreover, different cell types can be found inside a solid tumor (intra-tumor heterogeneity). Furthermore, in response to any given therapy, solid tumors inevitably evolve, leading to strong difficulties in managing cancer therapy. Therefore, there is a critical need in developing personalized therapy [Blanco et al., 2009; Guthi et al., 2010]. The combination of imaging and therapeutic capabilities in a same vector could provide a useful tool in addressing this challenge. Indeed, such theranostic platforms allow the molecular diagnosis by imaging to verify the expression of cancer biomarker to guide target-specific therapy. Furthermore, it enables to assess the efficacy of the treatment at different stages of the therapy then using those results to intelligently modify the strategy for cancer treatment (real-time monitoring) [Guthi et al., 2010; Lammers et al., 2010]. The multifunctional $\alpha_v\beta_3$-targeted nanoparticles developed in this study showed promising results in terms of anti-tumor efficiency and imaging abilities when combined to magnetic targeting. Finally, their imaging abilities could be useful to monitor the biodistribution of these multifunctional nanoparticles after injection to the patient in a first step. Thereafter, on the basis of this non-invasive imaging insight on target site, and possibly undesirable liver accumulation it would be possible to evaluate a benefice/risk ratio and, if favorable, select the patient for the treatment. This particular application could be of great interest to limit the treatment of non-responding patients and patients at high risk of undesirable toxicity.

This study also proves that MRI could be predictive of the anti-cancer treatment efficacy. This finding could be interesting from the perspective of a translational approach in the management of therapeutic treatment and personalized therapy, using these multifunctional nanoparticles as theranostics.

V. CONCLUSION

This study is the first to compare *in vivo* four targeting strategies for multifunctional nanoparticles in terms of anti-cancer efficacy, *ex-vivo* biodistribution, and MRI contrast agent efficiency. The most effective targeting strategy for imaging and therapeutic purposes was obtained by the use of a combination of active strategy using RGD-grafted nanoparticles and magnetic targeting.

VI. REFERENCES

Ahmed,N., Fessi,H., Elaissari,A., 2012. Theranostic applications of nanoparticles in cancer. Drug Discov Today, 17, 928-934.

Al-Jamal,K.T., 2013. Active drug targeting: lessons learned and new things to consider. Int J Pharm, 454, 525-526.

Alexiou,C., Arnold,W., Klein,R.J., Parak,F.G., Hulin,P., Bergemann,C., Erhardt,W., Wagenpfeil,S., Lubbe,A.S., 2000. Locoregional cancer treatment with magnetic drug targeting. Cancer Res, 60, 6641-6648.

Arias,J.L., Reddy,L.H., Othman,M., Gillet,B., Desmaele,D., Zouhiri,F., Dosio,F., Gref,R., Couvreur,P., 2011. Squalene based nanocomposites: a new platform for the design of multifunctional pharmaceutical theragnostics. ACS Nano, 5, 1513-1521.

Bertrand,N., Leroux,J.C., 2012. The journey of a drug-carrier in the body: an anatomo-physiological perspective. J Control Release, 161, 152-163.

Blanco,E., Kessinger,C.W., Sumer,B.D., Gao,J., 2009. Multifunctional micellar nanomedicine for cancer therapy. Exp Biol Med (Maywood), 234, 123-131.

Brindle,K., 2008. New approaches for imaging tumour responses to treatment. Nat Rev Cancer, 8, 94-107.

Chertok,B., Moffat,B.A., David,A.E., Yu,F., Bergemann,C., Ross,B.D., Yang,V.C., 2008. Iron oxide nanoparticles as a drug delivery vehicle for MRI monitored magnetic targeting of brain tumors. Biomaterials, 29, 487-496.

Cole,A.J., Yang,V.C., David,A.E., 2011. Cancer theranostics: the rise of targeted magnetic nanoparticles. Trends Biotechnol, 29, 323-332.

Danhier,F., Danhier,P., Magotteaux,N., De Preter G., Ucakar,B., Karroum,O., Jordan,B., Gallez,B., Preat,V., 2012a. Electron paramagnetic resonance highlights that the oxygen effect contributes to the radiosensitizing effect of paclitaxel. PLoS One, 7, e40772.

Danhier,F., Feron,O., Preat,V., 2010. To exploit the tumor microenvironment: Passive and active tumor targeting of nanocarriers for anti-cancer drug delivery. J Control Release, 148, 135-146.

Danhier,F., Le Breton A., Preat,V., 2012b. RGD-based strategies to target alpha(v) beta(3) integrin in cancer therapy and diagnosis. Mol Pharm, 9, 2961-2973.

Danhier,F., Lecouturier,N., Vroman,B., Jerome,C., Marchand-Brynaert,J., Feron,O., Preat,V., 2009a. Paclitaxel-loaded PEGylated PLGA-based nanoparticles: in vitro and in vivo evaluation. J Control Release, 133, 11-17.

Danhier,F., Ucakar,B., Vanderhaegen,M.L., Brewster,M.E., Arien,T., Preat,V., 2014. Nanosuspension for the delivery of a poorly soluble anti-cancer kinase inhibitor. Eur J Pharm Biopharm.

Danhier,F., Vroman,B., Lecouturier,N., Crokart,N., Pourcelle,V., Freichels,H., Jerome,C., Marchand-Brynaert,J., Feron,O., Preat,V., 2009b. Targeting of tumor endothelium by RGD-grafted PLGA-nanoparticles loaded with paclitaxel. J Control Release, 140, 166-173.

Desgrosellier,J.S., Cheresh,D.A., 2010. Integrins in cancer: biological implications and therapeutic opportunities. Nat Rev Cancer, 10, 9-22.

Fang,J.H., Lai,Y.H., Chiu,T.L., Chen,Y.Y., Hu,S.H., Chen,S.Y., 2014. Magnetic Core-Shell Nanocapsules with Dual-Targeting Capabilities and Co-Delivery of Multiple Drugs to Treat Brain Gliomas. Adv Healthc Mater.

Garanger,E., Boturyn,D., Coll,J.L., Favrot,M.C., Dumy,P., 2006. Multivalent RGD synthetic peptides as potent alphaVbeta3 integrin ligands. Org Biomol Chem, 4, 1958-1965.

Garinot,M., Fievez,V., Pourcelle,V., Stoffelbach,F., des Rieux A., Plapied,L., Theate,I., Freichels,H., Jerome,C., Marchand-Brynaert,J., Schneider,Y.J., Preat,V., 2007. PEGylated PLGA-based nanoparticles targeting M cells for oral vaccination. J Control Release, 120, 195-204.

Guthi,J.S., Yang,S.G., Huang,G., Li,S., Khemtong,C., Kessinger,C.W., Peyton,M., Minna,J.D., Brown,K.C., Gao,J., 2010. MRI-visible micellar nanomedicine for targeted drug delivery to lung cancer cells. Mol Pharm, 7, 32-40.

Hamoudeh,M., Al,F.A., Canet-Soulas,E., Bessueille,F., Leonard,D., Fessi,H., 2007. Elaboration of PLLA-based superparamagnetic nanoparticles: characterization, magnetic behaviour study and in vitro relaxivity evaluation. Int J Pharm, 338, 248-257.

Janib,S.M., Moses,A.S., MacKay,J.A., 2010. Imaging and drug delivery using theranostic nanoparticles. Adv Drug Deliv Rev, 62, 1052-1063.

Kim,D.H., Kim,K.N., Kim,K.M., Lee,Y.K., 2009. Targeting to carcinoma cells with chitosan- and starch-coated magnetic nanoparticles for magnetic hyperthermia. J Biomed Mater Res A, 88, 1-11.

Kranenborg,M.H., Boerman,O.C., Oosterwijk-Wakka,J.C., de Weijert,M.C., Corstens,F.H., Oosterwijk,E., 1998. Two-step radio-immunotargeting of renal-cell carcinoma xenografts in nude mice with anti-renal-cell-carcinoma X anti-DTPA bispecific monoclonal antibodies. Int J Cancer, 75, 74-80.

Kwon,I.K., Lee,S.C., Han,B., Park,K., 2012. Analysis on the current status of targeted drug delivery to tumors. J Control Release, 164, 108-114.

Lammers,T., Kiessling,F., Hennink,W.E., Storm,G., 2010. Nanotheranostics and image-guided drug delivery: current concepts and future directions. Mol Pharm, 7, 1899-1912.

Laurent,S., Mahmoudi,M., 2011. Superparamagnetic iron oxide nanoparticles: promises for diagnosis and treatment of cancer. Int J Mol Epidemiol Genet, 2, 367-390.

Lin,R.Y., Dayananda,K., Chen,T.J., Chen,C.Y., Liu,G.C., Lin,K.L., Wang,Y.M., 2012. Targeted RGD nanoparticles for highly sensitive in vivo integrin receptor imaging. Contrast Media Mol Imaging, 7, 7-18.

Ling,Y., Wei,K., Luo,Y., Gao,X., Zhong,S., 2011. Dual docetaxel/superparamagnetic iron oxide loaded nanoparticles for both targeting magnetic resonance imaging and cancer therapy. Biomaterials, 32, 7139-7150.

Liu,Y., Yang,Y., Zhang,C., 2013. A concise review of magnetic resonance molecular imaging of tumor angiogenesis by targeting integrin alphavbeta3 with magnetic probes. Int J Nanomedicine, 8, 1083-1093.

Lu,J., Ma,S., Sun,J., Xia,C., Liu,C., Wang,Z., Zhao,X., Gao,F., Gong,Q., Song,B., Shuai,X., Ai,H., Gu,Z., 2009. Manganese ferrite nanoparticle micellar nanocomposites as MRI contrast agent for liver imaging. Biomaterials, 30, 2919-2928.

Lubbe,A.S., Bergemann,C., Huhnt,W., Fricke,T., Riess,H., Brock,J.W., Huhn,D., 1996. Preclinical experiences with magnetic drug targeting: tolerance and efficacy. Cancer Res, 56, 4694-4701.

Lyons,J.A., Sheahan,B.J., Galbraith,S.E., Mehra,R., Atkins,G.J., Fleeton,M.N., 2007. Inhibition of angiogenesis by a Semliki Forest virus vector expressing VEGFR-2 reduces tumour growth and metastasis in mice. Gene Ther, 14, 503-513.

Maeda,H., Wu,J., Sawa,T., Matsumura,Y., Hori,K., 2000. Tumor vascular permeability and the EPR effect in macromolecular therapeutics: a review. J Control Release, 65, 271-284.

Melancon,M.P., Stafford,R.J., Li,C., 2012. Challenges to effective cancer nanotheranostics. J Control Release, 164, 177-182.

Mitra,A., Nan,A., Ghandehari,H., McNeill,E., Mulholland,J., Line,B.R., 2004. Technetium-99m-Labeled N-(2-hydroxypropyl) methacrylamide copolymers: synthesis, characterization, and in vivo biodistribution. Pharm Res, 21, 1153-1159.

Murphy,E.A., Majeti,B.K., Barnes,L.A., Makale,M., Weis,S.M., Lutu-Fuga,K., Wrasidlo,W., Cheresh,D.A., 2008. Nanoparticle-mediated drug delivery to tumor vasculature suppresses metastasis. Proc Natl Acad Sci U S A, 105, 9343-9348.

Oakes,J.M., Breen,E.C., Scadeng,M., Tchantchou,G.S., Darquenne,C., 2014. MRI-based measurements of aerosol deposition in the lung of healthy and elastase-treated rats. J Appl Physiol (1985).

Petros,R.A., DeSimone,J.M., 2010. Strategies in the design of nanoparticles for therapeutic applications. Nat Rev Drug Discov, 9, 615-627.

Pourcelle,V., Freichels,H., Stoffelbach,F., Auzely-Velty,R., Jerome,C., Marchand-Brynaert,J., 2009. Light induced functionalization of PCL-PEG block copolymers for the covalent immobilization of biomolecules. Biomacromolecules, 10, 966-974.

Prokop,A., Davidson,J.M., 2008. Nanovehicular intracellular delivery systems. J Pharm Sci, 97, 3518-3590.

Radermacher,K.A., Beghein,N., Boutry,S., Laurent,S., Vander Elst L., Muller,R.N., Jordan,B.F., Gallez,B., 2009. In vivo detection of inflammation using pegylated iron oxide particles targeted at E-selectin: a multimodal approach using MR imaging and EPR spectroscopy. Invest Radiol, 44, 398-404.

Radermacher,K.A., Magat,J., Bouzin,C., Laurent,S., Dresselaers,T., Himmelreich,U., Boutry,S., Mahieu,I., Vander Elst L., Feron,O., Muller,R.N., Jordan,B.F., Gallez,B., 2012. Multimodal assessment of early tumor response to chemotherapy: comparison between diffusion-weighted MRI, 1H-MR spectroscopy of choline and USPIO particles targeted at cell death. NMR Biomed, 25, 514-522.

Rizzo,L.Y., Theek,B., Storm,G., Kiessling,F., Lammers,T., 2013. Recent progress in nanomedicine: therapeutic, diagnostic and theranostic applications. Curr Opin Biotechnol, 24, 1159-1166.

Schleich,N., Sibret,P., Danhier,P., Ucakar,B., Laurent,S., Muller,R.N., Jerome,C., Gallez,B., Preat,V., Danhier,F., 2013. Dual anticancer drug/superparamagnetic iron oxide-loaded PLGA-based nanoparticles for cancer therapy and magnetic resonance imaging. Int J Pharm, 447, 94-101.

Son,H.N., Nam,J.O., Kim,S., Kim,I.S., 2013. Multiple FAS1 domains and the RGD motif of TGFBI act cooperatively to bind alphavbeta3 integrin, leading to anti-angiogenic and anti-tumor effects. Biochim Biophys Acta, 1833, 2378-2388.

Stromhaug,P.E., Berg,T.O., Gjoen,T., Seglen,P.O., 1997. Differences between fluid-phase endocytosis (pinocytosis) and receptor-mediated endocytosis in isolated rat hepatocytes. Eur J Cell Biol, 73, 28-39.

Talelli,M., Rijcken,C.J., Lammers,T., Seevinck,P.R., Storm,G., van Nostrum,C.F., Hennink,W.E., 2009. Superparamagnetic iron oxide nanoparticles encapsulated in biodegradable thermosensitive polymeric micelles: toward a targeted nanomedicine suitable for image-guided drug delivery. Langmuir, 25, 2060-2067.

Taurin,S., Nehoff,H., Greish,K., 2012. Anticancer nanomedicine and tumor vascular permeability; Where is the missing link? J Control Release, 164, 265-275.

Wang,M., Thanou,M., 2010. Targeting nanoparticles to cancer. Pharmacol Res, 62, 90-99.

Xie,J., Lee,S., Chen,X., 2010. Nanoparticle-based theranostic agents. Adv Drug Deliv Rev, 62, 1064-1079.

Yang,H.W., Hua,M.Y., Liu,H.L., Tsai,R.Y., Pang,S.T., Hsu,P.H., Tang,H.J., Yen,T.C., Chuang,C.K., 2012. An epirubicin-conjugated nanocarrier with MRI function to overcome lethal multidrug-resistant bladder cancer. Biomaterials, 33, 3919-3930.

Yang,Y., Yu,K., Zhang,H., Dai,J., Deng,Z., 2014. In vitro assessment of the dual-targeting behavior of a peptide-based magnetic resonance imaging contrast agent. Int J Mol Med, 33, 215-220.

Zhang,F., Huang,X., Zhu,L., Guo,N., Niu,G., Swierczewska,M., Lee,S., Xu,H., Wang,A.Y., Mohamedali,K.A., Rosenblum,M.G., Lu,G., Chen,X., 2012. Noninvasive monitoring of orthotopic glioblastoma therapy response using RGD-conjugated iron oxide nanoparticles. Biomaterials, 33, 5414-5422.

CHAPTER V.

DISCUSSION AND PERSPECTIVES

TABLE OF CONTENTS

I. PRINCIPAL FINDINGS OF THE STUDIES

The main objectives of this thesis were (i) to develop PLGA-based nanoparticles as multifunctional entities by co-encapsulation of an anti-cancer drug (PTX) and a contrast agent (SPIO) for both anti-cancer therapy and magnetic resonance imaging; (ii) to compare four targeting strategies of these multifunctional nanoparticles in terms of anti-tumor efficacy, biodistribution and MRI contrast enhancement. The four targeting strategies were passive targeting (PT), active $\alpha_v\beta_3$ integrin targeting by grafting RGD (RGD), magnetic targeting (MT) and the combination of the two latest (RGD+MT).

In this thesis we prepared and characterized multifunctionnal PLGA-based nanoparticles loaded with SPIO along with an anti-cancer drug (PTX or DOX). One part of these particles was grafted with RGD to allow active targeting. Table 1 summarizes the major physico-chemical characteristics of the developed nanoparticles as well as the efficacy of the targeting strategy used in terms of tumor accumulation, *in vivo* anticancer efficacy and local disturbance induced by SPIO in MRI (measured by T_2 RSD of the tumor region).

Nanoparticles presented a spherical morphology and a size of 240 nm. Relaxometry studies and phantom MRI demonstrated their efficacy as T_2 contrast agent. Significant cellular uptake by CT26 cells of nanoparticles was shown by Prussian blue staining and fluorescent microscopy for non-grafted nanoparticles. While SPIO did not show any toxicity in CT-26 cells, PTX-loaded nanoparticles had a cytotoxic activity. PTX-loaded nanoparticle (5 mg/kg) with or without co-encapulated SPIO induced *in vivo* a regrowth delay of CT26 tumors. This regrowth delay was even better for RGD grafted and magnetic targeted nanoparticles. The best in vivo regrowth delay was obtained for RGD+MT-treated mice. Electron Spin Resonance spectroscopy and Magnetic Resonance Imaging (MRI) were used to both quantify and visualize the accumulation of theranostic nanoparticles into the tumors. We demonstrated that, compared to untargeted or single targeted nanoparticles, the combination of both active strategy and magnetic guidance drastically enhanced (i) nanoparticle accumulation into the tumor tissue (ii) contrast in MRI (diagnosis purpose). Double targeting of nanoparticles to tumors by different mechanisms could be a promising translational approach for the management of therapeutic treatment and personalized therapy.

Table 1. Major physico-chemical characteristics of the developed nanoparticles and efficacy of each targeting strategy in terms of tumor accumulation, in vivo anticancer efficacy and local disturbance induced by SPIO in MRI (measured by T_2 RSD of the tumor region).

	Passive targeting	**Magnetic targeting**	**Active targeting**	**Active + Magnetic targeting**
Size	243 ± 9.9 nm		245 ± 1.2 nm	
Zeta potential	-0.02 ± 0.01 mV		-0.42 ± 0.6 mV	
PTX loading	1.84 ± 0.4 mg/100 mg of polymer		1.85 ± 0.2 mg/100 mg of polymer	
SPIO loading	10.4 ± 1.9 mg/100 mg of polymer		10.1 ± 0.6 mg/100 mg of polymer	
R_2 20MHz	127 $mM^{-1}s^{-1}$		145 $mM^{-1}s^{-1}$	
Msat	15.1 ± 0.1 Am^2/kg		14.1 ± 0.1 Am^2/kg	
Anticancer efficacy (MST)	13 days	15 days	15 days	21 days
Biodistribution (% of the i.d. in tumor)	0.13 %	0.74 %	0.35 %	1.12 %
MRI (T2W image + measured mean RSD)	 0.144	 3.39	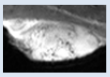 0.33	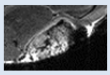 4.44

Abbreviations: i.d. = injected dose, Msat = saturation magnetization, MST = mean survival time, RSD = relative standard deviation, T2W = T_2-weigthed

II. OPEN QUESTIONS AND PERSPECTIVES

Considering all the results presented in this thesis, there are still remaining numerous questions to be answered and point to be discussed. Some points and questions are discussed below based on the literature, on the results obtained and on my personal opinion. An opening on potential perspectives is discussed based on these questions.

II.1. WAS THE CT-26 TUMOR MODEL APPROPRIATE?

All experiments of the thesis were performed on CT26-bearing BALB/c mice. CT-26 cell line is a syngenic murine colon adenocarcinoma cell line induced in BALB/c mice by N-nitroso-N-methylurethane [Chen et al., 2002]. This tumor model was chosen because of its sensibility to paclitaxel [Yang et al., 2013] and its vasculature appropriate for the EPR effect [Lyons et al., 2007]. Moreover, the tumor growing rate of this cell line was relatively reproducible. The main advantages of this model in the studies conducted in this thesis were: (i) the easy-to-manipulate characteristic of this sub-cutaneous tumor allowing simple tumor volume measurements and (ii) the superficial location of the tumor allowed an effective and easy magnetic targeting as well as an easy localization in MR images. Although this ectopic animal model was convenient for these proof-of-concept studies, this tumor model presents some limitations. Data obtained from such a model may not necessarily represent the actual orthotopic tissue microenvironments, which is critical for proper development [Chen et al., 2002]. Indeed, tumor vasculature has been shown to develop to a lesser extent in subcutaneous tumor model than in orthotopic model showing more vessels in the periphery of the tissue [Borgstrom et al., 2013].

In a view of a translational approach and to further investigate the relevance of our findings, an orthotopic model should be used. For instance, the murine melanoma B16-F10 could be appropriate [Thomas et al., 2014]. Given its superficial localization, it should be a good choice for magnetic targeting application. Moreover, this tumor model has been shown to express $\alpha_v\beta_3$ [Boles et al., 2010]. Testing our formulations in this model to confirm our results could be a first step.

In a second step, another interesting application of an orthotopic model could be studying the efficacy of magnetic targeting in tracting nanoparticles to a more deeply situated tumor. For instance, we could test our formulations in an orthotopically implanted U87MG glioma

model. Indeed, this model has been shown to be well vascularized and to express $\alpha_v\beta_3$ [Wegscheid et al., 2014]. Moreover, the location of the tumor although more deeply situated than in the skin is still not too deep and could be potentially suitable for magnetic targeting. Furthermore, since effectiveness of the currently available treatment is very limited due to the development of resistance mechanisms by tumor cells [Fan et al., 2013; St-Coeur et al., 2013], personalized therapy could be of great interest in this cancer type to allow early identification of treatment-resistant patients. Finally, since glioblastoma is infiltrative, complete resection is virtually impossible and relapse almost inevitable [Brandes et al., 2008]. Therefore, using RGD-grafted multifunctional nanoparticles could be interesting to visualize and preferentially entered the remaining unremoved tumor cells. However, in order to overcome the BBB penetration issue, intracranial administration based on the convection enhanced delivery method should be used to administer the treatment directly into the peritumoral brain tissue [St-Coeur et al., 2013].

II.2. IS SPIO A GOOD CONTRAST AGENT FOR MRI?

Magnetic resonance imaging (MRI) is a clinical widely used non-invasive imaging technique, presenting a high spatial resolution, which is suitable for cancer detection and therapeutic response assessment [Brindle, 2008; Liu et al., 2013]. Imaging technique based on magnetic resonance spectroscopy such as MRI provides ideal imaging modalities. Indeed, this technique responds to a series of criteria needed for such aim including (i) providing high-resolution morphological images, (ii) offering functional information in regard with anatomy, (iii) avoiding the use of ionizing radiation and (iv) being relatively easy to perform [Krishna et al., 2001]. However, its major limitation consists of a relatively low sensitivity. Superparamagnetic iron oxides (SPIO) as excellent MRI contrast agent address this limitation. Indeed, SPIO can produce predominant T_2 relaxation effect with excellent sensitivity and biocompatibility when compared to other MRI agents such as chelates of paramagnetic ion (Gd^{3+}-DTPA). This results in a strong signal reduction on T_2-weighted images [Ittrich et al., 2013; Reddy et al., 2012]. Hence, SPIO are considered as negative contrast agents. Moreover, given their reactivity to an externally applied magnetic field, SPIO are among the most suitable candidate to achieve magnetic targeting abilities by using an external magnet [Laurent et al., 2011].

However, when SPIO concentration is very high, the T_2 decreases so fast that the software failed to give a proper T_2 curve fitting resulting in a non-exponential relationship and thus, an

incorrect T_2 value. This phenomenon was observed in the results obtained for magnetic targeting and the combination of magnetic and active targeting in the *in vivo* MRI experiment in this thesis. Therefore, we measured a relative standard deviation of these T_2 values in the region of interest. RSD is a measure of tumor heterogeneity after the SPIO injection. This method is commonly used in MRI when T_2 signal is too heterogeneous [Oakes et al., 2014]. Nevertheless, in this thesis, SPIO injected dose was determined considering those found in the literature and the minimal concentration detected by MRI (using the *in vitro* MRI phantom study). Thus, further studies should investigate the proper SPIO dose to be injected in order to optimize (i) the decrease in T_2 relaxation of the tumor tissue and (ii) the maximum concentration threshold above which MRI is not discriminative anymore. This could be assessed by *in vitro* MRI phantom studies by increasing SPIO concentration in the phantom samples.

Furthermore, a major concern in using SPIO is their relatively unpopularity among the radiologists. Although SPIOs and USPIOs have been approved by the FDA and EMEA for use in the past, various commercial form including ferumoxides (Endorem®/Feridex®) have been withdrawn from the market after several years of commercialization due to their limited use by radiologists [Corot et al., 2013]. Indeed, radiologists blame the SPIO to be negative contrast agents and, consequently, to produce image contrasts more difficult to interprete than a positive contrast agent resulting in hyperintense signal in MRI. This pitfall contradicts SPIO as a good choice for tumor diagnosis.

However, in my opinion, since this developed theranostic system does not intend to diagnose the presence of a nascent tumor but visualize nanoparticle accumulation in tumor when its location is already precisely known, such SPIO utilization could be accountable. Indeed, since many tumors are visualized hyperintense using MRI, a negative contrast agent could be indicated to characterize tumor accumulation. Nevertheless, effective elimination of SPIO should be investigated to ensure proper diagnosis if MRI is required for another further medical examination (given the tendency of SPIO to accumulate in various tissues).

Pharmacokinetic studies should be performed to determine the half-life of our multifunctional nanoparticles as well as the time needed for complete clearance from the body. Those informations could be relevant since a compromise between long circulation time to reach sufficient tumor accumulation and efficient elimination of SPIO to avoid signal perturbations if another MRI is required. Therefore, blood samples following administration of a finite dose

of multifunctional nanoparticles should be taken over time and SPIO concentration should be measured.

II.3. WHAT ABOUT THE SPIO ACCUMULATION-MEDIATED TOXICITY?

SPIO-based multifunctional nanoparticles have been shown to be massively taken up in the liver (30 – 35 % of the injected dose). This phenomenon is well known and extensively described in the literature [Bertrand et al., 2012]. Zhang *et al*. reported an accumulation of RGD-grafted magnetite PLGA-based nanoclusters of 35% of the injected dose in the liver [Zhang et al., 2012]. Incidentally, SPIO-loaded nanoparticles are usually used as contrast agent for liver imaging [Lu et al., 2009]. This particular point raises the question of the toxicity of such accumulation. Analysis of the literature shows conflicting results on the toxicity of SPIO. Some studies have shown that SPIO could generate a production of ROS in liver cells that could lead to toxicity [Bae et al., 2011]. However, this toxicity seems to depend on the particle shape, size, charge and dose. Moreover, in normal circumstances, the injected iron is expected to be sequestered by Kupffer cells, metabolized and regulated by normal physiological iron homeostatic mechanisms [Laurent et al., 2014]. This SPIO sequestration seems to protect liver cells from apoptosis since only free iron oxides proved to be toxic. Indeed, Jain *et al.* showed that the intra-venous administration of oleic acid coated SPIO (10 mg Fe/kg) did not result in any notable alteration of the liver functionality [Jain et al., 2008]. Nevertheless, repeated dosing of SPIO in short intervals would not be a desirable option in imaging and drug delivery since it could lead to a surpassed transferrin iron-binding capacity and, therefore, to high free iron concentration [Laurent et al., 2014; Reddy et al., 2012]. Hence, in a view of a translational approach, further toxicity assessment should be performed. In a cellular point of view, at high concentration (>600µg Fe/ml) the ferric ions released from SPIO into the acidic endolysosomal compartments have been shown to have a negative influence on cell homeostasis with consequences like affected actin cytosqueleton, diminished cell proliferation and ROS production. However, it is yet unclear what the precise effect of these factors is on cell viability as all cells have defence mechanisms, which allows them to deal with certain levels of oxidative stress [Soenen et al., 2011]. This point highlights again the importance of toxicity assessments in evaluating nanoparticle efficiency as at non-toxic concentrations of IONPs.

In a first step, *in vitro* toxicity should be assessed on hepatocytes to investigate the type of cell death mediated by SPIO and the influence of PLGA encapsulation. Apoptosis, necrosis, autophagy as well as ROS production should be assessed using adequate assays.
In a second step, *in vivo* test should be performed. Apoptosis in liver after injection of SPIO-loaded nanoparticles should be investigated by a TUNEL assay on histological sections. However, *in vivo* evaluation of the toxicity should be performed as well to investigate ROS production. For instance, evaluation of the lipid hydroperoxide level in serum samples 24h after injection should provide interesting data over the oxidative stress [Jain et al., 2008].

II.4. IS THERE A REAL INTEREST TO COMBINE ACTIVE AND MAGNETIC TARGETING?

Active targeting presents an important issue constituting the most limitations: since targeted nanomedicines have no mean of self-propulsion, reaching the target site and thereby, accumulating in the tumor tissue only relies on EPR-mediated extravasation and all the pitfalls related to it [Kwon et al., 2012; Lammers et al., 2008]. In this context, the only advantage in functionalizing nanoparticles relies in the higher chance of internalization. Another important point that needs to be considered is the fact that despite the rather easy in vitro demonstration of receptor-mediated targeting, in vivo efficacy is more difficult to show. Moreover, even if a better internalization is demonstrated in vivo, the entire amount of drug localized in the tumor is often still lower than 0.01% of the injected dose [Jain and Stylianopoulos, 2010]. Indeed, before reaching their specific receptor expressed on tumor cells, targeted-nanomedicine face different challenges including escaping target receptor present on normal tissue, heterogeneity in receptor expression by tumor cells or according to the disease stage and a possible receptor saturation limiting targeting efficiency [Duncan and Gaspar, 2011].

Both targeted and non-targeted systems arrive at the tumor via the EPR effect. Magnetic targeting promotes the accumulation of nanoparticles near the magnet and, thus, near tumor cells. However, to date, studies showed that this strategy did not promote nanoparticles entrance into the cells [Bae et al., 2011; Kocbek et al., 2013]. Mechanisms of tumor internalization for both non-targeted and magnetically-targeted nanoparticles mostly involve macropinocytosis [Kocbek et al., 2013; Kumari et al., 2011]. On the contrary, RGD-targeted nanoparticles are internalized by both tumor cells and endothelial cells (which are expressing $\alpha_v\beta_3$integrin) via receptor-mediated endocytosis, as abovementioned.

Consequently, nanoparticles intratumoral distribution could shift from the extracellular compartment to the tumor cell intracellular compartment [Prokop et al., 2008]. Therefore, combining active targeting (RGD) and magnetic targeting (MT) could enhance anti-tumor efficacy by both an enhanced accumulation (by MT) and an enhanced entrance (via $\alpha_v\beta_3$ receptor-mediated endocytosis by RGD targeting).

Moreover, for non-grafted nanoparticles only the EPR effect can explain the accumulation of drug-loaded nanocarriers into the tumor. By contrast, RGD-targeted nanoparticles exert a double active targeting of both endothelial and cancer cells. Indeed, $\alpha_v\beta_3$integrin is expressed on endothelial cells of neoangiogenic vessels, allowing the binding of circulating RGD-nanoparticles resulting in subsequently tumor cells death by lack of oxygen and nutrients, and on tumor cells [Danhier et al., 2010; Folkman, 1971]. This putative anti-angiogenic effect of the active targeting of drug-loaded RGD-nanoparticles may constitute an advantage to the RGD-nanoparticles treatment since this effect does not rely on the penetration of nanoparticles into tumor interstitium which is complicated by the high interstitial fluid pressure [Bouzin et al., 2007; Jain, 1987]. Figure 2 represents the putative complementarity between these two targeting strategies.

Finally, analysis of the literature shows that most studies having demonstrated *in vivo* efficacy of their theranostics in both the therapeutic and the imaging approach use combined targeting strategies. Indeed, researchers usually face the issue of poor tumor accumulation leading to difficulties in terms of *in vivo* anti-tumor efficacy or *in vivo* imaging efficacy. Indeed, percentage of the injected dose reaching the tumor is rarely above 1 %. Moreover, accumulation in healthy tissue such as liver and spleen is often larger than 35 %. In this context, there is a rationale to combine different strategies in a same nanomedicine to overcome the limitations of each one taken separately, making those multi-modal nanotheranostics. This strategy has gained much interest among the scientist during the past few years. Promising results have been reported. In this thesis, we demonstrated using ESR spectroscopy a 3- and 2-fold increase in tumor accumulation using a combination of magnetic and active targeting compared to active targeting and magnetic targeting, respectively, when used separately [Schleich et al., 2014]. Interesting results were also obtained for the combination of PDT and active targeting [Reddy et al., 2006]. This combination allowed to drastically improve the survival rate of 9L glioma-bearing rats when compared to PDT when used separately. Similarly, the interest of combined strategies was also confirmed in a study

conducted by Fan *et al.* in which focused US and magnetic targeting displayed drastic contrast enhancement in susceptibility weighted images compared to focused ultrasound as a unique targeting strategy [Fan et al., 2013].

In my opinion and considering the results obtained in this thesis and the literature, there is a real interest in combining magnetic targeting (mostly useful to accumulate nanotheranostics into tumor tissue) and RGD-mediated targeting strategy for enhancing cell internalization and anti-angiogenic effect. However, further studies could be interesting to perform in order to investigate this complementary relationship between both strategies.

To investigate the complementarity of active and magnetic targeting, immunohistochemistry should be performed on frozen tumor sections. Endothelium could be labeled using a CD-31 monoclonal antibody and a secondary Alexa-fluor 488-labeled antibody. FITC-grafted PLGA could be used to label nanoparticles [Danhier et al., 2012]. Finally, nuclear labeling should be performed using DAPI. Sections could be, thereafter analyzed by a fluorescent microscope to assess if the combining strategy allows improving cellular internalization when compared to magnetic targeting alone.
Another interesting study should investigate whether the combination of both targeting strategies could overcome the absence of EPR effect. Therefore, it could be interesting to assess their efficacy in a tumor model known to exhibit practically no EPR effect such as metastatic liver, pancreatic and prostate cancer [Maeda, 2012]. For instance an orthotopic model of DU 145 MN1 prostate cancer cell line could be used [Korbel et al., 2014].

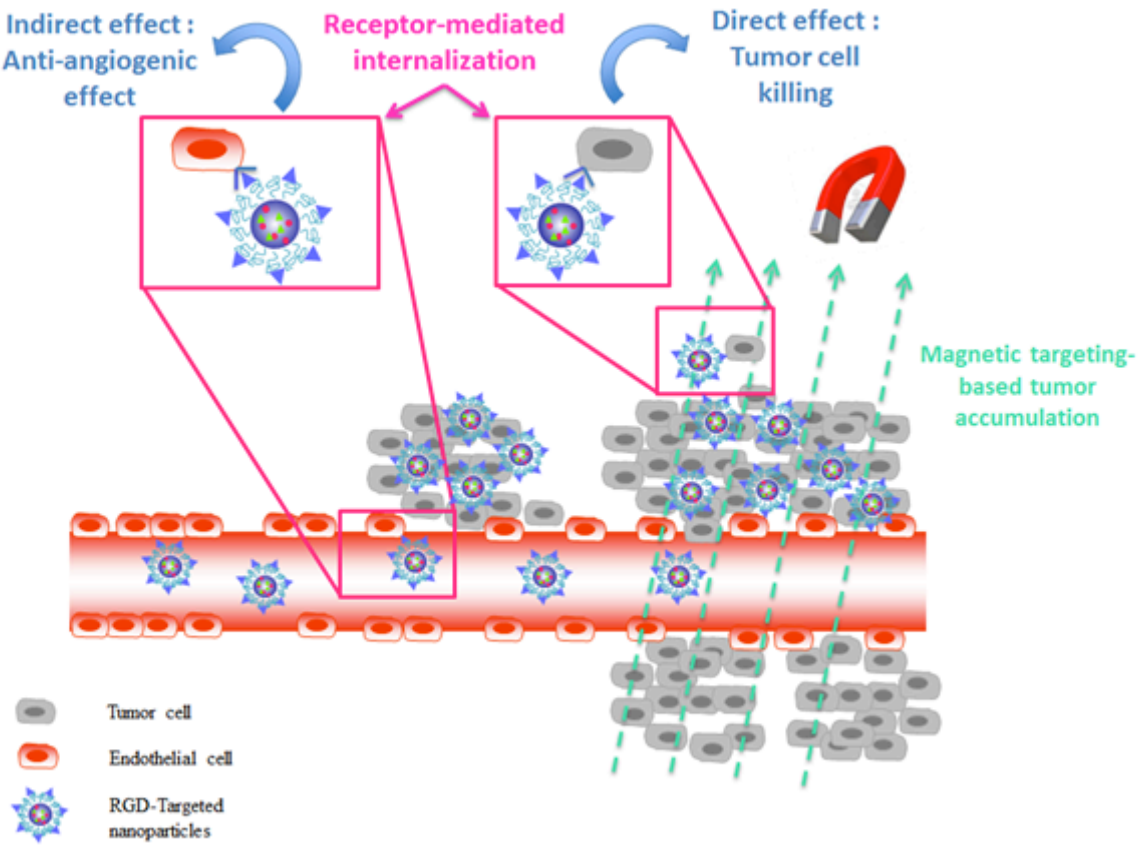

Figure 2. Schematic representation of the complementarity between magnetic and active targeting. Normally, RGD-grafted nanoparticles only accumulate in tumor interstitium via EPR effect. Magnetic targeting has the potential to improve nanoparticles accumulation by magnetic force attraction. Once RGD sequence is recognized by either tumor or endothelial cells, internalization occurs leading to an anti-tumor effect mediated by both a direct and an indirect effect, respectively.

II.5. ARE THESE MULTIFUNCTIONAL NANOPARTICLES COMBINING MAGNETIC AND ACTIVE TARGETING SUITABLE FOR CLINICAL TRANSLATION?

Magnetic targeting into clinic

Lübbe *et al.* were the pioneers in using an external magnetic field to guide a treatment in patients [Lubbe et al., 1996]. Later, numerous studies used this method with magnetic field strength ranging from 0.4 to 4 T [Alexiou et al., 2000; Arias et al., 2011; Chertok et al., 2008; Kim et al., 2009]. For superficial tumors, this strategy can be easily transposable into clinic by placing the permanent magnet outside of the body at the surface of the tumor. However, the success of this targeting strategy is limited by inadequate magnetic gradients, thus, by the

distance between the magnets and the target site. Indeed, to allow magnetic targeting, magnetic forces should exceed the linear blood flow rates in arteries (10 cm s−1) or capillaries (0.05 cm s−1). Since magnetic gradient decreases as a function of the distance with the magnetic source, magnetic targeting should be more effective in regions closer to the magnets limiting its application to superficial tumors [Alexiou et al., 2000; Laurent et al., 2011]. Nevertheless, many strategies to overcome this problem are under investigation. In most cases, the magnetic field gradient is generated by a strong permanent magnet, such as Nd–Fe–B. This type of magnet is known to enhance the depth of magnetic field by up to 10 - 15 cm [Laurent et al., 2014]. However, such a distance could not allow magnetic targeting of tumor localized deeper in the body. For such tumor, it seems that the particles could be focused to the tumor region by using rotating magnetic fields [Alexiou et al., 2000; Huang et al., 2010]. Another proposed strategy is to improve the quality of the source (e.g. using a MRI system magnet as a source [Riegler et al., 2010]). Finally, another solution could involve magnetic implants near the tumor region [Polyak et al., 2008].

Since the magnetism is size-dependent, particles size can also influence the attraction by the magnet. Indeed, small particles are less susceptible to be attracted than large particles [Alexiou et al., 2000]. Magnetic targeting efficacy is also dependent on the saturation magnetization, which refers to the maximum magnetization possible. Generally, nanoparticles with higher saturation magnetization are preferred because they provide higher sensitivity and efficiency [Colombo et al., 2012]. Our particles showed a relatively low saturation magnetization (Ms) compared to free SPIO described in the literature [Larumbe et al., 2012; Shamim et al., 2007]. Indeed, while the use of a polymer coating around SPIO has been shown to increase relaxivities (R_2) or reduce transverse relaxation times (T_2) making, thus, more effective contrast agent, at the same time, it is associated with a change in the anisotropy constant leading to a further reduction in magnetization [Kolhatkar et al., 2013]. This phenomenon constitutes another limitation to magnetic targeting. This limitation could be reduced by further investigating the modulation of nanoparticles physical parameters (size, shape, composition, and shell-core architecture) to optimize the properties of these magnetic nanoparticles for improved magnetic targeting applications.

EPR effect into clinic

Most of the currently developed nanoparticular systems rely on this passive targeting via the EPR effect. Nevertheless, this strategy has recently known disenchantment. Since passive

targeting is highly dependent on tumor vascularization and given this vascularization is highly heterogeneous depending on the patient (inter-variability) and depending on the disease stage or even on the tumor areas (intra-variability), EPR effect is a highly heterogeneous phenomenon. Moreover, EPR effect has shown to be much more important in animal models compared to human. This is due to the much faster growth of animal tumors compared to patients. This speed increase results in more leaky vasculature and consequently in larger EPR effect [Lammers et al., 2012]. Secondly, due to the high interstitial pressure and dense extracellular matrix, penetration of the carrier is quite limited [Nichols et al., 2014]. Interestingly, some pharmacological treatment interfering with extracellular matrix (matrix degrading enzymes, inhibitors of fibrosis) or enhancing extravasation (inflammatory mediators such as TNF-α) have been shown to promote tumor penetration when co-administered [Kumagai et al., 2009; McKee et al., 2006].

Formulation challenges

The vast majority of multifunctional nanomedicine systems described in literature is suffering from high cost of manufacture and material as well as complexity or limitations of production process and analytical characterization [Peer et al., 2007]. Indeed, these kinds of nanoplatform combining different components are difficult to synthesize and scale-up by the pharmaceutical industry since their production involves many different synthetic and purification steps decreasing their commercial attractiveness [Lammers et al., 2012]. For nanocarrier-based theranostics, only few excipients evaluated as matrix materials or stabilizing agents in the literature, have a solid track record of preclinical and clinical experience to overcome the regulatory obstacles that assure quality and safety of new nanomedicines. In this thesis, keeping regulatory sciences in mind, we have used PLGA, a FDA approved polymer for parenteral drug delivery and SPIO for their FDA approval as MRI contrast agents in a view of a translational approach.

Moreover, since pharmacokinetics and toxicology of nanocarriers are strongly dependent on the physico-chemical properties, minor changes in manufacture may have a major impact on their behavior in vivo. As a consequence, nanocarriers-manufacturing process requires precise control to limit batch-to-batch variability [Wacker, 2013].

Furthermore, a major challenge with theranostic therapies arises from the opposing time line and concentrations of imaging and therapeutic agents. Indeed, although the main goal in

imaging is to deliver the smallest amount of imaging agent for a short time to ensure a strong signal-to-noise ratio, the amount of drug desired to induce a strong anti-cancer effect must be the highest as possible (maximum tolerated dose) [Svenson, 2013]. Consequently, there is a formulation challenge to address in order to ensure a maximum drug delivery and a minimum imaging agent. This challenge could be more easily addressed by nanocarrier-based theranostic compared to SPIO-conjugate due to the encapsulation of various amount of drug and imaging agent that nanocarriers offer. Moreover, this issue could be easily solved by maintaining the original two-step process in which the same nanocarrier is used to encapsulate at first the imaging agent in order to visualize biodistribution and tumor accumulation and, thereafter, the anti-cancer drug to treat the patient [Svenson, 2013].

Finally, another important limitation to clinical translation is the toxicological concern of using organic solvent such as dichloromethane (DCM) in the formulation process. DCM is part of the Class 2 solvents in the FDA guidance for industry classification on residual solvents. In this guidance, solvents in Class 2 (Table 2) should be limited in pharmaceutical products because of their inherent toxicity [http://www.fda.gov]. Indeed, concerns relating to the carcinogenic potential of dichloromethane arose in the 1980s and since, have been subjected to many toxicology studies. This carcinogenicity has been attributed to the glutathione-S transferase-theta 1 (GST-T1)-catalyzed metabolic pathway of DCM resulting in the production of two highly reactive intermediates, formaldehyde and S-(chloromethyl)glutathione, and carbon dioxide [Cooper et al., 2011; Graves et al., 1994]. FDA's regulatory guidance gives for DCM a maximal residual concentration of 600 ppm [http://www.fda.gov]. Alternatives like using Class 3 solvents, which are considered as less toxic and of lower risk to human health could be used in the future perspectives. These include ethyl acetate, a solvent in which oleic acid-coated SPIO, paclitaxel, and our polymers are predicted to be solved based on chemical models (http://showme.physics.drexel.edu/onsc/models/multisolvent.php). However, this should be tested experimentally. Litterature shows examples where ethyl acetate has been used to formulate Poly(D,L-lactic acid) and PLGA nanoparticles using a similar emulsion/diffusion technique as used in this thesis [Sahana et al., 2008; Trimaille et al., 2003]. Further studies should investigate the use of this solvent to replace DCM in order to meet regulatory criteria.

All these limitations show the long way multifunctional nanoparticles combining active and magnetic targeting need to travel before reaching the market.

II.6. WHAT IS THE REAL INTEREST OF NANOTHERANOSTICS IN ANTI-CANCER THERAPIES?

Many publications claim that theranostics can be used for the simultaneous diagnosis and treatment. Actually, their suitability for real diagnosis is questionable. The diagnosis purpose of theranostics should not refer to the identification, the localization and/or the staging of tumors but to the pre-selection of patients, to the prediction of potential therapeutic responses, and/or to the longitudinal monitoring of treatment efficacy [Rizzo et al., 2013].

Solid tumors are known to be highly heterogeneous either depending on the cancer type, patient or even on the disease stage (inter-tumor heterogeneity). Moreover, different cell types can be found inside a solid tumor (intra-tumor heterogeneity). Furthermore, in response to any given therapy, solid tumors inevitably evolve, leading to strong difficulties in managing cancer therapy. Therefore, there is a critical need in developing *personalized therapy* [Blanco et al., 2009; Guthi et al., 2010].

At first, personalized therapy has been widely studied in the terms of genetic and genomic. The principle of this personalized medicine is based on *ex vivo* tumor molecular profiling or whole-genome profiling. Briefly, it relies on the evaluation of genetic sequences to confirm the expression of a biomarker. Thereafter, patients are selected for the treatment regarding this level of expression [Kalia, 2013; Tessari et al., 2013]. This method has been proved to be effective in assuring optimal efficacy and hence, is currently being used clinically in various cancer therapy [Lammers et al., 2012]. However, as the amount of information generated by an individual patient's tumor genomic profiling increases, it become more and more difficult for the clinicians to analyze, interpret, and act on this information [Van Allen et al., 2013]. In this context, nanotheranostics have emerged as high potential tools to make the personalized therapy easier. Indeed, visualizing and quantifying the overall level of target site accumulation is far easier than genome analysis.

A successful clinical application of this personalized therapy concept is the clinically approved Zevalin® (a radioimmunotherapeutic directed against CD-20) for the treatment of Rituximab-failed non-Hodgkins lymphoma. The therapeutic schedule involves the injection on day one of ^{111}Indium ibritumomab tiuxetan followed by whole-body planar gamma imaging (SPECT) obtained 48–72 h later in order to assess biodistribution. If the patients

present an appropriate biodistribution, they receive the active agent, ^{90}yttrium ibritumomab tiuxetan, on day 8 [Beaven et al., 2012]. However, to date, all the theranostics involved in clinical studies rely on the use of PET or SPECT agents and, hence on ionizing radiations.

In my point of view, this particular challenge of personalized therapy is the real interest of nanotheranostics. Indeed, such theranostic platforms allow the molecular diagnosis by imaging to assess the expression of cancer biomarker to guide target-specific therapy. Moreover, administration of such theranostic platform allows a non-invasive visualization of nanocarriers biodistribution and, consequently, evaluation of tumor accumulation and unintended accumulation in healthy tissue. Furthermore, it enables to assess the efficacy of the treatment at different stages of the therapy then using those results to intelligently modify the strategy for cancer treatment (real-time monitoring) [Guthi et al., 2010; Lammers et al., 2010]. The multifunctional $\alpha_v\beta_3$-targeted nanoparticles developed in this thesis showed promising results in terms of anti-tumor efficiency and imaging abilities when combined to magnetic targeting. In clinical management of cancer therapy, their imaging abilities could be useful to monitor the biodistribution of these multifunctional nanoparticles after injection to the patient in a first step. Thereafter, on the basis of this non-invasive imaging insight on target site, and possibly undesirable liver accumulation, it would be possible to evaluate a benefice/risk ratio and, if favorable, select the patient for the treatment. This particular application could be of great interest to limit the treatment of non-responding patients and patients at high risk of undesirable toxicity.

In this thesis, we have observed that there was a link between treatment response and tumor accumulation of the multifunctional nanoparticles assessed using MRI. This observation led to the hypothesis that MRI could be predictive of the treatment response. To confirm this hypothesis, we should image mice before treatment and measure tumor volume using T_2-weighted MRI (more precise compared to the caliper). Thereafter, treatment should be injected and re-imaged. This operation should be repeated every two days and tumor volume should be measured to monitor treatment response. This experiment could confirm our hypothesis and explore another application of theranostic (real-time monitoring of the treatment response). Moreover, determining the link between tumor vessel maturation and the preferential accumulation of targeted and untargeted nanoparticles could be interesting to design a time schedule of administration to both treat and image tumors. Therefore, we could

correlate the T_2 contrast due to the accumulation of SPIO-loaded RGD-nanoparticles imaged by MRI with the T_1 contrast obtained by DCE-MRI (at 11.7 T) after the injection of monogadolinium macrocyclic compound (Gd-DOTA) [Baudelet et al., 2006; Boles et al., 2010; Schmieder et al., 2008]. This technique has emerged as a non-invasive imaging technique of the tumor vasculature. By analyzing the kinetics of contrast-media uptake and wash-out, DCE-MRI provides information on perfusion and permeability and, consequently, vessel maturation [Baudelet et al., 2006].

III. REFERENCES

Alexiou,C., Arnold,W., Klein,R.J., Parak,F.G., Hulin,P., Bergemann,C., Erhardt,W., Wagenpfeil,S., Lubbe,A.S., 2000. Locoregional cancer treatment with magnetic drug targeting. Cancer Res, 60, 6641-6648.

Arias,J.L., Reddy,L.H., Othman,M., Gillet,B., Desmaele,D., Zouhiri,F., Dosio,F., Gref,R., Couvreur,P., 2011. Squalene based nanocomposites: a new platform for the design of multifunctional pharmaceutical theragnostics. ACS Nano, 5, 1513-1521.

Bae,J.E., Huh,M.I., Ryu,B.K., Do,J.Y., Jin,S.U., Moon,M.J., Jung,J.C., Chang,Y., Kim,E., Chi,S.G., Lee,G.H., Chae,K.S., 2011. The effect of static magnetic fields on the aggregation and cytotoxicity of magnetic nanoparticles. Biomaterials, 32, 9401-9414.

Baudelet,C., Cron,G.O., Gallez,B., 2006. Determination of the maturity and functionality of tumor vasculature by MRI: correlation between BOLD-MRI and DCE-MRI using P792 in experimental fibrosarcoma tumors. Magn Reson Med, 56, 1041-1049.

Beaven,A.W., Shea,T.C., Moore,D.T., Feldman,T., Ivanova,A., Ferraro,M., Ford,P., Smith,J., Goy,A., 2012. A phase I study evaluating ibritumomab tiuxetan (Zevalin(R)) in combination with bortezomib (Velcade(R)) in relapsed/refractory mantle cell and low grade B-cell non-Hodgkin lymphoma. Leuk Lymphoma, 53, 254-258.

Bertrand,N., Leroux,J.C., 2012. The journey of a drug-carrier in the body: an anatomo-physiological perspective. J Control Release, 161, 152-163.

Blanco,E., Kessinger,C.W., Sumer,B.D., Gao,J., 2009. Multifunctional micellar nanomedicine for cancer therapy. Exp Biol Med (Maywood), 234, 123-131.

Boles,K.S., Schmieder,A.H., Koch,A.W., Carano,R.A., Wu,Y., Caruthers,S.D., Tong,R.K., Stawicki,S., Hu,G., Scott,M.J., Zhang,H., Reynolds,B.A., Wickline,S.A., Lanza,G.M., 2010. MR angiogenesis imaging with Robo4- vs. alphaVbeta3-targeted nanoparticles in a B16/F10 mouse melanoma model. FASEB J, 24, 4262-4270.

Borgstrom,P., Oh,P., Czarny,M., Racine,B., Schnitzer,J.E., 2013. Co-implanting orthotopic tissue creates stroma microenvironment enhancing growth and angiogenesis of multiple tumors. F1000Res, 2, 129.

Bouzin,C., Feron,O., 2007. Targeting tumor stroma and exploiting mature tumor vasculature to improve anti-cancer drug delivery. Drug Resist Updat, 10, 109-120.

Brandes,A.A., Tosoni,A., Franceschi,E., Reni,M., Gatta,G., Vecht,C., 2008. Glioblastoma in adults. Crit Rev Oncol Hematol, 67, 139-152.

Brindle,K., 2008. New approaches for imaging tumour responses to treatment. Nat Rev Cancer, 8, 94-107.

Chen,Y., Chang,K.J., Hwang,L.H., Chen,C.N., Tseng,S.H., 2002. Establishment and characterization of a rectal cancer model in mice: application to cytokine gene therapy. Int J Colorectal Dis, 17, 388-395.

Chertok,B., Moffat,B.A., David,A.E., Yu,F., Bergemann,C., Ross,B.D., Yang,V.C., 2008. Iron oxide nanoparticles as a drug delivery vehicle for MRI monitored magnetic targeting of brain tumors. Biomaterials, 29, 487-496.

Colombo,M., Carregal-Romero,S., Casula,M.F., Gutierrez,L., Morales,M.P., Bohm,I.B., Heverhagen,J.T., Prosperi,D., Parak,W.J., 2012. Biological applications of magnetic nanoparticles. Chem Soc Rev, 41, 4306-4334.

Cooper,G.S., Scott,C.S., Bale,A.S., 2010. Insights from epidemiology into dichloromethane and cancer risk. Int J Environ Res Public Health, 8, 3380-98.

Corot,C., Warlin,D., 2013. Superparamagnetic iron oxide nanoparticles for MRI: contrast media pharmaceutical company R&D perspective. Wiley Interdiscip Rev Nanomed Nanobiotechnol, 5, 411-422.

Danhier,F., Feron,O., Preat,V., 2010. To exploit the tumor microenvironment: Passive and active tumor targeting of nanocarriers for anti-cancer drug delivery. J Control Release, 148, 135-146.

Danhier,F., Pourcelle,V., Marchand-Brynaert,J., Jerome,C., Feron,O., Preat,V., 2012. Targeting of tumor endothelium by RGD-grafted PLGA-nanoparticles. Methods Enzymol, 508, 157-175.

Duncan,R., Gaspar,R., 2011. Nanomedicine(s) under the microscope. Mol Pharm 8 (6), 2101–2141.

Fan,C.H., Liu,W.L., Cao,H., Wen,C., Chen,L., Jiang,G., 2013. O6-methylguanine DNA methyltransferase as a promising target for the treatment of temozolomide-resistant gliomas. Cell Death Dis, 4, e876.

Folkman,J., 1971. Tumor angiogenesis: therapeutic implications. N Engl J Med, 285, 1182-1186.

Graves,R.J., Callander,R.D., Green,T., 1994. The role of formaldehyde and S-chloromethylglutathione in the bacterial mutagenicity of methylene chloride. Mutat. Res, 320, 235–243.

Guthi,J.S., Yang,S.G., Huang,G., Li,S., Khemtong,C., Kessinger,C.W., Peyton,M., Minna,J.D., Brown,K.C., Gao,J., 2010. MRI-visible micellar nanomedicine for targeted drug delivery to lung cancer cells. Mol Pharm, 7, 32-40.

Huang,Z., Pei,N., Wang,Y., Xie,X., Sun,A., Shen,L., Zhang,S., Liu,X., Zou,Y., Qian,J., Ge,J., 2010. Deep magnetic capture of magnetically loaded cells for spatially targeted therapeutics. Biomaterials, 31, 2130-2140.

Ittrich,H., Peldschus,K., Raabe,N., Kaul,M., Adam,G., 2013. Superparamagnetic iron oxide nanoparticles in biomedicine: applications and developments in diagnostics and therapy. Rofo, 185, 1149-1166.

Jain,R.K., 1987. Transport of molecules in the tumor interstitium: a review. Cancer Res, 47, 3039-3051.

Jain,R.K., Stylianopoulos,T., 2010. Delivering nanomedicine to solid tumors, Nat Rev Clin Oncol, 7 (11), 653–664.

Jain,T.K., Reddy,M.K., Morales,M.A., Leslie-Pelecky,D.L., Labhasetwar,V., 2008. Biodistribution, clearance, and biocompatibility of iron oxide magnetic nanoparticles in rats. Mol Pharm, 5, 316-327.

Kalia,M., 2013. Personalized oncology: recent advances and future challenges. Metabolism, 62 Suppl 1, S11-S14.

Kim,D.H., Kim,K.N., Kim,K.M., Lee,Y.K., 2009. Targeting to carcinoma cells with chitosan- and starch-coated magnetic nanoparticles for magnetic hyperthermia. J Biomed Mater Res A, 88, 1-11.

Kocbek,P., Kralj,S., Kreft,M.E., Kristl,J., 2013. Targeting intracellular compartments by magnetic polymeric nanoparticles. Eur J Pharm Sci, 50, 130-138.

Kolhatkar,A.G., Jamison,A.C., Litvinov,D., Willson,R.C., Lee,T.R., 2013. Tuning the magnetic properties of nanoparticles. Int J Mol Sci, 14, 15977-16009.

Korbel,C., Jung,V., Kamradt,J., Stockle,M., Unteregger,G., Menger,M.D., Saar,M., 2014. High-Resolution Ultrasound Allows Percutaneous Initiation and Surveillance of Prostate Cancer in an Orthotopic Murine Model. Urol Int.

Krishna,M.C., Devasahayam,N., Cook,J.A., Subramanian,S., Kuppusamy,P., Mitchell,J.B., 2001. Electron paramagnetic resonance for small animal imaging applications. ILAR J, 42, 209-218.

Kumagai,M., Kano,M.R., Morishita,Y., Ota,M., Imai,Y., Nishiyama,N., Sekino,M., Ueno,S., Miyazono,K., Kataoka,K., 2009. Enhanced magnetic resonance imaging of experimental pancreatic tumor in vivo by block copolymer-coated magnetite nanoparticles with TGF-beta inhibitor. J Control Release, 140, 306-311.

Kumari,A., Yadav,S.K., 2011. Cellular interactions of therapeutically delivered nanoparticles. Expert Opin Drug Deliv, 8, 141-151.

Kwon,I.K., Lee,S.C., Han,B., Park,K., 2012. Analysis on the current status of targeted drug delivery to tumors. J Control Release, 164, 108-114.

Lammers,T., Hennink,W.E., Storm,G., 2008. Tumour-targeted nanomedicines: principles and practice. Br J Cancer, 99, 392-397.

Lammers,T., Kiessling,F., Hennink,W.E., Storm,G., 2010. Nanotheranostics and image-guided drug delivery: current concepts and future directions. Mol Pharm, 7, 1899-1912.

Lammers,T., Kiessling,F., Hennink,W.E., Storm,G., 2012. Drug targeting to tumors: principles, pitfalls and (pre-) clinical progress. J Control Release, 161, 175-187.

Larumbe,S., Gomez-Polo,C., Perez-Landazabal,J.I., Pastor,J.M., 2012. Effect of a SiO2 coating on the magnetic properties of Fe3O4 nanoparticles. J Phys Condens Matter, 24, 266007.

Laurent,S., Mahmoudi,M., 2011. Superparamagnetic iron oxide nanoparticles: promises for diagnosis and treatment of cancer. Int J Mol Epidemiol Genet, 2, 367-390.

Laurent,S., Saei,A.A., Behzadi,S., Panahifar,A., Mahmoudi,M., 2014. Superparamagnetic iron oxide nanoparticles for delivery of therapeutic agents: opportunities and challenges. Expert Opin Drug Deliv, 1-22.

Liu,Z., Wang,F., 2013. Development of RGD-based radiotracers for tumor imaging and therapy: translating from bench to bedside. Curr Mol Med, 13, 1487-1505.

Lu,J., Ma,S., Sun,J., Xia,C., Liu,C., Wang,Z., Zhao,X., Gao,F., Gong,Q., Song,B., Shuai,X., Ai,H., Gu,Z., 2009. Manganese ferrite nanoparticle micellar nanocomposites as MRI contrast agent for liver imaging. Biomaterials, 30, 2919-2928.

Lubbe,A.S., Bergemann,C., Huhnt,W., Fricke,T., Riess,H., Brock,J.W., Huhn,D., 1996. Preclinical experiences with magnetic drug targeting: tolerance and efficacy. Cancer Res, 56, 4694-4701.

Lyons,J.A., Sheahan,B.J., Galbraith,S.E., Mehra,R., Atkins,G.J., Fleeton,M.N., 2007. Inhibition of angiogenesis by a Semliki Forest virus vector expressing VEGFR-2 reduces tumour growth and metastasis in mice. Gene Ther, 14, 503-513.

Maeda,H., 2012. Vascular permeability in cancer and infection as related to macromolecular drug delivery, with emphasis on the EPR effect for tumor-selective drug targeting. Proc Jpn Acad Ser B Phys Biol Sci, 88, 53-71.

McKee,T.D., Grandi,P., Mok,W., Alexandrakis,G., Insin,N., Zimmer,J.P., Bawendi,M.G., Boucher,Y., Breakefield,X.O., Jain,R.K., 2006. Degradation of fibrillar collagen in a human melanoma xenograft improves the efficacy of an oncolytic herpes simplex virus vector. Cancer Res, 66, 2509-2513.

Nichols,J.W., Bae,Y.H., 2014. EPR: Evidence and fallacy. J Control Release.

Oakes,J.M., Breen,E.C., Scadeng,M., Tchantchou,G.S., Darquenne,C., 2014. MRI-based measurements of aerosol deposition in the lung of healthy and elastase-treated rats. J Appl Physiol (1985).

Peer,D., Karp,J.M., Hong,S., Farokhzad,O.C., Margalit,R., Langer,R., 2007. Nanocarriers as an emerging platform for cancer therapy. Nat Nanotechnol, 2, 751-760.

Polyak,B., Fishbein,I., Chorny,M., Alferiev,I., Williams,D., Yellen,B., Friedman,G., Levy,R.J., 2008. High field gradient targeting of magnetic nanoparticle-loaded endothelial cells to the surfaces of steel stents. Proc Natl Acad Sci U S A, 105, 698-703.

Prokop,A., Davidson,J.M., 2008. Nanovehicular intracellular delivery systems. J Pharm Sci, 97, 3518-3590.

Reddy,G.R., Bhojani,M.S., McConville,P., Moody,J., Moffat,B.A., Hall,D.E., Kim,G., Koo,Y.E., Woolliscroft,M.J., Sugai,J.V., Johnson,T.D., Philbert,M.A., Kopelman,R., Rehemtulla,A., Ross,B.D., 2006. Vascular targeted nanoparticles for imaging and treatment of brain tumors. Clin Cancer Res, 12, 6677-6686.

Reddy,L.H., Arias,J.L., Nicolas,J., Couvreur,P., 2012. Magnetic nanoparticles: design and characterization, toxicity and biocompatibility, pharmaceutical and biomedical applications. Chem Rev, 112, 5818-5878.

Riegler,J., Wells,J.A., Kyrtatos,P.G., Price,A.N., Pankhurst,Q.A., Lythgoe,M.F., 2010. Targeted magnetic delivery and tracking of cells using a magnetic resonance imaging system. Biomaterials, 31, 5366-5371.

Rizzo,L.Y., Theek,B., Storm,G., Kiessling,F., Lammers,T., 2013. Recent progress in nanomedicine: therapeutic, diagnostic and theranostic applications. Curr Opin Biotechnol, 24, 1159-1166.

Sahana,D.K., Mittal,G., Bhardwaj,V., Kumar,M.N., 2008. PLGA nanoparticles for oral delivery of hydrophobic drugs: influence of organic solvent on nanoparticle formation and release behavior in vitro and in vivo using estradiol as a model drug. J Pharm Sci, 97, 1530-42.

Schleich,N., Po,C., Jacobs,D., Ucakar,B., Gallez,B., Danhier,F., Préat,V., 2014. Comparison of active, passive and magnetic targeting to tumors of multifunctional paclitaxel/SPIO-loaded nanoparticles for tumor imaging and therapy. J Control Release.

Schmieder,A.H., Caruthers,S.D., Zhang,H., Williams,T.A., Robertson,J.D., Wickline,S.A., Lanza,G.M., 2008. Three-dimensional MR mapping of angiogenesis with alpha5beta1(alpha nu beta3)-targeted theranostic nanoparticles in the MDA-MB-435 xenograft mouse model. FASEB J, 22, 4179-4189.

Shamim,N., Hong,L., Hidajat,K., Uddin,M.S., 2007. Thermosensitive polymer (N-isopropylacrylamide) coated nanomagnetic particles: preparation and characterization. Colloids Surf B Biointerfaces, 55, 51-58.

Soenen,S.J., Himmelreich,U., Nuytten,N., De Cuyper,M., 2011. Cytotoxic effects of iron oxide nanoparticles and implications for safety in cell labelling. Biomaterials, 32, 195-205.

St-Coeur,P.D., Touaibia,M., Cuperlovic-Culf,M., Morin,P., Jr., 2013. Leveraging metabolomics to assess the next generation of temozolomide-based therapeutic approaches for glioblastomas. Genomics Proteomics Bioinformatics, 11, 199-206.

Svenson,S., 2013. Theranostics: are we there yet? Mol Pharm, 10, 848-856.

Tessari,A., Palmieri,D., Di,C.S., 2013. Overview of diagnostic/targeted treatment combinations in personalized medicine for breast cancer patients. Pharmgenomics Pers Med, 7, 1-19.

Thomas,S.N., Vokali,E., Lund,A.W., Hubbell,J.A., Swartz,M.A., 2014. Targeting the tumor-draining lymph node with adjuvanted nanoparticles reshapes the anti-tumor immune response. Biomaterials, 35, 814-824.

Trimaille,T., Pichot,C., Elaïssari,A., Fessi,H., Briançon,S., Delair,T., 2003. Poly(d,l-lactic acid) nanoparticle preparation and colloidal characterization. Colloid Polym. Sci., 281, 1184–1190.

Van Allen,E.M., Wagle,N., Levy,M.A., 2013. Clinical analysis and interpretation of cancer genome data. J Clin Oncol, 31, 1825-1833.

Wacker,M., 2013. Nanocarriers for intravenous injection--the long hard road to the market. Int J Pharm, 457, 50-62.

Wegscheid,M.L., Morshed,R.A., Cheng,Y., Lesniak,M.S., 2014. The art of attraction: applications of multifunctional magnetic nanomaterials for malignant glioma. Expert Opin Drug Deliv, 11, 957-975.

Yang,X.Y., Li,Y.X., Li,M., Zhang,L., Feng,L.X., Zhang,N., 2013. Hyaluronic acid-coated nanostructured lipid carriers for targeting paclitaxel to cancer. Cancer Lett, 334, 338-345.

Zhang,F., Huang,X., Zhu,L., Guo,N., Niu,G., Swierczewska,M., Lee,S., Xu,H., Wang,A.Y., Mohamedali,K.A., Rosenblum,M.G., Lu,G., Chen,X., 2012. Noninvasive monitoring of orthotopic glioblastoma therapy response using RGD-conjugated iron oxide nanoparticles. Biomaterials, 33, 5414-5422.